Cardiff University

Optimisation of Radiolabelling Methodologies for Lymphocyte Tracking by PET Imaging

A thesis submitted to the Cardiff University School of Medicine in candidacy for the degree of Doctor of Philosophy

by

Hanan Almutairi

Supervised by:

Principal supervisor: Dr Stephen Paisey

Co-supervisor: Prof Ann Ager

2024

Abstract

Cell tracking and labelling have become rapidly growing areas of research in clinical practice, particularly in the context of monitoring and evaluating immune cells and cell-based therapies. In order to effectively implement these therapies in the clinic, it is essential to have a comprehensive understanding of how cells behave and distribute within the body post-administration. The two main preclinically evaluated ^{89}Zr-tracers that have been applied for direct cell labelling are ^{89}Zr-DFO-NCS for cell surface labelling and ^{89}Zr-oxine for intracellular labelling. Although numerous publications have addressed the labelling of cells with ^{89}Zr-oxine and ^{89}Zr-DFO-NCS, direct comparisons between these two cell labelling methods remain limited. A study conducted in 2021 by Friberger *et al.,* provides an insightful *in vitro* comparison of these methodologies. In addition, further research by Friberger *et al*., in 2023 expands upon this comparison by investigating the efficacy of these two labelling techniques *in vivo*. Therefore, the primary objective of this project was to optimise direct *in vitro* labelling of lymphocytes with ^{89}Zr complexes, specifically ^{89}Zr-oxine and ^{89}Zr-DFO-NCS, allowing for *in vivo* tracking of radiolabelled cells via PET/CT imaging in a mouse model using these two compounds simultaneously. In particular, the thesis addressed the following objectives. Chapter 1 provided a general background and an introduction to the topic. Chapter 2 described the methods and materials used in the research project. Chapter 3 discussed the initial attempts to label donor lymphocytes with ^{89}Zr-oxine and ^{89}Zr-DFO-NCS complexes and track the labelled cells *in vivo* by PET/CT imaging in a mouse model in part 1. Part 2: presented the development of the labelling method for ^{89}Zr-oxine and EL4 cells for *in vivo* PET imaging. Chapter 4 presented the optimised parameters established from the labelling of EL4 cells to perform *in vitro* radiolabelling for the *in vivo* tracking of CTLL2 cells via PET/CT imaging in a mouse model. Finally, Chapter 5 summarised the study, highlighted any limitations

encountered, and presents suggestions for future work. We have shown that both ^{89}Zr-oxine and ^{89}Zr-DFO-NCS were successful in labelling T cells and tracking the movement and distribution of the labelled cells in mice using PET/CT imaging.

Acknowledgements

The completion of this doctoral dissertation does not simply reflect years of scholarly work, but also the generous support, encouragement and wisdom that I received from many people. I would like to thank each and every one of them for their contribution in my journey because without them, this achievement would not have been possible.

First of all, I would like to thank Kuwait University for their financial support. Their support was the cornerstone of this research, and I am eternally grateful for their assistance.

Secondly, I would like to express my sincere gratitude to my main supervisor Dr Stephen Paisey for his intellectual support and guidance during this study, as well as for his consistent encouragement His guidance has been significant in my personal and professional development, reaching well beyond the bounds of academics, transforming me into a judicious researcher and an astute thinker. Dr Paisey, your impact on my path is eternal.

I also wish to extend my heartfelt thanks to my co-supervisor, Professor Ann Ager. Her sharp analytical insights and constructive feedback have consistently elevated the quality of my work. Her keen sense for detail and scholarly rigor have made an indelible imprint on my academic journey.

I am particularly grateful to my mentor, Dr Ian Brewis for his knowledge and encouraging support in perfecting my research skills. Dr Brewis, your gifts of unequalled opportunities for development as a researcher are greatly valued.

I would like to express my sincere gratitude to my esteemed colleagues Abdulla Alenezi, Markella Alatsatianos and Ruban Peter. The collaborative atmosphere we developed has made

my doctoral journey a lot more meaningful. Your valuable contributions to my study, as well as the moral support you gave me, have made this academic life much more enjoyable and less challenging.

Lastly, I must mention the endless help of my family. Though this journey, my foundation has been your love, encouragement and emotional support. It would be an understatement to say that I am grateful for your unwavering faith in me. You have been my shelter when times were tough and source of happiness during victory. I am blessed to have you in my life.

In conclusion, I express my sincere thanks to all those who participated either directly or indirectly in the completion of this Ph.D., your influence has not only contributed to this academic piece but also amply benefitted my life by so much more words can define.

Thank you.

Abbreviations

Indium-111	^{111}In
Carbon-11	^{11}C
Oxygen-15	^{15}O
Fluorine-18	^{18}F
Copper-64	^{64}Cu
Gallium-68	^{68}Ga
Germanium-68	^{68}Ge
Yttrium-86	^{86}Y
Zirconium-89	^{89}Zr
Technetium-99	^{99}Tc
Acridine orange/propidium podide	AO/PI
Bioluminescence imaging	BLI
Biological services unit	BSU
Benzyl	Bz
Chimeric antigen receptor	CAR
Cluster of differentiation 4	CD4
Cluster of differentiation 8	CD8
Cell labelling efficiency	CLE
Concanavalin A	ConA
Circulating progenitor cells	CPCs
Computed tomography	CT
Cytotoxic T lymphocyte cells	CTLs

Dendritic cell	DC
P-isothiocyanatobenzyl-desferrioxamine	Df-Bz-NCS
Desferrioxamine	DFO
Dulbecco's modified eagle's medium	DMEM
Dimethyl sulfoxide	DMSO
1,4,7,10-tetraazacyclododecane-1,4,7,10-tetraacetic acid	DOTA
Diethylenetriaminepentaacetic acid	DTPA
1-ethyl-3-(3-dimethyl-aminopropyl)-carbodiimide	EDC
Ethylenediaminetetraacentic acid	EDTA
Fetal calf serum	FCS
US Food and Drug Administration	FDA
Fluorodeoxyglucose	FDG
4-(2-hydroxyethyl)-1-piperazineethanesulfonic acid	HEPES
Hexamethylpropyleneamine oxime	HMPAO
Human bone marrow-derived mesenchymal stem cells	hMSCs
High performance liquid chromatography	HPLC
Immunity and infection	I & I
Interleukin	IL
Instant thin layer chromatography	ITLC
Labelling efficiency	LE
Line of response	LOR
Magnetic activated cell sorting	MACS
Acetonitrile	MeCN
Methanol	MeOH

Major histocompatibility complex	MHC
Magnetic particle imaging	MPI
Magnetic resonance imaging	MRI
Mesenchymal stem cell	MSC
Sodium carbonate	Na_2CO_3
Sodium chloride	NaCl
Sodium hydroxide	NaOH
Isothiocyonate (chemical group)	NCS
Natural killer	NK
1,4,7-triazacyclononane-N,N',N"-triacetic acid	NOTA
Neural stem cells	NSCs
Optical imaging	OI
Phosphate buffered saline	PBS
Positron emission tomography	PET
Personal investigator licence	PIL
Project licence	PPL
Research and development	R & D
Red blood cell	RBC
Roswell Park Memorial Institute	RPMI
Room temperature	RT
Single photon emission computed tomography	SPECT
Superparamagnetic iron oxide	SPIO
T cell receptor	TCR
1,4,8,11-tetraazacyclotetradecane-1,4,8,11-tetraacetic acid	TETA

Tetrafluorophenyl	TFP
Regulatory T cell	Treg
Ultrasound	US
White blood cell	WBC

Abbreviations of units

Injected activity	IA
Injected activity/organ	IA/g
Kilobecquerel	KBq
Molar	M
Megabecquerel	MBq
Milligram	mg
Millilitre	ml
Millimolar	mM
Microlitre	µl
Micrometre	µm

Table of contents

List of figures

List of tables

Chapter 1: Introduction

1.1 Background

More than a century and a half ago, Rudolf Virchow's observation of white blood cells in cancerous tissues during the 1860s was a key moment in the history of medicine. It suggested a connection between long-lasting inflammation and cancer, forming the basis for the field of cancer immunology and, as a result, the development of treatments that use the immune system.[1] Expanding on this idea, William Coley carried out important experiments in the 1890s by injecting tumours with bacteria that had been killed by heat. Astonishingly, these injections often caused the tumours to become smaller, which was a significant step forward for research in immune-based treatments.[2]–[4]

In 1908, Paul Ehrlich substantiated Coley's findings by demonstrating that the immune system could spontaneously suppress several tumours.[5] Concurrently, Murphy and Morton from the Rockefeller Institute in the United States were engaged in mouse studies, leading them to propose a theory in 1915. They suggested that even non-specific activation of immune cells, especially lymphocytes, might be a viable approach for treating cancer.[6] However, subsequent human trials proved largely unsuccessful, resulting in the abandonment of this hypothesis and the dismissal of cancer immunotherapy as a viable treatment option for several decades.[5] A significant advancement in cancer immunotherapy occurred with the introduction of Thomas and Burnet's ground breaking theory of cancer immunosurveillance in 1957.[5] They posited that lymphocytes could serve as guardians, identifying and potentially eradicating cells transformed by mutations.[5],[7] Yet, this theory was hindered by a lack of understanding of tumour-specific antigens and the technical challenges in cultivating lymphocytes *in vitro*, delaying further progress.[5] The concept of immune surveillance

resurfaced in 1974, when Stutman's research indicated that nude mice with compromised immune systems developed cancer more frequently than their normal counterparts.[8],[9] Around this period, the discovery of natural killer cells lent further credence to the human immune system's capabilities.[5],[10],[11] Although Burnet and Thomas's hypothesis of cancer immunosurveillance was proposed in the mid-twentieth century, it wasn't until the end of the twentieth century that the work of Schreiber, Dunn, Old, and their teams confirmed the role of T cells in anti-tumour surveillance and immune responses.[7],[11]–[14] This was followed by further discoveries, including insights into immunoediting, the mechanisms of cancer cell evasion, and the recognition that immunosuppressed patients have a significantly higher risk of developing cancer.[15]–[17]

The interplay between T cells, immunotherapy, and cancer treatment is crucial. T cells, a vital component of the immune system, are capable of recognizing and destroying cancer cells. However, cancer cells can suppress T cell activity to evade immune detection.[18] Immunotherapy seeks to enhance the body's immune response against cancer cells, offering a more targeted approach than traditional treatments like chemotherapy and radiotherapy, which often harm healthy cells alongside cancerous ones.[19] The specificity of immunotherapy and cell-based therapy results in fewer side effects and improved patient outcomes.[20] Driven by breakthroughs in immunology and the understanding of tumour immune evasion; these therapies have shown effectiveness in treating cancers like melanoma, lung cancer, and leukaemia.[21]

Notable immunotherapeutic approaches are Adoptive T cell transfer therapy, which infuses autologous or allogeneic T cells into cancer patients, and chimeric antigen receptor T (CAR-T) cell therapy, which uses genetically modified T cells.[22] These methods have shown considerable success in treating hematologic malignancies. Advances in genome editing,

proteomics, and metabolomics have opened doors for multi-faceted approaches addressing various aspects of cancer treatment.[22],[23] These therapies have achieved remarkable success in clinical trials, with some patients experiencing complete cancer remission. Immunotherapy is emerging as a transformative approach to cancer treatment.[24]

Understanding the biology of the tumour microenvironment and monitoring the effectiveness of therapies are among the central challenges facing immune cellular therapies. Molecular imaging is, therefore, necessary in the *in vivo* tracking of immune cells together with mechanisms such as Single Photon Emission Computed Tomography (SPECT), Positron Emission Tomography (PET), Magnetic Resonance Imaging (MRI), fluorescence imaging (FLI), bioluminescence imaging (BLI), and Ultrasound (US). In this way, the tracking method can give helpful information on the effectiveness of immunotherapy, which will help optimise treatment strategies. For example, knowledge about immune cell mechanisms by imaging will help develop combination therapies and further predict the patient's response to immunotherapy.[21] Such information from *in vivo* targeted imaging is indispensable in defining the dynamics of immunotherapy and potential therapy targets. This technique is essential in predicting the treatment outcome and identifying patients more likely to benefit from immunotherapy.[25]–[27]

As an alternative approach, PET imaging by direct cell labelling has emerged as a new paradigm in immunotherapy since it offers a non-invasive quantitative tool to study the efficacy of adoptive cell transfer-based therapies. The first attempts at direct cell labelling, where cells are labelled *in vitro* and re-injected for tracking *in vivo,* in nuclear medicine started with using radiolabelled red blood cells for imaging the blood flow in the 1950s.[28] Since then, advancements in labelling have resulted in the development of new radiotracers and techniques and the adoption SPECT imaging of ^{111}In and ^{99m}Tc labelled white blood cells as standard

clinical techniques for imaging inflammation and infection.[29],[30] Whilst these clinical SPECT imaging techniques have proved to be extremely useful there has been recent focus on the development of direct cell labelling PET tracers to take advantage of the increased sensitivity and quantifiability PET imaging can offer.[31]–[33]

The two main preclinically evaluated ^{89}Zr-tracers that have been applied for direct cell labelling are ^{89}Zr-DFO-NCS for cell surface labelling and ^{89}Zr-oxine for intracellular labelling. Although numerous publications have addressed the labelling of cells with ^{89}Zr-oxine [34], [35] and ^{89}Zr-DFO-NCS [36],[37], direct comparisons between these two cell labelling methods remain limited. A study conducted in 2021 by Friberger *et al.,* provides an insightful *in vitro* comparison of these methodologies.[38] In addition, further research by Friberger *et al*., in 2023 expands upon this comparison by investigating the efficacy of these two labelling techniques *in vivo*.[39] Therefore, the primary objective of this project is to optimise direct *in vitro* labelling of lymphocytes with ^{89}Zr complexes, specifically ^{89}Zr-oxine and ^{89}Zr-DFO-NCS, allowing for *in vivo* tracking of radiolabelled cells via PET/CT imaging in a mouse model using these two compounds simultaneously.

1.2   Aims of the thesis and thesis outline

The primary objective of this thesis was to optimise ^{89}Zr complexes, specifically ^{89}Zr-oxine and ^{89}Zr-DFO-NCS, for *in vivo* tracking of radiolabelled CD8 T cells via PET/CT imaging in a mouse model. To achieve this goal, the following chapters were proposed.

- **Chapter 1** provides a general background and an introduction to the topic.
- **Chapter 2** describes the methods and materials used in the research project.

- **Chapter 3** discusses the initial attempts to label donor lymphocytes with ^{89}Zr-oxine and ^{89}Zr-DFO-NCS complexes and track the labelled cells *in vivo* by PET/CT imaging in a mouse model in part 1. Part 2: presents the development of the labelling method for ^{89}Zr-oxine and EL4 cells for *in vivo* PET imaging.

- **Chapter 4** presents the optimised parameters established from the labelling of EL4 cells to perform *in vitro* radiolabelling for the *in vivo* tracking of CTLL2 cells via PET/CT imaging in a mouse model.

- **Chapter 5** summarises the study, highlights any limitations encountered, and presents suggestions for future work.

1.3   Immune system

The immune system is a complex system comprising different types of tissues, organs, and cells (Figure 1-1) which unite to protect us against bacteria, viruses, parasites, and harmful substances. Broadly, the immune system is split into two main types: innate and adaptive. It is essential to differentiate these two types, as they will help understand how the immune system works.[40] The body's innate immune system serves as the initial line of defence, providing nonspecific protection against various pathogens. It includes physical barriers such as the skin and mucous membranes and specialised cells such as neutrophils, macrophages, dendritic cells, and natural killer cells.[40]–[44] On the other hand, the adaptive immune system mounts a more targeted response to pathogens. It involves specific cell types such as B and T lymphocytes. Cellular immunity occurs when specialised T cells recognise specific antigens displayed on pathogenic or abnormal cells, whereas B cell-mediated humoral immunity produces antibodies. These responses play a crucial role in combating infections and help detect abnormalities such as cancers for disease prevention.[41] Until recently, scientists

believed that innate and adaptive immunity acted independently, but the evidence shows more interdependency of their processes that blurs these boundaries. Both innate and adaptive immune cells secrete cytokines that are crucial in the regulation of inflammation as well as cellular communication.[41],[45]

1.3.1 Lymphocytes

Lymphocytes, a category of leukocytes, are integral to the adaptive immune response. They have specialized capabilities in recognizing and neutralizing discrete pathogenic entities. There are two types of lymphocytes: B and T lymphocytes. These two types have different functions but work together to protect the immune system.[41],[46]-[48] B lymphocytes, emerging from hematopoietic stem progenitors in the bone marrow, constitute the humoral segment of acquired immunity mediated by immunoglobulins. Antigen stimulation drives B lymphocyte activation and differentiation into antibody-generating plasma and memory B cells. The secreted antibodies neutralize or eliminate specific antigens. Memory B cells confer lasting immune memory, enabling accelerated reactions to subsequent antigen exposures, thus preventing recurrent infections.[41],[46] T lymphocytes also arise from bone marrow hematopoietic stem cells but mature in the thymus gland. This developmental process enables tailored immune responses to novel threats without autoreactivity. Rather than directly destroying pathogens, T cells coordinate infected or aberrant cell elimination by stimulating other immune cell types through cytokines and cytotoxic granules.[41],[46],[49]

1.3.1.1 Development and differentiation of T lymphocytes

Upon maturation, T cells remain inactive until they encounter antigens presented by dendritic cells or macrophages. This interaction links the innate and adaptive immune systems. T cells

are transformed into three specialized subtypes when activated, each of which has unique functions: Helper T cells (CD4 T cells) coordinate the immune response by activating and guiding other immune cells, including B cells and cytotoxic T cells. The role of cytotoxic T cells (CD8 T cells) is to combat and eliminate infected and abnormal cells, including cells infected by viruses or tumours. Regulatory T cells are cells that control and suppress immune responses in order to prevent autoimmune diseases. This differentiation process is crucial in how T cells contribute to the adaptive immune response. It emphasizes their role in primarily supporting cell-mediated immunity, directing the elimination of infected or abnormal cells by stimulating other immune cells through cytokines and cytotoxic granules.[41],[46]–[48]
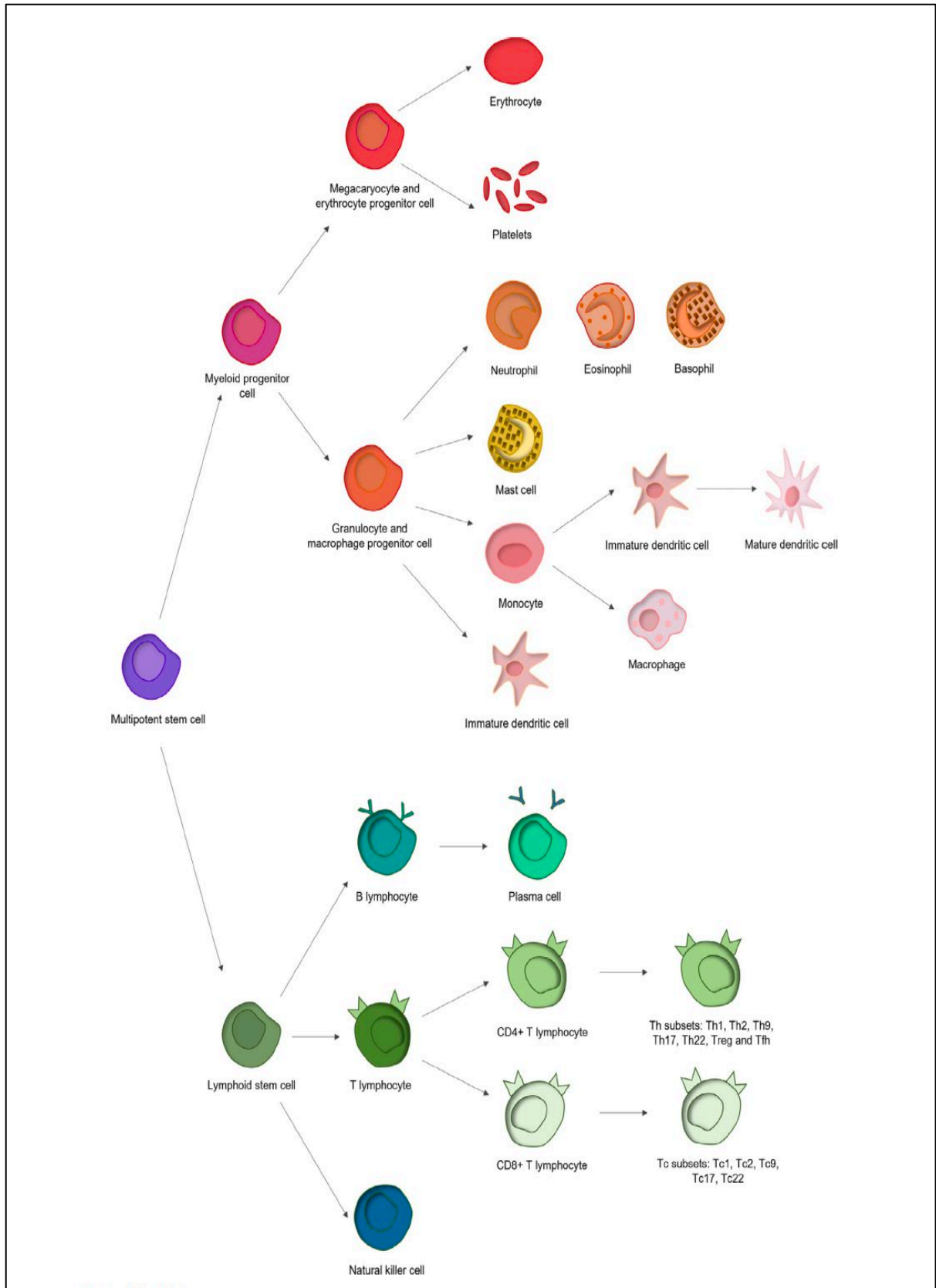
Figure 1-1: Cells of the immune system. This figure was taken from reference [41].

1.3.1.2 Activation of Naïve CD8 cytotoxic T lymphocytes (CTLs)

Naïve CD8 cytotoxic T lymphocyte (CTLs) activation is critical to the cancer immunity cycle and immunosurveillance. Naive CTLs are T cells which have not yet met with respective antigens and remain inactive. Optimal activation of naive CTLs necessitates three discrete signals: antigen recognition, co-stimulatory and cytokine signalling. The first activation signal is antigen recognition, which happens when the T Cell Receptor (TCR) of a naive CTL pairs with its specific antigen presented by primary histocompatibility class I molecules owned by antigen-presenting cells. This interaction is the first stimulus for CTL activation, which is performed through an antigen-specific way. The second signal refers to co-stimulation, which occurs when the CTL's CD28 control binds to CD80/CD86 on the antigen-presenting cell. T cell activation and clonal expansion are, in turn, enhanced by this co-stimulatory signal. Third, stimulatory cytokines such as interleukin-2 and interferon-gamma signal for CTL proliferation, differentiation and acquisition of effector functions.[50]

Naive CTLs, once activated, differentiate into effector CTLs, which can detect and remove cancer cells. Effector CTLs enter the tumour sites, infiltrate the tumour microenvironment, and recognize the cancer cells expressing its antigen. Afterwards, CTLs cause the cancer cells to undergo apoptosis, a process triggered by discharging cytotoxic granules into the cancerous cells and ultimately leading to the regression of the tumour.[50]

Indeed, the activation of CTLs marks a crucial stage in the cancer immunity cycle, Figure 1-2, which is a sequence of events the immune system undergoes to identify and eliminate cancer cells.[51] This cycle involves (1) Release of cancer antigens from tumour cells; (2) Presentation of cancer antigens on the primary histocompatibility complex class (MHC) by antigen-presenting cells; (3) recognition of cancer antigens on the MHC by the T cell receptor,

resulting in T cell activation; (4) Trafficking of activated T cells; (5) Infiltration into the tumour; (6) Recognition of cancer antigens on the MHC within the tumour; (7) Attack on tumour cells, resulting in tumour cell injury/death.[20]

In a nutshell, triggering of the naive CD8 cytotoxic T cells through antigen contact, co-stimulation, and cytokine endorsement is necessary for the production of effector CTLs that can contribute to the cancer immunity cycle and immunosurveillance, which detects and eliminates malignant cells. This stresses the relevance of CTL responses in cancer immunity.[20]
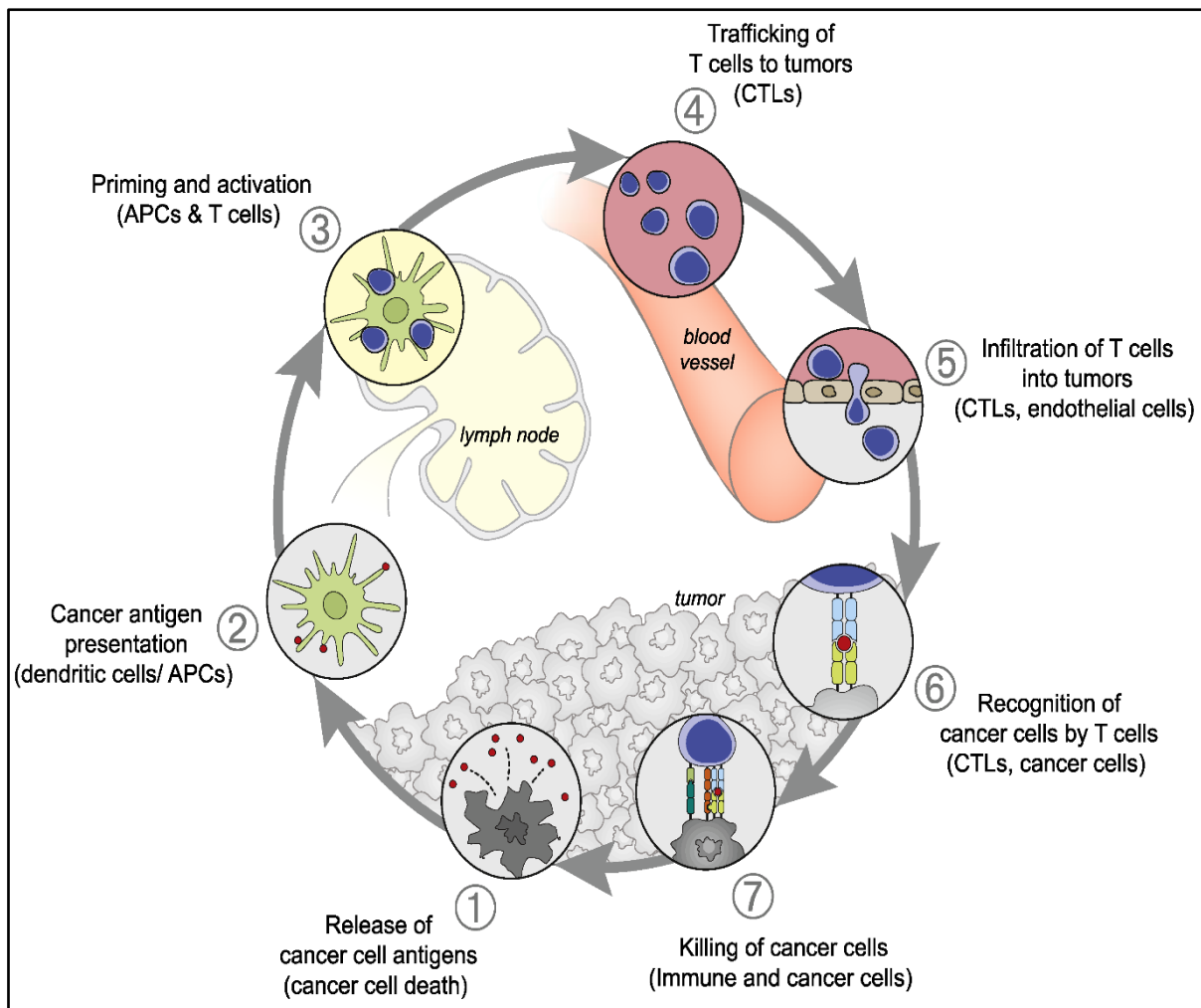
Figure 1-2: Cancer-immunity cycle. This figure was adopted from reference [20].

1.4   Overview of cell labelling and *in vivo* tracking methodologies

Cell labelling is essential for studying cellular biology, particularly in immunology and cell-based therapies. This process involves the attachment of radioactive isotopes to cells, enabling researchers and clinicians to track their movement and distribution within the body. The use of immune cells as potential therapeutics for conditions such as cancer and autoimmune disease has led to an increased demand for non-invasive methods of cell trafficking, such as molecular imaging. This technique allows for longitudinal tracking of target cells *in vivo*, providing valuable insights into the migration, homing, and overall behaviour after injection or transplantation. Additionally, molecular imaging can also be used to predict therapy response in some instances, making it a powerful tool for understanding the biology of the tumour microenvironment.[29],[52]–[54]

Cell labelling methods can be generally categorised into direct and indirect (Figure 1-3). Direct cell labelling involves directly attaching the radioisotope to the cell surface or intracellularly. In contrast, indirect labelling involves using a carrier molecule that binds to a specific marker on the cell surface and subsequently carries the radioisotope to the cells of interest. Both methods have advantages and limitations, and the choice of labelling method depends on the specific goals and requirements of the study.[29],[52],[53] Table 1-3 presents comparative overview of labelling strategies and imaging modalities for cell tracking in preclinical and clinical studies. Although this research focuses on the direct *in vitro* labelling of cells, we will briefly mention the indirect cell labelling method.

1.4.1 Indirect cell labelling and tracking

Indirect cell labelling techniques involve the genetic modification of target cells to express reporter genes upon their transfer, enabling sustained visibility of labelled cells over extended periods. This method allows for continuous *in vivo* imaging, offering the potential to track cell viability and proliferation using reporter genes that encode proteins specifically active in living cells, such as the ATP-dependent sodium-iodide symporter (NIS).[55],[56]

Furthermore, indirect labelling can be tailored to target specific immune cell subtypes through the expression of particular antigens. Reporter gene imaging, involving integrating genes like HSV1-TK under controlled promoters leading to specific protein expression, enables targeted imaging upon injecting a radiolabelled agent. Although less cytotoxic than direct labelling, this method requires careful consideration to maintain cell functionality and minimize immunogenicity.[56],[57]

In the context of stem cell tracking, indirect labelling has been utilized for the non-invasive monitoring of transplanted human endothelial progenitor cells, demonstrating its potential for assessing tissue distribution and engraftment in myocardial infarction.[58] Additionally, indirect labelling strategies have been explored for tumour-targeting proteinaceous drugs, offering a more significant number of radiolabelled molecules with various modifications and localizations compared to direct labelling approaches.[59]

The use of indirect labelling for non-invasive cell tracking in cancer therapy has been a subject of interest, with the potential to visualize genetic events in living subjects through various imaging modalities such as optical, radionuclide, and magnetic resonance imaging. This approach has shown promise in imaging molecular pathways and reporter genes, providing insights into cellular processes and gene expression *in vivo*.[59] Despite its advantages, the

complexity of this approach, the potential to alter cell functionality, associated costs, the need for specialized equipment and expertise, and the significant regulatory burden present additional challenges to its widespread adoption in clinical settings. However, with advancements in gene editing technologies, the safe incorporation of reporter genes into the genome appears increasingly feasible.[55],[57]

1.4.2 Direct *(in vitro)* cell labelling and tracking

Direct *ex vivo* or *in vitro* cell labelling involves attaching an imaging label to the cell surface or inside the cells before administering it. This technique provides a simple way to track cells in clinical and research settings, avoiding the complexities of genetic manipulation. Direct cell labelling with radionuclides has significantly advanced biomedical research and clinical applications. It involves labelling cells with a radiotracer *in vitro* or *ex vivo* before reintroducing them into the body. This enables imaging or therapeutic applications.[29],[55],[60] The attached radiolabel facilitates tracking the cells *in vivo*, revealing valuable information about their location, movement, and potentially their function. Common radionuclides used are long-lived isotopes like indium-111 and Zirconium-89, enabling imaging over relatively long periods.[29],[60]

The cell labelling process involves multiple steps. First, cells are exposed to a radiolabelling agent like a radiometal complex or radioisotope. The cells then absorb the agent through diffusion or active transport. After labelling, the cells are washed to remove excess radiotracer. The labelled cells are injected into the subject, followed by *in vivo* imaging to assess their distribution over time. The key criterion is that the label must remain fixed inside or on the cells for sufficient time for imaging purposes.[29],[60]

Indium-111 labelled white blood cell (WBC) scanning is a nuclear medicine imaging technique utilized to locate regions of inflammation and infection in the body.[29] The radiolabelled leukocytes are allowed 24 hours to migrate to sites of infection or inflammation before obtaining images. Areas of abnormal accumulation of the tagged white blood cells on scintigraphic images indicate infectious or inflammatory foci. While this method is considered the gold standard radionuclide technique for diagnosing most infections in patients with intact immune systems, it has some drawbacks. The *in vitro* cell labelling process is labour-intensive, time-consuming, requires handling of blood products, and is not widely available at all institutions.[62] However, despite these limitations, Indium-111 labelled WBC scanning remains an important and useful diagnostic nuclear medicine procedure for detecting infection and inflammation.[29]

In nuclear medicine, labelled red blood cells serve as a diagnostic radiopharmaceutical.[63],[64] A prime example is Technetium-99m-labelled red blood cells, revolutionizing cardiovascular imaging.[28] These are used for blood pool imaging, detecting vascular malformations, and determining red cell mass.[28] Technetium also labels red blood cells to locate intestinal bleeding. Technetium-99m- labelled erythrocytes scans are recommended to confirm gastrointestinal bleeding and can be effective in localizing the site of bleeding.[29],[63],[64]

Furthermore, one of the key applications of the direct cell labelling technique is in tracking the fate, biodistribution, and migration behaviour of autologous patient-derived cells following administration. This has been particularly useful in oncology, where it has been used to track the short-term delivery of cells in patients with cancer.[52] A specific example of this application is the *in vivo* tracking of Th1 cells using PET imaging. This method has been used to reveal the quantitative and temporal distribution of Th1 cells and their specific homing in

lymphatic tissue. The study found that Th1 cells homed to the peri thymic lymph nodes of naive mice. Interestingly, intravenously administered Th1 cells homed predominantly into the lung and spleen.[65] Direct cell labelling is also used in the diagnosis and treatment of cancer. Radioimmunotherapy, a targeting therapy for cancer, uses monoclonal antibodies labelled with a radionuclide directed against tumour-specific antigens.[66]

Various direct labelling methods exist. For instance, natural killer cells can be labelled with Carbon-11 using surface protein binding with methyl iodide. Similarly, bone-marrow derived dendritic cells can be labelled with Fluorine-18 using N-succinimidyl-4-fluorobenzoate.[29],[59]

Direct cell labelling offers several advantages. It is a relatively simple process that can be applied to any chemical probe capable of entering cells and binding to the radionuclide.[29],[55] The technique allows for fast, efficient cellular uptake, with high cellular retention of the radionuclide.[29] This makes it a valuable tool for tracking the movement and location of cells *in vivo*. However, limitations exist. The imaging time window depends on the radionuclide's half-life.[29] Radiotracer efflux from cells can restrict techniques.[29] Cell proliferation information is lost as radionuclides redistribute between dividing daughter cells (label dilution).[29] Potential radiotoxicity from delivering radionuclides into cells is a concern, partially mitigated by surface labelling.[29] Not only that but also, labelling is laborious, requiring radiation shielding.[67]

The impact of labelling on cell viability has been studied for Superparamagnetic Iron Oxide Particles (SPIO), showing that high concentrations of labelling reagents can lead to a decrease in overall cell yield.[68] Usefully, cell labelling efficiency can be determined by measuring the decrease in the spin-spin relaxation time of the water proton in cell samples containing labelled

cells.[68] These studies highlight the importance of assessing the impact of labelling agents on cell viability and functionality to optimize their use in preclinical and clinical settings.[68] Despite these complications, superparamagnetic iron oxide (SPIO) nanoparticles have shown promise for labelling stem cells for cellular magnetic resonance imaging (MRI), offering superb spatial resolution and repeated non-invasive imaging of magnetically labelled cells *in vivo*.[69] However, it has been observed that daughter cells of SPIO-labelled cells tend to lose some labelling due to cell proliferation, emphasizing the need to maintain high labelling efficiency over successive passages.[69]

In conclusion, direct cell labelling agents demonstrate various adaptabilities and potential applications, each with unique properties. However, careful consideration of stability, toxicity, and the impact of cell division on signal retention is essential. The effects on cell viability and function necessitate a cautious approach in selecting and applying these agents, underlining the need for careful evaluation to optimize their use in preclinical and clinical settings.[29],[56]
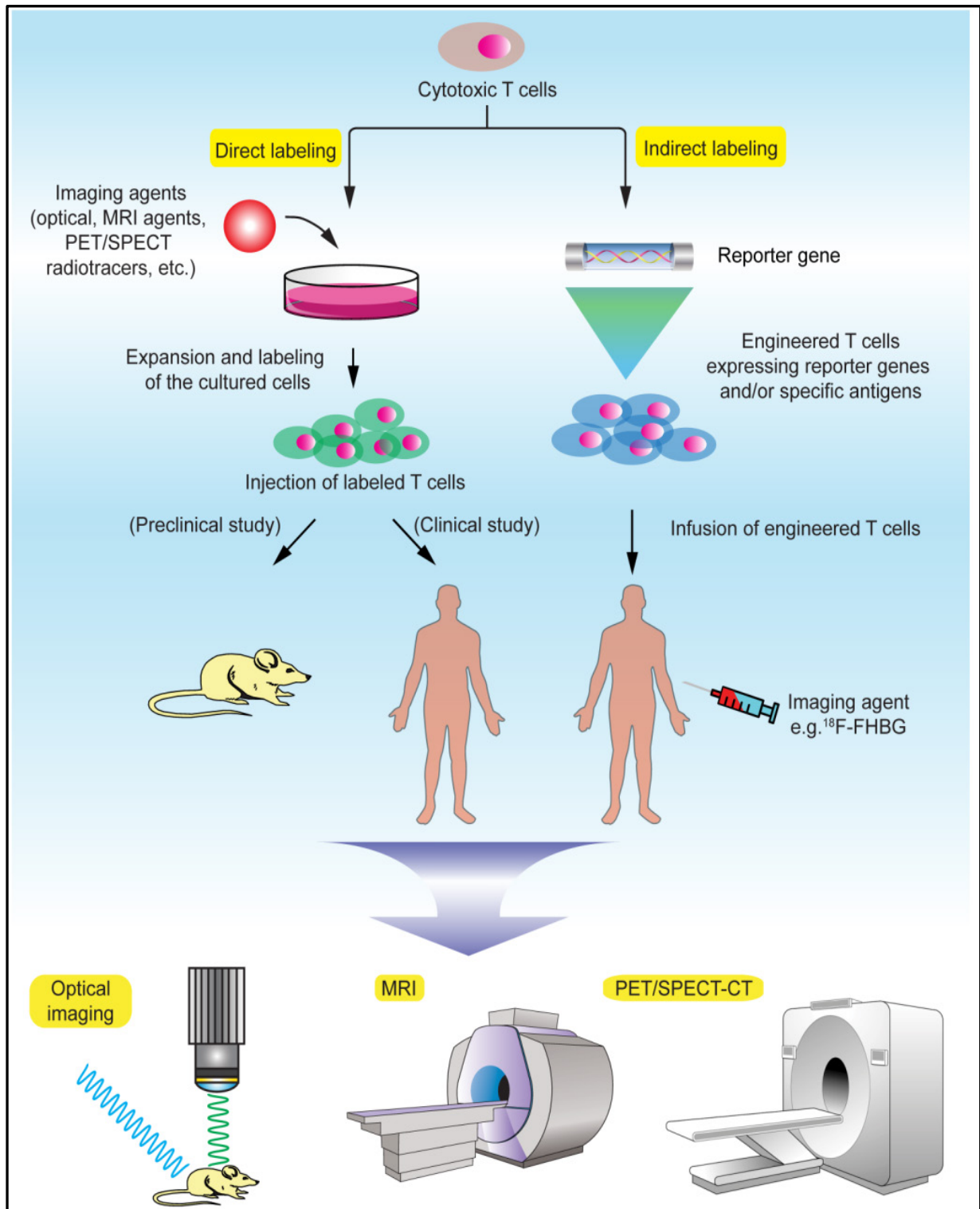
Figure 1-3: A schematic representation of non-invasive T cell tracking using molecular imaging. Direct *in vitro* cell labelling involves introducing radioactive or fluorescent tags into cells before administering them to a subject. In contrast, indirect labelling involves transducing a reporter gene into the cell before transplantation, which is then visualized by injecting a probe or substrate. Labelled cells can be tracked using optical imaging, MRI, PET, SPECT, CT, or a combination of these methods. The figure was taken from reference [109].

1.5 Molecular imaging modalities for cell tracking

Advancements in immunology and cell-based therapies have led to an increase in the tracking of specific cell types in the body. Researchers have found that certain cells, such as neutrophils and eosinophils [70],[71], exhibit distinct distribution patterns in conditions such as asthma and chronic obstructive pulmonary disease, and there is a significant interest in tracking T cells [72] and dendritic cells [73] in cancer and autoimmune diseases. Additionally, advancements in the separation and isolation of different leukocyte types and an increased understanding of the roles of these cells have opened new possibilities for tracking individual immune cell types through imaging, leading to the utilisation of cell labelling in various applications, including cancer, atherosclerosis, stroke, transplant medicine, asthma, and allergy.[54],[74]

Molecular imaging is a rapidly developing field with applications in various disciplines, including biology, chemistry, computer science, engineering, and medicine. It allows for the visualisation of cellular and subcellular processes within living subjects. In particular, non-invasive, *in vivo* cell tracking is an emerging approach with significant implications for immune cell therapies.[30],[54],[75]–[77] Molecular imaging is indispensable in resolving critical inquiries within therapy. Beyond shedding light on T cell functionality, *in vivo,* cell tracking with molecular imaging technologies can furnish quantifiable data on T cell homing, infiltration capabilities, and the quantification and duration of T cell presence within tumours. Such data crucially mirrors the dynamics of the tumour microenvironment and the efficacy of therapeutic interventions.[52]–[55] The development and testing of cell-based immunotherapies is greatly enhanced by the ability to follow the trafficking of therapeutic cells *in vivo* via this non-invasive, clinically compatible technique which is not limited by depth and does not require a biopsy.[54],[78]

Imaging modalities applied in preclinical and clinical arenas for tracking immune and stem cells include Optical Imaging (OI) such as Bioluminescence Imaging (BLI) and Fluorescence Imaging (FLI), Computed Tomography CT, Magnetic Resonance Imaging (MRI), Positron emission Tomography (PET) and single photon emission computed tomography (SPECT). Each has inherent advantages and limitations. Selecting the optimal modality depends on the relevant cellular process and expected readout for a particular T cell therapy study.[30],[54],[75]–[77]

1.5.1 Optical Imaging (OI)

Optical imaging (OI) offers non-invasive visualization of cellular processes with high spatial resolution, including bioluminescence imaging (BLI) and fluorescence imaging (FLI), which is crucial to cell imaging. By employing light and optical systems, these advanced imaging modalities can produce detailed images of internal cellular structures, providing valuable insights into cellular processes.[79] BLI is a suitable and effective method for investigating cancer biology and treatment. Furthermore, BLI has been demonstrated to be helpful in visualizing dynamic cellular processes in live animals as well as in monitoring cell movement and gene expression.[80]

OI methods have exceptional sensitivity, with detection thresholds ranging from picomolar to femtomolar for the relevant optical reporters or contrasts. At a minimal cost, these optical imaging modalities can be used to assess the distribution, functionality, and viability of infused T cells in a rapid and long-term manner. Although this method excels at analysing cellular and molecular events, its utility in larger animals and clinical settings for humans is restricted by its inability to penetrate deep tissues. In biological tissues, OI has limitations due to its susceptibility to light scattering.[79] Also, advanced OI systems are complex and expensive,

which may limit their widespread use. Future advances in OI technology might address these limitations, increasing its utility in cell imaging.[81]–[84]

1.5.2 Ultrasound (US):

Ultrasound imaging is a valuable non-invasive technique for visualizing cellular processes, utilizing high-frequency sound waves reflected by internal structures to create images. It has been extensively used in various cell imaging applications, including apoptosis detection, stem cell tracking, tissue engineering, and molecular imaging.[85]

Apoptosis detection through ultrasound imaging has been successful *in vitro*, *in situ*, and *in vivo*, showcasing its high-resolution, non-invasive monitoring capabilities.[86] Stem cell tracking has also shown promise, despite low cell contrast, with a 3.8-fold increase in imaging intensity post-contrast agent injection [85] This potential has been demonstrated using a cell-culture system.[87] Ultrasound has been explored for differentiating benign and malignant thyroid nodules using elastography and MicroPure imaging [88] and detecting apoptosis in cancer therapy research.[89] It is a primary tool for imaging testicular germ cell tumours [90] and has a role in diagnosing, staging, and managing pancreatic diseases, work by Vazquez-Sequeiros *et al.* emphasizes endoscopic ultrasound's advantages and limitations.[91] In tissue engineering, ultrasound characterizes extracellular matrix deposition, estimates cell concentrations, and evaluates matrix morphology.[92] Molecular imaging advancements have led to targeted contrast agents, expanding ultrasound's capabilities to depict molecular and cellular processes.[93]

It is, however, essential to note that ultrasound imaging has some limitations. Because the contrast between target tissue and background is so low, it is challenging to visualize cellular

structures accurately. Ultrasound imaging also has the disadvantage of spot noise, adversely affecting cell image clarity. Furthermore, ultrasound imaging has limitations when it comes to imaging cells, including difficulty distinguishing benign from malignant nodules and accurately imaging deep-seated cellular structures.[94],[95]

1.5.3 Magnetic Resonance Imaging (MRI)

Magnetic Resonance Imaging (MRI) is a valuable tool in cell imaging, offering non-invasive visualization of cellular processes. This advanced imaging modality involves the manipulation of magnetic fields and radio waves to create detailed images of tissues and organs within the body. This non-invasive technique has been widely utilized in cell imaging, particularly in visualising labelled cells and tracking bacterial infections. MRI offers high spatial resolution, allowing for the precise localization of labelled cells within specific tissues. Additionally, it provides excellent soft tissue contrast, making it suitable for visualizing cellular structures with high detail. However, one critical limitation of MRI is its inability to detect certain cellular features, such as calcifications and artifacts created by patient movement during imaging.[96]

MRI has been employed in cell imaging to track magnetically labelled mesenchymal stem cells (MSCs), offering non-invasive monitoring of their distribution and migration within the body. For example, in a study by Sun *et al.,*[97] MRI was used to track magnetically labelled MSCs in rat kidneys with acute renal failure. Histological analyses showed that most of the labelled MSCs that tested positive for Prussian blue staining were in glomerular capillaries, corresponding to the areas where a loss in signal intensity was observed in the MRI. This demonstrates the potential of MRI in tracking labelled cells within specific anatomical locations. Furthermore, MRI has been instrumental in tracking bacteria through *in vivo* magnetic resonance imaging. Hoerr *et al.,*[98] established an *in vitro* cell labelling strategy that

can be transferred to other bacterial species, providing a conceptual advance in molecular MRI. This example highlights the versatility of MRI in visualizing cellular and molecular events within the body, extending its applications beyond traditional anatomical imaging.

Despite its advantages, MRI presents certain limitations in cell imaging. Its inability to detect certain cellular features, such as calcifications and artefacts created by patient movement during imaging, poses challenges in achieving precise cell imaging with MRI.[96] Additionally, the cost and availability of MRI equipment may limit its widespread use in specific settings, particularly in resource-constrained environments.

MRI boasts a superior spatial resolution to many other imaging modalities and unparalleled soft tissue differentiation, but it is disadvantaged by suboptimal sensitivity. To overcome this, superparamagnetic iron oxide (SPIO) nanoparticles have gained prominence in cell labelling for *in vivo* tracing, with numerous applications reaching the clinical trial phase.[99]–[107] A notable alternative development in this field is the advent of ^{19}F MRI, utilizing perfluorocarbon (PFC) as a novel mechanism for cell tracking. This technology distinctively identifies the ^{19}F nuclei within labelled T cells, yielding augmented specificity and quantification.[108],[109]

1.5.4 Nuclear medicine imaging

Nuclear medicine imaging uses small amounts of radioactive substances (radiotracers or radionuclides) to diagnose medical conditions. These radiopharmaceuticals are administered through injection, ingestion, or inhalation and accumulate in specific body areas for examination, such as malignant tumours or inflamed regions.[110],[111] The radiopharmaceuticals adhere to specific proteins within the body and emit gamma rays (or positrons which generate gamma rays) that gamma cameras or positron emission tomography

(PET) scanners can detect. Nuclear medicine imaging encompasses two essential techniques: SPECT and PET. SPECT uses gamma rays released by radiopharmaceuticals to generate three-dimensional images depicting the distribution of radioactive tracers throughout the patient's body. At the same time, PET employs positron-emitting radiopharmaceuticals to generate three dimensional images. Both methods enable the assessment of metabolic activity and physiological processes within the body.[110],[111]

Nuclear medicine imaging provides a crucial understanding of molecular processes in organs and tissues by capturing data on the dispersion and functioning of radiopharmaceuticals in the patient's body. This approach offers a distinct advantage over traditional imaging methods such as X-rays, CT scans, and MRI by delivering essential metabolic and functional information. Unlike standard imaging techniques focusing on anatomical specifics, nuclear medicine explores organ and tissue functionality, particularly important for early disease detection and informed therapeutic decision-making across various medical conditions.[111],[112]

SPECT and PET have transformed nuclear medicine by visualizing organ and tissue functionality through tracer accumulation driven by molecular processes, improving understanding of disease processes and guiding therapeutic interventions. These techniques diagnose and manage cardiovascular diseases, neurodegenerative diseases, infectious conditions, oncology, and endocrine disorders. Recent radiotracer developments for SPECT and PET have broadened applications to detect deep-seated infections and serve as biomarkers for brain metastases.[113],[114] Moreover, nuclear medicine imaging plays a crucial role in diagnosing and managing neurodegenerative diseases, as demonstrated by Tiepolt's comprehensive overview of the currently available radiotracers for imaging neurodegenerative diseases in research and routine clinical settings.[115] The advancement of new radiopharmaceuticals and improved imaging methods has broadened the use of nuclear

medicine imaging, particularly in oncology. It has been applied for diagnosing and monitoring different types of cancer, such as prostate cancer, leiomyosarcoma, and medullary thyroid carcinoma.[116]–[118] Additionally, combining SPECT/CT and PET/CT has significantly improved the accuracy of diagnosis and clinical usefulness of nuclear medicine imaging by precisely identifying and describing lesions across different anatomical areas.[119],[120]

Since the 1970s, radionuclide cell tracking has been used to detect sites of infection and inflammation through techniques such as gamma scintigraphy and SPECT using autologous leukocytes labelled with gamma-emitting radionuclides like ^{111}In and ^{99m}Tc.[29],[121] Additionally, radiolabelling of erythrocytes (RBCs) with ^{99m}Tc has been utilised for many years for cardiovascular imaging, blood-pool imaging, splenic function [78],[122], and gastrointestinal bleeding imaging.[123] Blood-cell radiolabelling is commonly performed in clinical nuclear medicine.[123],[124] However, the need for enhanced detection of small lesions and low numbers of cells and more precise quantification has led to increased interest in using PET for cell tracking. To gain a deeper understanding of the migration and homing, as well as the overall behaviour of cells after injection or transplantation, it is essential to find the most advanced methods for tracking cells *in vivo* over time.[29],[53] While conventional techniques for labelling cells have been successful in specific applications, detecting small lesions and small numbers of cells beyond the limits of gamma camera imaging using ^{111}In continues to be challenging. This has sparked interest in developing positron-emitting radiolabels for cells that can take advantage of the improved sensitivity, quantification, and resolution offered by PET compared to scintigraphy and SPECT. Several positron-emitting radionuclides and radiotracers have been evaluated for this purpose, including ^{68}Ga, ^{18}F, ^{64}Cu, and ^{89}Zr.[29],[53],[125]

1.5.4.1 Single Photon Emission Computed Tomography (SPECT)

The use of radioactive tracers in medicine has sparked interest in visualizing their precise distribution and measuring their 3-D uptake within the body. As a result, emission tomography was explored early on in the development of nuclear medicine and remains a significant theme for technological advancement. Single Photon Emission Computed Tomography has undergone extensive development since its initial demonstration by Kuhl and Edwards in 1963.[126],[127] SPECT is an imaging technique that relies on detected gamma rays from gamma-emitting radioisotopes, developed from planar imaging (2D), using multiple gamma camera angles to reconstruct a 3D view.[128] The SPECT principle involves the detection of gamma rays which are directly emitted from SPECT radio-isotopes. Each SPECT isotope has its own specific gamma emission energy range, which allows a SPECT scanner to distinguish between co-injected isotopes. This is in contrast to PET scanning, which relies on isotopes with different decay characteristics and detects only 511 KeV gamma rays. Imaging is conducted using a gamma detector, which produces a set of two-dimensional projection images detected from different angles. In general, one, two, or three detectors are slowly rotated around the patient's body to acquire the data necessary to reconstruct 3-D images. Collimators, typically made of lead or tungsten, play a vital role in this process since they collect only the photons incident perpendicular to the detector crystal, thereby preventing off-angle emission from degrading the quality of the image. Consequently, SPECT is less sensitive than PET because the collimator rejects many diagonally emitted photons, Figure 1-4. Despite this limitation, recent technological advances, such as micro-pinhole apertures, have improved the sensitivity, field of view, and spatial resolution of SPECT images.[33],[53],[54],[129]

The rotating gamma camera has historically dominated clinical utility, but there have been significant technological advancements in organ-specific dedicated SPECT systems. The

introduction of a hybrid SPECT/CT imaging modality has allowed for more accurate localization in 3D space and provided valuable information about localized function in internal organs. Although the development and acceptance of SPECT/CT have been relatively slow, combining the functional imaging from SPECT with the anatomic imaging from CT has become increasingly popular due to its facilitation of optimal clinical utility. This combination utilizes a specific algorithm to reconstruct projections and produce spatial images of administered radioisotope distributions.[126],[128] SPECT offers the advantage of allowing the detection of photons of different energies at the same time, which enables the simultaneous imaging of multiple radioisotopes. It is, therefore, possible to track several different cell populations that have been labelled with different radioisotopes simultaneously.[130]
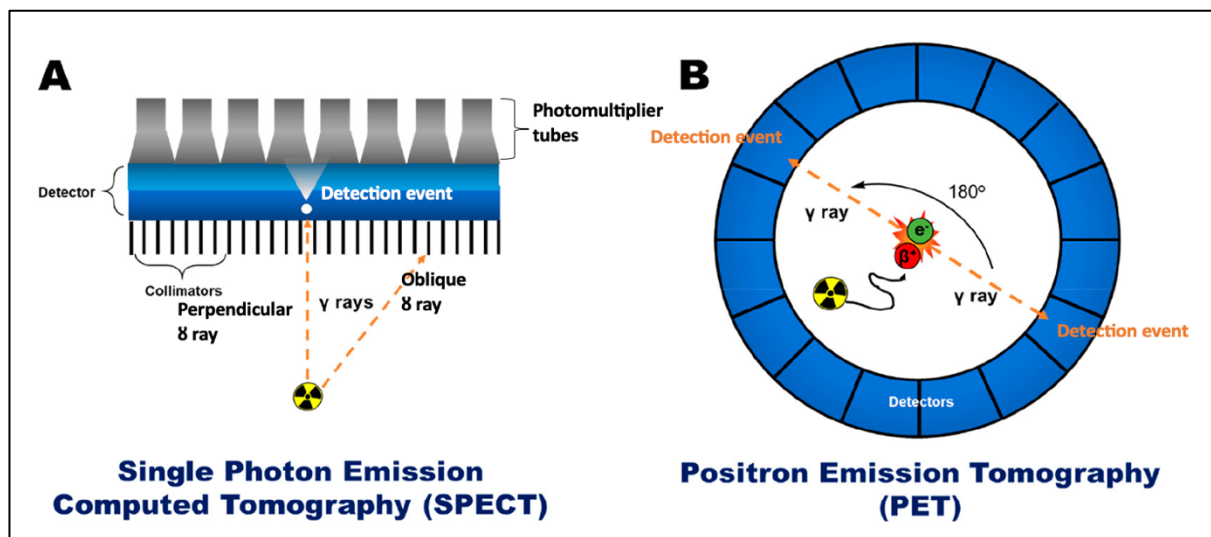
Figure 1-4: A schematic comparison between two imaging modalities, (A) SPECT and (B) PET. The SPECT technique utilises a gamma camera that generates a planar projection by rotating around the subject, resulting in a three-dimensional tomographic reconstruction. In contrast, the PET scanner employs a ring detector capable of simultaneously detecting emissions for a full 360º arc around the sample. SPECT isotopes emit a single gamma photon per disintegration meaning that collimation is required to reduce image blurring by ensuring that only perpendicular gamma rays reach the detector. Oblique gamma rays are blocked by the collimator. This process coupled with the rotating flat panel detector design of a SPECT scanner greatly reduce the sensitivity of the scanner. Meanwhile PET isotopes emit positrons which upon annihilation with an electron generate 2 gamma photons travelling in directly opposite directions. By pairing coincident gamma ray detections on opposite sides of the PET ring detector PET scanners are able to accurately localise annihilation events without the need for collimation. This detection method coupled with 360º ring detector give PET scanners a greatly improved sensitivity over SPECT cameras. This figure was copied from [29].

1.5.4.2 Positron Emission Tomography (PET)

Positron Emission Tomography (PET) has evolved significantly since its inception, with each development marking a new chapter in the imaging modality's history, Table 1-1. The journey began in 1932 when Carl David Anderson's discovery of the positron garnered him the Nobel Prize in Physics in 1936.[131] Progressing through the timeline, in 1934, Ernest Lawrence conceived and constructed the first cyclotron. Lawrence's work on the cyclotron was a significant achievement in physics, leading to his Nobel Prize in Physics in 1939.[132] In 1951, Sweet's innovation of a primary brain probe utilizing positrons at Massachusetts General Hospital (MGH) initiated the clinical application of this technology.[133],[134] By 1962, Brownell developed the earliest form of a multiple-detector PET scanner for clinical imaging at MGH.[132] The first commercial PET/CT system was developed in 2003, combining PET and CT modalities for enhanced anatomical and functional imaging.[132],[135],[136] Furthermore, in 2010, novel PET radiopharmaceuticals were introduced.[132] Further, in 2019, developments in total body PET scanner technology are expected to result in an increase in sensitivity by up to 40-fold for the whole body and by up to 4-5-fold for a single organ, thereby enhancing PET's sensitivity and clinical utility, providing a promising and highly sensitive means of imaging labelled cells.[137]

PET imaging is a widely used, non-invasive, and extremely sensitive modality in research and clinical settings. It has found extensive application in both clinical and preclinical research, offering valuable insights into disease mechanisms and the development of innovative treatment strategies. By using a radiotracer such as ^{18}F-FDG, typically administered intravenously (i.v.), PET can detect diseases, characterize their stage and progression, and assess the response to therapeutic intervention. When combined with high-resolution anatomical imaging methods like CT or MRI, PET can pinpoint the signal's source.[138]

The PET imaging process employs positron-emitting radionuclides. These radionuclides undergo decay, emitting positrons, which are the antimatter counterparts of electrons. In the case of ^{89}Zr, positron decay would look like the following: **^{89}Zr = Y + β$^+$ + v**. The energy released in the decay is divided between the positron and neutrino (and the residual energy of the daughter), which means that the positron energy is not monoenergetic but emits in a range of energies. The neutrino is always ejected simultaneously with the positron but is not detected. For radionuclides used in PET, the range of the positron in tissue is in the order of 1-10 mm.[139] The energy of the emitted positrons can vary depending on the parent nucleus. For instance, the most commonly used tracer, ^{18}F, has an average and maximum positron emission energy of 300 KeV and 600 KeV, respectively. On the other hand, ^{82}Rb has an average and maximum energy of 1500 KeV and 3350 KeV, respectively. The emitted positron travels a finite distance within a tissue medium before undergoing annihilation. This distance is defined as the positron range, which varies with positron energy and is isotope-specific, e.g. 0.6 mm for ^{18}F, 1.2 mm for ^{89}Zr, and 2.9 mm for ^{68}Ga.[140]

When a positron is emitted, it quickly loses its kinetic energy as it travels through tissue. The positron then collides with an electron, resulting in annihilation. This process converts their rest masses into two photons of 511 keV, following Einstein's law ($E=mc^2$). The PET camera's ring of detectors detects these photons, which can be used to locate the origin of the annihilation event along a line of response (LOR). A PET reconstruction algorithm generates three-dimensional images showing the tracer distribution throughout the patient's body.[141] The process of generating images acquired by PET involves several steps. Initially, a positron-emitting radionuclide is administered to the subject. The radionuclide travels through the body and accumulates in specific tissues or organs. The radionuclide decays and emits positrons, which annihilate with electrons to produce gamma photons. These photons are detected by the PET scanner, which uses this information to calculate the LORs. The LORs are then used to

reconstruct an image of the radionuclide's distribution within the body. By calculating all LORs, the place where the annihilation occurred can be reconstructed.[142] This is basically the principle of coincidence systems. Notice that this location does not refer to the location where the positron decay took place, but rather to the line along which the decay occurred.

Image reconstruction in PET is a complex process that can be performed using various algorithms. The raw data from the PET scan is typically stored in list mode format and can be converted into 2D sinograms using single slice rebinning (SSRB), multi-slice rebinning (MSRB), or Fourier rebinning (FORE). These sinograms are then reconstructed using algorithms such as filtered-back projection (FBP), 2D ordered-subsets expectation-maximization (OSEM), or 3D algorithms like 3D-OSEM or 3D maximum a posteriori (MAP). The choice of algorithm affects the image quality, with 3D algorithms generally providing better spatial resolution and recovery rates.[144],[145]

The sensitivity of a PET scanner is defined as the percentage between emitted and measured annihilation photons. It is influenced by several factors, including the detector material, the dead space or packing fraction, the crystal length, and the solid-angle coverage of the detector ring. Scanners with longer axial fields of view (FOVs) and smaller bore diameters usually exhibit the highest sensitivity. The spatial resolution of a PET scanner is defined as the distance at which two infinitely small point sources can still be distinguished from each other. This is influenced by factors such as the size and arrangement of the detector elements, the type of scintillator material used, and the method used to reconstruct the image. Typical preclinical PET scanners exhibit a spatial resolution in the order of 1.5 - 2.5 mm, measured at full width at half maximum (FWHM) of the point spread function in the central field of view (cFOV).[146]

Two factors influence the image resolution in a PET scan. The first factor is the size and type of detectors used, while the second is the energy of the positron used. As the positron's energy increases, the distance it travels before it annihilates increases, resulting in reduced image resolution. Several technological advances have been made in PET cameras, including digital cameras, time-of-flight PET cameras, and total body PET cameras, which are improving the field. There is an essential reason for this since the radiation dose from 37 MBq of ^{89}Zr-labelled antibody is estimated to be around 20 mSv, which may be a limitation when it comes to clinical use.[141]

Year	Key events in the development of PET
1932	Carl David Anderson discovered the positron, leading to the Nobel Prize in Physics in 1936.
1934	Ernest Lawrence conceived and constructed the first cyclotron. Lawrence's work on the cyclotron was a significant achievement in physics and led to his Nobel Prize in Physics in 1939.
1951	Sweet developed a primary brain probe at Massachusetts General Hospital, marking the first use of positrons in medical applications.
1962	Brownell developed the early form of a multiple-detector PET scanner for clinical imaging at MGH.
1974 – 1976	Ido prepared the first FDG.
1976	Abass Alavi and his team at the University of Pennsylvania administer FDG to human volunteers for the first time.
1976 - 1980	Synthesis of FDG, expanding PET's application in medical diagnostics.
1977	Sokoloff and his team developed the autoradiographic method to measure regional cerebral glucose metabolism, foundational for FDG PET imaging.
1977 - 1978	The introduction of Bismuth Germanate (BGO) as PET scanner detector material improves sensitivity and resolution.
1979	Phelps demonstrate the tracer kinetic model of FDG.
1984 - 1985	Introduction of the Block Detector, innovating PET detectors and improving scan efficiency.
1984 - 1986	Development of the first mini-cyclotron and automated chemistry, revolutionizing PET molecular preproduction.
1985 - 1990	Development of the match/mismatch principle for cardiac viability, advancing cardiac PET imaging.
1987 - 1990	Siemens and GE entered the PET market, beginning PET as a clinical service.
1990 – 1991	Formation of the Institute for Clinical PET and introduction of whole-body PET imaging for oncology.
1997 - 1998	FDA Reform Bill and HCFA reimbursement for PET in lung cancer and cardiovascular disease, a significant breakthrough in clinical PET applications.
1998	The prototype of the first integrated PET/CT scanner was produced by David Townsend and colleagues at the University of Pittsburgh.
2001	The introduction of Time-of-Flight (TOF) PET, a major technical innovation in PET imaging, offers improved spatial resolution.
2001	Development of the first commercial PET/CT system, combining PET and CT modalities for enhanced anatomical and functional imaging.
2008	Introduction of digital silicon photomultiplier technology in PET scanners, improving timing resolution and overall PET performance.
2010	Advancements in PET radiopharmaceuticals, including novel tracers for various diseases and conditions, contribute to the expanding clinical applications of PET.
2015	Emergence of total-body PET scanners, allowing simultaneous whole-body imaging and providing a comprehensive view of physiological processes.
2019	Construction of the world's first total-body PET/CT scanner, enhancing effective sensitivity by about 40 times for total-body imaging and 4-5 times for single organs.

Table 1-1: Key events in the development of PET. Adapted from [132],[134]–[136],[147].

1.5.5 Multimodality imaging

Each of the primary imaging modalities has its own set of benefits and drawbacks as summarised in Table 1-2. Therefore, the current trend in medical imaging is to integrate technologies to produce 'multimodal' or 'hybrid' imaging techniques to increase diagnostic performance and compensate for the deficiencies of individual imaging systems while exploiting their strengths.[148]

PET and X-ray computed tomography (PET/CT) are the most famous examples of multimodal imaging systems. The merging of PET and CT was deemed such a milestone in medical imaging that only one of the leading manufacturers of medical imaging systems produces stand-alone PET scanners.[149] Soon after the introduction of PET/CT scanners, SPECT/CT machines entered the market. The birth of these integrated imaging systems was prompted by one of the fundamental limitations of nuclear imaging: the modality lacks an anatomical reference frame, which can present challenges in accurately interpreting collected pictures.[150] Since PET and SPECT can only offer information on the location of molecules, CT is now commonly employed to add anatomical context.[151]

Researchers in the medical imaging community have been inspired by the success of PET/CT and SPECT/CT to test out other combinations of imaging modalities, such as US and MRI.[151] Although not as common as CT, PET or SPECT combined with MRI is frequently utilised therapeutically. This is because while anatomical guiding is MRI's primary usage, the technology's other prospective applications—like the quantification of magnetic/polarized molecules *in vivo* are also significant. These applications may be leveraged to create multimodality probes for PET/MRI that can image many metabolic processes simultaneously or consecutively *in vivo* depending upon scanner design.[148]

The complementary nature of these two imaging modalities has prompted the construction of prototype PET/MRI scanners. While PET's temporal resolution and quantification are excellent, and the information it delivers is driven by molecular processes, the technology's spatial resolution is lacking. Similarly, MRI's excellent spatial resolution gives information at the anatomical level, but the technique's poor temporal resolution limits its usefulness.[148] The integration of PET and MRI will result in high sensitivity, quantifiability, spatial resolution, and temporal resolution. Utilising PET and MRI together for cell tracking might provide information on the intra-organ distributions of cells utilising PET to picture and quantify the biodistributions of delivered cells throughout the body. Hybrid imaging probes that can provide signal and contrast in both PET and MRI are being developed at the same time as innovative PET/MRI systems.[152]

1.5.6 Key strengths and limitations of PET and SPECT over anatomical techniques such as classical CT and MRI

PET and SPECT are two fundamental nuclear imaging modalities that play a pivotal role in studying molecular and biochemical processes within living organisms. PET functions on the principle of detecting high-energy gamma photons resulting from the annihilation of emitted positrons with electrons, a unique process specific to PET isotopes such as ^{18}F and ^{89}Zr. The interaction creates two gamma photons moving at 180-degree angles from each other, which is captured by the PET camera. One key advantage of PET imaging lies in its exceptional precision and sensitivity in detecting gamma rays through coincidence detection, where two sections of the detector register the emitted photons during isotope disintegration and positron annihilation.[155] This mechanism enables accurate spatial localization of radiopharmaceuticals, allowing for the production of high-resolution images with typically 5 – 7 mm spatial resolution in clinical settings.[156]

Both PET and SPECT imaging modalities exhibit extensive depth penetration, allowing for thorough examination of biological processes and comprehensive visualization of cellular distributions in whole-body scans. The temporal resolution of both systems, ranging from seconds to minutes, facilitates dynamic tracking of cellular events post-administration. Notably, PET boasts a higher sensitivity, detecting tracer concentrations in the range of 10^{-11}-10^{-12} M, surpassing SPECT's sensitivity of 10^{-10}-10^{-11} M.[157] This difference in sensitivity underscores PET's advantage in applications such as cell tracking, where quantifying the proportion of cells reaching a target organ is crucial. Despite PET's superior spatial resolution and quantitative capabilities, SPECT has the advantages of being more widely accessible and less costly, which can be a determining factor in its preference for certain clinical and research applications.[149],[154],[157],[158]

PET and SPECT offer distinct advantages over anatomical imaging techniques like CT and MRI, primarily due to their ability to detect biochemical alterations preceding anatomical changes, often the harbingers of disease.[149],[154],[158] This early detection capability is a cornerstone of their diagnostic superiority. Nonetheless, the spatial resolution of PET and SPECT is suboptimal—ranging from 1 to 2 mm in preclinical settings—making detailed organ imaging and visualization of intra-organ cell distribution a challenge.[157] To compensate for this and the absence of an anatomical reference frame, multimodality imaging that combines PET or SPECT with CT or MRI has emerged, synergizing molecular with anatomical imaging to enhance diagnostic precision.[157]

Safety profiles also delineate the limitations of these modalities, as they involve ionizing radiation, with PET and SPECT scans subject to annual exposure limits of 5 mSv for the public and up to 50 mSv for radiation workers. This underscores the need for judicious use in clinical studies. While PET's high sensitivity and quantitative capabilities are key strengths, its spatial resolution is inferior to that of MRI.[157] Conversely, SPECT's cost-effectiveness and accessibility contrast with its lower sensitivity and coarser spatial resolution, which is inferior to clinical PET.[149],[154],[157],[158]

Both PET and SPECT, requiring minimal amounts of the imaging agent, mitigate concerns about chemical toxicity and pharmacological effects. Their high sensitivity and unlimited penetration depth permit the comprehensive investigation of many biological processes and disease states in living subjects. Despite the differences, both imaging techniques continue to provide invaluable insights in clinical and research contexts.[149],[154],[157],[158] The combined advantages of PET imaging make it a powerful, tool for spatial and longitudinal tracking of different (therapeutic) cell types offering superior sensitivity for cell tracking compared to other imaging modalities.[33],[159] Thus providing the most promising pathway towards cell tracking *in vivo* and at the whole-body level, making it particularly amenable to clinical translation.[157],[160]

Modality	MRI	MPI	US	FI	BLI	PET	SPECT
Main clinical applications	Structural imaging	Tracer imaging	Structural imaging	Not Specified	Not Specified	Tracer imaging	Tracer imaging
Form of energy used	Radiofrequency waves	Radiofrequency waves	High-frequency sound waves	Visible to infrared light	Visible to infrared light	Gamma rays from Annihilation of positrons	Gamma rays
Contrast agents/tracers	Gadolinium, iron oxide particles	Iron oxide particles	Microbubbles	Not Specified	Not Specified	Radioactive tracers	Radioactive tracers
Spatial Resolution (mm)	0.01 - 0.1 (small-animal MRI); 0.5 - 1.5 (clinical MRI)	1 mm	0.04 - 0.1 (small-animal US); 0.1 - 1 (clinical US)	< 1 (FRI); 1 (FMT)	3 - 5	1 - 2 (microPET); 6 - 10 (clinical PET)	0.5 - 2 (microSPECT); 7 - 15 (clinical SPECT)
Temporal resolution	Seconds to hours	< 1 second to minutes	< 1 second	Not Specified	Not Specified	Minutes	Minutes
Sensitivity	Low (mM-μM)	High	Low (~ μM)	High	High	High (fM)	High (pM-fM)
Required molecular probe Mass (ng)	$10^3 - 10^6$	~30 ng	$10^3 - 10^6$	$10^3 - 10^6$	$10^3 - 10^6$	1 - 100	1 - 100
Patient risk	Heating and peripheral nerve stimulation	Heating and peripheral nerve stimulation	Heating and cavitation	Not Specified	Not Specified	Radiation	Radiation
Cost	High	Medium	Low	Low (FRI); Medium-High (FMT)	Low	High	Medium
Advantages	High spatial resolution; superb soft tissue discrimination	Not Specified	High sensitivity; portable	High sensitivity; multiplexed imaging	High sensitivity; high throughput	High sensitivity; quantitative; tracer amount of probe	High sensitivity; quantitative; tracer amount of probe

Table 1-2: Comparison of common clinical imaging modalities used for cell imaging. Adapted from [161],[162].

Types of cells	Labelling strategy	Imaging modality	Tracer	Subject	Duration	Purpose	Clinical translation	Reference
DC	Direct	FLI	NIR-QD	Mouse	3 days	Tracking study	Limited	[75]
		PET	^{18}F-SFB	Mouse	4 h	Tracking study	Yes	[163]
		SPECT	^{111}In	Human	24 – 48 h	Tracking study	Yes	[164]
		SPECT	^{111}In /^{99m}Tc-HMPAO	Human	48 – 72 h	Tracking study	Yes	[163]
	Indirect	BLI	Fluc	Mouse	4 days	Tracking study	Limited	[165]
		PET	NIS/^{124}I	Mouse	4 days	Tracking study	Yes	[165]
		MRI	FTH	Mouse	48 h	Tracking study	Yes	[166]
Macrophage	Direct	FLI	NIR nanoparticles	Mouse	3 – 24 h	Tracking to inflammation	Limited	[167]
		MRI	SPIO	Mouse	24 h	Tracking to inflammation	Yes	[168]
		MRI	Magnetic nanoparticles	Mouse	3 – 24 h	Tracking to inflammation	Yes	[167]
		MRI	SPIO	Mouse	6 - 13 days	Tracking rheumatoid arthritis	Yes	[169]
	Indirect	BLI	Fluc	Mouse	0 - 21 days	Tracking to inflammation	Limited	[170]
		PET	NIS/^{124}I	Mouse	7 days	Tracking to inflammation	Yes	[171]

Types of cells	Labelling strategy	Imaging modality	Tracer	Subject	Duration	Purpose	Clinical translation	Reference
Macrophage	Indirect	PET	NIS/^{124}I	Mouse	8 - 21 days	Tracking to inflammation	Yes	[170]
		PET/CT	^{18}F-FB	Mouse	3 h	Tracking lung carcinoma	Yes	[172]
T cells	Direct	MRI	IOPC-NH^2	Rat	24 – 48 h	Tracking study	Yes	[168]
		MRI	PPEP/^{19}F	Mouse	48 h	Tracking study	Yes	[173]
	Indirect	BLI	Fluc	Mouse	24 h	Tracking study	Limited	[174]
		PET/CT	sr39tk/^{18}F-FHBG	Mouse	1 - 21 days	Melanoma tumour targeting	Yes	[175]
B cells	Direct	FLI	NIR nanoparticles	Mouse	1 - 15 days	Tracking study	Limited	[176]
		PET/CT	^{89}Zr-anti-B220	Mouse	15 – 72 h	Biodistribution	Yes	[177]
	Indirect	MRI	SPIO	Mouse	1 - 15 days	Tracking study	Yes	[177]
NK	Direct	FLI	NIR dye	Rat	24 h	Tracking study	Limited	[178]
		PET	^{11}C	Mouse	0.5 – 1 h	Tracking study	Yes	[179]
		SPECT	^{111}In	Human	0.5 – 144 h	Tracking and therapy study	Yes	[180]
		SPECT	^{111}In	Human	6 – 96 h	Tracking study	Yes	[180]

Table 1-3: Comparative overview of labelling strategies and imaging modalities for cell tracking in preclinical and clinical studies. This table was adapted from [54] and further added to from various sources and literature.   Abbreviations that were not used in the text before; NIR: near infrared, QD: quantum dot, SFB: fluorobenzoate, NIS: sodium iodide symporter, HMPAO: hexamethylpropyleneamineoxime, SPIO: superparamagnetic iron oxide, Fluc: firefly luciferase, FB: fluorobenzene, IOPC: iron oxide nanoparticles coated, PFPE: perfluoropolyethers, sr39tk: mutant type of HSV-thymidine kinase, and FHBG: fluorohydroxymethyl butyl guanine.

1.5.7 Radioisotopes for SPECT imaging and SPECT Clinical applications

SPECT imaging, a vital tool in clinical settings, particularly in cardiology, neurology, and oncology, utilizes a spectrum of radioisotopes for diagnostic purposes (see Table 1-4). These isotopes include metallic elements like ^{111}In and ^{99m}Tc, as well as non-metallic elements like ^{123}I and ^{125}I, which are tagged to different biological targets (cells, antibodies, small molecules) and offer varying half-lives suitable for tracking biological processes from several hours to days. The primary radioisotopes employed in SPECT, such as ^{99m}Tc and ^{111}In, are chosen for their optimal half-lives and energy characteristics.

^{99m}Tc, notably versatile, is used in various radiopharmaceuticals such as ^{99m}Tc-DTPA and ^{99m}Tc-MAG3 for renal function assessments; ^{99m}Tc-MDP for bone scans; ^{99m}Tc-MAA for lung perfusion studies; and ^{99m}Tc-ECD for cerebral imaging. Its properties include emitting 142 keV gamma rays with a 6.02-hour half-life, allowing adequate time for radiolabelling procedures and compatibility with nuclear medicine imaging systems. This isotope is derived from a ^{99}Mo/^{99m}Tc generator, with compounds to be labelled typically available as lyophilised kits in hospital radiopharmacy, facilitating the formulation of ^{99m}Tc compounds.[29],[121]

On the other hand, ^{111}In, with a longer half-life of 2.8 days, is advantageous for antibody labelling in SPECT imaging, making it suitable for monitoring molecular processes over extended periods. It has been pivotal in studying cell trafficking, particularly in imaging the migration of white blood cells for detecting infection and inflammation and has been used for over three decades in nuclear medicine for labelling autologous leukocytes.[29],[121]

In routine clinical applications, SPECT/CT employs isotopes like ^{201}Th and ^{99m}Tc-labelled sestamibi in cardiology for evaluating myocardial blood flow [181],[182], ^{111}In-capromab pendetide in oncology for identifying metastatic disease sites from prostate cancer [183], and

[188]Re-HEDP for treating painful bone metastases [184]. SPECT's clinical applications have extended over three decades, notably in mapping the distribution of autologously labelled leucocytes within inflammatory regions, generally using ^{111}In-oxine or ^{99m}Tc-HMPAO as labelling agents prior to patient injection.[29],[121] While the application of direct cell labelling in SPECT imaging is well-established in diagnostic contexts, its clinical use in cell therapies has been limited. This hesitancy largely stems from concerns about cytotoxicity, which could impede long-term cell viability or alter the therapeutic phenotype. In SPECT, these concerns are amplified due to the high levels of radioactivity required for sufficient signal generation. It has been demonstrated that significant, time-dependent toxicity has been observed *in vitro* in mesenchymal stem cells (MSCs) [185], hematopoietic progenitor cells (HPCs) [186], and lymphocytes [187], all of which have been labelled with Indium-111 (^{111}In). However, clinical applications are evident despite these challenges. In addition, ^{111}In-oxine with Technetium-99m Hexamethylpropyleneamine Oxime (^{99m}Tc-HMPAO) were used as a tracking agents in cancer therapy for primed dendritic cells.[188] In cirrhosis, MSCs were labelled with ^{111}In-oxine and tracked for up to 10 days after injection [189] and ^{99m}Tc-labelled bone marrow mononuclear cells were monitored for 24 hours in stroke patients [190]. There is a trade-off involved in selecting SPECT isotopes with longer half-lives, such as ^{111}In, with a half-life of 68 hours, as opposed to ^{99m}Tc, with a half-life of 6 hours. Although it provides extended cell tracking, it also poses the risk of increased radioactive exposure and potential toxicity. The advancement of reporter genes for SPECT and direct labelling has provided the potential for extended cell tracking. This approach has not yet been validated in patient studies using SPECT.[53] SPECT has thus become a staple in modern nuclear medicine, providing invaluable insights into physiological processes and aiding in detection, diagnosis, and management of various diseases.[29],[121]

While SPECT was not used in the present work, it has significantly impacted routine clinical nuclear medicine imaging and warrants mention in this thesis.

radionuclide	half-life	max. energy (keV)	decay	production	common production reaction
^{198}Au	2.7 d	960	β^-, γ	cyclotron	^{197}Au(n,γ)^{198}Au
^{199}Au	3.1 d	452.6	β^-, γ	cyclotron	^{198}Au(n,γ)^{199}Au
^{67}Ga	78.3 h	300	Auger e$^-$, γ	cyclotron	^{68}Zn(p,2n)^{67}Ga
^{111}In	2.81 d	245	Auger e$^-$, γ	cyclotron	^{111}Cd(p,n)^{111}In
^{123}I	13.3 h	159	Auger e$^-$, γ	cyclotron	^{127}I(p,5n)^{123}Xe
^{125}I	60.5 d	35	Auger e$^-$, γ	nuclear reactor	^{124}Xe(n,y)^{125}Xe $\rightarrow$ ^{125}I
^{131}I	8.0 d	610	β^-, γ	nuclear reactor	^{130}Te(n,γ)^{131}Te $\rightarrow$ ^{131}I
^{188}Re	16.9 h	155	β^-, γ	generator	^{188}W/^{188}Re
^{99m}Tc	6.0 h	140	γ	generator	^{99}Mo/^{99m}Tc

Table 1-4: **Properties of various radionuclides used for SPECT Imaging.** Copied from [29].

1.5.8 Radioisotopes for PET imaging and PET applications

The choice of radionuclide is of key importance as it affects image quality, quantification accuracy and radiation burden for patients and personnel. The selection of the PET radioisotope must consider its physical and chemical properties. The decay half-life, for instance, must be long enough for the chemical preparation process, synthesis, purification and analysis, and for a biological process to allow the accumulation at target organs and the clearance from the blood pool of the radiopharmaceutical. Another factor that should be examined is β^+ emission energy, which determines the distance that positrons travel before annihilating and influences the PET scan's resolution (see Table 1-5). The development of radiopharmaceuticals for rapid

biological processes is limited to short-lived PET isotopes. In contrast, long-lived isotopes have garnered attention in cell labelling and tracking and immune-PET imaging. Several positron-emitting radionuclides and radiotracers, such as ^{11}C, ^{18}F, ^{68}Ga, ^{64}Cu, and ^{89}Zr, have been evaluated for these purposes.[29]

radionuclide	half-life	max. energy (keV)	decay	production	common production reaction
^{15}O	2.1 min	1732	β^+	cyclotron	^{15}N(p,n)^{15}O
^{13}N	9.9 min	1199	β^+	cyclotron	^{16}O(p,α)^{13}N
^{11}C	20.4 min	961	β^+	cyclotron	^{14}N(p,α)^{11}C
^{68}Ga	67.6 min	1899	EC, β^+	generator	^{68}Ge/^{68}Ga
^{18}F	109.7 min	634	EC, β^+)	cyclotron	^{18}F(F$^-$): ^{18}O(p,n)^{18}F
^{62}Cu	9.7 min	2926	β^+	generator	^{62}Zn/^{62}Cu
^{64}Cu	12.7 h	656	EC, β^+, β^-	cyclotron	^{64}Ni(p,n)^{64}Cu
^{89}Zr	78.4 h	900	EC, β^+	cyclotron	^{89}Y(p,n)^{89}Zr
^{124}I	4.2 d	2100	EC, β^+	cyclotron	^{124}Te(p,n)^{124}I
^{52}Mn	5.6 d	1434	β^+	cyclotron	^{52}Cr(p,n)^{52}Mn

Table 1-5: Properties of a selection of radionuclides used for PET imaging. Copied from [29].

1.5.8.1 Fluorine-18 (^{18}F):

Fluorine-18 (^{18}F) is a PET isotope with a relatively short physical half-life of 110 minutes. Typically, ^{18}F is used as ^{18}F-fluorodeoxyglucose (^{18}F-FDG) in clinical applications. ^{18}F-FDG is an analogue of glucose, which can be taken up and incorporated by glucose-metabolizing cells, particularly tumour cells, similarly to glucose.[191] After initial phosphorylation, ^{18}F-FDG cannot be metabolized by enzymes past hexokinase in the glycolytic pathway. Therefore, it is trapped and has a slow clearance, which results in an accumulation of ^{18}F-FDG inside cells that PET scanners detect. While ^{18}F-FDG has been used to diagnose a variety of malignant

cells, including tumour staging, it is not specific for tumour cells. Several studies have demonstrated that infected and inflammatory cells also take up this tracer. ^{18}F-FDG was even found to accumulate in carotid plaques three hours after radiotracer injection.[192]

Several efforts have been conducted to label autologous leukocytes using ^{18}F-FDG; however, glucose has been previously found to affect the efficiency as well as stability of the process.[193] By incubating leukocytes directly with ^{18}F-FDG at 37 degrees Celsius for 20 minutes while using heparin as an anticoagulant Forstrom *et al.,* achieved near-optimal labelling efficiency of 78 %.[194] After incubation for 60 minutes, the cells were viable even though the radiolabel loss increased from 13 % at one hour to 26 % after four hours.[194] However, ^{18}F-FDG was inefficient at labelling leukocytes with efficiencies lower than those observed with ^{111}In-oxine.[195]–[197]

Prince and colleagues reported that the efflux rate of ^{18}F-FDG from labelled dendritic cells post-labelling exceeded 20 % per hour.[198] Autologous human bone marrow cells were labelled and imaged with ^{18}F-FDG during acute myocardial infarction.[199] The ^{18}F-FDG-labelled bone marrow cells (BMCs) and CD34-positive cells were found to have 92 to 96 % cell viability. After intracoronary infusion, this tracer was also able to detect infarcted myocardium.[199] So, this technique might help trace the homing of BMCs after myocardial infarction and tracking their distribution. When autologous T lymphocytes were labelled with ^{18}F-FDG, their labelling efficiency was similar to that of ^{111}In-oxine (64 % to 68 %) and was superior to ^{99m}Tc-HMPAO (31 %). Even though these tracers did not decrease cell viability, they reduced T lymphocyte cytotoxic properties as measured by ^{51}Cr released assay and decreased cell proliferation.[200] Researchers attempted to study the tracking of circulating progenitor cells (CPCs) in acute myocardial infarction by labelling human and pig CPCs with ^{18}F-FDG. They found that the labelling efficiency reached a maximum of 90 % after 30 minutes

of incubation at 37 °C. However, it was found that the tracer was significantly dissociated from the radiolabelled cells within two hours, to around 23 % to 28 %. PET/CT imaging of labelled cells in pig MI models successfully confirmed their delivery to the myocardium infarction.[201] The researchers also attempted to use phloretin, a glucose transport inhibitor, to prevent the washout of ^{18}F-FDG.

However, despite its effectiveness *in vitro* in preventing glucose release in red blood cells, it was unsuccessful *in vivo* when tested with neural stem cells (NSCs) in a tumour inflammation model.[202] The use of ^{18}F-FDG for labelling cells has certain drawbacks such as low labelling efficiency, stability, and short physical half-life of ^{18}F. This limits the ability to track labelled cell migration for prolonged periods.[191]

1.5.8.2 Gallium-68 (^{68}Ga):

Gallium-68 (^{68}Ga), a short-lived positron-emitting isotope with a half-life of 67.7 minutes, predominantly decays by positron emission (89 %) and electron capture (EC) (11 %). A key disadvantage is its high positron energy (mean β^+ energy 836.0 keV, maximum β^+ energy 1899.1 keV) which reduces its efficacy for medical applications.[203] In aqueous solutions, gallium exists in the Ga(III) form, maintaining its state in physiological conditions. Gallium, a hard acid according to the HSAB classification, prefers coordination with hard bases like O and N, often forming a six-coordinate octahedral geometry with chelating ligands. In pH ranges relevant for radiolabelling biomolecules (pH 3 - 7), gallium forms insoluble hydroxide (Ga(OH)$_3$). To prevent colloidal formation during the ^{68}Ga-labelling process, weak acids such as acetate, citrate, or oxalate are used.[204]–[206]

Initially, ^{68}Ga was used in nuclear medicine before ^{99m}Tc radiopharmaceuticals and 2-deoxy-2-[^{18}F]fluoro-D-glucose (2-[^{18}F]FDG) became clinical standards. However, the cumbersome handling of early ^{68}Ge/^{68}Ga generators led to its temporary side-lining in favour of ^{99m}Tc and ^{18}F.[207] Interest in ^{68}Ga resurged with more user-friendly generators, particularly with the development of chemistry for ^{68}Ga-labelled radiopharmaceuticals.[208] Today, ^{68}Ga is prominent in publications and clinical trials among positron-emitting radiometals.[209]

Since 1977, ^{68}Ga has been used in various studies, such as labelling erythrocytes and platelets with ^{68}Ga-oxine, showing high labelling efficiency in RBCs but inconsistent yields with platelets. Successful *in vivo* imaging of these labelled dog cells highlighted high blood pool organs and detected endothelial injury.[210] Further, lipophilic complexes like ^{68}Ga-tropolone and ^{68}Ga with 2-mercaptopyridine-N-oxide (MPO) were explored for platelet labelling, with ^{68}Ga-MPO showing reproducible labelling and viability for imaging aorta injury in rabbits.[211],[212] However, its short half-life (68 min) limits its application in sequential studies. Despite its promise, ^{68}Ga-MPO's short lifespan in circulation and rapid decay hindered its effectiveness in early-stage studies and in detecting pulmonary embolus lesions.[211]

1.8.5.3 Copper (^{64}Cu):

Copper (Cu) has several radioisotopes available, including ^{60}Cu, ^{61}Cu, ^{62}Cu, ^{64}Cu, and ^{67}Cu, which can label cells. Most of these isotopes are positron emitters produced using either a cyclotron (^{60}Cu, ^{61}Cu, ^{64}Cu) or a generator (^{62}Cu). Copper isotopes have shown promise in labelling peptides [213] and cells [197] with ^{64}Cu exhibiting particularly striking characteristics for studying cell migration. ^{64}Cu decays primarily through electron capture (41 %), positron emission (19 %) and beta (40 %) particles.[218] Due to its intermediate half-life of 12.7 hours, it can be used to label molecules with intermediate *in vivo* distributions. The low β^+ energy

^{64}Cu permits high spatial resolution imaging, and the emitted Auger electrons make it a potential radionuclide for therapeutic purposes.[219]

Lipophilic tracers such as bis(thiosemicarbazone) ligands (PTSM) [217], tropolonate [197], and PEG conjugates [217], ^{64}Cu can be labelled with cells. Copper is redox-active and chemically labile under physiological conditions, making it challenging to be chelated by pharmaceutical ligands and possibly leading to decomplexation *in vivo*. This property, however, has been successfully exploited by a widely studied complex known as the ^{64}Cu diacetyl-bis(N4-methylthiosemicarbazone) (ATSM) for imaging hypoxic tumours.[220]

1.8.5.4 Zirconium-89 (^{89}Zr)

In the 1950s and 1960s atomic testing period ^{93}Zr and ^{95}Zr emerged as major fission products. Several early zirconium radiochemistry studies were published in the National Academy of Sciences (NAS) report.[221] Zirconium is in Group IVB of the periodic table, and there are 38 known isotopes of zirconium, but only five exist naturally. In this regard, ^{96}Zr, ^{91}Zr, ^{92}Zr, ^{95}Zr, and ^{93}Zr represent the ratios of 2.80 %, 11.22 %, 17.15 %, 17.38 %, and 51.45 %, respectively. Only ^{89}Zr, however, is useful for PET imaging.[232] Early interests in fission/ fallout led to animal studies investigating the biological distribution of ^{93}Zr and ^{95}Zr. The toxicity and biodistribution of ^{95}Zr in rats or mice were studied. Through autoradiography, ^{89}Zr was shown to have a high affinity for bones and a low toxicity level in rats.[275] One of the earliest studies (probably the first one published) on the distribution of ^{89}Zr in the human body was performed in 1957. Mealey studied the dynamics of excretion of ^{89}Zr from the bloodstream and its distribution between plasma proteins. He reported the possibility of applying ^{89}Zr for the "external localization" of human brain tumours.[222]

It was not until the mid-2000s that there was renewed interest in using [89]Zr as a potential PET isotope for labelling monoclonal antibodies *in vivo* for cancer imaging.[223] Additionally, [89]Zr has been used for direct cell labelling [224] and nanoparticle and liposome labelling and tracking.[225],[226] While research is ongoing, [89]Zr is becoming an essential and promising radiometal for immuno-PET due to the long half-life (T$_{1/2}$: 78,4 h) which is well matched with long biological half-lives of large proteins and cells.[227]–[230] Another reason for the current interest in [89]Zr is that the nuclear decay characteristics of [89]Zr are suitable for the labelling of antibodies. Through both positron emission (22.7 %) and electron capture (76.6 %), [89]Zr decays into [89m]Y, which then decays into stable [89]Y via gamma-ray emission (909 keV) with a half-life of 15.7 seconds, Figure 1-5.[231] A relatively low positron energy of E$_{mean}$ = 396 KeV (E$_{max}$ = 902 KeV) and a positron mean range of 1.3 mm (a positron max range of 3.8 mm) enables images of high resolution.[232]
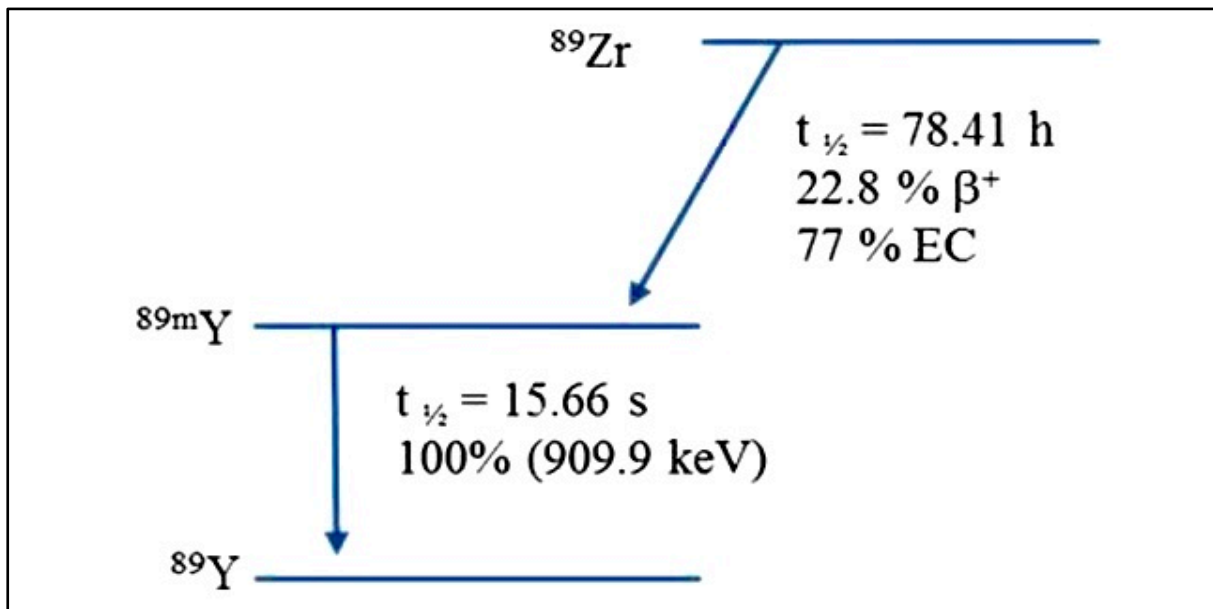
Figure 1-5: Decay scheme for [89]Zr. This figure was adapted from reference [231].

1.5.9 The cyclotron:

With the exception of ^{68}Ga and ^{62}Cu which are generator produced, all of the PET isotopes mentioned above are cyclotron produced. In a cyclotron, the radionuclide is obtained after the bombardment of a target material with high-energy protons or deuterons. In a generator, a parent radionuclide, the mother isotope, is loaded onto a stationary phase, and eluted regularly during decay to obtain a solution containing the daughter isotope. The cyclotron, a fundamental particle accelerator, plays a crucial role in the production of radionuclides for various applications, including medical imaging and cancer therapy. This sophisticated device is designed to accelerate charged particles, such as protons and deuterons, to high energies, enabling the bombardment of target materials to produce specific radioisotopes. The cyclotron has significantly contributed to the advancement of nuclear medicine, providing a reliable and efficient method for generating a diverse array of radioisotopes used in diagnostic and therapeutic procedures.[233]

The design of a cyclotron typically consists of two hollow semi-circular electrodes, known as dees, placed in a strong magnetic field. The dees are connected to an alternating current (AC) power supply, which creates an oscillating electric field within the cyclotron. The magnetic field causes the charged particles to move in a circular path, while the alternating electric field accelerates the particles as they cross the gap between the dees. This process allows the particles to gain energy with each revolution, ultimately reaching the desired energy level for radionuclide production.[234]

The mechanism of work of a cyclotron involves the use of electromagnetic fields to accelerate charged particles in a spiral path. The particles are injected into the centre of the cyclotron. They are subjected to a combination of electric and magnetic fields, causing them to spiral

outward and gain energy with each revolution. This process continues until the particles reach the desired energy level, at which point they are extracted and directed towards a target material. Upon collision with the target, the high-energy particles induce nuclear reactions, producing specific radionuclides.[234]

The role of the cyclotron in radionuclide production is paramount, as it enables the synthesis of specific radioisotopes essential for various medical procedures. The production of medical radioisotopes using cyclotrons has been a subject of extensive research and development, with numerous studies focusing on optimising production methods, target materials, and separation techniques. These efforts have successfully produced a wide range of radioisotopes, including those used in PET and targeted radionuclide therapy.[235]

Despite its numerous advantages, the cyclotron production of radionuclides also presents particular challenges and limitations. One of the critical challenges is the need for specialized infrastructure and expertise to operate and maintain cyclotron facilities. Additionally, producing specific radionuclides may require complex target materials and irradiation conditions, which can impact the efficiency and cost-effectiveness of the production process. Furthermore, the regulatory aspects associated with the production and distribution of cyclotron-produced radionuclides require stringent adherence to quality control and safety standards to ensure these radioisotopes' safe and effective use in clinical settings.[236]

In conclusion, the cyclotron is a critical component of nuclear medicine, enabling the synthesis of a diverse range of radioisotopes for medical imaging and therapeutic applications. The ongoing research and development in this field continue to enhance the capabilities of cyclotron facilities, producing high-quality radionuclides that are essential for advancing diagnostic and therapeutic procedures in nuclear medicine. While the cyclotron production of

radionuclides presents specific challenges, its significant contributions to nuclear medicine underscore its importance in providing essential radioisotopes for clinical applications.[237]

1.5.10 ^{89}Zr production

^{89}Zr is produced in a cyclotron by the proton bombardment of ^{89}Y; ^{89}Y(p,n)^{89}Zr [238],[239] or deuterium bombardment of ^{89}Y; ^{89}Y(d,2n)^{89}Zr.[240]-[242] The cyclotron target material for these reactions can be in different physical forms, such as solid, liquid or gas. Natural yttrium foils, which are used as solid target materials for both reactions of ^{89}Zr production, can be bombarded with protons or deuterons; such solid target materials can be in the form of a foil [243], pellet [243], sputtering [244] or deposition [245] of yttrium. Verel *et al.,* studied and explained the most common production procedure for ^{89}Zr in 2003. They produced the ^{89}Zr on ^{89}Y target in the form sputtered on copper, via bombardment with 14 MeV protons for 2 – 3 h.[227] ^{89}Zr can be produced with 99.9 % purity using ^{89}Y target material (which has a 100 % natural abundance) of between 5 and 1000 μm thickness employing the ^{89}Y(p,n)^{89}Zr reaction.[246],[247] Different studies mentioned the use of ^{89}Y foils with different thicknesses. Wooten *et al.* studied ^{89}Y foil of 0.25 mm thickness and bombarded it with 15 MeV protons. The process yields and products vary depending on the form of the target material.[248] Therefore, different research groups investigated new target materials or different yttrium foil features to provide high yields of ^{89}Zr production via the ^{89}Y(p,n)^{89}Zr process.[249],[250] Pandey *et al.,*[251] and De Grado et *al.,*[252] studied the different liquid targets for proton irradiation. The yield they found is lower when using liquid targets than solid targets for ^{89}Zr production.[251]–[253] ^{89}Y solid target material has some advantages, such as being non-reactive, low cost, and commercially available. In the ^{89}Y(p,n)^{89}Zr reaction, ^{89}Y is bombarded by 14 – 15 MeV protons, and this method is more common than the other ^{89}Y(d,2n)^{89}Zr reaction.[254]–[256] In the ^{89}Y(d,2n)^{89}Zr reaction, a 5.6 MeV beam energy is required for the

deuterium reaction. The ^{89}Y(d,2n)^{89}Zr is not the most common reaction for ^{89}Zr production due to the high deuteron energy requirement, even though this reaction provides a high yield.[228],[257]

The Zweit group utilized natural yttrium pellets to produce ^{89}Zr using the ^{89}Y(d,2n)^{89}Zr reaction: the starting material was irradiated with a 16 – 17 MeV optimum energy beam of deuterons and then purified in an ion-exchange column to obtain a 66.6 MBq/μAh yield of ^{89}Zr with a minor fraction of long-lived ^{88}Zr (0.008 %). Using a similar reaction, high-purity ^{89}Zr production was experimentally reported by Tang and co-workers and theoretically calculated by the Sadeghi group.[250],[258] Despite the higher yield of the ^{89}Y(d,2n)^{89}Zr reaction compared to the ^{89}Y(p,n)^{89}Zr reaction, application of the ^{89}Y(d,2n)^{89}Zr reaction in medical accelerators is still restricted. This is due to the fact that common small medical cyclotrons are not capable of producing the high-energy deuterons required for the ^{89}Y(d,2n)^{89}Zr reaction. Although several medical cyclotrons, such as the GE PETtrace 800 or IBA Cyclone 18/9, have two beam currents, the deuteron energy is insufficient to produce a high yield of ^{89}Zr. Hence, the ^{89}Y(p,n)^{89}Zr reaction is the more practical approach to producing ^{89}Zr in these kinds of machines.[231]

Link and co-workers carried out the first ^{89}Y(p,n)^{89}Zr reaction, who employed an ^{89}Y source on Y foil, which was irradiated with 13 MeV protons. After irradiation, the Y foil was dissolved in HCl solution, and ^{89}Zr (IV) was extracted via multistep extraction using 4,4,4-trifluoro-1-(2-thienyl)-1,3-butanedione (TTA) and then HNO_3/HF. Purification by anion exchange with 1 M HCl/0.01 M oxalate resulted in an 80 % yield of ^{89}Zr (99.99 % purification). A similar protocol using a thin Y foil l was reported by the Dejesus group.[231],[243],[259] Based on the same starting material of a Y foil target, several studies modified parameters such as foil thickness, time of irradiation, energy, and beam current in an attempt to improve production

yields.[177],[257],[261] However, the increase of beam energy over 13 MeV inevitably causes the undesirable production of long-lived ^{88}Zr via the ^{89}Y(p,2n)^{88}Zr reaction. The Queern group worked on the production of ^{89}Zr using sputtered yttrium on the niobium coin. They found that a reduction of beam energy from 17.8 to 12.8 MeV or 12.5 MeV using a 0.75 mm thick aluminium degrader yielded good results with no ^{88}Zr observed.[262]

The use of solid targets can be limited by a lack of facilities, so liquid targets have also been utilized to produce ^{89}Zr. For instance, Pandey and co-workers irradiated yttrium (III) nitrate in a nitric acid solution. Although their results showed a yield of only 4.4 MBq/µAh for two hours of irradiation at a 40 µA beam current, which is barely adequate for a solid target, this yield was still better than what has been achieved with conventional liquid targets.[263]

1.5.11 ^{89}Zr purification

After the irradiation process, ^{89}Zr should be purified from the impurities.[264] ^{88}Zr (392 keV), ^{88}Y (898 and 1836 keV) and ^{56}Co (896 keV) are the possible impurities resulting from the production process of ^{89}Zr in a cyclotron.[246] ^{88}Y and ^{88}Zr impurities are formed after bombardment as side products, whilst ^{56}Co comes from iron impurities in the yttrium target. ^{48}V, ^{156}Tb, and ^{65}Zn are further common impurities, and they come from titanium and gadolinium impurities and copper supports in the target, respectively.[244],[265] All these radionuclide impurities are separated from ^{89}Zr using a hydroxamate functionalized column.[266],[267] double extraction protocols are generally applied for ^{89}Zr purification, followed by anion exchange. Non-radioactive metal impurities are also removed by anion exchange using a hydroxamate-modified resin.[268],[269] Separation methods such as solvent extraction [259], cation and anion chromatography [243] and solid-phase hydroxamate resin [227] are used to obtain high radionuclide purity.[270] Separation processes and methods are essential due to the chelator affinity and potential biological uptake of impurities. Several studies investigated the separation of ^{89}Zr from the yttrium target.[259],[271],[272] Verel *et al.,*[227] used a hydroxamate

column to purify the [89]Zr from the target. The column was developed via two steps with the 2,3,5,6-tetrafluorophenol-chelate ester (TFP) and 1-ethyl-3-(3-dimethyl-aminopropyl)-carbodiimide (EDC) chemicals by themselves to provide the highest reproducible separation. In the end, [89]Zr was purified with more than 99 % purity.[227] Meijs *et al.,* also used a hydroxamate column to separate [89]Zr from bulk [89]Y with more than 99.99 % efficiency by using an oxalic acid solution.[273] Other studies mentioned that hydroxamate-modified resin cation exchange chromatography is the best method for [89]Zr purification from [89]Y targets.[240],[251],[259],[274] [89]Zr production process should be followed by a quality control process. Radionuclide purity and chemical purity tests were done as quality control after [89]Zr production terminated.[259] Dabkowski *et al.,* also studied the impurities of [89]Zr production. They found only limited quantities of impurities. Before purification, the activity of [88]Zr as an impurity was found to be 0.0007 – 0.0012 %, whereas the values decreased to 0.0005 – 0.0010 % after purification.[275] The chemical impurities may be copper, aluminium or iron, depending on the yttrium target system and its supporting metal components. Several methods, such as polarography, atomic absorption, mass, and PIXE analysis also analysed these impurities.[259]

Kandil *et al.* studied the separation of [89]Zr using different methods.[276] They used Triphenyl Phosphine Oxide (TPPO) as a reagent for separating [89]Zr from yttrium by ion-exchange chromatography and solvent extraction. In addition to radionuclide and chemical purity analysis, yield measurements were also carried out. When the yield was measured, different parameters and uncertainties were accounted for, such as the average energy range in the target, irradiation parameters, theoretical yield and batch yield of radionuclide, and chemical and radionuclide impurities.[276]

In the early studies by Mealey *et al.,* [89]Zr was prepared and administered in the form of [89]Zr-citrate (formulated in 1 % sodium citrate, pH 6-7).[222] The findings by Baroncelli and Grossi that hydroxamic acids have a high specific affinity for zirconium and can form very stable complexes paved the way to more efficient production and specific separation processes of [89]Zr from the yttrium target material.[277] Meijs *et al.,* were the first to describe the separation of [89]Zr from the yttrium target with an in-house prepared hydroxamate

resin by eluting the no carrier added ^{89}Zr with 1.0 M oxalic acid.[244] Oxalic acid can keep ^{89}Zr in solution very stably as ^{89}Zr-oxalate, given that oxalate as a ligand needs to have a stronger affinity to ^{89}Zr than to the hydroxamate resin itself. Holland *et al.* showed that the concentration of oxalic acid in the solution with ^{89}Zr did not impact the formation of complexes with the DFO chelator.[257] ^{89}Zr can also be produced as ^{89}ZrCl$_4$ or converted to ^{89}ZrCl$_4$ from ^{89}Zr-oxalate in a 2-step procedure via a QMA cartridge.[278] Although ^{89}ZrCl$_4$ is very reactive, hygroscopic and prone to form oxychloride hydrates that are hard to chelate [279][280] it has shown to be the favourable starting material to label tetraazamacrocyclic ligands such as the 1,4,7,10-tetraazacyclododecane *N,N',N''*, *N'''*-tetraacetic acid (DOTA) chelator compared to ^{89}Zr-oxalate yielding complexes with "extraordinary stability".[256] Therefore, the chemical form of the isotope is essential and often decisive for the subsequent radiochemistry but also for applications where oxalic acid can be a major problem due to its toxicity and where it can't be removed from the tracer solution. Both ^{89}Zr-oxalate and ^{89}ZrCl$_4$ offer the possibility of choosing the better-starting compound depending on the chelation chemistry and application.

Most hydroxamate resins currently used by different institutions and described in the literature are prepared in-house. Hence, minor differences in the experimental data are typical and expected. The material and methods chapter in this thesis describes in more detail the production of ^{89}Zr that was used during this work. One of the main advantages of the cyclotron production of ^{89}Zr is that there is no need to use an isotopically enriched target material since yttrium as the starting material is a monoisotopic element, which is also cheap and makes the production process affordable and efficient.[281]

1.5.12 ^{89}Zr chemistry, chelator design, and radiolabelling

1.5.12.1 Stable Zr chelators for protein labelling

In PET imaging, the chemistry of ^{89}Zr and the design of chelators are critical for the stability and effectiveness of radiopharmaceuticals. ^{89}Zr is uniquely stable predominantly existing in the 4+ oxidation state (Zr(IV)) and binds readily to chelators featuring three hydroxamic acid moieties.[273],[282],[283] In aqueous solutions, Zr^{4+} forms coordination complexes with high coordination numbers, preferring anionic oxygen donors, but in neutral solutions, it often exists in polynuclear and polymeric forms, hindering effective chelation.[284],[285]

Chelators, vital for linking radiometals to targets, significantly affect radiometal-labelled compounds' biological properties, biodistribution, stability, and selectivity.[270],[280] A variety of ligands, such as DOTA [287], TETA [288], NOTA [289], DTPA [289], EDTA [289], and DFO [290], are used for ^{89}Zr radiolabelling, each influencing the stability and behaviour of the radiometal in different ways. For instance, while EDTA binds ^{89}Zr with two nitrogen, four oxygen atoms, and two exogenous water molecules, DOTA and DTPA coordinate ^{89}Zr solely via the ligand's constituent atoms.[291],[292]

The stability of ligand-^{89}Zr complexes varies. Meijs *et al.,*[282] noted significant deterioration of the ^{89}Zr-DTPA complex in human serum within 24 hours. Though DFO is FDA-approved and safe for *in vivo* use [273] ^{89}Zr-DFO complexes exhibit relatively poor stability.[257],[293] Several preclinical studies have reported significant bone accumulation of dissociated ^{89}Zr from labelled antibodies.[231],[286] Unchelated ^{89}Zr, in forms like ^{89}Zr-chloride and ^{89}Zr-oxalate, leads to bone uptake of approximately 15 % ID/g and 20 % ID/g respectively at 8 hours post-injection *in vivo*. Zirconium's high affinity for phosphates suggests that ^{89}Zr is likely

chelated by hydroxyapatite, forming the matrix of bones.[294] However, in human immuno-PET imaging studies, the [89]Zr-DFO complex does not seem to experience the same degree of dechelation and subsequent bone uptake observed in mice, indicating a variance in stability between species.[295],[296] This led to the exploration of bioactive molecules like thiol-derivatives and maleimide for conjugation to DFO,[297],[298] with DFO-p-Bz-NCS emerging as a popular choice due to its simple conjugation reaction. Perk *et al.,* studied DFO-p-Bz-NCS for [89]Zr radiolabelling, observing high serum stability and selective *in vivo* accumulation.[299] This chelator forms a thiourea bond with primary amine proteins, showing promising results in both *in vitro* and *in vivo* experiments.[300],[301] Despite DFO-Bz-NCS's popularity, derivatives like DFO-Sq also show potential as promising chelating agents.[302]

Overall, the stability and efficiency of [89]Zr-chelation are vital for successful PET imaging. The exploration of more stable octadentate ligands and ongoing research into predicting the thermodynamic stability of [89]Zr-tracers are responses to concerns about *in vivo* stability and radiation dose from dissociated [89]Zr.[292],[303]

1.5.12.2 Lipophilic complexes for direct cell labelling

The use of radiometal ionophore complexes for the direct radiolabelling of cells has been a common practice in nuclear medicine for several decades. These complexes consist of a radiometal and an ionophore, an organic ligand that allows for the passive diffusion of metal ions through lipid bilayer cell membranes. As far as we know, the use of oxine for directly labelling cells with radionuclides was first reported by McAfee and colleagues in the 1970s. They described the synthesis of ^{99m}Tc-oxine and ^{111}In-oxine complexes for the labelling of red blood cells and white blood cells.[29],[121] However, the ^{111}In-oxine formulation was withdrawn from the European market due to insufficient medical demand, although it is now

available in the EU from alternative sources like Curium. This withdrawal led to the use of ^{99m}Tc HMPAO for leukocyte labelling and tracking, the primary application of the tracer in clinical settings at that time. Nonetheless, the growing need for tracking cells over extended periods has revived interest in ^{111}In-oxine for *in vivo* tracking of cellular therapies both preclinically and clinically.[29]

8-Hydroxyquinoline, or oxine, is a metal-chelating ligand that has been found to bind to a variety of metals through the pyridyl nitrogen and deprotonated hydroxyl group, resulting in the formation of neutral, lipophilic metal complexes.[29],[305],[306] These complexes have been tested with various radionuclides, including ^{57}Co [307], ^{59}Fe [307], ^{69}Ga [307], ^{68}Ga [210], ^{201}Tl [210], and ^{89}Zr [29] for cell labelling. Lipophilic complexes of oxine are often metastable and dissociate inside cells, where the radiometal may bind to intracellular proteins with chelating groups or other metal-chelating ligands, Figure 1-6.[29],[308] Effective radio-ionophore agents should facilitate rapid uptake and slow radionuclide efflux while maintaining the viability and function of cells. Figure 1-7 presents a schematic representation of ^{89}Zr cell labelling methodology utilizing oxine as an ionophore.
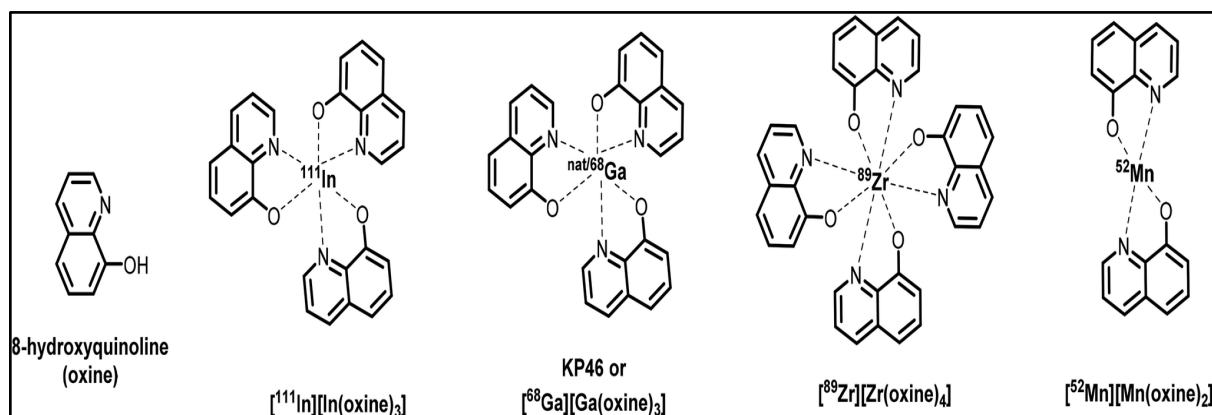
Figure 1-6: Chemical structures of oxine and oxine metal complexes. This figure copied from reference [309].
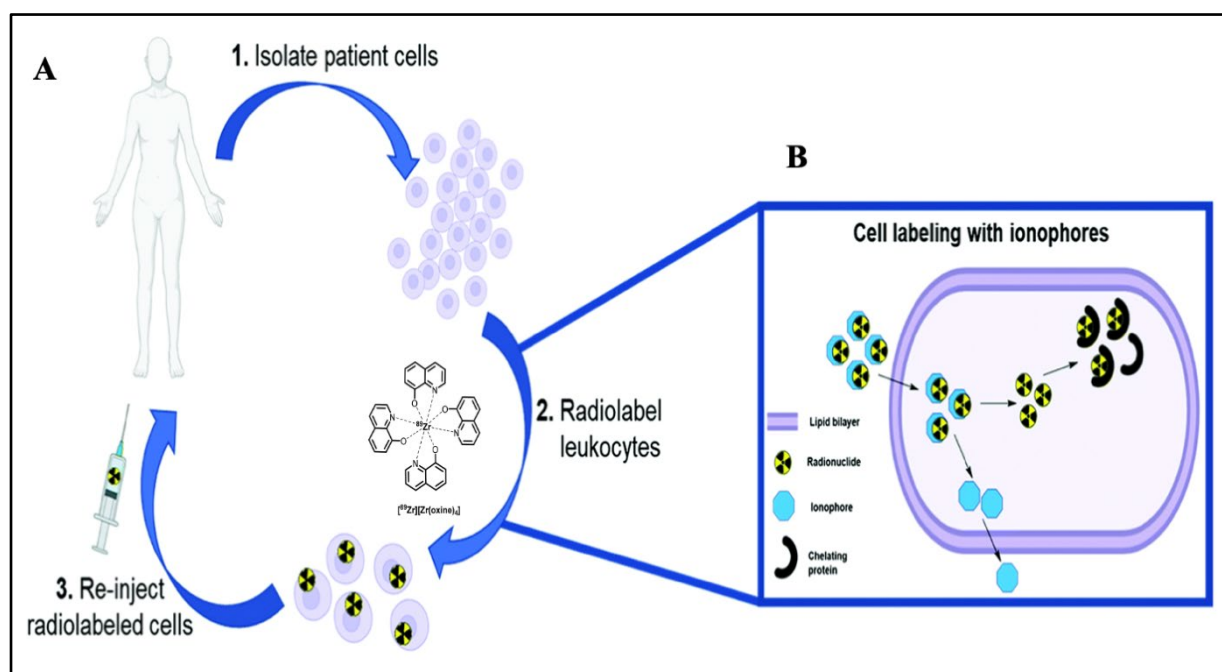
Figure 1-7: Schematic representation of ^{89}Zr cell labelling methodology utilizing oxine as an ionophore. Section **(A)** illustrates the direct cell labelling stages *in vitro* where (1) cells are isolated from a subject, donor, or culture, (2) the isolated cells are radiolabelled *in vitro* through incubation with ^{89}Zr-oxine, and (3) these radiolabelled cells are subsequently reintroduced into the subject for diagnostic or therapeutic purposes. Section **(B)** zooms in on the process of cell labelling with ionophores, demonstrating that (1) the lipophilic, metastable ^{89}Zr-oxine complex penetrates the lipid bilayer of the cell membrane, (2) once internalized, the complex disassembles, allowing the radiometal ion Zr^{4+} to be trapped by cellular components, and (3) the ionophore is expelled from the cells. The figure is reproduced with alterations from reference [309].

As PET becomes more readily available, research efforts have turned towards exploring PET tracers for cell labelling. PET imaging has demonstrated superior sensitivity, spatial resolution, and quantification compared to SPECT imaging in clinical settings.[29],[33],[53],[129] One particularly promising compound for this purpose is ^{89}Zr-oxine, which has a half-life of 3.27 days. Developing a PET tracer for long-term cell tracking using ^{89}Zr as an alternative to ^{111}In-oxine has been made possible due to the similarities in the half-lives and preferred ligand types of In^{3+} and Zr^{4+}.[308] Several studies have demonstrated the effective cell labelling and tracking properties of ^{89}Zr-oxine, which has been extensively evaluated in preclinical studies both *in vitro* and *in vivo*. In addition, its longer half-life and improved cellular retention of the radionuclide compared to ^{111}In allow for extended *in vivo* tracking of various cell types using PET for up to two weeks.[29],[34],[38],[310],[311]

Chapter 2: Methods and materials:

All primary reagents and solvents were procured from Sigma-Aldrich or Merck. These were employed in their received state unless specified otherwise.

2.1 Production of ^{89}Zr

The production of ^{89}Zr took place at the institutional cyclotron facility of PETIC through the proton irradiation of a Yttrium target, adhering to the techniques delineated by Walther *et al.,*[177] and Dabkowski *et al.,*[312]. In essence, a disc composed of natural ^{89}Y foil (300 μm in thickness) was positioned within a bespoke aluminium holder. This was subsequently inserted into a COSTIS Solid Target System (STS) that was affixed to an IBA Cyclone (18/9) cyclotron, which had been enhanced with a niobium beam degrader measuring 400 μm. Subjected to an irradiation period of 4 hours, the disc received a beam energy of 40 μA. Post-irradiation, the disc remained within the cyclotron for an additional 12 h interval to facilitate the decay of any transient ^{89m}Zr isotope to ^{89}Zr prior to its extraction for purification processes. The resultant activity ranged between 1.5 and 2 GBq.

2.2 Separation of ^{89}Zr

The synthesized ^{89}Zr was then subjected to dissolution in hydrochloric acid (HCl) to facilitate its separation from the initial material. To achieve this, 2 M HCl (6 ml) was added dropwise over 4 minutes with rapid stirring to the irradiated disc to produce a grey mixture containing partially dissolved particulate matter. Caution HCl must be added slowly to avoid overspill due to vigorous effervescence. Once effervescence had subsided 200 μl of 30 % hydrogen peroxide followed by 600 μl of 6 M HCl were added and the resultant mixture was heated with stirring

to 80 °C for 60 minutes to yield a pale-yellow solution. Once cooled the solution was passed dropwise through as solid phase extraction column containing 125 mg of hydroxymate functionalised ion exchange resin (prepared in-house via the methods of Verel *et al.*[227], (see below). The ^{89}Zr was trapped on the column whilst the waste yttrium starting material flowed through the column. The column was washed with a further 12 ml of 2 M HCl and 25 ml of deionised water to remove waste yttrium before the ^{89}Zr was liberated from the column by dropwise addition of 1 M oxalic acid (3 ml) collected in 3×1 ml fractions. The most concentrated fraction typically contained 800 – 1000 MBq of ^{89}Zr.

2.3 Preparation of the hydroxamate resin

The hydroxamate-functionalised ion exchange resin was employed for the distinct separation of the ^{89}Zr product from the ^{89}Y target substance. The resin's preparation closely adhered to the protocol set out by Verel *et al.,*[227]. Briefly, 1.0 g of Accell Plus CM cation exchange resin, 225 μl of 1 M HCl (aqueous), 1.0 ml of MeCN containing 200 mg/ml or 1.2 M TFP in and 400 mg of EDC (equating to 2.08 mol) were sequentially added to 8.0 ml of water, and the final to a final pH ranging from 5.5 to 6.0. This composite was allowed to agitate gently on a thermomixer for 1 h at RT. It is crucial to note that only gentle shaking and not vigorous stirring was employed to preserve the resin's particulate structure, ensuring an unhindered flow of the ^{89}Zr solution through the column.

Additional constituents were incorporated: 315 μl of 1 M HCl (aqueous), 1 ml of MeCN containing 200 mg of TFP (1.2 mM) and 400 mg of EDC (2.08 mM) and the solution, subjected to another hour of gentle shaking at room temperature. After the reaction, the TFP-ester-activated resin was carefully separated by filtration using an empty solid-phase extraction (SPE) cartridge equipped with a 20 μm frit. The filtered resin was then cleansed by passing 30

ml of MeCN through the cartridge. Separately 700 mg hydroxylamine hydrochloride was dissolved in 1 ml of 1 M NaOH plus 2 ml of MeOH to give a final concentration 10 mM and agitated as described above for 15 min giving a final pH of 5.0 - 5.5. This resultant solution was then introduced to the TFP-ester-activated resin in the SPE cartridge, and the ends were capped, and the mixture was shaken for 18 h on a thermomixer (1000 rpm, room temperature). The resin was then washed with 50 ml deionised water and dried at room temperature in the SPE cartridge under vacuum for 18 h. This product is stable for 6 months if stored at -20 °C. 125 mg portions of the product are activated immediately prior to use by washing in a 1 ml fritted SPE cartridge with MeCN (75 ml), saline (10 ml) and 2 M HCl (2 ml).

2.4 Synthesis of [89]Zr-oxine complex

[89]Zr-oxine was synthesized in an aqueous solution for cell labelling using the method described in this previously published work.[70] An aliquot of [89]Zr-oxalate in 1 M oxalic acid, generally 200 to 250 MBq in 200 μl, was neutralised to pH 7 ± 0.2 by the addition of freshly made 0.5 M Na_2CO_3. The concentration of oxalic acid was reduced from 1 M to 0.1 M by the addition of distilled water (dH$_2$O). On the day of the experiment, oxine solution (1 mg/ml) was made by combining an equivalent quantity of oxine, 8-hydroxyquinoline (10 to 20 mg), with chloroform (10 to 20 ml). Generally, 2 ml of the oxine solution was added to an equal amount of neutralised [89]Zr in 0.1 M oxalic acid. The resulting biphasic mixture was shaken at 1000 rpm for 1 h at RT. Following phase separation, the bottom layer (chloroform extract) was collected and transferred to a 15 ml Falcon tube. If the first [89]Zr extraction produced sufficient activity (1 – 20 MBq), an additional 2 ml oxine solution (1 mg/ml of oxine/chloroform solution) was added, to the [89]Zr-oxalate solution and the mixture mixed overnight. If the first extraction yielded less than 1 MBq, the pH of the aqueous [89]Zr-oxalate solution was checked and corrected to 7.0 ± 0.2 before adding the second 2 ml portion of the oxine solution. After

separation, this generally provided 60 - 140 MBq of ^{89}Zr-oxine in the bottom chloroform layer. The chloroform was evaporated using dry air, revealing a powdered ^{89}Zr oxine residue of light cream colour. This was redissolved in 10 – 20 μl of fresh dimethyl sulfoxide (DMSO). Once fully dissolved, it was diluted with 2 ml of phosphate-buffered saline (PBS). Typically, after solubilisation and transfer to a new sample tube, 1 – 20 MBq of ^{89}Zr-oxine was separated from the first extraction and 50 to 80 MBq from the second extraction.

2.5 Synthesis of ^{89}Zr-DFO-NCS (Desferrioxamine) complex

^{89}Zr-DFO-NCS complex was synthesized for cell labelling according to the method described by Bansal *et al.,*[36] ^{89}Zr-oxalate in 1 M oxalic acid ($\approx$ 100 MBq) was neutralised to pH 7 $\pm$ 0.2 by the addition of freshly prepared 0.5 M Na_2CO_3. 3.8 mg of desferrioxamine (DFO-Bz-NCS; Macrocyclics, Inc, USA) was dissolved in 1009 μl of DMSO. 8 μl of the freshly prepared DFO solution was added to the neutralised ^{89}Zr-oxalate and incubated for 1 hour at 37 $^{\circ}$C and 550 rpm. Radio-Instant thin-layer chromatography (radio-iTLC) was employed to determine the radiochemical purity of the ^{89}Zr-DFO-NCS product; 500 μl of 50 mM DTPA (pH 7.4) was used as the eluent. Then, on the line at the bottom of the radio-iTLC paper, 5 μl of ^{89}Zr-DFO-NCS product sample was added. Following that, sufficient time (5 to 10 minutes) was allowed for the product in the eluent to migrate along the radio-iTLC paper. Finally, the counts within the radio-iTLC paper were determined using a ScanRAM radio-TLC scanner (LabLogic, UK). Typically, the reaction proceeds quantitatively, requiring no further purification.

2.6 Mice details

In all mouse experiments, C57BL/6 type female mice (aged 6 to 12 weeks) were utilised for both donor and recipient mice, and they were purchased from Charles River Laboratories in

the UK. In this project, all mouse experiments were conducted under the project licence (PPL) P2FB675AB and the personal investigator licence (PIL) I4A6AF191. All experimental protocols and animal handling were carried out in accordance with PPL, PIL, and UK Home Office guidelines.

2.7 Tissue culture

Unless otherwise stated, all the components of the cell culture medium were provided by Thermo Fisher Scientific except for the fetal calf serum, which was provided by Gibco.

2.7.1   Isolation of cells

2.7.1.1 Mixed lymphocytes

The procurement of fresh mixed lymphocytes was performed as described here: At the outset, C57BL/6 mice were culled in compliance with schedule one procedures (CO_2 inhalation followed by cervical dislocation) at the Biological Services Unit (BSU). Following this, splenocytes and/or lymph nodes were harvested and preserved in 5 ml of chilled phosphate-buffered saline (PBS) for transport to the tissue culture facility. In the primary tissue culture lab of the Immunity and Infection Department, the harvested spleens and/or lymph nodes were homogenized by being pressed through a 70 μm cell strainer (BD Pharmingen) with a rubber plunger's end, followed by rinsing the strainer with 5 ml of chilled PBS. After centrifugation at 350 g for 5 minutes at 4 ℃, the supernatant was removed. The cell suspension then underwent red blood cell (RBC) lysis following the guidelines provided by the manufacturer (Biolegend; 420301), with a resting period on ice for 5 minutes and intermittent vertexing. A subsequent centrifugation was performed for 5 minutes at 350 g at 4 ℃. The lymphocytes were

purified, washed twice with PBS, and their count was determined with a hemocytometer. The final step involved suspending the lymphocytes in sterile PBS and their conveyance on ice to the R & D preclinical lab for cell labelling studies, securely contained within a 15 ml Falcon tube.

2.7.1.2 CD8 T cells

To attain primary murine CD8 T cells, the same steps as those used for the isolation of mixed lymphocytes was followed by negative isolation by magnetic activated cell sorting (MACS) for CD8 positive splenocytes according to the manufacturer's protocol (Stem Cell; 17953). CD8 T cells were isolated by initially preparing the cell sample to a density of 1×10^8 cells/ml within a volume ranging from 0.1 to 2 ml, according to the EasySep™ protocol. Rat Serum was then added at a concentration of 50 µl/ml. This mixture was transferred to a 5 ml polystyrene tube. An Isolation Cocktail was added to the sample at 50 µl/ml. The sample was then mixed and incubated at room temperature (RT) for 10 min. Post incubation, RapidSpheres™ were vortexed for 30 sec to ensure particles were evenly dispersed. These were added to the sample at 75 µl/ml, followed by mixing and a further incubation at RT for 2.5 min. The volume of the sample was brought up to the required 2.5 ml with the MACS buffer (PBS/2 % FCS with 1mM EDTA), mixed by gentle pipetting up and down 2 - 3 times. The tube, without its lid, was placed into the magnet and incubated at RT for an additional 2.5 min. To finalize, the magnet and tube were inverted in a single motion, allowing the enriched cell suspension to be collected into a new tube. The isolated CD8 T cells were thus prepared and ready for use.

2.7.2 Cultivation of cells

2.7.2.1 EL4 mouse lymphoma T cell line

The EL4 mouse lymphoma T cell line, used in the optimization experiments, was kind gift from Prof Ann Ager. Cells were cultivated in accordance with ATCC guidelines.[313] EL4 cells were maintained in Dulbecco's Modified Eagle's Medium (DMEM) (4.5 g/L glucose) supplemented with 4 mM L-glutamine, 10 % FCS, 100 IU penicillin, 100 μg/ml streptomycin and 1 mM sodium pyruvate. Cells were maintained in suspension and housed in a 5% CO_2 incubator at 37 ºC within a humidified atmosphere. Cell culture was started at 2×10^5 cells/ml and maintained between 1×10^5 and 1×10^6 cells/ml. T-75 flasks were used for subculturing this product. Medium renewal was carried out every 2 to 3 days. Cells were tested for mycoplasma contamination at regular intervals, typically every 4 weeks on actively growing cell lines and upon receipt of externally sourced cells and upon thawing of frozen cell lines, no mycoplasma contaminations were detected for the duration of this project.

2.7.2.2 CTLL2 mouse cytotoxic T cell line

CTLL2 cells are a clone of cytotoxic T cells derived from C57BL/6 mice.[314] Cells were purchased from ATCC (item code ATCC TIB-214). This cell line was cultured under as per ATCC guidelines.[314] CTLL2 cells were cultured in RPMI 1640 medium (4.5 g/L glucose), enriched with 2mM L-glutamine, 1 mM sodium pyruvate, 100 IU penicillin, 100 μg/ml streptomycin, 10 % FCS, and 10 % T.stim with Concanavalin A (ConA), (Scientific Laboratory Supplies, product code 354115). Cells were maintained in suspension and incubated in a 5% CO_2 incubator at 37 ºC within a humidified atmosphere. The culture medium for cells was refreshed two to three times a week. Subculturing of actively

growing suspension cultures was performed prior to the cell density reaching 2×10^5 cells/ml to prevent rapid depletion of Interleukin-2 (IL-2) and subsequent loss of cell viability. The cultures were inoculated at densities ranging from 1×10^4 to 2×10^4 viable cells/ml. For subculturing these cells, T-75 flasks were utilized. This approach ensured optimal growth conditions and maintained cell culture health. Cells were tested for mycoplasma contamination at regular intervals, typically every 4 weeks on actively growing cell lines and upon receipt of externally sourced cells and upon thawing of frozen cell lines no mycoplasma contaminations were detected for the duration of this project.

2.8 Freezing and thawing of cells

Prior to freezing, the cells were centrifuged at a speed of 350 g for 5 minutes. The resulting pellet was resuspended in 1 ml of freezing medium, consisting of FCS supplemented with 10% DMSO. This suspension was then transferred to a cryovial. To ensure successful cryopreservation and subsequent recovery of the cells, the vials were placed in a freezing container filled with isopropyl alcohol. This container was stored overnight at -80 ºC before being transferred to liquid nitrogen for long-term storage.

For the thawing process, the cryovial was rapidly warmed in a water bath. The thawed cells were then transferred to 10 ml of cell complete medium for the chosen cell line prewarmed to 37 °C. Following a subsequent centrifugation at 350 g for 5 minutes, the supernatant was discarded. The remaining pellet was resuspended in the culturing medium and cultivated in a suitable cell culture flask or plate.

2.9 Cell counting and viability assessment

Cells were counted, and viability was determined using either manual or automated cell counting.

2.9.1 Manual cell counting method using trypan blue exclusion

The trypan blue exclusion assay is commonly utilised protocol to determine cell viability within a cell suspension. The underlying principle of this method is premised on the ability of live cells, characterised by their unimpaired cell membranes, to exclude particular dyes such as trypan blue. Conversely, cells that have been compromised or are non-viable are unable to preclude the penetration of the dye, leading to the staining of their cytoplasm.

In order to perform this assay we followed the procedure suggested by StemCell Technologies [315]. To begin, a suitable volume of cell suspension (20 - 200 μl) was carefully resuspended and mixed with an equal volume of 0.4 % trypan blue dye. The mixture was then incubated at room temperature (15 ºC - 25 ºC) for 5 minutes, allowing the dye to penetrate the cell membranes and stain only the non-viable cells. Next, 10 μl of the stained cell mixture was carefully placed into the hemocytometer chamber using a 20 μl pipettor. The coverslip was positioned over the chambers, and the hemocytometer which was then positioned under a microscope for visual assessment. Both the unstained (indicative of viable cells) and the stained (indicative of non-viable cells) cells were counted separately. The cells were counted in each of the four outside squares of the hemocytometer (Figure 2-1A), including those that lay on the bottom and left-hand perimeters using a hand tally counter. Cells that lay on the top and right-hand perimeters (Figure 2-1B) were excluded from the count.
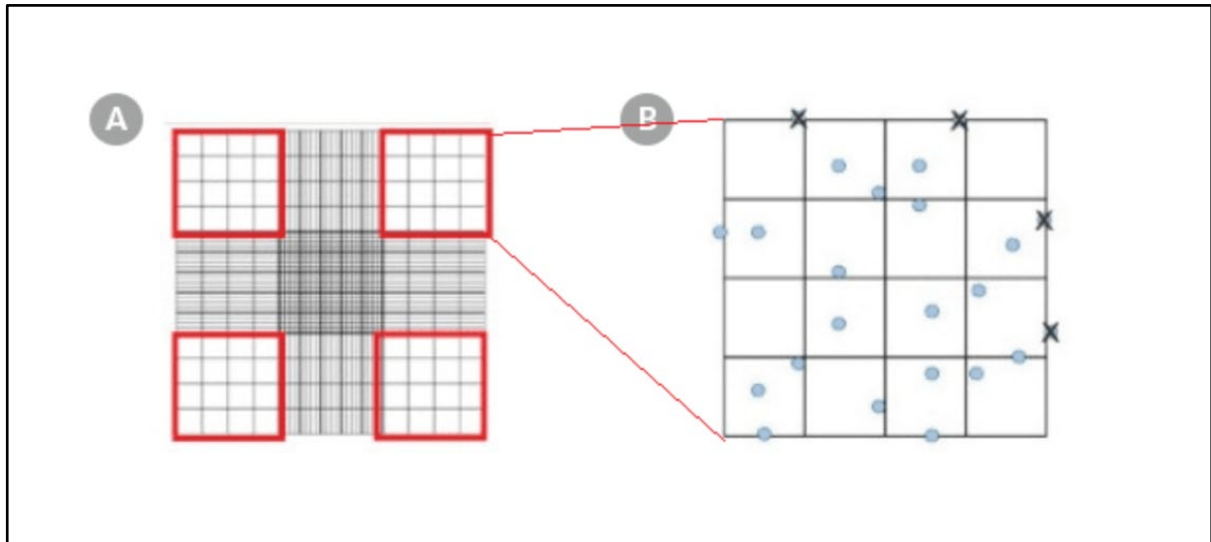
Figure 2-1: Hemocytometer Gridlines. Diagram of a hemocytometer highlighting **(A)** the four sets in red and **(B)** the 16 squares within one set designated for counting. This figure was taken from StemCell Technologies.[315]

The dilution factor was adjusted to ensure that the cell concentration was within the correct range, resulting in 50 - 100 cells per square in the hemocytometer. The total number of live cells (unstained cells) per millilitre was calculated using the following equation:

$$\text{Total number of live cells/ml} = \text{average live cell count per square} \times \text{dilution factor} \times 10^4$$

Cell viability was quantitatively expressed as a percentage, representing the ratio of live cells to the total cell population within a given sample. The viability percentage was calculated using the equation below. Whereas the number of viable cells refers to the count of unstained cells, the total number of cells represents the sum of both viable and non-viable cells within the observed field of the haemocytometer.

$$\text{Percentage of viable cells} = \left(\frac{\text{number of viable cells}}{\text{total number of cells}} \right) \times 100$$

2.9.2 Automated cell counting

Two automated cell counters were used in this project. Within the primary tissue culture laboratory of the Immunity and Infection Department, cell counts were performed using the LUNA-FL™ Dual Fluorescence Cell Counter, which operates with either a 1:1 Trypan Blue solution or a 1:10 Acridine Orange/Propidium Iodide (AO/PI) Cell Viability Reagent, supplied by Logos Biosystems and Thermo Fisher Scientific. In the R & D preclinical laboratory a LUNA-II™ Automated Cell Counter, which utilizes a 0.4% trypan blue stain was employed.

2.10 PET Imaging

Mice were intravenously administered with ^{89}Zr labelled cells suspended in 200 µl of PBS, followed by an intraperitoneal injection of iopamidol contrast agent (100 µl/mouse). Throughout the imaging procedure, anaesthesia was induced and maintained via the inhalation of 1 % - 2 % isoflurane in oxygen, delivered through a nose cone, while respiratory parameters were continuously monitored through a pressure pad coupled with differential pressure transducers designed for low-range pressure detection. The mice were scanned using a dedicated small animal nanoScan PET/CT scanner (Mediso Ltd., Hungary). Each imaging session consisted of a one-hour PET scan with a spatial resolution of 0.4 mm and an energy window ranging from 400 to 600 KeV, followed by a 3-minute CT scan with a tube voltage of 50 kVp, a tube current of 1 mA, an exposure time of 300 ms, and a total of 400 projections. The CT scans yielded a reconstructed resolution of 0.25 mm. This combined PET/CT imaging

protocol was replicated at time points of 20 h, 44 h, 68 h, 140 h, 188 h, 212 h, and 235 h post-tracer administration. In addition to imaging, whole-body radioactivity levels were quantified immediately following each scan by positioning each anesthetized mouse in a Capintec CRC-25 dose calibrator, set at calibrator mode 465, for instantaneous radioactivity measurement.

2.11   Image processing and analysis

By employing VivoQuant^{TM} 4.0, patch 3 software, the obtained PET/CT images underwent processing and analysis. Three-dimensional regions of interest (ROIs) were meticulously delineated around the targeted organs, including the lungs, liver, spleen, kidneys, and skeleton. The ROIs were then subjected to decay correction in order to calculate the percent of the administered dose (%IA) and the normalised percent of the dose per organ (%IA/g).

2.12   Statistical analysis

In this thesis, data analysis was carried out employing GraphPad Prism software, specifically version 8.2.1. Unpaired two-tailed t-tests were employed for comparisons involving two groups, while one-way ANOVAs, accompanied by multiple comparisons, were applied when comparing more than two groups. The results are presented in the format of mean ± standard deviation (SD). Correlations among continuous variables were evaluated using the Pearson correlation coefficient (r). The specific statistical test utilized for each comparison is indicated within the legend accompanying each table and/or figure. Statistical significance was determined based on P values, with values less than 0.05 being considered statistically significant. Significance levels were denoted as follows: $*P \leq 0.05$, $**P \leq 0.01$, $***P \leq 0.001$.

Chapter 3: Part 1: Initial attempts to label donor lymphocytes with ^{89}Zr-oxine and ^{89}Zr-DFO-NCS complexes and track the labelled cells *in vivo* by PET/CT imaging in a mouse model. Part 2: Development of the labelling method for ^{89}Zr-oxine and EL4 cells for *in vivo* PET imaging

3.1   Introduction

The aim of this project was to develop an optimised imaging methodology that would allow the long-term whole-body tracking of freshly harvested mouse donor lymphocytes in tumour bearing mice. PET imaging was selected as the imaging methodology due to its extremely high sensitivity, excellent tissue penetration and quantifiable whole-body 3D image outputs. A key requirement of this application is that the fresh donor lymphocytes could be rapidly labelled without need for genetic modification and the associated extended tissue culture processes. Therefore, a direct cell labelling methodology, which also offers advantages of high specificity and sensitivity, was required.[29],[55],[125],[316],[317] The isotope ^{89}Zr was chosen due to its long half-life (78.4 h, which enables up to 15 days of imaging, excellent imaging properties and established literature for labelling other cell types. Two of the most common chelators developed for ^{89}Zr are oxine and DFO-NCS. There has been considerable progress in the development of cell labelling strategies using ^{89}Zr-oxine and ^{89}Zr-DFO-NCS.[38] The main difference between these two radiotracers is the cell labelling mechanism. The mechanism of action of ^{89}Zr-oxine is based on its ability to diffuse through cell membranes due to its lipid solubility. In contrast, ^{89}Zr-DFO-NCS is reported to conjugate ^{89}Zr directly with cell surface proteins for PET tracking. This process involves chelating ^{89}Zr with deferoxamine-NCS and covalently binding the NCS group to a primary amine group on the surface of membrane

proteins.[36],[38] The result is that the majority of ^{89}Zr radioactivity is found in the membranes of the labelled cells rather than in the cytoplasm and nucleus.[29],[36],[38]

The development of ^{89}Zr PET tracers, particularly ^{89}Zr-oxine, for cell labelling has seen significant advancements. Preclinical models have demonstrated the potential of ^{89}Zr-oxine in direct cell labelling and cellular tracking, with superior sensitivity compared with conventional SPECT imaging methods.[29],[34],[38],[125],[318] The ionophore properties of 8-hydroxyquinoline (oxine) for ^{89}Zr cell labelling have been emphasised especially for PET tracking of T cells in breast tumours.[319]

In a specific study, the biodistribution of ^{89}Zr-oxine labelled human bone marrow-derived mesenchymal stem cells was evaluated by assessing the impacts on cellular functionality, viability, proliferation, apoptosis, differentiation, morphology, phenotype, and *in vivo* behaviour using micro-PET/CT imaging.[320] Another study demonstrated the use of the ^{89}Zr-oxine complex for PET cell imaging, underscoring its practicality for direct cell labelling without further purification.[310] However, some studies have indicated that the ^{89}Zr-DFO-NCS labelling strategy may be superior to ^{89}Zr-oxine in terms of increased cell stability and viability.[36],[322]

In the past few years, ^{89}Zr-oxine has been assessed in numerous preclinical trials *in vitro* and *in vivo* for labelling and monitoring therapeutic cells. The results of these studies have been summarized in Table 3-1. The potential of ^{89}Zr-oxine for PET imaging in cell-based therapies was further explored by assessing its cytotoxicity and application in visualising lung delivery of cell/gene cancer therapy.[323] One study highlighted the need for optimising labelling conditions to maintain the viability, proliferation and differentiation of bone marrow cells, emphasising the criticality of dose control in preserving cell functionality.[324] Sato *et al,.*

contributed significantly to this field by demonstrating the efficient and stable retention of [89]Zr-oxine in various cell types, including chimeric antigen receptor T cells (CAR-T cells), human bone marrow-derived mesenchymal stem cells (hMSCs), and regulatory T cells (Tregs).[310] This stable retention of [89]Zr-oxine is crucial for its successful application in prolonged cell tracking and monitoring in preclinical studies, as noted in further research.[325][326] The utility of [89]Zr-oxine extends to PET-based biodistribution studies. A particular study showcased this by labelling CAR-T cells with [89]Zr-oxine and analysing their product attributes for biodistribution studies, thereby highlighting its usefulness in characterising the *in vivo* distribution of engineered T cells.[326]

Furthermore, Weist *et al.,* reported a cell labelling with [89]Zr-oxine that was more efficient than previous methods. This efficiency was attributed to the specific cell type, or the higher cell concentration used in the labelling experiments. This finding underscores the importance of considering cell-specific factors and labelling conditions when assessing the efficacy of [89]Zr-oxine for cell tracking.[325] The medium-term *in vivo* cell tracking potential of [89]Zr-oxine was demonstrated by the successful radiolabelling efficiency of human regulatory T cells, supporting PET tracking beyond one week.[327]

The chelate's hydrophobicity prevents efflux from the cell. High labelling efficiency can be achieved; human mesenchymal stem cells (hMSCs) labelled with [89]Zr-oxine for just 30 min at 37°C demonstrated 98% labelling efficiency. Labelled cells retain viability and normal function, with no impact on migration, differentiation capacity, or immunosuppressive properties.[320]

[89]Zr-oxine cell labelling has proven particularly useful for tracking various immune cell types. T cells were one of the first evaluated; both CD4+ and CD8+ T cells have been labelled with

[89]Zr-oxine and PET imaging has been performed to track their biodistribution in mice. Excellent labelling efficiency (~ 90 %) was achieved without impacting viability or function. *In vivo*, [89]Zr-oxine enabled precise quantification of T cell trafficking to lymph nodes.[325] Natural killer (NK) cells have also been successfully labelled with [89]Zr-oxine and tracked *in vivo*. Labelling did not alter NK cell viability, phenotype, cytotoxicity, or antitumor functionality *in vitro*. PET imaging revealed biodistribution patterns and enabled quantification of NK cell accumulation at tumour sites.[328] Dendritic cells (DCs) are another key immune cell type amenable to [89]Zr-oxine labelling. Radiolabelled DCs have been used to study trafficking to draining lymph nodes and to quantify DC participation in tumour immunotherapy regimens.[329] Likewise, the survival and biodistribution of macrophage adoptive cell transfer has been evaluated with [89]Zr-oxine labelling.[317] High labelling efficiency was achieved in all these cell types without impairment of viability or functionality.[330] In addition to immune cells, [89]Zr-oxine labelling has proven valuable for tracking mesenchymal, neural, and other stem cell types. Early work demonstrated effective [89]Zr-oxine labelling of adipose-derived stem cells (ASCs) without impact on differentiation or proliferation.[320] *In vivo* PET imaging revealed biodistribution to the liver, lungs, and spleen following intravenous injection. Bone marrow-derived human MSCs have also been labelled with [89]Zr-oxine and tracked long-term after different transplantation routes, providing quantification of cell survival.[320] [89]Zr-oxine enables tracking of not only mesenchymal but also neural stem cells, giving insight into cell delivery, viability, and distribution following transplantation. labelled rat neural stem cells (NSCs) with [89]Zr-oxine and longitudinal PET imaging was performed after intracerebral transplantation in rat stroke models. Quantification revealed the dynamics of NSC persistence and disappearance in the weeks following transplantation. Similar NSC tracking approaches have been performed by using [89]Zr-oxine labelled human NSCs. PET imaging provided unique

insight into the biodistribution, viability, and tumour-targeting capacity of injected therapeutic NSCs.[320]

[89]Zr-oxine cell labelling provides several key advantages that have supported its growing use across diverse applications. One of the key advantages of [89]Zr-oxine is its ability to passively diffuse into cells, enabling straightforward cell labelling. This mechanism allows for the efficient and effective labelling of various cell types without the need for genetic engineering, making it a clinically applicable alternative to reporter gene imaging.[331] The simplicity and ease of implementation of [89]Zr-oxine labelling have been demonstrated in various studies, highlighting its potential for non-invasive tracking over a week post-injection, which is crucial for longitudinal studies and monitoring of cell migration and biodistribution.[323],[332] Additionally, high labelling efficiency can be achieved regardless of cell type, with up to 98% of cells successfully labelled after short incubations of 30-60 minutes.[38] Excellent intracellular retention of [89]Zr has also been demonstrated, even after long-term culture of labelled cells.[224] Crucially, the process of radiolabelling of immune cells such as lymphocytes, macrophages, and bone marrow-derived dendritic cells with [89]Zr-oxine does not impede their functionality, provided that the labelling doses are optimal. For instance, the activation, proliferation, and cytokine expression (IFN-γ and IL-2) post-TCR stimulation in CD8 T cells labelled with [89]Zr-oxine remain unaffected.[310] Likewise, the viability, cytotoxicity, or cytokine production of CAR-T cells labelled with [89]Zr-oxine are not compromised.[325] The labelling of dendritic cells with [89]Zr-oxine does not interfere with their LPS-induced activation or their capacity to present antigens and activate T cells.[310] The only observed exception is that [89]Zr-oxine labelling of bone marrow cells, even at low radioactivity doses (10.9 kBq/10^6 cells), initially slows down the proliferation post-GM-CSF stimulation *in vitro*. Nevertheless, the differentiation ability of these labelled bone marrow cells is preserved both *in vitro* and *in vivo*.[311] These studies suggest that the optimal labelling doses, which are

approximately 11 - 44 kBq/10^6 cells depending on the cell type and condition, minimize cellular toxicity while still allowing for PET imaging.[224] Once cells are labelled with [89]Zr-oxine, the [89]Zr is stably retained within the cells.[310],[311],[333] However, the death of labelled cells leads to the rapid release of free [89]Zr. *In vivo*, free [89]Zr is excreted via the kidney, but a small fraction may be absorbed into the bone matrix hydroxyapatite. This minor bone uptake can be reduced by administering deferoxamine, a chelating agent used clinically for treating iron overload and hemochromatosis.[311] Once bound to deferoxamine, the [89]Zr is quickly excreted through the urinary tract.[224]

While offering many advantages, [89]Zr-oxine cell labelling is not without limitations. One drawback is radiation dose to labelled cells due to [89]Zr decay. While cell functionality remains largely unaffected, some studies suggest changes in hematopoietic stem cell differentiation capacity and multipotency at very high doses. Dosimetry studies are still needed to fully elucidate dose effects. Additionally, efflux of the label has been observed in some cell types, highlighting the need for optimization of labelling procedures. Long-lived [89]Zr also means extended radiation exposure to patients that may hinder translation of cell tracking techniques to humans. Furthermore, the toxicity of [89]Zr-oxine is dependent on the amount used for labelling and varies between cell types, requiring individual evaluation with each prospective cell therapy.[334] The lack of standardized methods and tracer kits poses another challenge. Recent advancements have led to the development of an optimized formulation of [89]Zr-oxine that allows rapid, stable, high-yield preparation of [89]Zr-oxine in a single step, without further processing of commercially available zirconium-89. This formulation contains oxine, polysorbate 80, and 4-(2-hydroxyethyl)-1piperazineethanesulfonic acid (HEPES).[318]

The use of [89]Zr-DFO, particularly [89]Zr-DFO-NCS (also referred to as [89]Zr-DBN), has gained significant attention in immune-PET imaging. Desferrioxamine (DFO) is the most commonly

used chelator for ^{89}Zr.[302],[335]. Bansal *et al.,* developed ^{89}Zr-DFO-NCS as a novel cell labelling agent for PET-based cell trafficking studies through a two-step process involving the production and isolation of ^{89}Zr and the subsequent synthesis of ^{89}Zr-DFO-NCS. This method results in a high conversion rate of ^{89}Zr complexation with DFO in an aqueous solution, facilitating direct cell labelling without further purification. The synthesis of ^{89}Zr-DFO-NCS involves chelating ^{89}Zr with DFO conjugated to an isothiocyanate (NCS) group, forming a stable complex ideal for cell labelling. The NCS group in ^{89}Zr-DFO-NCS reacts with primary amine groups on cell surface membrane proteins, leading to the covalent attachment of the radiolabel to the cells. This covalent binding mechanism enhances its stability, making ^{89}Zr-DFO-NCS suitable for long-term *in vivo* tracking. One of the significant advantages of using ^{89}Zr-DFO-NCS over previous cell labelling methods is its stability. The covalent attachment of ^{89}Zr-DFO-NCS to cells reduces efflux of the radiolabel, enabling effective PET-based monitoring of *in vivo* cell trafficking over extended periods. Moreover, the general nature of the ^{89}Zr-DFO-NCS labelling method allows for the broad labelling of various cell types, which is attributable to the mechanism by which ^{89}Zr-DFO-NCS covalently binds to cell surface proteins, independent of cell type. This versatility is particularly beneficial because it is not limited to specific cell types or reliant on the presence of certain biomarkers. It leverages the abundance of primary amines on the cell surface, facilitating the labelling of various cell types. This broad applicability is advantageous for research and clinical applications involving diverse cell populations, eliminating the need for cell-specific optimisation of labelling protocols and circumventing potential limitations associated with targeting processes that might impact cellular function or viability.[36]

The ^{89}Zr-DFO-NCS complex has been extensively researched for its potential in longitudinal tracking of cell therapies, particularly in chimeric antigen receptor (CAR) T cell trafficking. This complex enables the assessment of cell survival, proliferation, and biodistribution, which

are crucial aspects in the context of cell-based therapies.[322],[335] Bansal *et al.,* contributed to this field by reporting the distribution of ^{89}Zr- labelled human mesenchymal stem cells (hMSCs) in mouse models. Their findings confirmed the biostability of the radiolabel bound to the DFO moiety, suggesting the ^{89}Zr-DFO-NCS labelling method's suitability for monitoring stem cell engraftment and cell trafficking.[36]

Another study highlighted the efficacy of ^{89}Zr-DFO-NCS labelling in human immune cells, achieving radioactivity concentrations up to 0.5 MBq/10^6 cells without adversely affecting cellular viability. Importantly, cell efflux studies demonstrated high radiolabel stability, with virtually no tracer loss for up to seven days.[37] However, preclinical studies have raised concerns about the suitability of DFO as a chelator, noting that the ^{89}Zr– DFO complex is partly unstable, leading to ^{89}Zr release and subsequent accumulation in bone tissue, which can reach values greater than 10 % ID/g.[286],[293],[302],[336] This instability questions the long-term stability of the ^{89}Zr– DFO complex under physiological conditions, potentially impacting its clinical translation and use in longitudinal studies.[337],[338] To address these concerns, alternative chelators such as DFO* have been developed, aiming to improve the stability of ^{89}Zr complexation and reduce bone uptake over time.[317] Direct comparisons of different chelators, including DFO and DFO*, have been conducted to identify the most suitable chelator for stable ^{89}Zr-radiolabeling of antibodies in clinical settings.[339],[340]

In summary, while ^{89}Zr-oxine offers the advantage of straightforward cell labelling through passive diffusion into cells, it is important to consider its limitations, particularly the efflux problems observed in various studies. The stability of the ^{89}Zr–DFO complex in addressing efflux issues has been highlighted, although its partial instability *in vivo* and bone accumulation pose significant challenges. The extensive literature on ^{89}Zr-oxine and ^{89}Zr-DFO-NCS

provides valuable insights into their respective advantages and limitations, contributing to the ongoing refinement of cell labelling strategies for PET imaging.

The use of radioactive labelling approaches for cellular imaging can be very challenging, particularly due to the specific activity per cell, which must not substantially affect the phenotypic, survivability, or functioning of the labelled cells. In an ideal situation, radioactivity levels should not adversely affect any of the above properties while being sufficient to permit the detection of labelled cells upon imaging. In events that require tracking cells for an extended period, such as tracking stem cells or therapeutic cells, the ability of labels to retain their activity is essential in allowing long-term imaging of the cells that are being tracked. To accomplish this, estimating the radioactivity density of labelled cells that is needed for detection will be valuable for determining the radiolabelling density that combines optimal cell survival with *in vivo* detection.[125]

Direct cell radiolabelling involves several key concepts, including cellular uptake/labelling efficiency, cellular retention of the radiolabel, and cell viability and functionality.

- **Cellular uptake/labelling efficiency:** Labelling efficiency (LE %) is an important metric for assessing direct cell labelling agents, as it measures the amount of radioactivity associated with cells after the labelling process. It is typically expressed as a percentage and is calculated by dividing the cell-associated activity by the cell-associated activity plus the activity in the supernatant. Additionally, other units of measurement such as activity/cell, percentage activity added per milligram of protein, or a ratio of intracellular/extracellular radioisotope concentration may be used to provide additional information. A high labelling efficiency is desirable to reduce the waste of expensive radionuclides and minimise purification steps. The calculation and comparison of cellular uptake of radiotracers should be carefully

considered for each radiotracer, both when designing studies and interpreting results from the literature. The importance of labelling efficiency lies in its ability to provide a measure of the accuracy, efficiency and effectiveness of the direct cell labelling process, which can be utilised for various biological mechanisms and therapeutic effects *in vivo*.[29],[31],[341]

- **Cellular retention of the radiolabel:** Direct cell radiolabelling is a technique that employs radiotracers to study cellular function. A key aspect of this method is ensuring that the radiotracer is retained within or on the surface of the cells after the radiolabelling process has been completed. This is critical because radioactive emissions cannot be controlled, and all radiotracer signals will be acquired by the detector, regardless of their origin. To mitigate this issue, several strategies must be employed. The first strategy is to optimise the retention of the radionuclide throughout the study by considering the interactions between the radiotracer and various cellular components, as well as its metabolism within the cell. Additionally, it is essential to ensure that the radiotracer used does not cause significant damage to the cells. The second approach is to eliminate any unincorporated radiotracer by washing the cells before further use, *in vitro* or *in vivo*, ensuring that the radioactivity is associated with the cells of interest. Cellular retention, which is calculated similarly to labelling efficiency, is a measure of the ability of cells to retain the radiolabel over time, determining the duration and intensity of the radiolabel's signal, which can impact the accuracy and sensitivity of imaging or therapeutic approaches. Factors that influence cellular retention include the stability of the radiolabel, the rate of clearance by the body, and the properties of the cells themselves.[29],[342],[343]

- **Cell viability and functionality:** Methods of direct cell labelling must not adversely affect target cell viability, proliferation, movement, and behaviour. This is because the radioactive signals generated by directly labelled cells do not indicate whether the cells are

alive or functioning normally. This is significant because cells that are dying or dead have different circulating patterns and release their radiolabel more quickly, leading to misleading images. Assessing the damage that the radiolabelling method may cause to the target cells over time, ideally corresponding to the desired *in vivo* imaging time frame, is thus essential. Additionally, the functionality of radiolabelled cells must also be ensured, as methods that may impair the ability of cells to perform their normal functions, such as CAR T cells, would limit the effectiveness of imaging or therapeutic approaches. The impact of radiolabelling on cell viability and functionality can be caused by the radiotracer, the labelling conditions, and the chemical compounds used to mediate radiolabelling; thus, performing suitable controls in the absence of radioactivity to establish the potential cause for any observed effects on cell viability or functionality is also critical.[29],[342],[343]

Although numerous publications have addressed the labelling of cells with [89]Zr-oxine [34],[35] and [89]Zr-DFO-NCS [36],[37], direct comparisons between these two cell labelling methods remain limited. A study conducted in 2021 by Friberger provides an insightful *in vitro* comparison of these methodologies.[38] In addition, further research by Friberger in 2023 expands upon this comparison by investigating the efficacy of these two labelling techniques *in vivo*.[39] Therefore, part 1 of this chapter presents initial attempts at labelling lymphocytes with [89]Zr-oxine and [89]Zr-DFO-NCS complexes and tracking the labelled cells *in vivo* via PET/CT imaging in a mouse model. Additionally, part 2 of this chapter focuses on the development of the labelling method of [89]Zr-oxine and EL4 cells for pre-clinical *in vivo* PET imaging in wild-type mice, intending to achieve satisfactory labelling efficiency, optimal survival and detection of labelled cells. The development of the labelling method involved optimisation of the parameters that were not standardised in our previous radiolabelling experiments listed in part 1 of this chapter. This included the initial amount of [89]Zr-oxine activity per constant cell count, duration of the cell labelling reaction, oxine concentration

(mg/ml) in cell suspension, type of medium for suspending cells during cell labelling reaction time, type of cell labelling reaction and incubation vs shaking cells during cell labelling. As part of the development of ^{89}Zr-oxine cell labelling and EL4 cells, variation in cell viability due to the absence of a suitable cell culture hood was also evaluated.

Types of cells	Purpose	Duration	Labelling efficiencies (%)	Reference
Bone marrow cells	*In vivo* tracking and quantification in a bone marrow transplantation model	7 days	26 - 30	[311]
Dendritic cells (DCs), activated **cytotoxic T cells** (CTLs), **natural killer cells** (NKs)	*In vitro* labelling study and *in vivo* tracking of CTLs to B16-OVA melanoma tumours	7 days	43.9 ± 17.4 (DCs), 13.0 ± 1.4 (naïve CTLs)	[310]
Human CD19+ CAR T cells	Trafficking of intraventricular injected IL13Ra2-CAR T cells to tumour sites	7 days	75 ± 17	[325]
Mesenchymal Stem cells (MSCs) transduced to express TNF-related apoptosis inducing ligand (TRAIL)	*In vivo* tracking and biodistribution of MSC-TRAILs to mesothelioma tumours	7 days	43.0 ± 3.6	[323]
Natural killer cells	*In vivo* tracking and biodistribution in healthy rhesus macaques	7 days	Not explicitly quantified	[328],[344]
Vγ9Vδ2 subtype of human **γδ-T cells**	*In vivo* tracking of γδ-T cells in a xenograft model of breast cancer	7 days	46.6 ± 3.4	[319]

Table 3-1: Applications of ^{89}Zr-oxine in preclinical cell labelling and imaging studies.

3.2   Methods and materials:

3.2.1   Part 1: Series of initial attempts for cell labelling experiments

Each series of experiments involved isolating specific cells (CD8 T cells or mixed lymphocytes) from the spleens and lymph nodes of donor mice on the day of the radiolabelling experiment. The details of the cell isolation procedures are fully discussed in Chapter 2. The cells were prepared for labelling by centrifuging (250 g or 350 g as per Table 3-2) for 5 min at room temperature and discarding the supernatant. Radiolabelling was initiated using specific amounts of ^{89}Zr-oxine or ^{89}Zr-DFO-NCS (as per Table 3-2) per calculated cells in PBS. The radiolabelling reactions were performed in a thermomixer for 30 min or 1 h (as per experiment) at 37 °C and a shaking speed of 300 or 550 rpm (as per Table 3-2). Immediately after the cell labelling reaction, the cells were spun and the supernatants were discarded. The cells were then washed with PBS to remove unattached ^{89}Zr, and radioactivity was measured in both cell pellets and supernatants after each wash to calculate labelling efficiency (LE) %. Cell number and viability were determined using the trypan blue assay or automated cell counter. When successful cell radiolabelling was obtained, radiolabelled cells were intravenously injected into recipient mice, and PET/CT images were acquired at various time points after injection. Each experiment faced unique challenges, which led to modifications in subsequent experiments, as outlined in Table 3-3.

3.2.1.1 Series 1:

This series aimed to radiolabel freshly isolated CD8 T cells with ^{89}Zr-oxine and ^{89}Zr-DFO-NCS complexes to allow parallel comparison of both ^{89}Zr-oxine labelled CD8 T cells and ^{89}Zr-DFO-NCS labelled CD8 T cells *in vitro* and *in vivo*. Unfortunately, unsatisfactory cell labelling

results, including low efficiency and the absence of viable labelled cells meant the experiment had to be terminated and the recipient mice were not injected.

3.2.1.2 Series 2:

In response to the unsatisfactory outcomes of series 1, this series is a second attempt at a side-by-side comparison of the two labelling approaches for ^{89}Zr complexes (^{89}Zr-oxine and ^{89}Zr-DFO-NCS) with CD8 T cells. However, because of unacceptable viability results of the isolated cells, the experiment had to be prematurely ended before fulfilling its goals.

3.2.1.3 Series 3:

The purpose of this series was to radiolabel freshly harvested mixed lymphocytes, instead of the CD8 T cell sub population, thus avoiding the extra cell handling processes required to isolate and purify the CD8 T cells. Cells were radiolabelled with ^{89}Zr-oxine and ^{89}Zr-DFO-NCS successfully, allowing us to proceed and inject the radiolabelled cells into recipient mice. However, the intravenous injections were only successful in mice receiving ^{89}Zr-DFO-NCS labelled cells (n = 2), and PET/CT images were acquired for those mice to allow for *in vivo* trafficking of the labelled cells, unlike the case with mice receiving ^{89}Zr-oxine labelled cells (n = 2).

3.2.1.4 Series 4:

In this series, we aimed to validate the cell labelling results and *in vivo* distribution of ^{89}Zr-DFO-NCS labelled lymphocytes obtained from series 3. Additionally, to label lymphocytes with the ^{89}Zr-oxine complex to allow for comparison between both labelling methodologies

and to compare between ^{89}Zr-oxine labelled cells and ^{89}Zr-DFO-NCS labelled cells *in vivo*. Unfortunately, we were unable to inject radiolabelled cells into recipient mice, and the experiment had to be terminated due to unsatisfactory cell labelling results, including insufficient uptake of the radiolabelled cells.

3.2.1.5 Series 5:

To achieve successful cell labelling for *in vivo* monitoring of lymphocytes labelled with the ^{89}Zr-oxine complex, this series involved labelling mixed lymphocytes exclusively with ^{89}Zr-oxine. However, because of poor quality tail vein injections in the recipient mice, the study was terminated without acquiring PET/CT images.

3.2.1.6 Series 6:

To address the injection failures in series 5, this series aimed to repeat the later experiment to achieve successful radiolabelling of lymphocytes with ^{89}Zr-oxine complex and to allow *in vivo* monitoring of ^{89}Zr-oxine labelled lymphocytes. In this series, the viability of the ^{89}Zr-oxine labelled lymphocytes was very low (most of the labelled cells were dead cells). Accordingly, the plan of this series was modified to maximise the use of the obtained labelled cells. Therefore, we proceeded and successfully injected the labelled cells into recipient mice intravenously to monitor the *in vivo* distribution of the injected low viability labelled cells. PET/CT images were acquired at 0 h, 23 h, 48 h, 138 h, and 186 h after tracer administration, (n = 1).

3.2.2 Part 2: Series of labelling optimisation experiments in the EL4 cell line

After the previous radiolabelling failures, a series of *in vitro* only labelling optimisation experiments were carried out on a readily available test cell line.

3.2.2.1 Optimisation of the starting amount of ^{89}Zr-oxine per constant EL4 cell count (MBq/cell count)

In this experiment, we aimed to evaluate the effect of changing the amount of starting ^{89}Zr-oxine activity per constant El4 cell count on the labelling efficiency and labelled cell viability. Furthermore, we aimed to determine the amount of ^{89}Zr-oxine start activity that would result in acceptable cell labelling efficiency while preserving the viability of labelled cells. This experiment was performed over more than one day based on the availability of ^{89}Zr-oxine activity.

In total, 15 samples each containing 10×10^6 EL4 cells were loaded with ascending amounts of ^{89}Zr-oxine activity, ranging from 8 to 41 MBq in 2 ml of PBS. The cell labelling reaction between the EL4 cells and the ^{89}Zr-oxine complex was then started for 30 min at 37 $^{\circ}$C and a mixing speed of 550 rpm using a thermomixer. Cells were centrifuged immediately following the reaction. Supernatants were discarded and cells were washed up to three times with 1 ml of PBS to remove any unlabelled ^{89}Zr-oxine. The supernatant activity after every wash and the final cell pellet activity were measured using a dose calibrator set on the 465 setting to calculate LE %. LE % was calculated as the percentage of radioactivity in the final cell pellet compared with the total activity of the cell pellet and supernatants combined. The labelled cells in PBS were then transferred to a new tube to determine their count and viability using the manual Trypan Blue method. Table 3-4 presents experimental details and results for the 15 samples

involved in the optimisation of the starting amount of ^{89}Zr-oxine per constant cell count (MBq/cell count).

3.2.2.2 Optimisation of the labelling period between ^{89}Zr-oxine and EL4 cells

The process of cell labelling involves the addition of a tracer to cells *in vitro*, followed by an incubation period to allow the cells to take up the radioactive tracer. From this point on, it is important to determine the optimal cell labelling reaction timing that will maximise radiolabelling efficiency while allowing the labelled cells to preserve their viability. Thus, in this experiment, two cell labelling periods of 15 and 30 min were evaluated to determine their effects on the labelling efficiency and viability of labelled cells.

In total, six samples each containing 10×10^6 EL4 cells were loaded with ^{89}Zr-oxine activity in 2 ml of PBS buffer. On three of the six samples, radiolabelling reactions were conducted for 15 min. On the other three samples, radiolabelling reactions were conducted for 30 min. Both cell labelling reactions were performed at 37 $^{\circ}$C and 550 rpm using a thermomixer. The cells were centrifuged immediately after the reaction, and the supernatants were discarded. The cells were washed with 1 ml of PBS three times to eliminate any unlabelled ^{89}Zr-oxine, and then transferred to new tube. Labelling efficiency, labelled cell count and viability were determined. Table 3-5 presents details and results for the six samples that were involved in the optimisation of the labelling period between ^{89}Zr-oxine and EL4 cells.

3.2.2.3 Optimisation of the oxine concentration in the El4 cell suspension in the absence of radioactivity (mg/ml)

According to our cell labelling optimisation experiments in sections 3.2.2.1 and 3.2.2.2, there was a variation in the oxine concentration among the tested samples. This variation was due to differences in the yield of ^{89}Zr-oxine that was recovered following the ^{89}Zr-oxalate and oxine reactions. Consequently, we were unable to determine whether the results achieved for the LE % and labelled cell viability were achieved through optimisation of the cell labelling parameters or variation in the oxine concentration (mg/ml) among tested samples. Because of this, we could not tell if the results we observed were the result of the cell labelling parameters we were testing, such as the starting dose per cell count and the duration of the cell labelling reaction, or if the variation in oxine concentration (mg/ml) among tested samples contributed to the results. Thus, this experiment was designed to mimic the conditions under which cells are labelled without utilising radioactivity. The experiment tested five oxine concentrations ranging from 0.5 mg/2 ml to 2.5 mg/2 ml of PBS, with three repetitive samples per tested oxine concentration.

On the day of the experiment, a fresh oxine solution was prepared (1mg/ml) in the preclinical laboratory, to mimic the steps involved in radiolabelling extraction experiments, the oxine solution was aliquoted into individual sample tubes. The chloroform solution was then evaporated with dried air. The remaining oxine powder at the bottom of the tube was then dissolved with 20 µl of DMSO and 2 ml of PBS for each sample. Five oxine concentrations, 0.5, 1, 1.5, 2, and 2.5 mg per 2 ml, were prepared in triplicate. A total of 15 samples were prepared with five different oxine concentrations. These samples were then used to resuspend cell pellets containing 10×10^6 EL4 cells for mock cell labelling.

The samples were then placed in a thermomixer, where reactions between the EL4 cells and oxine were performed for 30 min at 37 $^\circ$C and a mixing speed of 550 rpm. Cells were centrifuged immediately after the reaction was completed. Supernatants were discarded, and cells were washed three times with PBS before being transferred into a new tube. Cells were counted and viability was determined using an automated cell counter. Table 3-7 includes experimental details and results related to the optimisation of the oxine concentrations (mg/2 ml) in the cell suspension when no ^{89}Zr-oxine radioactivity was involved.

3.2.2.4 Comparison between the effects of suspending EL4 cells in complete medium (DMEM medium supplemented with 4 mM L-glutamine, 10 % FCS, 100 IU penicillin, 100 µg/ml streptomycin and 1 mM sodium pyruvate) and PBS on cell viability and cell yield in the absence of radioactivity

This study aimed to determine the best medium for suspending EL4 cells during the labelling reaction with the ^{89}Zr-oxine complex for optimal cell labelling results. A comparison was made between the effects of suspending EL4 cells in a complete growth medium (DMEM medium supplemented with 4 mM L-glutamine, 10 % FCS, 100 IU penicillin, 100 µg/ml streptomycin and 1 mM sodium pyruvate) and those in PBS buffer on cell viability and cell yield. The medium optimisation experiment took place in the main tissue culture laboratory where EL4 cells had been cultured and grown in sterile conditions. Six samples were prepared for this study with 10×10^6 EL4 cells per sample. Three samples were loaded with 2 ml of complete growth medium and the other three samples with 2 ml of PBS. All samples were then incubated in a CO_2 incubator at 37 $^\circ$C simultaneously for 30 min. Cells were centrifuged immediately after the incubation period. Supernatants were discarded, and cells were washed three times with 1 ml of PBS before being transferred into a new tube. Cells were counted and viability was determined using an automated cell counter. A summary of the details and results for the

six samples that were used in the comparison between suspending the EL4 cells in two media and incubating them for 30 min at 37 $^{\circ}$C in a CO_2 incubator on cell viability in the absence of radioactivity is presented in Table 3-9.

3.2.2.5 Optimisation of the incubation method for EL4 cells in the absence of radioactivity

The purpose of this experiment was to optimise the incubation type of EL4 cells in the absence of ^{89}Zr-oxine radioactivity. In terms of the incubation type of the cells, we compared incubating cells in a cell incubator with shaking cells at a particular speed using a thermomixer. Each cell incubation type was performed for 30 min at 37 $^{\circ}$C. There were two shaking speeds tested: 300 and 550 rpm.

Nine samples were prepared for this study. Each sample had 10×10^6 EL4 cells in a complete growth medium in 15 ml Falcon tubes. In the preclinical laboratory, cells were centrifuged at 350 g for 5 min at room temperature and their supernatants were removed. Subsequently, the samples were suspended in 2 ml of PBS. Three samples were incubated at 37 $^{\circ}$C in a cell incubator for 30 min. The other six samples were placed in a thermomixer. Of the six samples, three were shaken at a speed of 300 rpm, whereas the other three were shaken at 550 rpm. The six samples were shaken for 30 min at 37 $^{\circ}$C. 30 minutes later, the nine cell samples were centrifuged and their supernatants were discarded. Cells were washed three times with 1 ml of PBS before being transferred into new tubes. Cells were counted, and viability was determined with an automated cell counter. Table 3-10 presents results for the optimisation of the incubation methods of EL4 cells in the absence of radioactivity.

3.2.2.6 Handling and incubating of EL4 cells in two labs, one of which lacks a class II cell culture hood, to determine the effects of the absence of a cell culture hood on the cell viability.

The culturing and growing of the EL4 cells that were used in the optimisation of the cell labelling experiments took place in the main tissue culture laboratory of the Immunity and Infection department (I & I). To do so, a class II cell culture hood was used to create a sterile environment in the main tissue culture lab. The optimisation experiments of the radioactive cell labelling techniques were taking place in the preclinical laboratory lab at PETIC, where there was no cell culture hood. Thus, the work was not completely performed under sterile conditions. Therefore, the goal of this experiment was to apply some basic cell culture procedures to two groups of cells in two different labs, one of which did not have a cell hood, to see how that would affect cell viability.

A total of six samples were prepared. Each sample contained 10×10^6 EL4 cells in a complete growth medium contained in 15 ml Falcon tubes. Three cell samples were allowed to complete the whole experiment in the main tissue culture lab in I & I, where all the cell work was done in the cell culture hood. In the pre-clinical lab, the remaining three cell samples were taken and used in the same way as the ones in the I & I department, but without a cell culture hood.

These procedures were conducted on the cells from both groups. The cells were centrifuged at 350 g for 5 min at room temperature, and their supernatants were removed. The cells were then suspended in 2 ml of complete medium. The cells were then incubated in a 5 % CO_2 incubator at 37 °C for 30 min. 30 minutes later, the cells were centrifuged, and the supernatants were discarded. The cells were then washed three times with 1 ml of PBS before being transferred into new tubes. Cell viability was determined by counting the cells using an automated cell

counter. Table 3-11 presents details and results of the handling and incubation of EL4 cells in two laboratories, one of which did not have a class II cell culture hood for studying the effect of the absence of a cell culture hood on the viability of cells.

3.2.2.7 Applying the optimised parameters to the radiolabelling of EL4 cells with ^{89}Zr-oxine complex

In this experiment, we applied all the optimised cell labelling parameters as determined by the earlier experiments in this chapter to label the EL4 cells with the ^{89}Zr-oxine complex. The cell labelling results after optimisation will be then evaluated in terms of labelling efficiency, cell viability and cell yield.

Three samples were prepared in the following composition: 10×10^6 EL4 cells suspended in 2 ml complete growth medium were labelled with 18 MBq of ^{89}Zr-oxine, with an oxine concentration of 0.333 mg/2 ml in the final cell suspension. The cell labelling reaction was carried out for 30 min at 37 $^{\circ}$C and a mixing speed of 350 rpm using a thermomixer. Cells were centrifuged immediately after completion of the cell labelling reaction for 5 min at RT and 350 g, and supernatants were discarded. Labelled cells were washed with 1 ml PBS up to three times to remove any unattached ^{89}Zr-oxine and the radioactivity of the cell pellets and supernatants were then measured after each wash to evaluate the radiolabelling efficiency. Labelled cells were then transferred to a new Eppendorf tube to measure cell count and viability. Cells were counted and viability was measured using an automated cell counter. The labelled cell samples were then transferred into cell flasks in a complete growth medium and incubated in a CO_2 cell incubator at 37 $^{\circ}$C to be monitored *in vitro* after cell labelling. ^{89}Zr-oxine labelled EL4 cells were incubated for up to 72 h. The efflux of the ^{89}Zr-oxine activity from the labelled cells, labelled cell count, and viability were evaluated at the following time

points after cell labelling: 0 min, 24 h, 48 h, and 72 h. The experimental details and results of the application of the optimised parameters to the radiolabelling of EL4 cells with the ^{89}Zr-oxine complex are provided in Table 3-12.

3.3   Results

3.3.1   Part 1: Series of cell labelling experiments

3.3.1.1 Series 1:

On the day scheduled for radiolabelling of cells, a total of 1.15×10^8 CD8 T cells with a viability of 72 % were obtained from the splenocytes of eight donor mice. These cells were then subjected to parallel radiolabelling reactions for 1 h at 37 °C and a mixing speed of 500 rpm utilising the following composition: 44.4 MBq of ^{89}Zr-oxine per 57.5×10^6 cells and 45.4 MBq of ^{89}Zr-DFO-NCS per 57.5×10^6 cells. The results of the labelling of the CD8 T cells with the zirconium-89 complexes revealed that 0.6×10^6 CD8 T cells with a viability of 13.3 % were labelled with 0.53 MBq of the ^{89}Zr-oxine complex, whereas no viable CD8 T cells were obtained from the of 0.71 MBq of the ^{89}Zr-DFO-NCS complex. The labelling efficiencies were found to be 1.2 % and 1.6 %, while the cell yields were 1.1 % and 2 %, respectively. Due to the unsatisfactory outcomes of cell labelling, including poor efficiency and the absence of viable labelled cells, the experiment was stopped at this point.

3.3.1.2 Series 2:

Using a negative selection kit and LS columns from StemCell Technologies, the isolation of CD8a+ T cells from the spleens of six donor mice was unsuccessful. Despite a pre-sorting stage

yielding 45 million T cells with a viability rate of greater than 90 %, counting the cells post-sorting revealed that they were all dead cells. As a result, the intended radiolabelling experiment could not be performed.

3.3.1.3 Series 3:

The outcome of the experiment revealed that 150×10^6 freshly obtained mixed lymphocyte cells, displaying 85 % viability, were isolated from the splenocytes and lymph nodes of two donor mice. The process of labelling the cells with radioactivity was initiated using 37.2 MBq of ^{89}Zr-oxine per 75×10^6 cells in 2 ml of PBS, as well as 62 MBq of ^{89}Zr-DFO-NCS per 75×10^6 cells in 2 ml of PBS. In the radiolabelling of mixed lymphocytes with zirconium-89 complexes, it was determined that 6×10^6 cells displayed 71 % viability and were labelled with 1.9 MBq of the ^{89}Zr-oxine compound, while 8.3×10^6 cells with a viability of 81.4 % were labelled with 3.1 MBq of the ^{89}Zr-DFO-NCS compound. As a result, the cell labelling efficiency was found to be 5 % for both cell labelling methods, with a cell yield of 8 % for the ^{89}Zr-oxine method and 11 % for the ^{89}Zr-DFO-NCS method. Additionally, it was observed that an amount of 4 MBq and 5 MBq of activity was affixed to the walls of the primary reaction tubes between the cells and the ^{89}Zr-oxine and ^{89}Zr-DFO-NCS complexes, respectively.

The quality of the tail vein injections for both recipient mice that were injected with the ^{89}Zr-oxine labelled lymphocytes was poor and resulted in tissue infiltrated injections, Figure 3-1. On the other hand, both mice that were injected with ^{89}Zr-DFO-NCS labelled lymphocytes received excellent tail vein injections, Figure 3-2. Accordingly, a PET/CT imaging series was performed after intravenous injection of ^{89}Zr-DFO-NCS labelled lymphocytes into mice (n = 2) to allow for non-invasive tracking of the injected cells. At 20 h post-activity administration, most of the activity was accumulated in the liver (%IA: 28.68 % ± 8.03 %), followed by the

skeleton (%IA: 9.23 % ± 0.05 %), lungs (%IA: 7.83 % ± 6.44 %), and kidneys (%IA: 7.49 % ± 7.07 %). Approximately 306 h after tracer administration, more activity was accumulated in the liver (%IA: 54.75 % ± 8.46 %), followed by the kidneys (%IA: 7.77 % ± 5.79 %), skeleton (%IA: 7.36 % ± 1.15 %), and spleen (%IA: 5.15 % ± 0.02 %), with minor accumulations in the lungs (%IA: 1.69 % ± 1.36 %). One of the most interesting and unexpected findings was the multiple focal hot spots of activity that were randomly distributed throughout the bodies of both mice, as illustrated in Figure 3-2. A detailed quantitative representation of the PET scans acquired for the mice at 20 h, 44 h, 68 h, 140 h, 164 h, and 306 h after intravenous injection of ^{89}Zr-DFO-NCS labelled lymphocytes is shown in Figure 3-3.
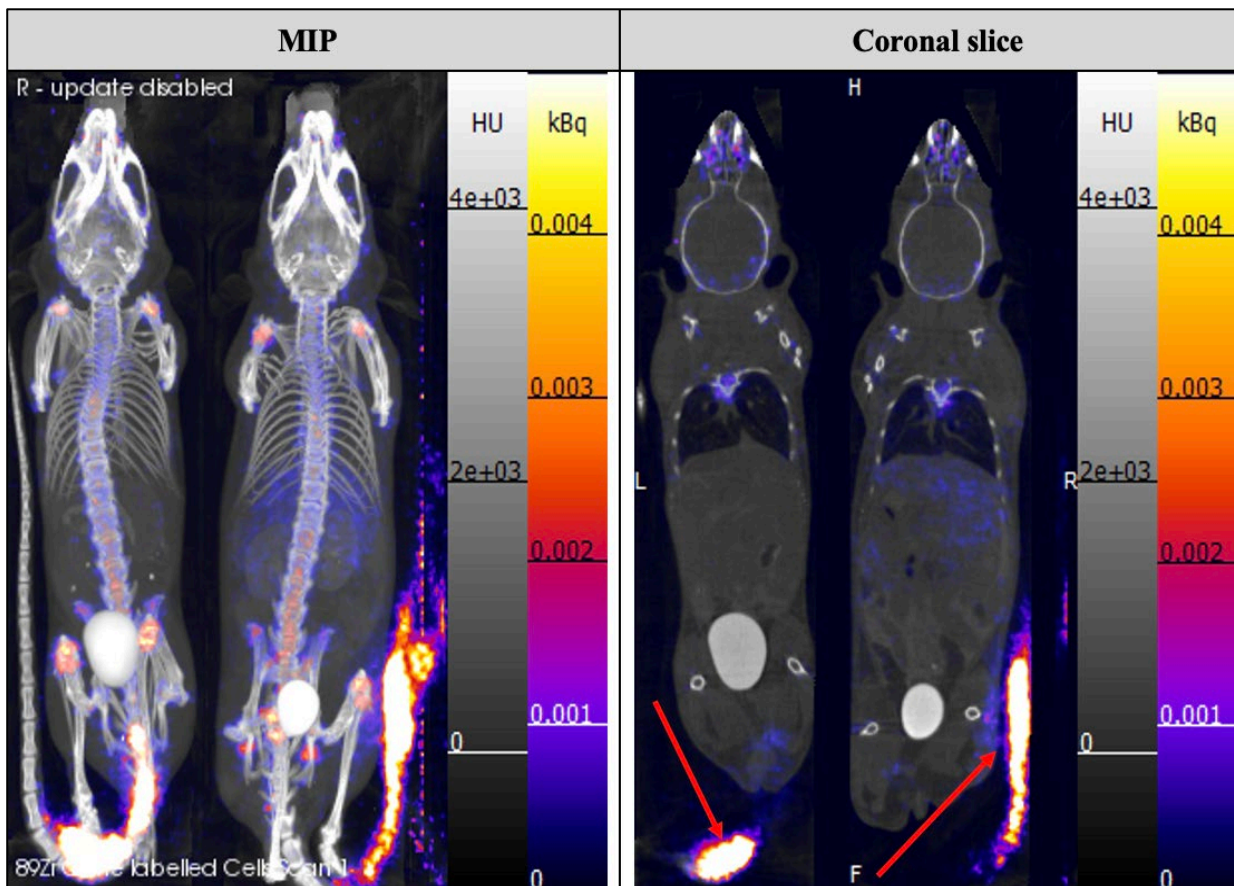
Figure 3-1: PET/CT imaging of ^{89}Zr-oxine labelled lymphocytes in a mouse model. MIP view and Coronal slice view of PET/CT image acquired 0 – 30 min after administration of radiolabelled cells into a C57BL/6 mouse. Most of the injected activity was accumulated at the site of injection because of the poor quality of tail vein injection, as indicated by arrows. This figure is related to the series 3 experiment, (n = 2).
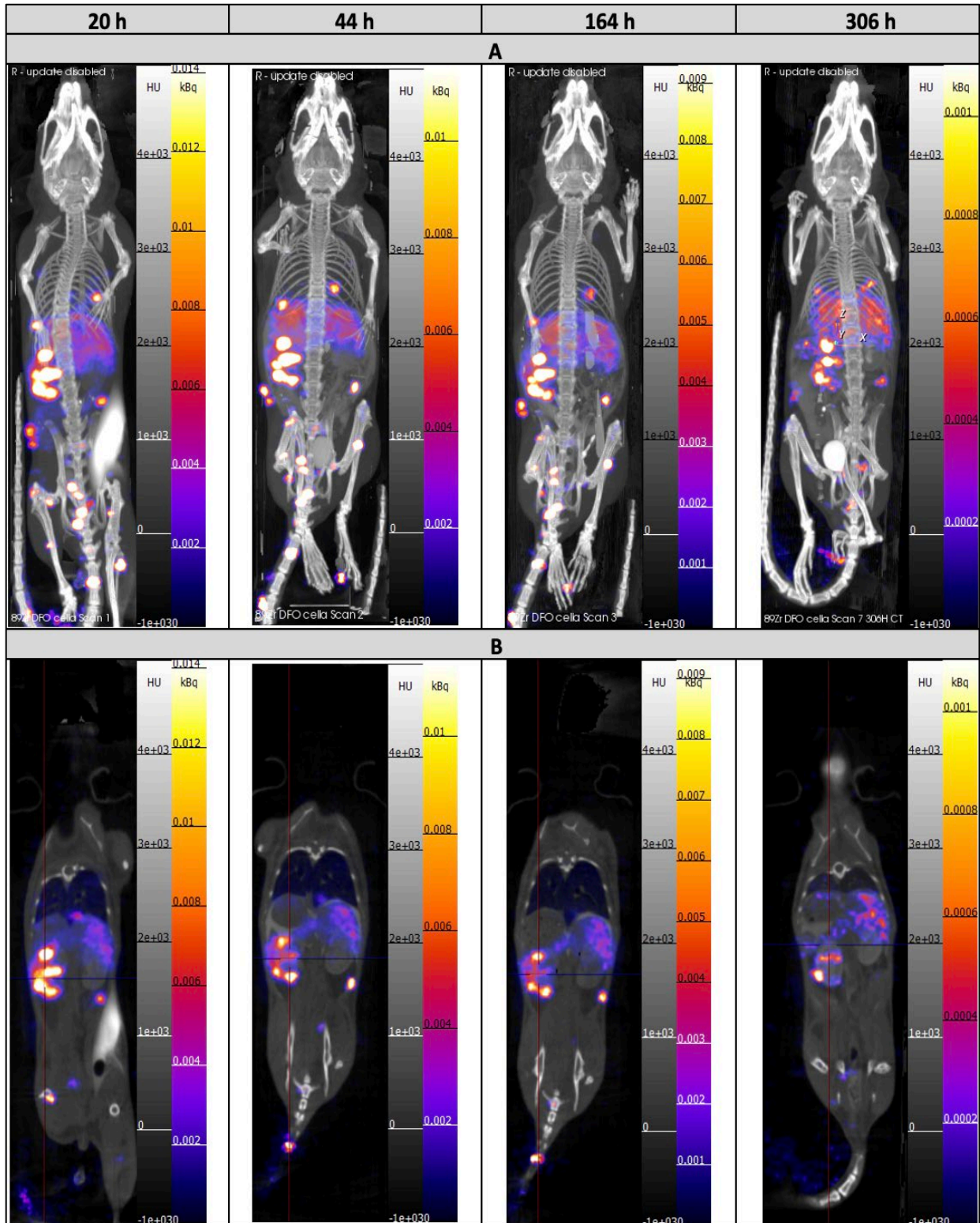
Figure 3-2: *In vivo* **tracking of** [89]**Zr-DFO-NCS labelled lymphocytes in healthy mice**. Series of whole-body **(A)** Maximum intensity projection (MIP) view PET/CT and **(B)** PET/CT coronal slice images of a C57BL/6 mouse injected with surface-labelled cells were acquired at 20 h, 44 h, 68 h, 140 h, 164 h, and 306 h following intravenous injection of the agent (n = 2). PET images are displayed as KBq, and the maximum intensity setting chosen to best highlight tissues of interest in scan 1 was decay corrected forward for each subsequent scan based upon the half-life of [89]Zr. This figure is related to the experiment in series 3.
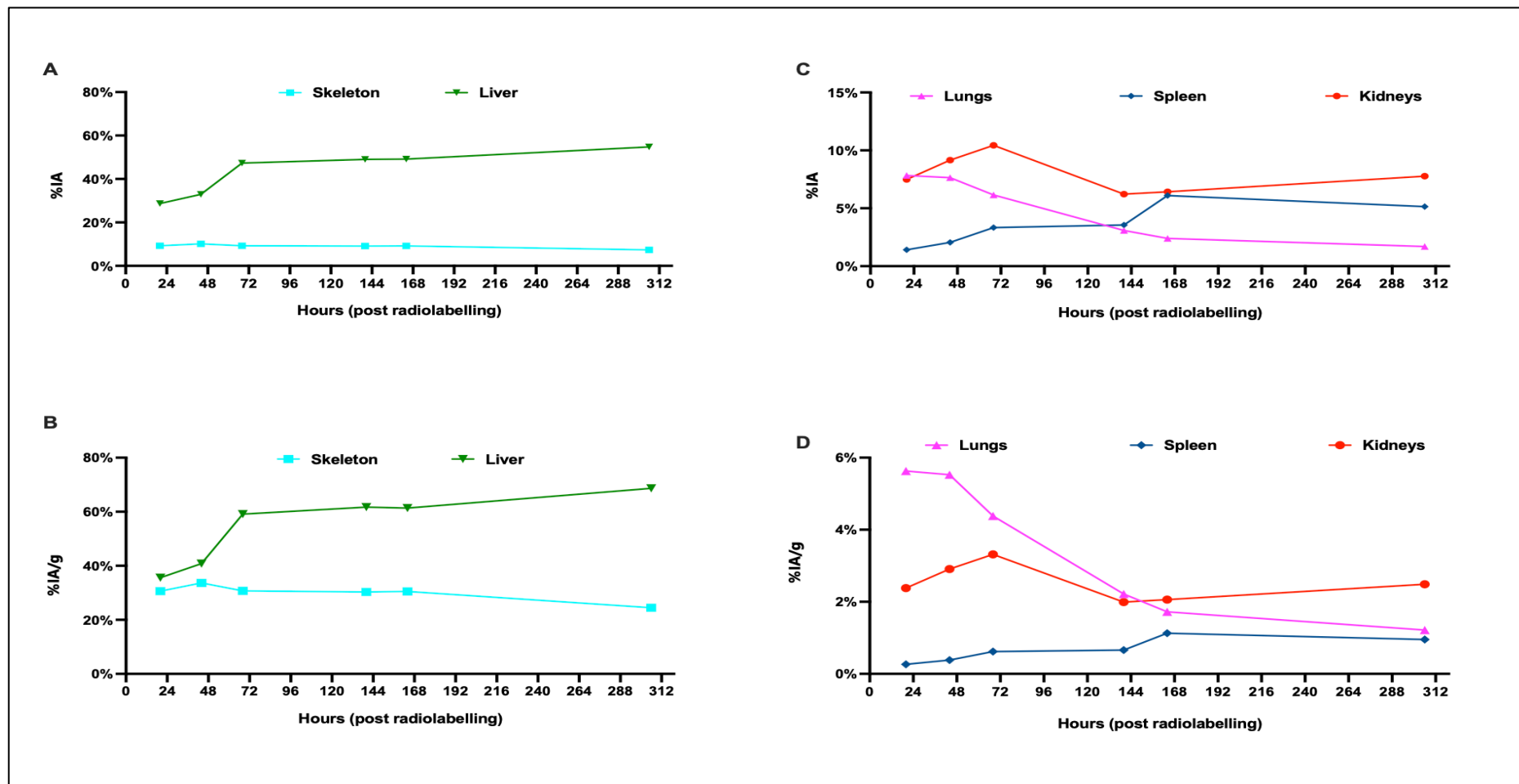
Figure 3-3: Time activity curves (TACs) for *the in vivo* distribution of ^{89}Zr-DFO-NCS labelled lymphocytes in a mouse model imaged with PET/CT. %IA and %IA/g were determined for target organs, skeleton, lung, liver, spleen, and kidneys throughout the experiment. Scans were acquired at 20 h, 44 h, 68 h, 140 h, 164 h, and 306 h following intravenous injection of the tracer. Graphs **(A)** and **(B)** indicate group average TACs of %IA and %IA/g for the skeleton and liver. **(C)** and **(D)** indicate group average TACs of %IA and %IA/g for the lungs, spleen, and kidneys. The displayed data are mean, (n = 2).

3.3.1.4 Series 4:

The experimental findings indicate that 170×10^6 mixed lymphocytes with 93.1 % viability were isolated from the splenocytes of four donor mice on the day of the experiment. The radiolabelling processes were initiated with the addition of 96.5 MBq ^{89}Zr-oxine per 85×10^6 cells in 2 ml PBS and 106 MBq ^{89}Zr-DFO-NCS per 85×10^6 cells in 2 ml of PBS. The radiolabelling of mixed lymphocytes with zirconium-89 complexes led to 14.4×10^6 cells with 82.76 % viability being labelled with 0.33 MBq of the ^{89}Zr-oxine compound, whereas 9.8×10^6 cells with 77.8 % viability were labelled with 2 MBq of the ^{89}Zr-DFO-NCS compound. Accordingly, the labelling efficiencies were 0.34 % and 1.9 %, and the cell yields were 17 % and 11.5 %, respectively. A total of 30 MBq and 49.5 MBq of activity were attached to the walls of the primary tubes (15 ml plastic Falcon tubes), where the radiolabelling reactions occurred between the cells and the ^{89}Zr-oxine and ^{89}Zr-DFO-NCS complexes, respectively. The experiment was terminated at this point because of unsatisfactory cell labelling results.

3.3.1.5 Series 5:

In total, 190×10^6 mixed lymphocytes with 85.08 % viability were isolated from the splenocytes and lymph nodes of three donor mice for use in the radiolabelling experiment. The cell labelling reaction was initiated between 99.1 MBq of ^{89}Zr-oxine and 190×10^6 cells in 4 ml of PBS for 30 minutes at a temperature of 37 $^{\circ}$C and a mixing speed of 550 rpm. As a result, 97×10^6 cells with a viability of 91.88 % were successfully labelled with 9.16 MBq of the ^{89}Zr-oxine compound. Accordingly, the labelling efficiency was 9.2 % and the cell yield was 51 %. A total of 36.4 MBq of activity was attached to the wall of the main tube (15 ml plastic Falcon tube), which was used to label the cells with the ^{89}Zr-oxine complex.

Despite our best efforts, we could not successfully administer the dose via the tail intravenously to mice. This was confirmed by PET/CT images. As expected, the three mice had a high concentration of injected activity in the tail region. The injected activity was predominantly observed in the tail area of the three mice. This strongly indicates that the given intravenous injections were of low quality and were likely to have been administered subcutaneously rather than intravenously. Consequently, no more PET/CT images were acquired, and the experiment was terminated at this stage.

3.3.1.6 Series 6:

A total of 210×10^6 mixed lymphocyte cells with 87 % viability were collected from the splenocytes of four donor mice on the day of the experiment. The cell radiolabelling reaction was then initiated between 210×10^6 mixed lymphocytes and 66 MBq of ^{89}Zr-oxine in 4 ml of PBS for 30 min at a temperature of 37 $^{\circ}$C and a rotation speed of 550 rpm. Consequently, 13.5×10^6 mixed lymphocytes with viability of 13.6 % were labelled with 13.17 MBq of ^{89}Zr-oxine. This resulted in a labelling efficiency of 20 % and a cell yield of 6.5 %. On the wall of the tube, where the main radiolabelling reaction between the cells and the ^{89}Zr-oxine complex was performed, a total of 15.23 MBq of activity was observed.

Following radiolabelling, a wild-type black mouse was successfully injected with 2.25×10^6 lymphocytes that had a viability of 13.6 % and were labelled with 1.41 MBq of ^{89}Zr-oxine through intravenous injection. Following the injection of low-viability lymphocytes labelled with ^{89}Zr-oxine into the mouse, a series of non-invasive PET/CT imaging was conducted to track the *in vivo* distribution of the injected labelled cells, Figure 3-5. PET imaging, 30 min after injection, indicated that the majority of radioactivity was found in the liver (%IA: 23.91 %), with smaller amounts detected in the skeleton (%IA: 5.39 %) and lungs (%IA: 3.92 %).

After 20 h, an increase in radioactivity was observed in the liver (%IA: 34.79 %), followed by the skeleton (%IA:11.40 %) and trace amounts in the kidneys (%IA: 1.75 %). At 136 h, the liver continued to be the main site of accumulation (%IA: 40.66 %), followed by the skeleton (%IA:15.51 %), and minimal amounts were found in the spleen (%IA: 1.69 %) and kidneys (%IA: 1.10 %). Figure 3-4 presents quantitative results of the PET scans taken at 0.5 h – 138 h post- injection of the [89]Zr-oxine labelled low-viability lymphocytes.
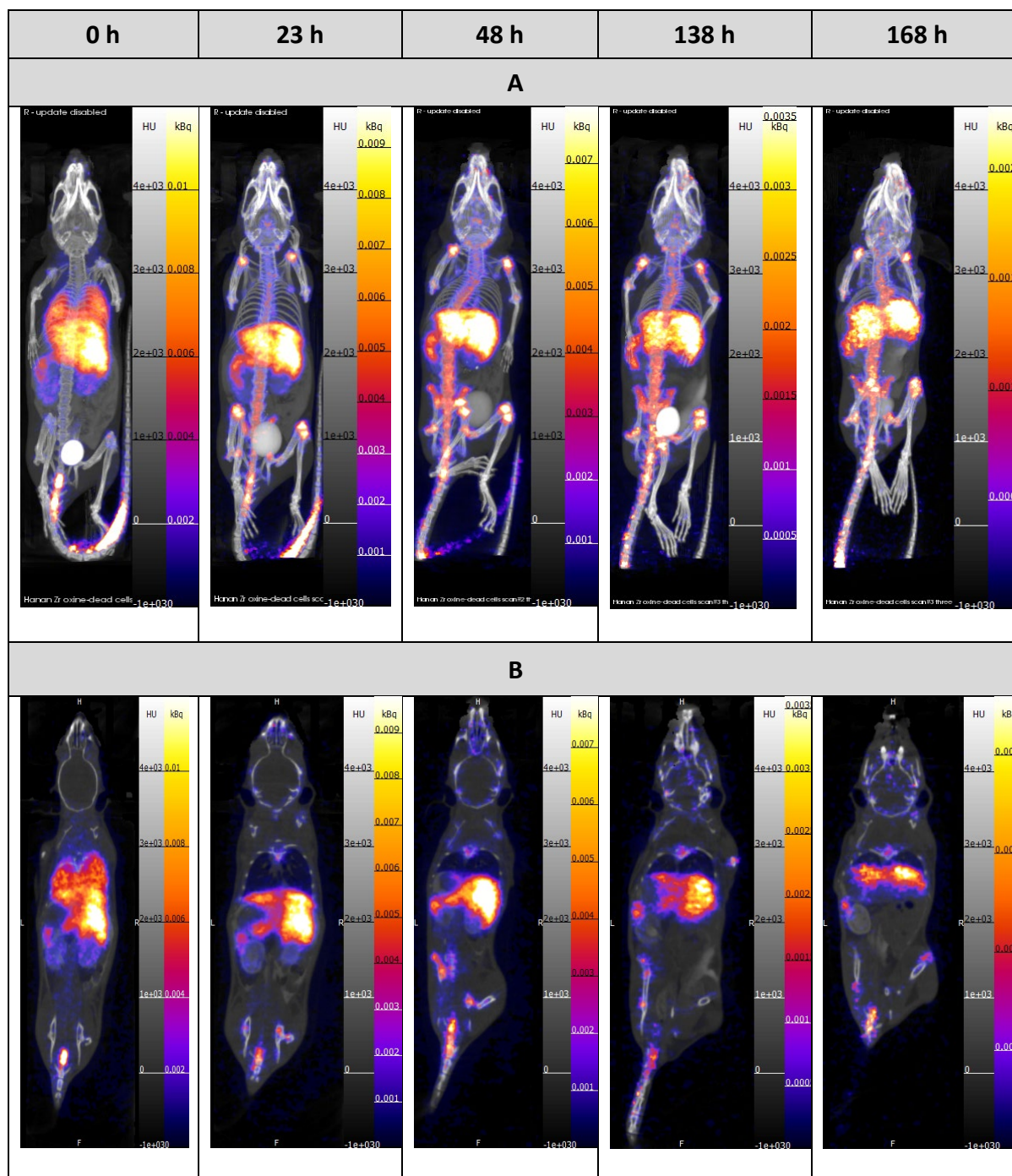
Figure 3-4: *In vivo* **tracking of** [89]**Zr-oxine labelled lymphocytes with low viability in healthy mice.**
Series of whole-body **(A)** Maximum intensity projection (MIP) view PET/CT and **(B)** PET/CT coronal
slice images of a C57BL/6 mouse injected with [89]Zr-oxine labelled lymphocytes with low viability were
acquired at 0 h, 23 h, 48 h, 138 h, and 168 h following intravenous injection of the agent (n = 1). PET
images are displayed as KBq, and the maximum intensity setting chosen to best highlight tissues of
interest in scan 1 was decay corrected forward for each subsequent scan based upon the half-life of [89]Zr.
This figure is related to the experiment in series 6.
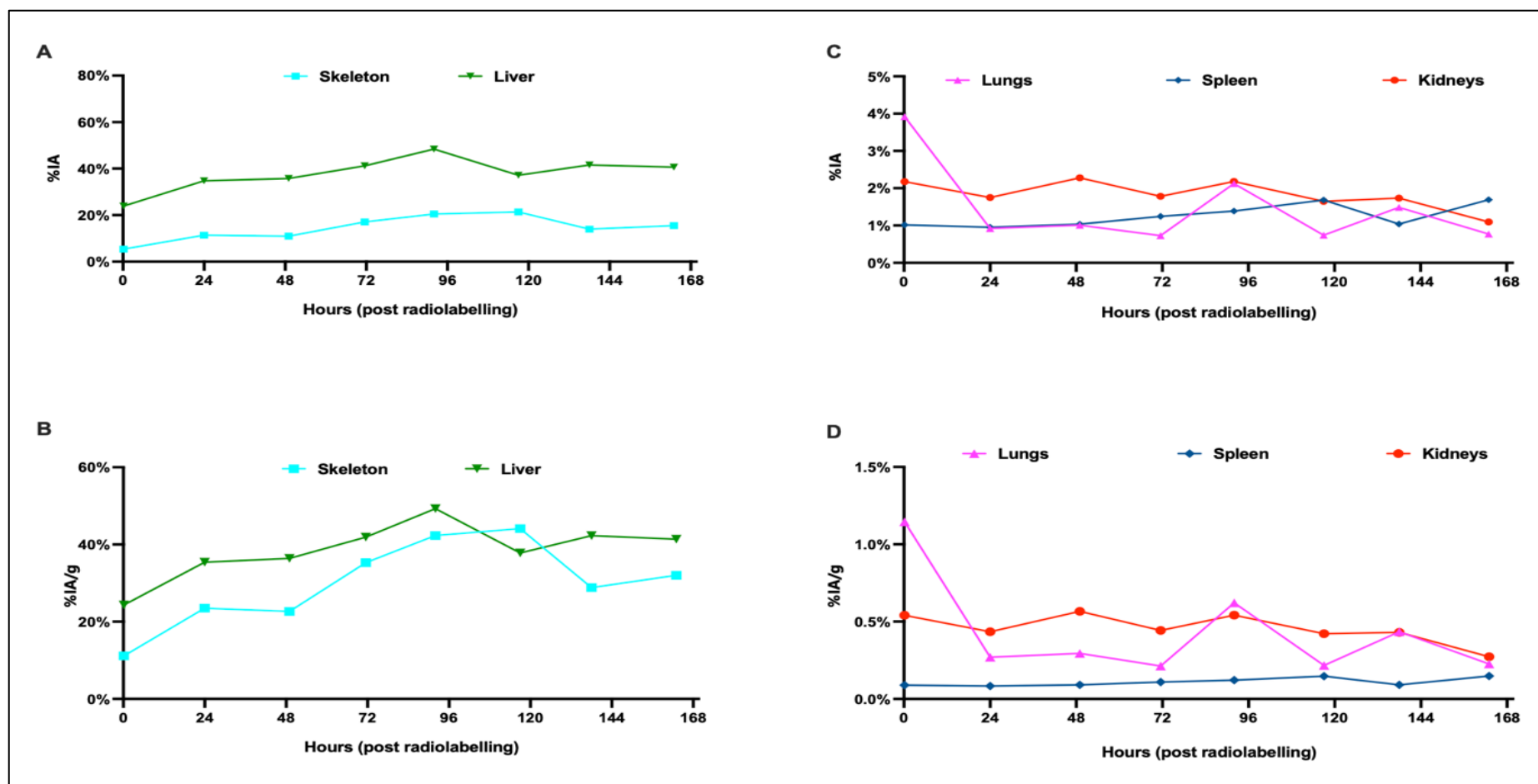
Figure 3-5: Time activity curves (TACs) for the *in vivo* distribution of ^{89}Zr-oxine labelled lymphocytes with low viability in a mouse model imaged with PET/CT. %IA and %IA/g were determined for target organs, skeleton, lung, liver, spleen, and kidneys throughout the experiment. Scans were acquired at 0 h, 23 h, 48 h, 138 h, and 168 h following intravenous injection of the tracer. **(A)** and **(B)** indicate group averaged TACs of %IA and %IA/g for the skeleton and liver. **(C)** and **(D)** indicate group averaged TACs of %IA and %IA/g for the lungs, spleen, and kidneys. The displayed data are mean, (n = 1).

Series No.	Series 1		Series 2	Series 3		Series 4		Series 5	Series 6
Cell type	CD8 T		N/A	Mixed		Mixed		Mixed	Mixed
^{89}Zr complexes	^{89}Zr-oxine	^{89}Zr-DFO-NCS	N/A	^{89}Zr-oxine	^{89}Zr-DFO-NCS	^{89}Zr-oxine	^{89}Zr-DFO-NCS	^{89}Zr-oxine	^{89}Zr-oxine
Start activity (MBq)	44.4	45.4	N/A	37.2	62	96.5	106	99.1	66
Initial cell count (×10⁶)	57.5	57.5	N/A	75	75	85	85	190	210
Initial cell viability (%)	72	72	N/A	85	85	93.1	93.1	85.1	87
Radiolabelling duration (min)	60	60	N/A	30	30	30	30	30	30
Relative centrifugal force (g)	250	250	N/A	350	350	350	350	350	350
Labelled cell count (×10⁶)	0.6	0.4	N/A	6	8.3	14	9.8	97	13.5
Labelled cell viability (%)	13.3	0	N/A	71	81.4	82.76	77.8	91.9	13.6
Labelled cell activity (MBq)	0.53	0.72	N/A	1.9	3.1	0.33	1.9	9.16	13.17
Labelling efficiency (%)	1.2	1.6	N/A	5	5	0.34	1.9	9.2	20
Cell yield (%)	1.1	0.7	N/A	8	11	17	11.5	51	6.5
Cell culture hood[1]	No								

Table 3-2: **Summary of the experimental details and results for the initial attempts to label lymphocytes with ^{89}Zr-oxine and ^{89}Zr-DFO-NCS complexes.**

---

[1] Indicating whether a class II cell culture hood was available for cell labelling experiments in the R&D lab in the pre-clinic PETIC department.

Series No.	Description	Outcome
1	This series aimed to perform parallel labelling experiments on CD8 T cells using ^{89}Zr-oxine and ^{89}Zr-DFO-NCS complexes. However, the experiment was terminated because of unsatisfactory cell labelling results, including low efficiency and the absence of viable labelling cells.	The experiment was terminated because of low efficiency and the absence of viable labelled cells.
2	In response to the unsatisfactory outcomes of the previous experiment, this series involved a side-by-side comparison of two labelling approaches for ^{89}Zr with CD8a+ T cells. However, because of unacceptable viability results of the isolated cells, the experiment had to be prematurely ended.	The experiment was prematurely ended due to unacceptable low viability results of the isolated CD8a+ T cells.
3	The purpose of this series was to radiolabel mixed lymphocytes using both ^{89}Zr complexes. Successful radiolabelling was achieved, and the labelled cells were subsequently injected into recipient mice. However, the injections were only successful in mice receiving ^{89}Zr-DFO-NCS labelled cells, and PET/CT images were acquired for those mice.	Successful radiolabelling of mixed lymphocytes using both ^{89}Zr complexes was achieved. Injections of labelled cells were successful only in mice receiving ^{89}Zr-DFO, and PET/CT images were acquired for these mice.
4	This series aimed to validate the labelling results obtained from a previous study and compare the biodistribution of the labelled lymphocytes with both ^{89}Zr complexes. Unfortunately, the experiment was halted because of insufficient uptake of the radiolabelled cells.	The experiment was halted because of insufficient uptake of the radiolabelled cells.
5	To achieve successful *in vivo* monitoring of lymphocytes labelled with the ^{89}Zr-oxine complex, this series involved re-labelling mixed lymphocytes exclusively with ^{89}Zr-oxine. However, because of poor-quality tail vein injections in the recipient mice, the study was terminated without acquiring PET/CT images.	The study was terminated because of poor-quality tail vein injections in the recipient mice, resulting in the inability to acquire PET/CT images.
6	To address the previous injection failures, this series aimed to repeat the experiment and achieve successful *in vivo* monitoring of lymphocytes labelled with the ^{89}Zr-oxine complex. Because of low cell viability, only one mouse received the labelled cells, and PET/CT images were acquired at different time points after tracer administration.	Because of low cell viability, only one mouse received the labelled cells, and PET/CT images were acquired at different time points after tracer administration.

Table 3-3: Description and outcome of initial attempts at labelling cells with ^{89}Zr-oxine and ^{89}Zr-DFO-NCS complexes.

3.3.2 Part 2: Series of labelling optimisation experiments in the EL4 cell line

3.3.2.1 Optimisation of the starting amount of ^{89}Zr-oxine per constant cell count (MBq/cell count)

To optimise the ^{89}Zr-oxine starting dose per constant EL4 cell count, 15 samples, each of which contained 10×10^6 EL4 cells, were loaded with ascending amounts of ^{89}Zr-oxine activity ranging from 8 MBq to 41 MBq in 2 ml of PBS. This was followed by cell labelling reactions, which were carried out for 30 min at 37 °C and 550 rpm. Table 3-4 presents the experimental details and results for the 15 samples that were involved in optimising the starting amount of ^{89}Zr-oxine per constant cell count (MBq/cell count).

When plotting starting amounts of ^{89}Zr-oxine radioactivity per 10×10^6 EL4 cells alongside labelled cell viability and labelling efficiency it became apparent that these factors were not correlated, Figure 3-6. When searching for factors to explain this surprising result it became apparent that the oxine concentration in the 2 ml PBS cell suspension was not standard across all samples. This was due to the variable efficiency of ^{89}Zr-oxine extraction which meant it was sometimes necessary to combine more than one extract of ^{89}Zr-oxine together to prepare individual cell labelling solutions, particularly for the highest amounts of activity. When the data was re-ordered to plot to rising amounts of excess oxine ligand per 2 ml of labelling solution alongside cell viability it became apparent that there was a threshold of 1.5 mg/2 ml at which there was a clear chemical toxicity of the excess non-radioactive oxine ligand in the labelling solution, Figure 3-7.

The concentration of oxine per cell suspension explains more of the variation in the viability of labelled cells than the amount of ^{89}Zr-oxine activity. In support of this, high labelled cell

viability was observed when oxine concentrations in the suspension were ≤1 mg/2 ml, despite the high starting ^{89}Zr-oxine activity used for labelling the cells, as seen in samples 7 (a) and 7 (b), whilst disappointingly low cell viabilities were seen for sample 1 (a) with a low starting activity of ^{89}Zr-oxine and a 2 mg/2 ml oxine concentration.

Sample	Starting ^{89}Zr-oxine activity (MBq/10×10^6 cells)	Oxine concentration (mg/2 ml)	Labelled cell uptake (MBq)	Labelling efficiency (%)	Labelled cell count (×10^6)	Labelled cell viability (%)
1 (a)	8.3	2.0	1.74	29.0	6.4	33.6
1 (b)	9.7	0.8	3.2	36.4	6.9	69
1 (c)	9.9	0.8	3.52	39.1	6.5	67.6
2	14.0	1.5	2.52	23.9	6.9	34.9
3 (a)	17.1	0.8	5.7	38.7	6.3	76.2
3 (b)	17.9	0.8	5.97	37.1	6.0	75
4 (a)	21.9	2.0	8.07	44.2	6.8	34.2
4 (b)	22.0	1.0	9.35	49.0	6.3	64.5
4 (c)	23.7	2.0	6.47	37.4	6.9	34.7
5 (a)	26.9	1.0	10.7	46.0	6.3	64.5
5 (b)	27.2	1.0	7.15	30.8	6.2	71.3
6	31.3	1.5	3.16	20.7	6.9	25.6
7 (a)	40.7	0.7	14.42	45.9	6.6	70.5
7 (b)	40.9	0.7	9.4	32.1	6.7	69.9
7 (c)	41.1	2.0	8.81	26.5	6.2	33.7

Table 3-4: The experimental details and results for the 15 samples involved in the optimisation of the starting amount of ^{89}Zr-oxine per constant cell count (MBq/cell count).
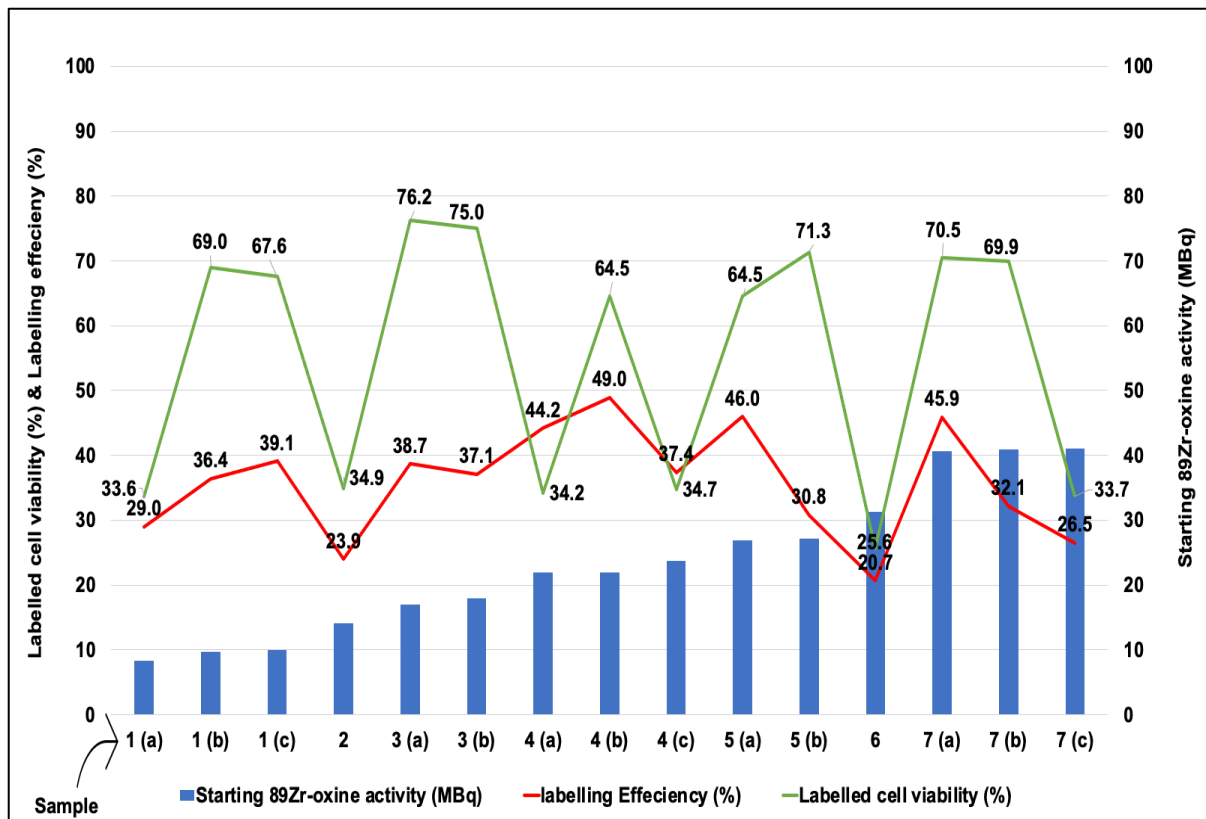
Figure 3-6: The experimental results for the optimisation of the initial amounts of ^{89}Zr-oxine per constant EL4 cell count (MBq/Cell count). An increase in ^{89}Zr-oxine activity per 10×10^6 EL4 cells has no apparent relationship with the viability of labelled cells or LE %.
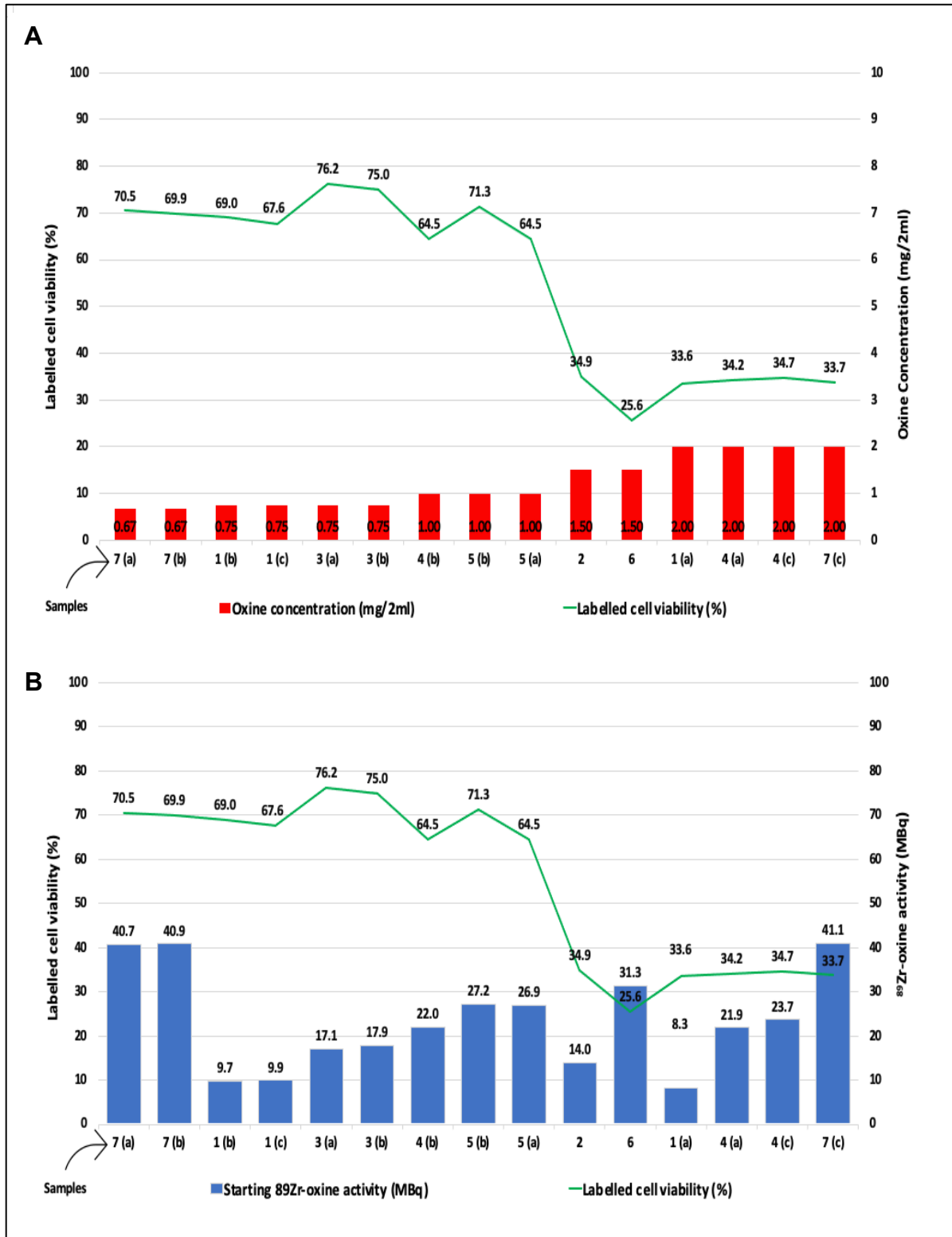
Figure 3-7: Comparative analysis of the oxine concentration (A) and ^{89}Zr-oxine activity (MBq) (B) on the labelled cell viability. The concentration of oxine per cell suspension explains more of the variation in the viability of the labelled cells than the amount of ^{89}Zr-oxine activity. An example of this is the high viability of cells observed in the samples when the oxine concentrations in cell suspensions were ≤1 mg/2 ml, despite the high ^{89}Zr-oxine activity initially used for labelling the cells.

3.3.2.2 Optimisation of the labelling period between ^{89}Zr-oxine and EL4 cells

To optimise the labelling period between the ^{89}Zr-oxine and EL4 cells, six samples, each of which contained 10×10^6 EL4 cells, were radiolabelled with ^{89}Zr-oxine. The experiment compared two labelling periods 15 min and 30 min, with three repeated samples per cell labelling period. In all samples, ^{89}Zr-oxine activity was loaded in 2 ml of PBS, and then cell labelling reactions were performed between ^{89}Zr-oxine and EL4 cells at 37 $^{\circ}$C and 550 g. The average ± SD starting ^{89}Zr-oxine activity for samples 1 (a), 1 (b), and 1 (c) was 11.0 MBq ± 0.1, and 9.3 MBq ± 0.9 for samples 2 (a), 2 (b), and 2 (c). The calculated average labelling efficiencies ± SD were as follows: 31.5 % ± 1.3 %, and 34.8 % ± 5.2 % for samples 1 (a), 1 (b), 1 (c) and 2 (a), 2 (b), 2 (c), respectively. The average viabilities ± SD for the ^{89}Zr-oxine labelled EL4 cells for samples 1 (a), 1 (b), and 1 (c) were 70.0 % ± 4.6 %, and 56.5 % ± 19.9 % for samples 2 (a), 2 (b), and 2 (c), respectively. Table 3-5 presents the details and results for the optimisation of the labelling period between the ^{89}Zr-oxine and EL4 cells. The effects of the two cell labelling periods of 15 min and 30 min on the labelling efficiency and viability of the labelled cells are illustrated in Figure 3-8. The statistical significance of the calculated results was determined by the application of a two-tailed, unpaired t-test, p values < 0.05 were considered significant. Accordingly, no significant difference was found between the effect of the two cell labelling periods on the labelling efficiency and labelled cell viability, Table 3-6.

Sample	^{89}Zr-oxine activity (MBq/10×10^6 cells)	Oxine concentration (mg/2 ml)	Cell uptake (MBq)	Labelling efficiency (%)	Labelled cell count (×10^6)	Labelled cell viability (%)
Cell labelling period of 15 min						
1 (a)	11.1	0.67	2.8	30.2	6.8	68.7
1 (b)	11.0	0.67	2.9	31.4	6.3	75.2
1 (c)	11.0	0.67	3.1	32.8	6.5	66.2
Cell labelling period of 30 min						
2 (a)	8.3	2.00	1.7	29.0	6.4	33.6
2 (b)	9.7	0.75	3.2	36.4	6.9	69
2 (c)	9.9	0.75	3.5	39.1	6.5	67

Table 3-5: **Details and results for the optimisation of the labelling period between ^{89}Zr-oxine and EL4 cells.** Two cell labelling periods were tested: 15 and 30 min. Six samples were involved, each containing 10×10^6 EL4 cells loaded with ^{89}Zr-oxine activity. Three samples were tested per cell labelling period.
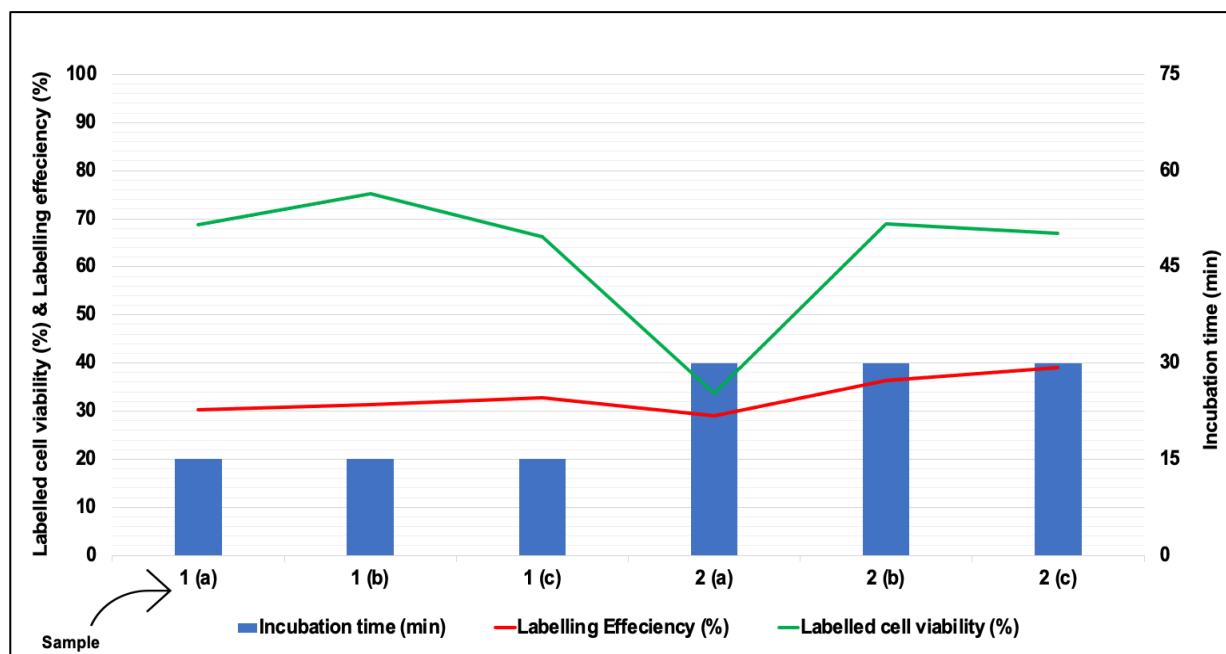
Figure 3-8: The effect of two cell labelling periods of 15 min and 30 min on the labelling efficiency and viability of the labelled cells. The displayed results were obtained by optimising the labelling period between the ^{89}Zr-oxine and EL4 cells. The study involved six samples containing 10×10^6 EL4 cells that were loaded with ^{89}Zr-oxine activity. Three samples were tested for each period of cell labelling.

Unpaired t-test for comparison between two cell labelling periods results	Mean difference (%)	Significant?	Summary	P Value
LE % for 15 min vs LE % for 30 min	3.367	No	ns	0.34
Cell viability for 15 min vs cell viability for 30 min	13.5	No	ns	0.31

Table 3-6: **The results of EL4 cells that were radiolabelled with ^{89}Zr-oxine for 15 and 30 min to assess the effects of the two labelling periods on the labelling efficiency and viability of the labelled cells**. A total of six samples containing 10×10^6 EL4 cells were labelled with the ^{89}Zr-oxine complex. For each period of cell labelling, three samples were tested. This study used a two-tailed, unpaired t-test to calculate statistical significance. P values < 0.05 were considered statistically significant while ns. represents no significance for p values > 0.05.

3.3.2.3 Optimisation of the oxine concentration in the EL4 cell suspension in the absence of radioactivity (mg/ml)

For the experimental optimisation of the oxine concentration in cell suspension in the absence of radioactivity, 15 samples each containing 10×10^6 El4 cells were loaded with different oxine concentrations (mg per 2 ml reaction volume), ranging from 0.5 mg/2 ml to 2.5 mg/2 ml of PBS. The experiment examined five oxine concentrations, with three replicates tested per oxine concentration. The oxine concentrations were as follows: 0.5 mg/2 ml for samples 1 (a-c), 1 mg/2 ml for samples 2 (a-c), 1.5 mg/2 ml for samples 3 (a-c), 2 mg/2 ml for samples 4 (a-c), and 2.5 mg/2 ml for samples 5 (a-c). For the above samples, the average EL4 cell viabilities ± SD were 79.6 % ± 0.7 %, 74.8 % ± 3.0 %, 44.4 % ± 3.4 %, 37.3 % ± 1.5 %, and 34.1 % ± 3.3 %, respectively, Table 3-7. The following significant results were obtained from this experiment: the oxine concentration was inversely correlated with the viability of the cells. However, the oxine concentrations of 0.5 and 1 mg/2 ml did not significantly alter the viability of the cells. The effects of these two oxine concentrations on cell viability were not significantly different. The cell viability ± SD for the cells that were suspended in these oxine

concentrations (0.5 mg/2 ml and 1 mg/2 ml) was 79.6 % ± 0.7 % and 75.73 % ± 2.17 %, respectively. Conversely, when the oxine concentration was increased to 1.5 mg per 2 ml of PBS cell suspension, a significant decrease in the viability of cells by an average ± SD of 31.33 % ± 1.2 % was observed, resulting in an average cell viability ± SD of 44.4 % ± 3.4 %. Cell viability continued to decline significantly when the oxine concentration in the cell suspension reached 2 mg per 2 ml or 2.5 mg per 2 ml, Figure 3-9. Table 3-7 and Figure 3-10 present a detailed statistical comparison of the effects of the five tested oxine concentrations on cellular viability that were carried out using one-way ANOVA with Tukey's multiple comparison test, and statistical significance was calculated. p values < 0.05 were considered statistically significant; * represents $p \leq 0.05$, ** represents $p \leq 0.01$, and *** represents $p \leq 0.001$. ns represents no significance for p values > 0.05.

This experiment has shown that for the ^{89}Zr-oxine cell labelling experiment, the oxine concentration should not exceed 1 mg/2 ml of the cell suspension to avoid a significant reduction in cell viability.

Sample	Starting cell count ($\times 10^6$)	Oxine concentration (mg/2 ml)	Cell viability (%)
1 (a)	10	0.5	80.1
1 (b)	10	0.5	78.8
1 (c)	10	0.5	80
2 (a)	10	1	78
2 (b)	10	1	72.2
2 (c)	10	1	74.1
3 (a)	10	1.5	42.6
3 (b)	10	1.5	42.3
3 (c)	10	1.5	48.3
4 (a)	10	2	35.8
4 (b)	10	2	38.7
4 (c)	10	2	37.4
5 (a)	10	2.5	32.7
5 (b)	10	2.5	37.8
5 (c)	10	2.5	31.7

Table 3-7: **The experimental details and results related to the optimisation of the oxine concentrations (mg/ml) in the cell suspension when no ^{89}Zr-oxine radioactivity was involved**. The oxine concentration within PBS varied between 0.5 mg/2 ml and 2.5 mg/2 ml for 15 samples containing 10×10^6 EL4 cells. Three replications were conducted for each oxine concentration.
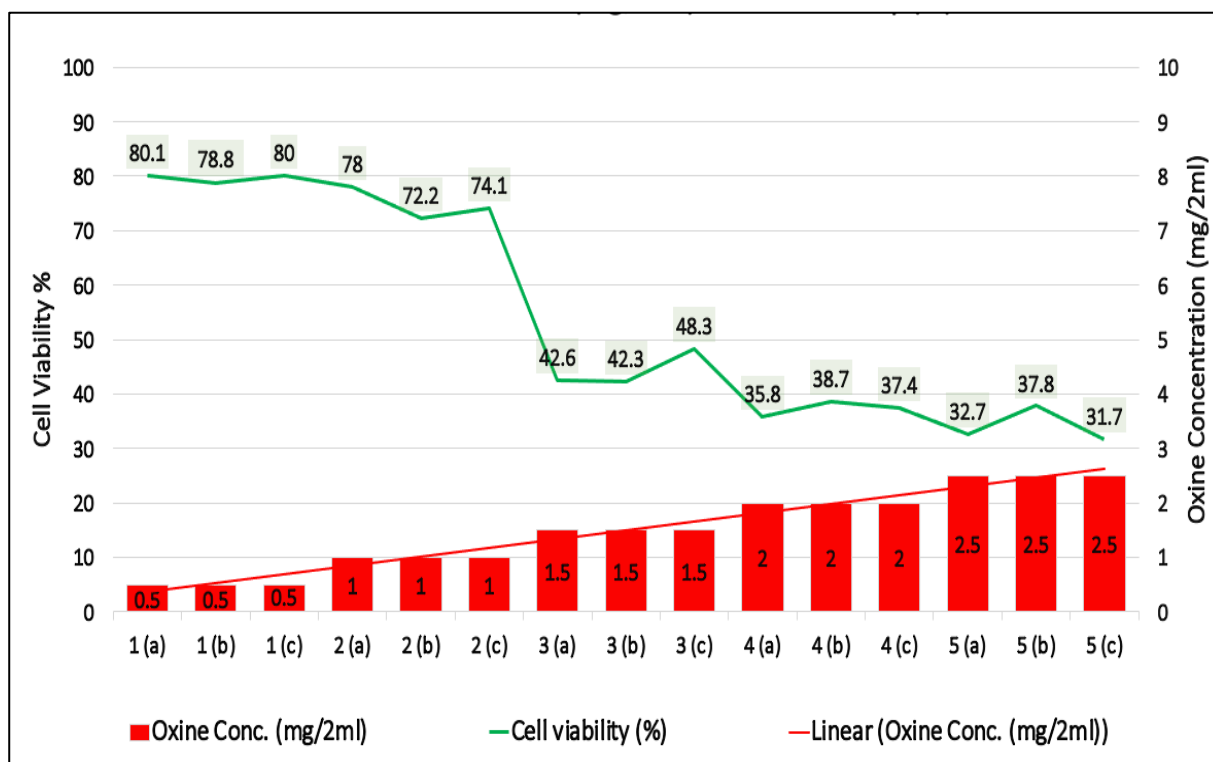
Figure 3-9: The relationship between oxine concentrations in cell suspension and cell viability results, based on the optimisation of the oxine concentration in cell suspension in the absence of radioactivity. In 15 samples containing 10×10^6 EL4 cells, five oxine concentrations of 0.5 mg/2 ml to 2.5 mg/2 ml of PBS were tested in triplicate. An increase in oxine concentrations in cell suspension had a direct negative impact on cell viability. A sharp decline in cell viability occurred when oxine concentrations reached 1.5 mg per 2 ml of cell suspension. Cell viability was further reduced when oxine concentrations of 2 mg/2 ml and 2.5 mg/2 ml were used in cell suspensions.

Tukey's multiple comparison test for cell viability at five oxine concentrations	Mean difference (%)	Significant?	Summary	Adjusted P Value
Initial vs 0.5 mg/2 ml	1.97	No	ns	0.88
Initial vs 1 mg/2 ml	5.87	No	ns	0.06
Initial vs 1.5 mg/2 ml	37.2	Yes	***	< 0.001
Initial vs 2 mg/2 ml	44.3	Yes	***	< 0.001
Initial vs 2.5 mg/2 ml	47.5	Yes	***	< 0.001
0.5 mg/2 ml vs 1 mg/2 ml	3.90	No	ns	0.32
0.5 mg/2 ml vs 1.5 mg/2 ml	35.2	Yes	***	< 0.001
0.5 mg/2 ml vs 2 mg/2 ml	42.3	Yes	***	< 0.001
0.5 mg/2 ml vs 2.5 mg/2 ml	45.6	Yes	***	< 0.001
1 mg/2 ml vs 1.5 mg/2 ml	31.3	Yes	***	< 0.001
1 mg/2 ml vs 2 mg/2 ml	38.4	Yes	***	< 0.001
1 mg/2 ml vs 2.5 mg/2 ml	41.7	Yes	***	< 0.001
1.5 mg/2 ml vs 2 mg/2 ml	7.10	Yes	*	0.02
1.5 mg/2 ml vs 2.5 mg/2 ml	10.3	Yes	**	0.001
2 mg/2 ml vs2.5 mg/2 ml	3.23	No	ns	0.51

Table 3-8: **Cell viability results from the experimental optimisation of the oxine concentration for the El4 cells in the absence of radioactivity.** 15 samples containing 10×10^6 EL4 cells were loaded with different oxine concentrations (mg/ml), ranging from 0.5 mg/2 ml to 2.5 mg/2 ml of PBS. The experiment examined five oxine concentrations, with three replicates per tested oxine concentration. Using one-way ANOVA with Tukey's multiple comparison test, statistical significance was calculated. p values < 0.05 were considered statistically significant; * represents $p \leq 0.05$, ** represents $p \leq 0.01$, and *** represents $p \leq 0.001$. ns represents no significance for p values > 0.05.
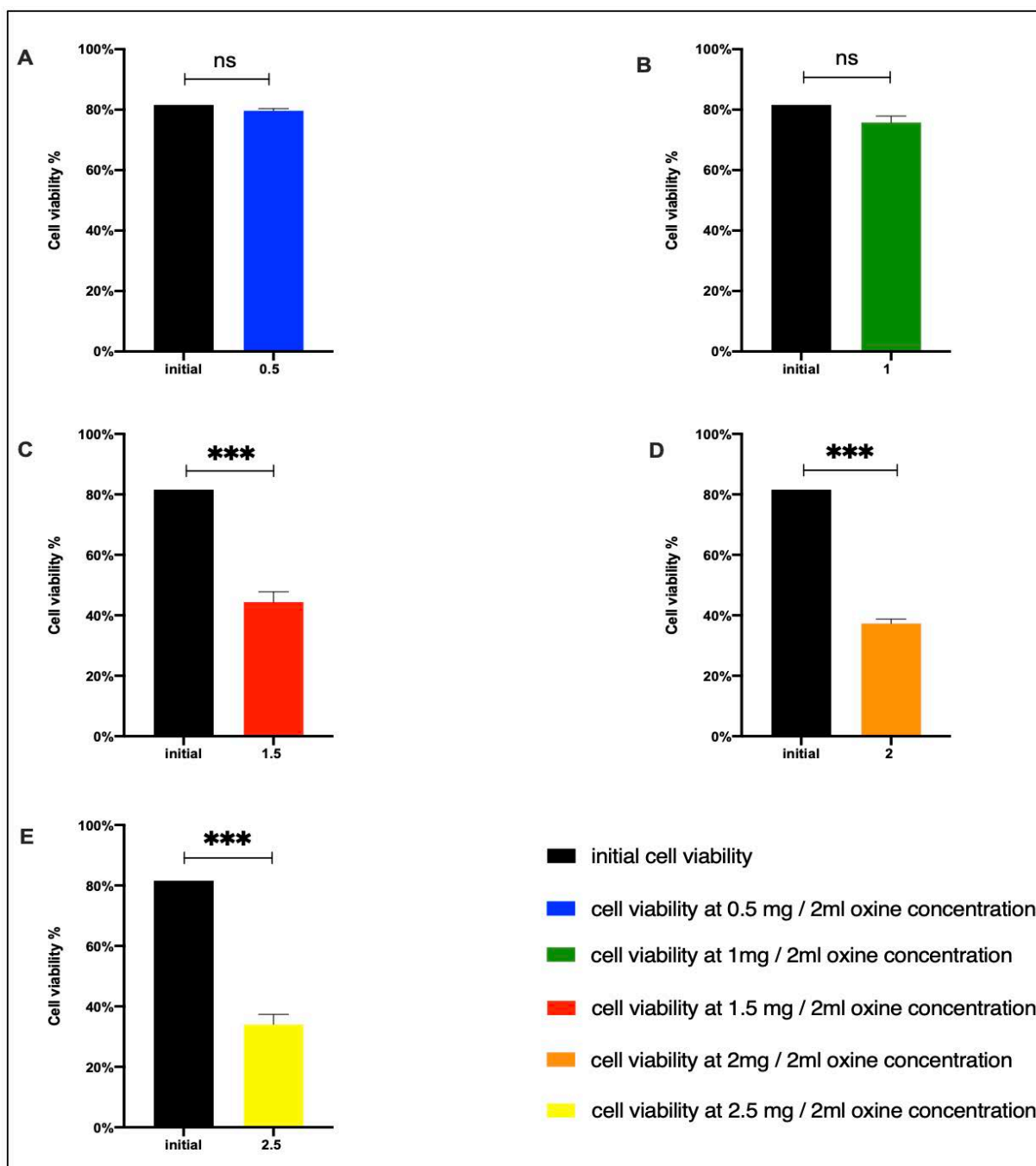
Figure 3-10: Cell viability results from the experimental optimisation of the oxine concentration for the EL4 cells in the absence of radioactivity. 15 samples containing 10×10^6 EL4 cells were incubated with different oxine concentrations, ranging from 0.5 mg/2 ml to 2.5 mg/2 ml of PBS. The experiment examined five oxine concentrations. The bar graphs represent the data as mean + SD (n = 3). (**A**) Initial cell viability vs cell viability after incubation with 0.5 mg/2 ml oxine concentration. (**B**) Initial cell viability versus cell viability after incubation with 1 mg/2 ml oxine concentration. (**C**) Initial cell viability versus cell viability after incubation with 1.5 mg/2 ml oxine concentration. (**D**) Initial cell viability versus cell viability after incubation with 2 mg/2 ml oxine concentration. (**E**) Initial cell viability versus cell viability at 2.5 mg/2 ml oxine concentration. Using one-way ANOVA with Tukey's multiple comparison test, statistical significance was calculated. p values < 0.05 were considered statistically significant; *** represents $p \leq 0.001$, and ns represents no significance for p values > 0.05.

3.3.2.4 Comparison between the effects of suspending EL4 cells in complete medium (DMEM with L-glutamine, penicillin/streptomycin and 10 % FCS) and PBS buffer on cell viability and cell yield in the absence of radioactivity

The results presented in Table 3-9 illustrate the cell viability of the six EL4 cell samples that were involved in the comparison that was carried out between the effects of suspending the EL4 cells in a complete cell culture medium (DMEM medium supplemented with 4 mM L-glutamine, 10 % FCS, 100 IU penicillin, 100 μg/ml streptomycin and 1 mM sodium pyruvate) versus PBS buffer on cell viability. The EL4 cells that were suspended in the cell culture medium and incubated for 30 min in a CO_2 incubator at 37 $^{\circ}$C had significantly higher cell viability than cells that were suspended in PBS buffer under the same incubation conditions.

The average cell viability ± SD for the three samples that were suspended in cell culture medium was 92.87 % ± 1.1 % compared with the average viability ± SD of 71.4 % ± 1.4 % for the other three samples that were suspended in PBS buffer. Accordingly, the results of cell viability were significantly different depending on the medium used for cell suspension. The viability of cells suspended in a cell culture medium was significantly higher than that of those suspended in PBS buffer by an average ± SD of 21.47 % ± 0.3 %, Figure 3-11.

Sample	Start cell count ($\times 10^6$)	Media (2 ml)	Recovered TOTAL cell count ($\times 10^6$)	Recovered LIVE cell count ($\times 10^6$)	Recovered DEAD cell count ($\times 10^6$)	Cell viability (%)
(1)	10	PBS	7.07	5.03	2.04	71.20
(2)	10	PBS	6.95	4.87	2.08	70.10
(3)	10	PBS	7.06	5.15	1.91	72.90
(4)	10	Complete medium	7.10	6.53	0.57	92.00
(5)	10	Complete medium	7.05	6.63	0.42	94.10
(6)	10	Complete medium	7.08	6.55	0.53	92.50

Table 3-9: **A summary of the details and results for the six samples used in the comparison between suspending the EL4 cells in two media and incubating them for 30 min at 37 °C in a CO$_2$ incubator on cell viability in the absence of radioactivity**. The two tested media were complete cell culture medium (DMEM medium supplemented with 4 mM L-glutamine, 10 % FCS, 100 IU penicillin, 100 μg/ml streptomycin and 1 mM sodium pyruvate) and PBS buffer. Each cell medium was tested with three samples.
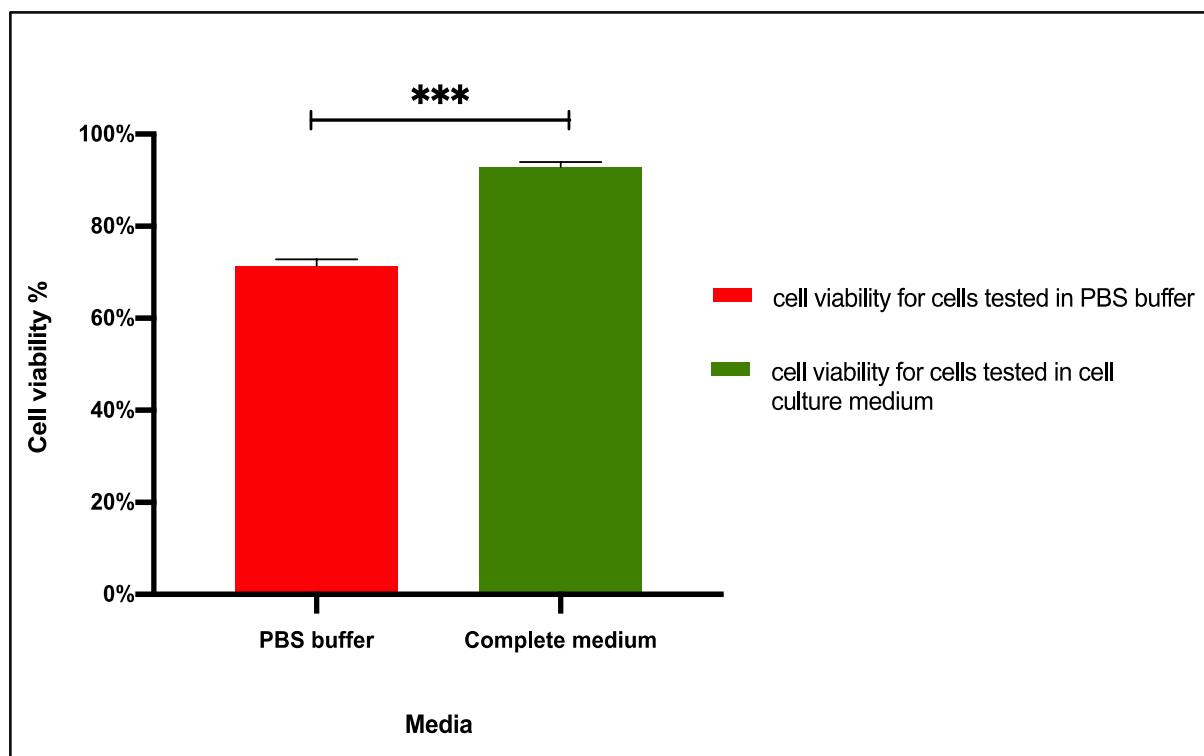
Figure 3-11: The effects of suspending cells in complete medium (DMEM medium supplemented with 4 mM L-glutamine, 10 % FCS, 100 IU penicillin, 100 μg/ml streptomycin and 1 mM sodium pyruvate) and PBS on cell viability in the absence of radioactivity. A total of six samples, each containing 10×10^6 EL4 cells suspended in a 2 ml medium, were involved, three samples per comparison. In the bar graphs, the data are presented as mean + standard deviation (n = 3). In this study, a two-tailed, unpaired t-test was used to calculate statistical significance. p values < 0.05 were considered statistically significant; *** represents p values ≤ 0.001.

3.3.2.5 Optimisation of the incubation method for EL4 cells in the absence of radioactivity

As shown in Table 3-10, the results present the cell viability and yield of the nine EL4 cell samples that were used to optimise the incubation methods to evaluate their effects on cell viability. In this study, all cells were suspended in 2 ml of the complete cell culture medium during the experiment. The samples were divided into three groups. The cells in the first group were incubated at 37 °C in a CO_2 cell incubator for 30 min without shaking. The cells from groups 2 and 3 were placed in a thermomixer for 30 min at 37 °C and two mixing speeds were

tested. A mixing speed of 300 rpm was applied to the cells from group 2, whereas a mixing speed of 550 rpm was applied to the cells from group 3.

One-way ANOVA and Tukey's multiple comparison tests were performed to examine the statistical significance of the results between the three groups of cells in terms of cell viability. Accordingly, cells from groups 1 and 2 had significantly higher cell viability than cells from group 3. Furthermore, cell viability results from groups 1 and 2 were not significantly different, as shown in Figure 3-12.

Based on the findings of this study, it is not recommended to mix cells at a speed of 550 rpm during the incubation process, as this will result in a significant decrease in the viability of the cells. Alternatively, it is essential to consider either mixing cells at a mixing speed of 300 rpm at 37 $^{\circ}$C for 30 min or incubating them in a CO_2 incubator to allow cells to maintain their viability.

Sample	Incubation method for 30 min at 37 °C	Start cell count ($\times 10^6$)	Recovered TOTAL cell count ($\times 10^6$)	Recovered LIVE cell count ($\times 10^6$)	Recovered DEAD cell count ($\times 10^6$)	Cell viability (%)	Cell yield (%)
1	Incubation in a CO_2 incubator	10	7.02	5.96	1.06	84.90	70.20
2	Incubation in a CO_2 incubator	10	7.13	5.99	1.14	84.00	71.30
3	Incubation in a CO_2 incubator	10	7.09	6.03	1.06	85.00	70.90
4	Mixed by a thermomixer at 300 rpm	10	7.11	6.06	1.05	85.20	71.10
5	Mixed by a thermomixer at 300 rpm	10	7.08	6.07	1.01	85.80	70.80
6	Mixed by a thermomixer at 300 rpm	10	7.07	6.06	1.01	85.70	70.70
7	Mixed by a thermomixer at 550 rpm	10	7.08	4.76	2.32	67.20	70.80
8	Mixed by a thermomixer at 550 rpm	10	6.98	4.89	2.09	70.10	69.80
9	Mixed by a thermomixer at 550 rpm	10	7.10	5.18	1.92	72.90	71.00

Table 3-10: The results for the optimisation of the incubation methods of the EL4 cells in the absence of radioactivity. The results of this study present the cell viability of the nine samples, each containing 10×10^6 EL4 cells that were incubated for 30 min at 37 °C per incubation method. Three samples were tested per incubation method. Three incubation methods were tested: (1) incubating cells in a CO_2 incubator, (2) mixing cells at 300 rpm using a thermomixer, and (3) mixing cells at 550 rpm using a thermomixer.
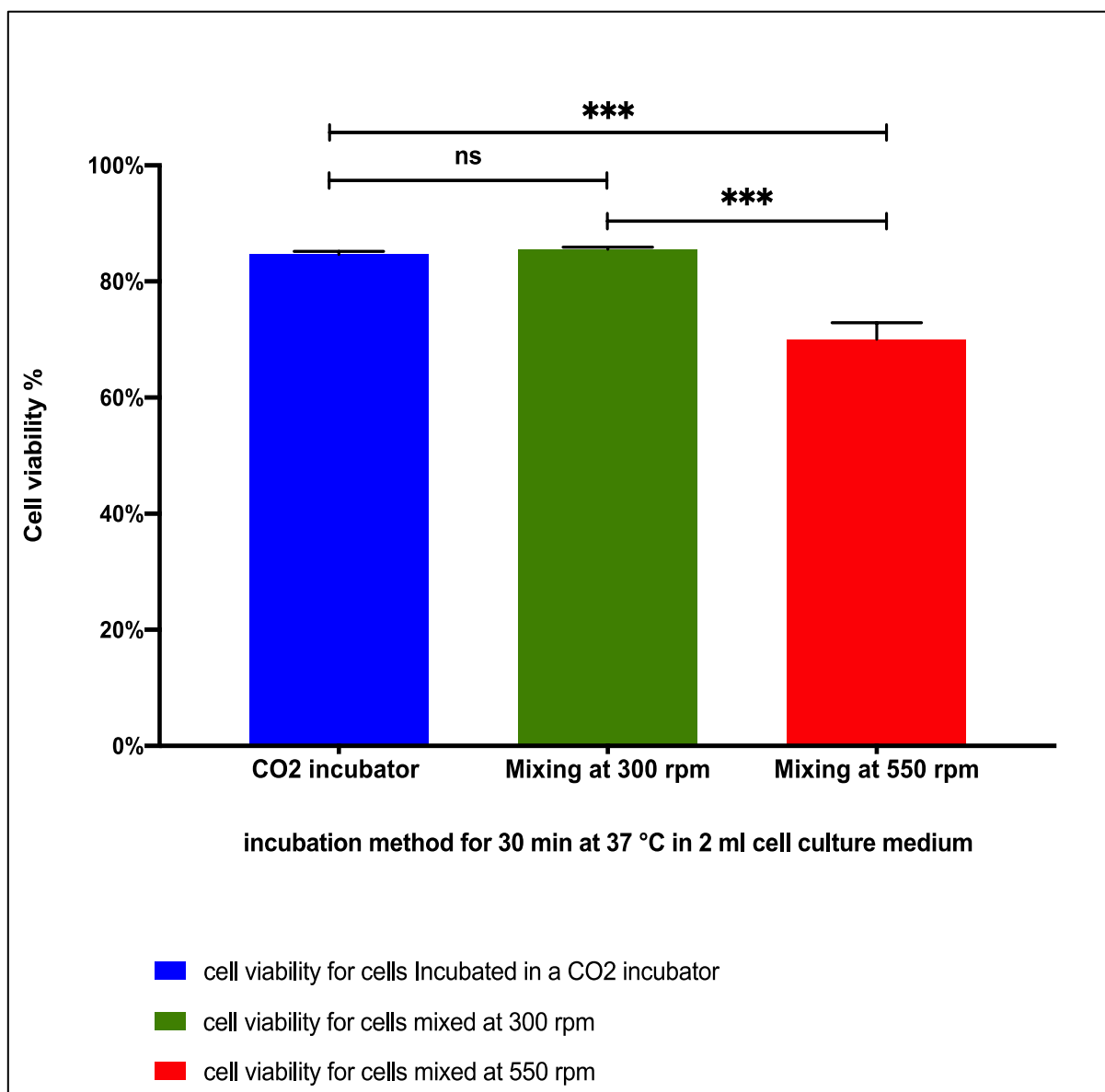
Figure 3-12: **The results of the experimental optimisation of the incubation methods of the EL4 cells in the absence of radioactivity.** The results present the cell viability of the nine samples, each containing 10×10^6 EL4 cells that were incubated for 30 min at 37 $^\circ$C per incubation method. Three samples were tested per in cubation method. Three incubation methods were tested: (1) incubating cells in a CO_2 incubator, (2) mixing cells at 300 rpm using a thermomixer, and (3) mixing cells at 550 rpm using a thermomixer. The data are displayed as the mean + SD (n = 3) in the bar graphs. The statistical significance of the results was determined using one-way ANOVA and Tukey's multiple comparison test. P values < 0.05 were considered statistically significant; *** representing p values ≤ 0.001, and ns indicates no significance for p values > 0.05.

3.3.2.6 Handling and incubating of EL4 cells in two labs, one of which lacks a class II cell culture hood, to determine the effects of the absence of a cell culture hood on the cell viability.

The results presented in Table 3-11 illustrate the cell viability of the six aliquots of EL4 cells included in this experiment. These cell viability results were used to evaluate how different using the same procedure but in two different labs, one of which lacks the cell culture hood, would influence the results of the experiment. EL4 cells were tested by applying the same basic cell culture procedures but in two different laboratories: the main tissue culture laboratory in the I & I department, where all procedures were conducted in a sterile cell culture hood, and the pre-clinical PETIC laboratory, where a tissue culture hood was not available.

The average cell viability ± SD for samples that were tested using a cell hood was 93.87 % ± 0.25 % compared with the average viability ± SD of 70.23 % ± 3 % for samples that were tested without using a cell culture hood. We determined whether there was a statistically significant difference between the viability of EL4 cells in the presence or absence of a cell culture hood using a two-tailed, unpaired t-test for comparison. P values < 0.05 were considered statistically significant, with *** representing p values ≤ 0.001. In this regard, the cells that were tested in the I & I laboratory under ideal sterile conditions using tissue culture cell hoods showed significantly higher cell viability by an average ± SD of 23.64 % ± 2.75 % compared with those tested in the R & D laboratory where no cell hood was available, Figure 3-13.

Sample	Start cell count (×10⁶)	Cell culture hood	Recovered TOTAL cell count (×10⁶)	Recovered LIVE cell count (×10⁶)	Recovered DEAD cell count (×10⁶)	Cell viability (%)
1	10	**With** culture hood	7.16	6.72	0.44	93.9
2	10	**With** culture hood	7.21	6.78	0.43	94.1
3	10	**With** culture hood	7.12	6.66	0.46	93.6
4	10	**Without** culture hood	7.18	5.02	2.16	69.9
5	10	**Without** culture hood	7.09	5.20	1.89	73.4
6	10	**Without** culture hood	7.2	4.85	2.35	67.4

Table 3-11: Effect of environment on cell viability Results of the handling and incubation of EL4 cells in two laboratories, one of which did not have a class II cell culture hood for studying the effect of the absence of a cell culture hood on the viability of cells. Six samples, each containing 10×10^6 EL4 cells, were suspended in 2 ml of a complete cell culture medium (DMEM medium supplemented with 4 mM L-glutamine, 10 % FCS, 100 IU penicillin, 100 μg/ml streptomycin and 1 mM sodium pyruvate). Three replicates per comparison.
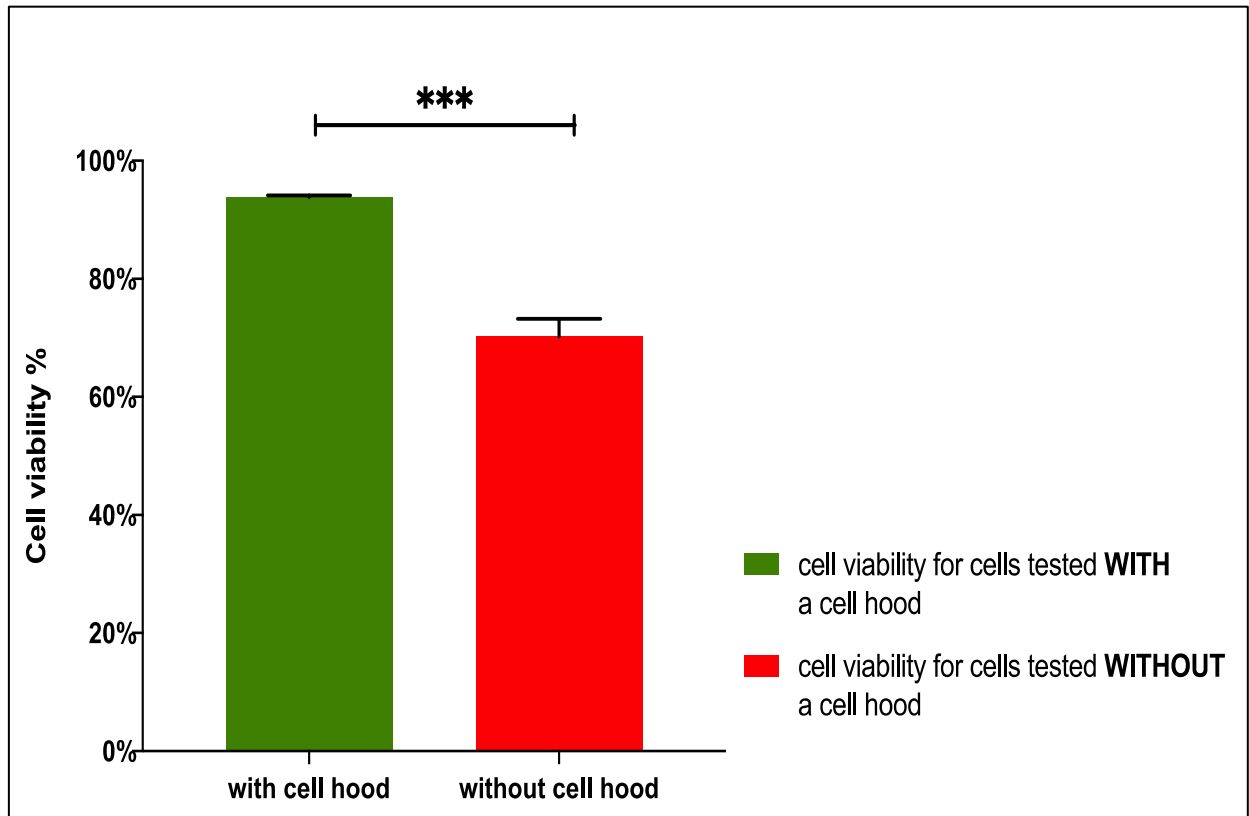
Figure 3-13: **Effect of environment on cell viability.** The results of the handling and incubation of EL4 cells in two laboratories, one of which did not have a class II cell culture hood for studying the effect of the absence of a cell culture hood on the viability of cells. Six samples, each containing 10×10^6 EL4 cells suspended in 2 ml of a complete cell culture medium were used (DMEM medium supplemented with 4 mM L-glutamine, 10 % FCS, 100 IU penicillin, 100 μg/ml streptomycin and 1 mM sodium pyruvate). In each comparison, three samples were tested. The data are presented as a bar graph indicating the mean and standard deviation (n = 3). The significance of the results was determined by a two-tailed, unpaired t-test. p values < 0.05 were considered statistically significant, with *** representing p values ≤ 0.001. ns representing no significance, p value > 0.05.

3.3.2.7 Applying the optimised parameters to the radiolabelling of EL4 cells with the ^{89}Zr-oxine complex.

Table 3-12 presents the experimental details and results of the application of the optimised parameters to the radiolabelling of EL4 cells with the ^{89}Zr-oxine complex. In this experiment, three consecutive samples were examined. Each sample was prepared as follows: 18 MBq of ^{89}Zr-oxine per 10×10^6 cells in 2 ml of culture medium (DMEM medium supplemented with 4 mM L-glutamine, 10 % FCS, 100 IU penicillin, 100 µg/ml streptomycin and 1 mM sodium pyruvate). total oxine amount was 1mg in each final 2 ml reaction volume. Labelling efficiency, viability, and the number of labelled cells were determined for each sample.

Cell viability, cell yield, and retention of activity within cells were calculated at the following intervals after cell labelling: 0 h, 24 h, 48 h, and 72 h, Table 3-13. In terms of the viability of ^{89}Zr-oxine labelled EL4 cells, the average ± SD values were 71.13 % ± 0.71 %, 18.87 % ± 0.72 %, 17.13 % ± 0.58 %, and 15.4 % ± 0.4 %. Furthermore, the average cell yields ± SD were 76.2 % ± 0.66 %, 43.4 % ± 4.7%, 39.1 % ± 3.2 %, and 17.97 % ± 5.5 %, respectively. Additionally, the averaged ± SD effluxes of activity from labelled cells at 24 h, 48 h, and 72 h post labelling were 38.9 % ± 2.45 %, 50.72 % ± 1.5 %, and 56.34 % ± 3.1 %, respectively. The results obtained following *in vitro* monitoring of the ^{89}Zr-oxine labelled EL4 cells at time intervals after labelling were analysed using the one-way ANOVA method with Tukey's multiple comparisons to determine whether statistically significant differences existed between the results obtained in terms of cell viability, cell yield and retention of activity within cells, as indicated in Table 3-14. Figure 3-14 presents time activity curves that were plotted following *in vitro* monitoring of ^{89}Zr-oxine EL4 cells in terms of cell viability, yield, and efflux of ^{89}Zr-oxine activity from labelled EL4 cells.

Sample	^{89}Zr-oxine activity (MBq/ 10×10^6 cells)	Cell uptake (MBq)	LE %	Labelled cell viability (%)	Labelled cell count (×10^6)
1 (a)	18	3.87	21.7	70.5	7.7
1 (b)	18	3.63	20.4	71.9	7.58
1 (c)	18	3.71	21	71	7.59

Table 3-12: **The experimental details and results of the application of the optimised parameters to the radiolabelling of EL4 cells with the ^{89}Zr-oxine complex**. Three consecutive samples were examined. Each sample was prepared as follows: 18 MBq of ^{89}Zr-oxine per 10×10^6 cells in 2 ml of culture medium (DMEM medium supplemented with 4 mM L-glutamine, 10 % FCS, 100 IU penicillin, 100 µg/ml streptomycin and 1 mM sodium pyruvate). Labelling efficiency, viability, and the number of labelled cells were determined for each sample.

Time	Sample	Labelled cell viability (%)	Labelled cell yield (%)	Total efflux of activity (%)
0 h	1 (a)	70.5	77	0
	1 (b)	71.9	75.8	0
	1 (c)	71	75.9	0
24 h	1 (a)	18.4	48.4	41.3
	1 (b)	19.7	39	36.4
	1 (c)	18.5	42.8	39
48 h	1 (a)	16.9	38	51.56
	1 (b)	17.8	42.7	49.01
	1 (c)	16.7	36.6	51.6
72 h	1 (a)	15.2	11.8	59.31
	1 (b)	15.9	19.7	53.14
	1 (c)	15.2	22.4	56.58

Table 3-13: **The results for applying the optimised parameters to the radiolabelling of EL4 cells with the ^{89}Zr-oxine complex.** Three consecutive samples were examined. In each sample, 18 MBq of ^{89}Zr-oxine was added per 10×10^6 cells in 2 ml of cell culture medium (DMEM medium supplemented with 4 mM L-glutamine, 10 % FCS, 100 IU penicillin, 100 µg/ml streptomycin and 1 mM sodium pyruvate). Cell viability, cell yield, and retention of activity within cells were calculated at the following intervals after cell labelling: 0 h, 24 h, 48 h, and 72 h.

	one-way ANOVA with Tukey's multiple comparisons test.	Mean difference	Significant?	Summary	Adjusted P Value
Cell Viability (%)	0 h vs 24 h	52.27	Yes	***	< 0.001
	0 h vs 48 h	54.00	Yes	***	< 0.001
	0 h vs 72 h	55.70	Yes	***	< 0.001
	24 h vs 48 h	1.73	Yes	*	0.04
	24 h vs 72 h	3.43	Yes	***	< 0.001
	48 h vs 72 h	1.70	Yes	*	0.04
Cell yield (%)	0 h vs 24 h	36.23	Yes	***	< 0.001
	0 h vs 48 h	40.53	Yes	***	< 0.001
	0 h vs 72 h	61.67	Yes	***	< 0.001
	24 h vs 48 h	4.3	No	ns	0.74
	24 h vs 72 h	25.43	Yes	**	0.001
	48 h vs 72 h	21.13	Yes	**	0.004
Total efflux of activity (%)	0 h vs 24 h	38.90	Yes	***	< 0.001
	0 h vs 48 h	50.72	Yes	***	< 0.001
	0 h vs 72 h	56.34	Yes	***	< 0.001
	24 h vs 48 h	11.82	Yes	***	< 0.001
	24 h vs 72 h	17.44	Yes	***	< 0.001
	48 h vs 72 h	5.62	Yes	*	0.05

Table 3-14: **Cell labelling results of ^{89}Zr-oxine with EL4 cells**. Cell labelling was performed using the following composition per sample (n = 3), 18 MBq of ^{89}Zr-oxine per 10×10^6 El4 cells, suspended in 2 ml of complete growth medium (DMEM medium supplemented with 4 mM L-glutamine, 10 % FCS, 100 IU penicillin, 100 µg/ml streptomycin and 1 mM sodium pyruvate). Significance was calculated for the results of cell viability, cell yield, and efflux of activity from cells at the following intervals: 0 h, 24 h, 48 h, and 72 h using one-way ANOVA with Tukey's multiple comparisons test. *** represents ≤ 0.001, ** represents $P \leq 0.01$, * represents $P \leq 0.05$, and ns. represents no significance.
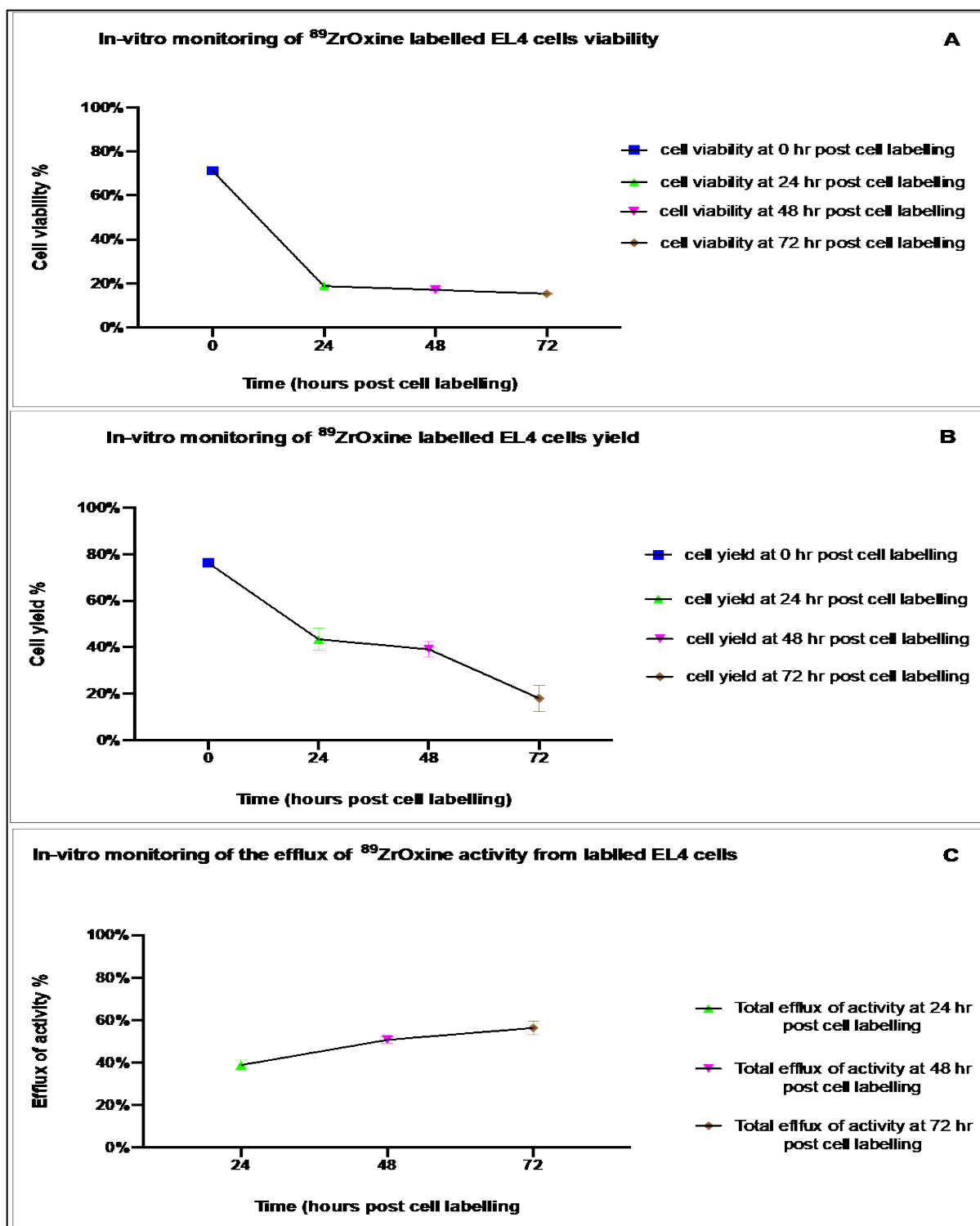
Figure 3-14: Results of *in vitro* monitoring of ^{89}Zr-oxine EL4- labelled cells. Three samples each containing 10×10^6 EL4 cells were loaded with 18 MBq of ^{89}Zr-oxine in 2 ml of complete cell medium (DMEM medium supplemented with 4 mM L-glutamine, 10 % FCS, 100 IU penicillin, 100 μg/ml streptomycin and 1 mM sodium pyruvate). The results of cell viability % (A), cell yield % (B), and efflux % of activity from cells (C) were plotted as a function of time at the following intervals post cell labelling: 0 h, 24 h, 48 h, and 72 h. The displayed data are mean + SD (n = 3).

3.4 Discussion:

In this chapter, we aimed to perform side-by-side labelling experiments of CD8 T cells with ^{89}Zr-oxine and ^{89}Zr-DFO-NCS complexes and track the labelled cells *in vivo* by PET/CT imaging in wild-type mice. This would allow us to compare the two cell labelling methodologies; in terms of cell labelling efficiency, labelled cell yields, labelled cell viability and *in vivo* biodistribution of the labelled cells. This chapter demonstrates several attempts at labelling zirconium-89 complexes to lymphocytes and tracking cells *in vivo* using PET/CT imaging.

In our first attempt to label the CD8 T cells using zirconium–89 complexes, a total of 1.15×10^8 CD8 T cells with a viability of 72 % were successfully isolated from eight donor mouse splenocytes using a CD8 T cell isolation kit for negative selection. Following the CD8 T cell labelling procedures with the ^{89}Zr complexes, the following cell labelling results were collected. There were 0.6×10^6 CD8 T cells with 13.3 % viability labelled with 0.53 MBq of the ^{89}Zr-oxine complex, whereas there were 0.4×10^6 dead cells (no viable CD8 T cells, all cells were dead) labelled with 0.71 MBq of the ^{89}Zr-DFO-NCS complex. Thus, the cell labelling efficiencies were 1.2 % and 1.6 %, and the labelled cell yields were 1.1 % and 0.7 %, respectively. As we can see from the results above, the cell labelling results were not satisfactory for the labelled cell viability, cell labelling efficiency and cell yields. In both cell labelling methods, we observed poor cell viability. The poor viability of the labelled cells might be related to the cell labelling procedures. For example, the labelling reaction time between the cells and the ^{89}Zr complexes in this experiment was accidentally set to 1 h instead of 30 min. Therefore, the prolonged cell and radioactivity labelling reaction for 1 h at 37 $^{\circ}$C and shaking speed of 550 rpm might be not optimal for the viability of the cells and needs to be optimised. Possibly, the poor viability of the labelled

166

cells resulted in low tracer uptake by the labelled cells. As a result, poor cell labelling efficiencies were achieved using both labelling methodologies.

Regarding the cell yields obtained from both the cell radiolabelling methodologies, only 1.1 % and 0.7 % of the total initial cells were recovered post the cell labelling methods with the ^{89}Zr-oxine complex and ^{89}Zr-DFO-NCS complex, respectively. This indicates a significant loss of cells during the labelling process. This may be related to the centrifuging speed that was used to spin the cells following the cell labelling reaction. In this case, the centrifuging speed was likely too low for the cells to sediment. Therefore, the centrifugation speed must be improved. In the absence of encouraging cell labelling results, the experiment was terminated at this stage.

Since we failed to produce satisfactory CD8 T cell labelling results from the previous experiment in series 1, we had to repeat the experiment with a better centrifugation parameter. Here are the results of our second attempt to label CD8 T cells with zirconium-89 complexes. The CD8 T cells isolated from the spleens of six donor mice using the CD8 T cell isolation kit for negative selection were not viable. We were surprised by this result, especially since in the previous experiment, we isolated CD8 T cells with viability over 72 % by following the same steps as before. We return to the steps for isolating the CD8 T cells. There was a total of 45×10^6 T cells with viability over 90 % were successfully isolated in the pre-sort stage of the CD8 T cells. This is a strong indicator that the cells died after this stage, i.e., during or after the CD8 T sorting stage, counting the cells post-sorting procedures indicated that there were no viable CD8 T cells. This suggested that cell death might be related to the serums that were used during the CD8 T cell sorting stage, which are rat serum, T cell cocktail, and EasySep Strep RapidSpheres. The experiment was terminated at this stage because we could not isolate any viable CD8 T cells.

Following the two unsuccessful attempts at labelling the CD8 T cells with the ^{89}Zr complexes and considering the sensitivity of CD8 T cells during the prolonged isolation procedures from donor mice and during the cell labelling process. we decided to simplify processes and switch to labelling the mixed lymphocytes instead of the CD8 T cells at this stage.

The results of the first attempts (series 3 and series 4) to label lymphocytes and ^{89}Zr complexes reveal the following. A total of 150×10^6 lymphocytes with 85 % viability were successfully isolated from the splenocytes and lymph nodes of two donor mice for cell labelling. The results from the cell labelling reactions that were conducted using 37.2 MBq of ^{89}Zr-oxine per 75×10^6 cells in 2 ml of PBS and 62 MBq of ^{89}Zr-DFO-NCS per 75×10^6 cells in 2 ml of PBS for 30 min at 37 $^\circ$C and at a shaking speed of 550 rpm were as follows 6×10^6 cells with 71 % viability were labelled with 1.9 MBq of the ^{89}Zr-oxine, and 8.3×10^6 cells with 81.4 % viability were labelled with 3.1 MBq of the ^{89}Zr-DFO-NCS. Accordingly, cell labelling efficiency was around 5 % for both cell labelling methods, cell yields were 8 % and 11 %, and amounts of 4 MBq and 5 MBq of activity were attached to the walls of the main tubes that were used for labelling reactions between the cells and radioactivity, respectively. labelling lymphocytes with ^{89}Zr complexes provided equal labelling efficiency, although unequal initial amounts of activity were used per cell labelling method. On the other hand, labelling lymphocytes with the ^{89}Zr-DFO-NCS compound was superior to labelling them with the ^{89}Zr-oxine compound in terms of cell yield and viability despite the higher starting activities. Although the cell labelling efficiency and cell yield results of labelling lymphocytes with ^{89}Zr complexes were not ideal, there was sufficient tracer uptake per labelled cell with considerably high viability obtained from each cell labelling method. Therefore, we injected the radiolabelled lymphocytes into a total of four recipient mice (2 mice per cell labelling method).

Attempts to administer tail vein injections to mice with [89]Zr-oxine labelled lymphocytes were unsuccessful, resulting in infiltrated doses in the tail region, Figure 3-1. Hence, PET/CT imaging was not possible. Conversely, the injections of [89]Zr-DFO- labelled lymphocytes into mice (n = 2) were successful, leading to a series of PET/CT imaging, Figure 3-2. Imaging tracked the injected cells *in vivo*. After 20 h of administration, most of the activity was observed in the liver (28.68 % ± 8.03 %), followed by the skeleton (%IA: 9.23 % ± 0.05 %), lungs (%IA: 7.83 % ± 6.44 %), and kidneys (%IA: 7.49 % ± 7.07 %). At 164 h post tracer administration, the highest activity was seen in the liver (%IA: 54.75 % ± 8.46 %), followed by the skeleton (%IA: 7.77 % ± 5.79 %), kidneys (%IA: 7.36 % ± 1.15 %), spleen (%IA: 5.15 % ± 0.02 %), and lungs (%IA: 1.69 % ± 1.36 %). At 306 h after tracer administration, more activity was present in the liver (%IA: 54.75 % ± 8.46 %), followed by the kidneys (%IA: 7.77 % ± 5.79 %), skeleton (%IA: 7.36 % ± 1.15 %), and spleen (%IA: 5.15 % ± 0.02 %), with minor accumulations in the lungs (%IA: 1.69 % ± 1.36 %). An unexpected finding was the presence of multiple focal hot spots of activity randomly distributed in both mice. The PET scans at 20 h, 44 h, 68 h, 140 h, 164 h, and 306 h post-injection are quantitatively represented in Figure 3-3.

In our study, the *in vivo* distribution of [89]Zr-DFO-NCS labelled lymphocytes was compared with the surface labelling of other cell types from the literature. Previous research found that [89]Zr-DFO-NCS labelled CAR T cell trafficking, as seen through PET imaging, showed low lung activity on day 7 compared with that the liver or spleen.[37] However, a study by Bansal *et al.,* involving mesenchymal stem cells labelled with [89]Zr-DFO-NCS showed high lung activity up to day seven, followed by liver liver.[36] In our study, the highest *in vivo* activity was observed in the liver (%IA: 54.75 % ± 8.46 %), followed by the skeleton (%IA: 7.77 % ± 5.79 %), kidneys (%IA: 7.36 % ± 1.15 %), spleen (%IA: 5.15 % ± 0.02 %), and lungs (%IA: 1.69 % ± 1.36 %). Unlike previous

research, our study showed significant activity uptake in the skeleton and kidneys on day seven. This may be due to the multiple hot spots randomly distributed with the tracer or the different cell types labelled with [89]Zr-DFO. Even with high skeleton and kidney activity, lung activity was still lower than liver or spleen activity, as observed in the labelled CAR T cells with [89]Zr-DFO.[37]

A particularly unexpected finding was the presence of multiple focal hot spots of activity that were randomly distributed throughout the bodies of both mice and were persistently observed in the whole series of PET/CT scans, as illustrated in Figure 3-2. These multiple focal hot spot patterns are difficult to explain because they do not follow a logical biological distribution pattern and are not focussed on any particular organ, suggesting that they arise from physical trapping, perhaps due to the aggregation of the cells. However, if this distribution is due to aggregation, it must occur after injection because any large clumps of poorly suspended aggregated cells injected into the tail vein would be expected to trap in the capillary beds in the lungs and in severe cases would kill the mice. Moreover, aggregation of the cells was not observed during cell counting processes before injection. To the best of our knowledge, no studies that have employed [89]Zr-DFO-NCS surface labelling for *in vivo* cell imaging have reported this pattern of distribution.[36],[37],[317],[345]

Consequently, for the validity of the findings presented in this study, it is essential that these experiments be repeated and that [89]Zr-oxine labelled lymphocytes be imaged successfully to determine if this distribution pattern is specific to these cells. However, if the choice labelling method adversely affects the distribution pattern of the cells, this is a very important finding that should be published. To conclude, this experiment provided *in vitro* results for labelling lymphocytes with both [89]Zr complexes, so we were able to compare these cell labelling approaches in terms of cell labelling efficiency, cell yield, and viability of the labelled cells. On the other hand,

we were unable to compare the *in vivo* biodistribution of labelled lymphocytes using both methods because of the unsuccessful tail vein injections of the ^{89}Zr-oxine labelled lymphocytes provided to both mice. Although this experiment provided useful information about tracking the movement of the ^{89}Zr-DFO-NCS labelled lymphocytes *in vivo*, this information was considered incomplete because of the lack of *in vivo* biodistribution of the ^{89}Zr-oxine labelled lymphocytes. Therefore, the labelling of lymphocytes with zirconium-89 complexes had to be repeated to achieve the targeted results.

Subsequently, we conducted the last experiment again to verify the *in vitro* labelling results of the lymphocytes and ^{89}Zr complexes obtained from the previous experiment and to enable the head-to-head comparison of the biodistribution of the labelled lymphocytes from both cell labelling methods. The results of the second attempt (series 4) to label lymphocytes with ^{89}Zr complexes reveal the following. A total of 170×10^6 lymphocytes with 39.1 % viability were isolated from the splenocytes and lymph nodes of four donor mice for cell labelling. As a result of the cell labelling reactions that were conducted using 96.5 MBq of ^{89}Zr-oxine per 85×10^6 cells in 2 ml of PBS and 106 MBq of ^{89}Zr-DFO-NCS per 85×10^6 cells in 2 ml of PBS, for 30 min at 37 $^\circ$C and at a shaking speed of 550 rpm, 14.4×10^6 cells with 82.76 % viability were labelled with 0.33 MBq of the ^{89}Zr-oxine, and 9.8×10^6 cells with 77.8 % viability were labelled with 2 MBq of the ^{89}Zr-DFO-NCS. Accordingly, the cell labelling efficiency was 0.34 % and 1.9 %, the cell yield was 17 % and 11.5 %, and 30 and 49.5 MBq of activity were attached to the walls of the reaction vials that were used for labelling reactions between the cells and ^{89}Zr-oxine and ^{89}Zr-DFO-NCS complexes, respectively. The labelling of lymphocytes with ^{89}Zr complexes in the second attempt (series 4) showed lower cell labelling efficiency for both labelling methods compared with the first attempt (series 3).

Unlike the first attempt, labelling lymphocytes with the ^{89}Zr-oxine compound was superior to labelling them with the ^{89}Zr-DFO-NCS compound in terms of cell yield and viability. Although there were sufficient labelled cells with considerably high viability resulting from each cell labelling method, tracer uptake by the labelled cells was low, especially for ^{89}Zr-oxine labelled cells. Although the initial amounts of ^{89}Zr were higher in this experiment, the labelling efficiency results were lower in both methods compared to the first attempt. This might be due to the significantly large amounts of ^{89}Zr that were attached to the tubes used for the cell and radioactivity reactions in this experiment, unlike the previous one. It is not clear why this excessively high vial labelling happened for this round of labelling. Because of the low activity of ^{89}Zr-oxine labelled cells, which is inadequate for *in vivo* imaging, the experiment was terminated at this stage.

Given that we had not been able to successfully image ^{89}Zr-oxine labelled lymphocytes, we decided to label lymphocytes again, but this time focussing only on the ^{89}Zr-oxine method. For the series 5 experiment, 190×10^6 lymphocytes were isolated from the splenocytes and lymph nodes of three donors with a viability of 85.1 % for cell labelling. As a result of the cell labelling reaction that involved 190×10^6 cells and 99.1 MBq of ^{89}Zr-oxine in 4 ml of PBS for 30 min at 37 $^{\circ}$C and a mixing speed of 550 rpm, 97×10^6 cells with 91.9 % viability were labelled with 9.16 MBq of ^{89}Zr-oxine. This indicates that the labelling efficiency was 9.2 % and the cell yield was 51 %. The results of this experiment were superior to those of previous labelling attempts with both ^{89}Zr complexes. This was our best experiment in terms of labelling efficiency and the percentage of recovered cells that were successfully labelled. The experiment demonstrated that we were able to successfully recover 51 % of the total lymphocytes and label them with an ^{89}Zr-oxine activity of 9.16 MBq (enabling *in vivo* long-term cell trafficking), while the labelled cells still maintained a high level of viability of 91.8 %.

Having achieved excellent labelling results, we continued and injected the recipient mice with lymphocytes labelled with ^{89}Zr-oxine. Unfortunately, the administration of the labelled cells into the mice via intravenous injections was not successful in all three mice. Early PET/CT images acquired 30 min after injection of the tracer revealed that the injected activity was concentrated in the tail area for all three mice. In this case, it is highly likely that the intravenous injections were of poor quality and were likely administered subcutaneously rather than intravenously. As a consequence, no more PET/CT images were acquired, and the experiment was abandoned. Despite the excellent results obtained for labelling lymphocytes and the ^{89}Zr-oxine complex, we did not succeed in tracking the labelled cells *in vivo* due to the poor quality of the intravenous injection despite our best efforts.

Because of the failure of the previous experiment (series 5) to achieve its primary objective of obtaining successful *in vivo* imaging of the ^{89}Zr-oxine labelled lymphocytes, the experiment was repeated. In the last cell labelling experiment described in series 6 in this chapter, 210×10^6 lymphocytes were isolated from four donors' splenocytes and lymph nodes with a viability of 87 % for cell labelling purposes. Cells were labelled with ^{89}Zr-oxine through the reaction between the cells and 66 MBq of ^{89}Zr-oxine in 4 ml of PBS for 30 min at 37 degrees Celsius and a shaking speed of 550 rpm. The result was that 13×10^6 cells with 13.6 % viability were labelled with 13.17 MBq of ^{89}Zr-oxine. Accordingly, the calculated labelling efficiency and cell yield were 20 % and 6.5 %, respectively. Although this experiment had the highest cell-labelling efficiency compared with previous cell-labelling experiments, the yield and viability of the labelled cells were considerably lower than those of most of our earlier cell-labelling experiments.

Despite the less-than-ideal outcomes of the cell labelling process, there were enough labelled cellsβwith a satisfactory ^{89}Zr-oxine activity to allow prolonged *in vivo* imaging of the cells. Therefore, we proceeded by administering 2.25×10^6 lymphocytes with a viability of 13.6 % that were labelled with 1.41 MBq of ^{89}Zr-oxine through intravenous injection to a mouse. Subsequently, a series of non-invasive PET/CT imaging was performed to monitor the movement of the cells *in vivo*, as shown in Figure 3-4. Thirty minutes after injection, the majority of radioactivity was detected in the liver (%IA: 23.91 %), with smaller amounts found in the skeleton (%IA: 5.39 %) and lungs (%IA: 3.92 %). After 20 h, an increase in radioactivity was noted in the liver (%IA: 34.79 %), followed by the skeleton (%IA: 11.40 %) and trace amounts in the kidneys (%IA: 1.75 %). At 136 h, the liver continued to be the main site of accumulation (%IA: 40.66 %), followed by the skeleton (%IA: 15.51 %), and minimal amounts were found in the spleen (%IA: 1.69 %) and kidneys (%IA: 1.10 %). Figure 3-4 illustrates the quantitative results of the PET scans taken at intervals ranging from 0.5 to 138 h after injection of the ^{89}Zr-oxine labelled low-viability lymphocytes.

The results of the *in vivo* distribution of ^{89}Zr-oxine labelled lymphocytes in our study were comparable to those reported in the literature. According to Charoenphun *et al.,* ^{89}Zr-oxine labelled myeloma cells were injected intravenously and observed in the lungs 30 min later. On day one, they migrated to the liver and spleen and remained there for seven days.[346] Similar results were reported for ^{89}Zr-oxine labelled dendritic cells by Sato.[310] Additionally, in a study involving CAR T cells conducted by Weist *et al.,* it was reported that the highest CAR T cell activity was observed in the spleen, followed by the liver.[325]

The death of labelled cells leads to the quick release of free ^{89}Zr, which is eliminated from the body through the kidneys.[210],[324] However, a small portion of free ^{89}Zr may be absorbed in the hydroxyapatite of the bone matrix.[224],[310],[311],[347] This could account for the higher activity uptake observed in the skeleton and kidneys during the *in vivo* tracking of low-viability lymphocytes labelled with ^{89}Zr-oxine in our study, in contrast to the *in vivo* tracking of live cells labelled with ^{89}Zr-oxine complex, as seen in previous studies.[34],[310],[325]

As shown in Table 3-2, the LE % for the labelling of lymphocytes with ^{89}Zr-oxine and ^{89}Zr-DFO-NCS complexes ranged between 0.34 % and 20 % and 1.6 % and 5 %, respectively. As a comparison to previously published results, naive dendritic cells and activated cytotoxic T cells were labelled with the ^{89}Zr-oxine complex in a study published by Sato *et al.,* and the calculated labelling efficiency ranged between 13.0 % and 43.9 %.[310] Furthermore, in a paper published by Bansal *et al.,* the ^{89}Zr-DFO-NCS (referred to as ^{89}Zr-DBN by these authors) was employed to label melanoma cells, dendritic cells and human mesenchymal stem cells. Based on the type of cell used, Bansal and his colleagues found that the labelling efficiency varied between 30 % and 50 % 30 min after labelling.[36]

Given the mixed results presented here in Table 3-2 and Table 3-3, it is apparent that this project requires intensive laboratory work that is exceedingly challenging in terms of both its technical requirements and the number of processing steps that must run smoothly and in sequence to yield useful results. Frustratingly the experiments failed at different stages each time for example when there was good cell isolation and labelling the tail vein injections failed. However, one key problem was the inconsistency in the results obtained from cell isolation and cell labelling between the experiments. Chances of overall success would be greatly improved if the reliability of these steps

could be improved. Therefore, the details of the procedures employed were closely analysed to determine the reasons why these experiments were not successful. Some conclusions might explain the results of these unsuccessful cell labelling attempts. First, there was a variation in the amount of starting ^{89}Zr activity per constant cell count. Second, one of the experiments failed because of the prolonged cell labelling reaction timing. Third, we observed differences in oxine concentrations (mg/ml) in repeated cell samples within one experiment due to variations in ^{89}Zr-oxine yield. Given these inconsistent results and repeated failures of experiments we aimed to optimise these parameters that were not standardised in previous radiolabelling experiments, such as the start amount of ^{89}Zr-oxine activity per constant cell count, the duration of the cell labelling reaction, oxine concentration (mg/ml) in cell suspension, the type of medium for suspending cells during cell labelling reaction time, type of cell incubation method and incubation vs shaking cells during incubation (two shaking speeds were tested). For these *in vitro* optimisation experiments we switched to an easily handleable and readily available cell line to reduce the number of animals required for the experiments and to introduce consistency in the viability and cell numbers at the start of each experiment. The variation in cell viability due to the absence of a suitable cell culture hood was also evaluated.

In our optimisation experiment for the ^{89}Zr-oxine starting activity per constant EL4 cell count, we found that labelled cell viability did not directly correlate with the increase in ^{89}Zr-oxine starting activity (MBq), as shown in Table 3-4 and Figure 3-6. However, oxine concentration (mg/ml), which was not standardised across all samples due to the variable yields of ^{89}Zr-oxine extraction, was shown to have clear threshold of cell toxicity. The variability in oxine concentration in the sample comes from the high variability in the extraction of ^{89}Zr from the aqueous phase stock solution by the 1mg/ml oxine in chloroform solution. The standardised method involved extracting

2 ml of neutralised ^{89}Zr in 0.1 M oxalic acid with 2 ml of chloroform overnight. The chloroform layer is removed, and the chloroform is evaporated to leave dried ^{89}Zr-oxine in 2 mg of excess oxine. This whole dried layer is dissolved in 20 µl of DMSO followed by 1980 µl of PBS and the required volume of the 2 ml solution is added to the cell pellet to give the desired activity of labelling solution. This method ensures there is always 2 mg of excess oxine in each 2 ml ^{89}Zr-oxine sample, however there is a very large variation in the extraction efficiency from one extraction to the next meaning sometimes repeat extractions need to be combined to achieve the desired amount of ^{89}Zr-oxine activity. This is particularly true because the preparation of the 15 samples involved in this study required relatively high levels of ^{89}Zr-oxine activity. Thus, mixing more than one extraction of ^{89}Zr-oxine was required, resulting in a lack of standardisation of oxine concentrations between samples involved in this experiment.

Therefore, we began to consider that the final radiolabelled cell viability was not directly related to the amount of start dose per known number of cells, as was originally thought, but was instead directly related to the oxine concentration (mg/ml) per cell suspension. This was demonstrated by samples 7 (a), 7 (b), and 7 (c) in Table 3-4, all of which were loaded with 41 MBq of ^{89}Zr-oxine per 10×10^6 EL4 cells, whereas a higher concentration of oxine was used in sample 7 (c). Samples 7 (a) and 7 (b) had oxine concentrations of 0.7 mg/2 ml, whereas sample 7 (c) had an oxine concentration of 2 mg/2 ml. Accordingly, samples 7 (a) and 7 (b) exhibited high and almost identical labelled cell viabilities, which were 70.5 % and 69.9 %, respectively, as compared to sample 7 (c), which exhibited nearly half of their viability, which was 33.7 %. Similar results were observed in samples 4 (a), 4 (b), and 4 (c), which were radiolabelled with a similar amount of ^{89}Zr-oxine activity of approximately 22.5 MBq. However, the oxine concentration in samples 4 (a) and 4 (c) was higher. In samples 4 (a) and 4 (c), the oxine concentration was 2 mg/2 ml, whereas in

sample 4 (b), it was 1 mg/2 ml. Therefore, samples 4 (a) and 4 (c) had low labelled cell viability of 34.2 % and 34.7 % compared with sample 4 (b), which had a labelled cell viability of nearly twice as much as samples 4 (a) and 4 (c), which was 64.5 %.

In light of the above findings, we replotted the data in Figure 3-6, but this time based on the ascending oxine concentration (mg/ml) in cell suspension versus labelled cell viability. From Figure 3-7, it is evident that there is an inverse relationship between cell viability and oxine concentration in the cell suspension. Hence, we concluded that our thought was correct when we found that the starting amounts of ^{89}Zr-oxine activity per constant EL4 cell count did not directly affect the viability of the labelled cells in the presence of oxine in the suspension. The figure also clearly demonstrates that once the concentration of oxine was raised to 1.5 mg per 2 ml cell suspension, a sharp drop in the viability of the labelled cells was observed. Considering these results, it has been concluded that when there was oxine in the cell suspension, it is the concentration of oxine per cell suspension that played the primary role in controlling the viability of the labelled cells, rather than the amount of starting ^{89}Zr-oxine in the suspension.

As reported by Man *et al*., the effect of ^{89}Zr-oxine on γδ T cell proliferation was not statistically significant at doses up to 20 mBq per cell; however, at 50 mBq per cell and higher, it became statistically significant. In addition, the radiolabelled γδ T cells were found to preserve their cytotoxic effects against tumour cells within 48 h of radiolabelling when labelled with ^{89}Zr-oxine activity up to 600 mBq per cell.[319] Weist *et al*., published a study demonstrating similar results when ^{89}Zr-oxine was used to radiolabel T cells and found to maintain their cytotoxicity after radiolabelling.[325] Furthermore, Sato *et al*., reported that labelling cells with the ^{89}Zr-oxine

complex did not affect cell viability, proliferation, or function when the cells were labelled at a specific activity of less than 2.4 kBq/10^6 cells.[310]

Using the results of our cell labelling experiments in comparison to those published in the literature, [310],[319],[325] we demonstrated that, despite the significantly high starting level of ^{89}Zr-oxine activity used to label the cells (4.1 MBq/10^6 cells), ^{89}Zr-oxine labelled EL4 cells preserved their viability at an oxine concentration of ≤ 1 mg/2 ml of the suspension. Therefore, it is worthwhile to reconsider looking for dose optimisation per cell count and per cell type, since it seems we can obtain high radiolabelled cell viability even when higher activity was added if the oxine concentration in cell suspension was ≤1 mg/2 ml. This will be a very useful finding, particularly if we are considering serial PET imaging scans up to 14 days post injection of the radiolabelled cells to recipient mice, to maintain a sufficient count rate during scanning even at very delayed PET scans.

To summarise the results obtained by optimising the amount of ^{89}Zr-oxine activity per constant number of EL4 cells for cell labelling, the results showed that at the activities tested no direct correlation existed between the initial amounts of ^{89}Zr-oxine per constant number of EL4 cells and either viability or cell yield, as shown in Figure 3-6. However, there was an inverse relationship between the concentration of oxine in the cell suspension and the viability of the labelled cells, Figure 3-7. Therefore, instead of the amount of ^{89}Zr-oxine activity in the cell suspension, the concentration of oxine per cell suspension accounted for most of the variation in the viability of the labelled cells. As a demonstration of this, high cell viability was observed when the oxine concentration in the suspension was ≤ 1 mg/2 ml, despite the high starting ^{89}Zr-oxine activity used for labelling the cells, as seen in samples 7 (a) and 7 (b).

Regarding the optimal duration of cell labelling, the effects of two cell labelling durations were evaluated on the cell labelling efficiency and labelled cell viability, as shown in Table 3-5 and Figure 3-8. The statistical significance of the calculated results was determined by the application of a two-tailed, unpaired t-test. P values < 0.05 were considered significant. Consequently, the study results indicated no significant difference between the effects of the two cell labelling periods on the efficiency of cell labelling and the viability of the labelled cells, Table 3-5. This would be true if the oxine concentration in the tested sample was the same, which was not the case in this experiment. This made it harder to determine how the duration of cell labelling affects the viability of cells, especially since lower concentrations of oxine were used in the three samples that were tested for a cell labelling period of 15 min. This led us to consider that the final radiolabelled cell viability might not be strongly related to the duration of the cell labelling reaction, but rather to the concentration of the oxine (mg/ml) per cell suspension, as was observed in the first optimisation experiment. The same pattern was observed when we examined samples 2 (a), 2 (b), and 2 (c). In fact, for these samples, the cell labelling reaction took place for the same duration of time and was conducted for 30 min. However, samples 2 (b) and 2 (c) had a lower oxine concentration of 0.75 mg/2 ml compared with sample 2 (a), which contained 2 mg/2 ml of oxine per cell suspension. Therefore, the viability of labelled cells was almost the same for samples 2 (b) and 2 (c), which were 69 % and 67 %, respectively, and higher than the cell viability of sample 2 (a), which was 33.6 %, Table 3-4.

In summary, the results obtained by optimising cell labelling duration for ^{89}Zr-oxine and EL4 could not clearly demonstrate how the duration of cell labelling affected cell viability and labelling efficiency. This was because the controlling factor, oxine concentration, was not standardised across repeated samples because the efficiency of oxine extraction varied. In contrast, there was

an inverse relationship between the concentration of oxine in the suspension of cells and the viability of the labelled cells. Therefore, it was difficult to determine the effect of the duration of the cell labelling reaction period on cell viability or labelling efficiency. According to the literature, both cell labelling periods have been used and verified in cell labelling studies. In a study conducted by Kurebayashi *et al*., CAR-T cells were incubated with ^{89}Zr-oxine for 15 min at room temperature or 4 $^{\circ}$C.[224] Sta Maria *et al*., also conducted a study in which CAR-T cells were incubated with ^{89}Zr-oxine for 30 min at 37 $^{\circ}$C.[316]

Following the results obtained from our first and second optimisation experiments, we designed an experiment to determine the optimal oxine concentration that must not be exceeded in our cell labelling experiments to preserve the viability of the labelled cells. The experiment that was conducted to optimise the oxine concentration in the cell suspension without radioactivity revealed the following significant results: there was a clear threshold above which the oxine concentration strongly affected cell viability, Figure 3-9. The results also revealed that oxine amounts of 500 µg and 1000 µg in 2 ml of cell suspension did not significantly affect the viability of cells. Furthermore, there was no significant difference between the effects of oxine amounts of 500 µg and 1000 µg in 2 ml cell suspension on the viability of the cells. However, it was found that when the concentration of oxine was increased to 1.5 mg per 2 ml of cell suspension, a significant drop in cell viability was observed by an average ± SD of 31.3 % ± 1.2 % in cell viability was observed, as shown in Figure 3-9 and Figure 3-10. This is, of course, a fundamental finding that should be carefully considered in the cell labelling experiment. In other words, for cells to remain viable, the oxine concentration in the cell suspension for cell labelling experiments must not exceed 1 mg per 2 ml of cell suspension. We now have a better understanding of one of the reasons why some of our earlier attempts to label ^{89}Zr-oxine with cells failed. If there was a low ^{89}Zr-oxine extraction

yield, we were required to mix more than one [89]Zr-oxine extraction to obtain the required activity for *in vivo* imaging. As a consequence, an oxine concentration of 1.5 – 2 mg per 2 ml of PBS for cell suspension was produced, which most likely had a role in the low and varying levels of cell viability observed.

In comparison to the literature, we used oxine amounts of 500 µg and 1000 µg which are higher than those reported for oxine complexing with radionuclides in the literature. For example, in early studies involving ^{111}In-oxinate, 150 µg of oxine in ethanol was used to complex with ^{111}In-InCl$_3$, whereas the commercially available kit for preparing ^{111}In-oxinate requires only 50 µg of oxine.[348] Another study used 150 g of oxine to complex with [68]Ga.[210] Although researchers have been attempting to minimise the amount of oxine used to minimise toxicity because oxine-related damage is dependent on the amount of oxine used. However, we found that the effect of oxine on cell viability is not only associated with the amount of oxine used but also with the type of cells.

As part of the process of developing the labelling method for [89]Zr-oxine and EL4 cells, two different mediums were tested to determine which medium to use for the cell suspension during the cell labelling reaction time to allow cells to preserve their viability. As can be seen in Table 3-9, it was found that viability for EL4 cells that were suspended in the complete cell culture medium and incubated in a CO_2 incubator at 37 °C for 30 min was significantly higher by an average ± (SD) of 22.8 % ± 1.75 % than the viability of EL4 cells that were suspended in the PBS buffer under the same incubation conditions, Figure 3-11. As a point of clarification, in our initial attempts to label [89]Zr-oxine with cells, cells were suspended in 2 ml of PBS buffer, not a complete cell culture medium, which probably contributed to the poor cell viability that was observed.

Therefore, the cell culture medium should be thought of as a cell suspension medium during the cell labelling reaction period for the labelling of ^{89}Zr-oxine and EL4 cells.

The incubation method, in which cells are given time to incubate and absorb radioactivity, was also considered as a part of developing the cell labelling method. Accordingly, we tested three methods for incubating the cells to determine the optimal cell incubation method that preserves cell viability. As shown in Table 3-10, the results of the experimental optimisation of the incubation method of EL4 cells in the absence of radioactivity are presented. The results of this study were based on the cell viability of nine samples, each containing 10×10^6 EL4 cells that were involved. Three samples were tested per incubation method, and the significance of the results was determined using one-way ANOVA and Tukey's multiple comparison test. As a result, cells that were incubated in a CO_2 incubator for 30 min at 37 $^{\circ}$C and cells that were mixed at a speed of 300 rpm for 30 min at 37 $^{\circ}$C had significantly higher viability than cells that were mixed at a speed of 550 rpm under the same mixing conditions. At the same time, there was not much difference between the cell viability results of cells that were incubated in a CO_2 incubator or cells that were mixed at a speed of 300 rpm for 30 min at 37 $^{\circ}$C, as shown in Figure 3-12.

It is worth noting that in our initial cell labelling experiments of ^{89}Zr-oxine and ^{89}Zr-DFO-NCS complexes with different cell lines, the cell labelling reaction was conducted for 30 min at 37 $^{\circ}$C and a mixing speed of 550 rpm. This was one of the reasons why we were not able to achieve adequate cell viability because the mixing speed of (550 rpm) was not optimal. According to the findings of this study, during the cell labelling time of the cells and radioactivity, using a thermomixer to mix cells at a mixing speed of 550 rpm is not advisable because it significantly decreases cell viability. To obtain better cell viability results, it is recommended that the cells and

radioactivity be incubated in a CO_2 incubator at 37 °C for 30 min or mixed at a speed of 300 rpm at 37 °C for 30 min.

Throughout all our experiments with [89]Zr-oxine and [89]Zr-DFO-NCS on lymphocytes and all our subsequent optimisation experiments, it is imperative to note that they were all conducted without a cell culture hood because this was not available in PETIC's preclinical laboratory. In other words, all our previous studies were not performed entirely under optimal sterile condition. Therefore, we wanted to determine the extent to which performing the cell labelling method without a cell hood negatively affected the results of cell viability in the conducted studies. Therefore, basic and similar cell culture procedures were applied to two groups of cells in two different labs, one of which lacked a cell hood.

In Figure 3-13, we present the results of the handling and incubation of EL4 cells in two laboratories, one of which did not have a class II cell culture hood, to examine the effect of the absence of such a hood on the viability of the cells. To determine the significance of the results, a two-tailed, unpaired t-test was conducted using six samples containing 10×10^6 EL4 cells under each condition. P values of < 0.05 were considered significant. It was shown in the results that cells tested in the I & I laboratory with tissue culture cell hoods were significantly more viable by an average $\pm$ (SD) of 23.63 % $\pm$ 0.78 % when compared to those tested in the R & D laboratory without cell hoods. In other words, handling cells and performing basic cell culturing procedures in the absence of a cell culture hood would significantly lower cell viability results by an average $\pm$ (SD) of 23.63 % $\pm$ 0.78 %. Accordingly, since PETIC's preclinical laboratory did not have a cell culture hood, there may have been another reason for the low viability seen in our early cell labelling studies. As a result, this is important to consider for upcoming cell labelling experiments;

we can increase the viability of cells by improving or adapting a sterile environment for radiolabelling, which can be accomplished by using a cell hood for all cell procedures.

Following the set of cell labelling optimisation experiments, many important results were obtained and considered. Accordingly, the cell labelling method of [89]Zr-oxine and EL4 cells was developed to the following scale: 20 MBq of [89]Zr-oxine activity per 10×10^6 El4 cells suspended in 2 ml of complete medium, with a maximum of 1 mg of oxine per 2 ml of cell suspension. In addition to restricting the oxine concentration $\leq$ 1 mg per 2 ml of cell suspension, a cell labelling reaction should be carried out by incubating cells and radioactivity in a CO_2 incubator at 37 °$^{\circ}$C for 30 min or mixing at a mixing speed of 300 rpm at 37 $^{\circ}$C for 30 min. These results must be carefully considered because they will undoubtedly improve cell labelling results in many aspects, including labelling efficiency, viability, yield of cells and retention of activity within cells.

As a result, all the optimised parameters were considered and applied to the labelling of [89]Zr-oxine with EL4 cells. Cell labelling reactions were conducted on three repetitive samples (n = 3) using the following composition per sample: 18 MBq of [89]Zr-oxine per 10×10^6 cells in 2 ml of complete medium, with an oxine concentration of 0.333 mg per 2 ml cell suspension, for 30 min at 37 $^{\circ}$C and at a mixing speed of 300 rpm. After applying the optimised parameters to the labelling of [89]Zr-oxine and EL4 cells, many successful cell labelling results were achieved. Before discussing the results of the experiment, it is very important to mention that the results of repeatedly tested samples were very similar in terms of labelled cell viability, cell yield, and retention of activity within labelled cells, Table 3-14. Even this result is considered a success in itself. In particular, if we wish to implement the optimised method in the future, the results confirm that we will achieve similar results.

A successful outcome in this experiment was the very low amount of activity that remained attached to the main reaction vial between the ^{89}Zr-oxine and EL4 cells. Hence, there was an average of just 0.24 MBq ± 0.13 activity that stuck on the tube out of the start amounts of ^{89}Zr-oxine activity of 18 MBq. This is a considerable improvement in comparison to our initial radiolabelling attempts, where we tended to lose a significant amount of activity due to sticking to the reaction Falcon tube that even might go up to 50 MBq, leading to insufficient cell uptake, which turned the cell labelling method to be unsuccessful.

Another success in this experiment was observed in the cell uptake of the repetitive EL4 cell samples. An average cell uptake of 3.73 MBq ± 0.1 was calculated from 18 MBq of ^{89}Zr-oxine activity that was used to initiate the cell labelling reaction. This is also an improvement over some of our initial radiolabelling attempts in which we tended to start with higher levels of activity up to 60 MBq, but we were able to retrieve only 4 MBq per radiolabelled cell. The reason for this was either an excessive amount of activity that tended to stick to the reaction tube or cell loss during the radiolabelling process, resulting in no radiolabelled cells at the end of the long radiolabelling process. Accordingly, the average ± SD calculated labelling efficiency for the ^{889}Zr-oxine labelled EL4 cells in this study was 21 % ± 0.65 %. Using the optimised cell labelling method, we obtained a LE % that was similar to previously published result in the study by Sato *et al.,* in which the ^{89}Zr-oxine complex was used to label dendritic cells and activated cytotoxic T cells and the calculated labelling efficiency ranged from 13.0 % to 43.9 %.[310]

In terms of the viability of the ^{89}Zr-oxine labelled EL4 cells, it was on average ± (SD) of 71.13 % ± 0.7 % for the consecutive replicates (n = 3), Table 3-12. This is not optimal cell viability, however, considering that the cell labelling experiment was acquired in a not very sterile lab

environment due to the absence of a cell culture hood during the time that this experiment was acquired. It was demonstrated by the experiment in section 3.3.2.6, that handling cells and performing basic cell culturing procedures in the absence of a cell culture hood would significantly lower cell viability results by an average ± (SD) of 23.63 % ± 0.78 %. Accordingly, this demonstrates that the labelling results of ^{89}Zr-oxine with EL4 cells, which were achieved after applying the protocol that we optimised, would improve by an average ± SD of 23.63 ± 0.78 % if a cell culture hood was used. This would enhance labelled cell viability to 94.76 % ± 1.48 % (SD) instead of 71.13 % ± 0.7 % (SD). In this case, the enhanced ^{89}Zr-oxine labelled cell viability would be 94.76 % ± 1.48 %, which indicates no significant decrease in the viability of cells post the application of the optimised cell labelling method.

To continue with the results that were achieved following the application of the optimised method on the radiolabelling of EL4 cells with ^{89}Zr-oxine complex. The most important success of this study was the yield of ^{89}Zr-oxine EL4 labelled cells. The optimised cell labelling method was able to achieve an average ± (SD) labelled cell yield of 76.2 % ± 0.66 % for the repetitive samples (n = 3) with average ± (SD) cell viability of 71.13 % ± 0.7 %, Table 3-12. Again, this represents an excellent result compared to many of our initial attempts to label ^{89}Zr-oxine and ^{89}Zr-DFO-NCS with different cell lines. Unlike in this experiment, many of our early cell labelling attempts ended up with either no radiolabelled cells at all or with completely dead radiolabelled cells, which turned the cell labelling method to be unsuccessful despite intensive and prolonged laboratory work. However, applying this optimised cell labelling method to the labelling of ^{89}Zr-oxine and EL4 cells resulted in a satisfactory yield of labelled cells, while cell viability remained preserved. Especially if we take into account the significant loss of cell viability that occurred in the absence of a cell culture hood, then we can project that the optimised cell labelling method, which resulted

in an average ± (SD) labelling cell yield of 76.2 % ± 0.66 %, could potentially obtain an enhanced cell viability ± (SD) of 94.76 % ± 1.48 % if carried out in the sterile conditions of a cell culture hood.

The ability of labelled cells to retain their activity for an extended time allows for long-term imaging of the cells. This is particularly important if we are considering serial PET imaging scans up to 14 days post injection of the radiolabelled cells to recipient mice to maintain a sufficient count rate during scanning even at very delayed PET scans. Table 3-13, Table 3-14, and Figure 3-14 show results for *in vitro* monitoring of ^{89}Zr-oxine EL4 labelled cells after applying the developed labelling method to determine their viability, yield, and efflux of activity from labelled cells up to 72 h post cell labelling method. At 24 h post cell labelling, there was a significant decrease in the labelled cell viability from 71.13 % ± 0.7 % to 18.87 % ± 0.7 %, which continued to decrease further to reach an average ± SD of 15.4 % ± 0.4 % at 72 h post cell labelling. A significant decrease in labelled cell yield was also observed from an average ± SD of 79.6 % ± 6.55 % labelled cells immediately following labelling down to 43.4 % ± 4.7 % and 17.97 % ± 5.5 % labelled cells after 24 and 72 h, respectively. One or both of the following factors could have contributed to the significant decline observed in our labelled cell viability and labelled cell count. The first is the effect of radioactive ^{89}Zr retention within cells, as *in vitro* monitoring of cell results demonstrated that ^{89}Zr remained attached to cells up to 72 h after radiolabelling by an average of 43.66 % ± 3.1 %. Second, the prolonged incubation and handling of cells under non-ideal cell culturing conditions caused by the absence of the cell culture hood led to the deterioration of labelled cell viability, especially over a prolonged *in vitro* monitoring period. This might explain the reason behind the quite low results for our labelled cell viability observed up to 72 h post labelling compared with those reported in the literature.[34],[35]

The efflux results of [89]Zr-oxine activity from labelled EL4 cells were encouraging and comparable to those reported in the literature. Despite the significant efflux of activity from labelled cells by an average ± SD of 38.9 % ± 2.45 % at 24 h post cell labelling, followed by a further efflux of activity, 43.66 % ± 3.1 % of the labelled activity remained attached to the cells until 72 h after labelling. In accordance with literature publications, Man *et al.*,[319] found that the retention of [89]Zr-oxine is determined by cell type and that approximately 50 % of the incorporated [89]Zr in labelled cells was released during *in vitro* incubation for one week. Furthermore, the results of tracer efflux reported by Man *et al.,* are similar to those observed with ^{111}In-oxinate labelled lymphocytes [350],[351], which is the most commonly used technique for cell tracking by nuclear imaging [319]. Studies by Charoenphun *et al.*,[34] and Sato *et al.*,[328] have investigated the chemotoxicity of [89]Zr-oxine as well as its significant efflux from cells following labelling, two problems commonly associated with oxine-based labelling. In their study, Charoenphun *et al.*,[34] observed a decrease in the viability of [89]Zr-oxine labelled 5 T33 myeloma cells from 93.3 % to 76.3 % ± 3.2 % in the first 24 h, as well as a significant efflux of 28.9 % of radioactivity 24 h following labelling. The same findings were observed by Sato *et al.*,[328] with [89]Zr-oxine labelled human and rhesus macaques' natural killer cells. They observed a broad range of viability of 60 % – 100 % in the radiolabelled cells over the first 24 h, which declined to 20 % – 30 % after 6 days. Furthermore, significant amounts of radioactivity were effluxed by these viable [89]Zr-oxine labelled cells following culture. Approximately 20 % – 25 % of the radioactivity was released from labelled cells within the first 24 h and 70 % – 80 % after 1 week of the culture period.[328]

3.5   Conclusion

Several attempts were made to radiolabel various cell lines with ^{89}Zr-oxine and ^{89}Zr-DFO-NCS in part 1 of this chapter. We analysed the unsuccessful trials to determine why they failed. These findings may explain why early cell labelling attempts were insufficient. First, ^{89}Zr activity per constant cell count varied. Second, one experiment did not succeed, most probably because of an error in setting the reaction duration for cell labelling. Third, variations in ^{89}Zr-oxine yield efficiency resulted in variations in the concentration of oxine (mg/ml) in replicate samples within a single experiment. Therefore, this chapter was dedicated to optimising the parameters that were not uniform in previous radiolabelling experiments. These were the starting amount of ^{89}Zr-oxine activity per constant cell count, the duration of the cell labelling reaction, the oxine concentration in the cell suspension, the medium in which the cells were suspended during the cell labelling reaction and incubating versus shaking cells for the cell labelling reaction. Along with the development of ^{89}Zr-oxine cell labelling and EL4 cells, the effect of not having a proper cell culture hood on cell viability was also examined.

Following the completion of the intended optimisation tests, significant conclusions were reached. First, optimising the amount of ^{89}Zr-oxine activity per constant number of EL4 cells for cell labelling could not clearly illustrate how the initial amounts of ^{89}Zr-oxine activity affected cell viability, primarily due to variation in the oxine concentration between repeated samples caused by variations in oxine extraction efficiency. However, oxine concentration accounted for most of the variation in tagged cell viability, not ^{89}Zr-oxine activity. The concentration of oxine in the cell suspension shows a clear toxicity threshold above which cell viability is significantly affected.

Despite the high starting ^{89}Zr-oxine activity used to label the cells, high cell viability was reported when the oxine concentration in the suspension was ≤1 mg/2 ml.

The results obtained from experiments to optimise cell labelling duration for ^{89}Zr-oxine and EL4 could not conclusively demonstrate how cell labelling duration affected cell viability due to the confounding effect of the variation in oxine concentration (mg/ml), which was again not standardised across repeated samples due to the variations in efficiency of oxine extraction. However, after controlling for oxine concentration in the samples the labelling duration did not appear to influence cell viability for the reaction times tested. Based on our cell labelling optimisation experiments, we found that the oxine concentration (mg/ml) within the cell suspension controlled the viability of the labelled cells, not the initial amount of ^{89}Zr-oxine activity per constant EL4 cell count nor the duration of the cell labelling reactions. Therefore, for the following experiment employing ^{89}Zr-oxine cell labelling, the oxine concentration should not exceed 1 mg/2 ml in the cell suspension to maintain cell viability. Additionally, the complete cell culture medium significantly enhanced cell viability compared with PBS buffer; hence, it should be used as a cell suspension medium for labelling ^{89}Zr-oxine and EL4 cells. According to this research, during the incubation method, using the thermomixer to mix cells and radioactivity at a mixing speed of 550 rpm significantly reduced cell viability, making it an unsuitable option for cell labelling. Instead, consider mixing cells at 300 rpm at 37 $^{\circ}$C for 30 min or incubating cells and radioactivity in a CO_2 incubator at 37 $^{\circ}$C for 30 min to improve cell survival in cell labelling studies. Moreover, because of the absence of the cell culture hood in the pre-clinical PETIC laboratory, the viability of tagged cells significantly dropped by an average of 23.64 %. This is a clear reason for the poor cell survivability observed in our early cell labelling tests. If we create or use a more

sterile environment for radiolabelling our cells, we can obtain significantly higher labelled cell viability.

Following this, all optimised parameters were applied to the labelling of ^{89}Zr-oxine and EL4 cells. Consequently, successful cell labelling results were obtained, which compared favourably to previously published cell labelling reactions with regard to the amount of activity that remains attached to the main reaction tube, labelling efficiency, labelled cell viability and labelled cell yield, as well as the efflux of activity from ^{89}Zr-oxine EL4 labelled cells. In light of these promising results with the developed cell radiolabelling method, the next step is to translate this optimised method to the radiolabelling of the target lymphocytes to evaluate its efficiency and enable *in vivo* imaging studies.

Chapter 4: *In vitro* radiolabelling for *in vivo* tracking of CTLL2 cells using PET/CT imaging in a mouse model with optimised parameters from EL4 cells

4.1 Introduction

It has been over a decade since we gained a better understanding of the cancer-immunity cycle, particularly how T cells stimulate antitumour immunity. Due to these advances, engineered cellular therapies have made significant advances and immune checkpoint blockade (ICB) therapies have been successfully developed and applied. In clinical settings, T cell-based therapeutics offer an opportunity to bridge the gap between preclinical models and human disease observations.[352]

CD8 T cells originate from lymphoid progenitor cells in the bone marrow and undergo further maturation in the thymus, emerging as naïve CD8 T cells. These cells, characterised by their ability to activate upon encountering specific antigens, display notable phenotypic and functional diversity, indicative of their heterogeneity.[353] Finding out about the cytotoxic properties of CD8 T cells, initially in the context of infectious diseases [354]–[358], has been a cornerstone in understanding their role in immune responses. Post-infection, these naïve cells proliferate and differentiate into effector CD8 T cells, capable of eliminating infected cells and protecting the host. A fraction of these effector cells then become memory cells, ready to respond rapidly to antigen re-exposure.[359]–[362]

It is important to note, however, that CD8 T cells become exhausted when they are repeatedly exposed to antigens, such as chronic viral infections or tumours, thereby resulting in a diminished ability to respond to subsequent antigen stimulations.[363]–[365] This insight has been crucial in tumour immunotherapy, leading to the development of strategies such as

adoptive cell therapy. This involves isolating, expanding, and activating patient CD8 T cells *in vitro* before reintroduction to the patient.[366],[367] A notable innovation in this area is chimeric antigen receptor (CAR) T cell therapy, in which patient CD8 T cells are genetically engineered to recognise cancer antigens effectively. The FDA has approved several CAR T cell therapies for haematologic malignancies.[260],[368]

CTLL2 cells are a clone of cytotoxic T cells derived from a C57BL/6 mouse that are dependent on interleukin-2 (IL-2) for growth and can be used to assay for IL-2.[314] Research has found these cells relevant because they can be used to develop bioassays for detecting murine IL12 and IL18. These cytokines have shown activity against various cancers and can act synergistically by upregulating their receptors mutually.[61] It has also been shown that CTLL2 cells can improve the detection of helper T lymphocyte precursors from bone marrow transplant patients, which are directed against alloantigens and correlate with the development of graft-versus-host disease.[321]

The increasing importance of cellular therapies has highlighted the need for effective *in vivo* cell tracking methodologies, with ^{89}Zr cell labelling for PET imaging emerging as a promising methodology. Two of the most common chelators developed for ^{89}Zr are oxine and DFO. There has been considerable progress in the development of cell labelling strategies using ^{89}Zr-oxine and ^{89}Zr-DFO.[38] A study by Man *et al*.,[318] introduced a novel advancement in the formulation of ^{89}Zr-oxine. This new method allows for a five-minute radiolabelling process, making it possible to produce ^{89}Zr-oxine from ^{89}Zr-oxalate in one step, resulting in stability for up to a week. This innovation offers a more efficient and clinically viable method for PET cell tracking, with a high yield (up to 85 %), overcoming limitations associated with previous methods that presented challenges for clinical use. The kit formulation is enhanced by higher concentrations of oxine and polysorbate 80 as well as increased HEPES concentration for

effective buffering, promising improvements in efficiency and safety related to [89]Zr-oxine PET cell tracking in clinical and preclinical settings.

Although numerous publications have addressed the labelling of cells with [89]Zr-oxine [34],[35] and [89]Zr-DFO-NCS [36],[37], direct comparisons between these two cell labelling methods remain limited. Research by Friberger *et al.*, in 2023 was conducted to evaluate and compare the biodistribution of cells labelled with two distinct radiotracers: [89]Zr-oxine and [89]Zr-DFO-NCS. The objective of this study was to use micro-PET/CT imaging for non-invasive, quantitative monitoring of cell biodistribution, thereby contributing to the optimisation of cell therapies.[39] This research involved the radiolabelling of human decidual stromal cells (hDSC) and rat macrophages (rMac) with two distinct radiotracers, chosen for their universal applicability across cell types. To account for varying migration patterns across different cell types *in vivo*, rMac and hDSC were selected from a diverse range of human and rat origins. In this study, micro-PET/CT imaging was used to monitor *in vivo* biodistribution over seven days after intravenous injection into rats. The findings revealed that although both radiotracers were effective for detecting cell biodistribution *in vivo*, distinct differences in the distribution patterns of the two radiotracers were observed. Cells labelled with [89]Zr-oxine exhibited more heterogeneous distribution than those labelled with [89]Zr-DFO-NCS. Furthermore, rMac cells showed higher uptake in the liver and spleen compared with hDSC, indicating cell type-dependent biodistribution. More specifically, cells labelled with [89]Zr-oxine showed immediate lung uptake and migrated to the liver immediately, whereas cells labelled with [89]Zr-DFO-NCS showed prolonged lung retention and higher lung uptake. Because of the different radiotracers, cells appear to behave differently and have different biodistributions. Additionally, the study noted that [89]Zr-oxine labelled cells had over 70 % higher liver uptake for both hDSC and rMac compared with [89]Zr-DFO-NCS labelled cells after 24 h. In contrast, [89]Zr-DFO-NCS labelled cells exhibited over 60 % higher lung uptake than [89]Zr-oxine labelled cells. These disparities

persisted up to day 7. Furthermore, dosimetry calculations further indicated that cells labelled with ^{89}Zr-DFO-NCS resulted in a higher effective dose (mSv/MBq) for both cell types. It is also likely that the prolonged uptake of ^{89}Zr-oxine labelled cells in the lungs contributed to a crossfire effect on the bone marrow, which resulted in a higher dose in the bones.

A key conclusion of the study is that radiotracer selection affects the behaviour and distribution of labelled cells *in vivo*. This shows care is required when selecting a radiolabelling method and highlights the need for careful validation of labelling methodologies used in each cell line of interest.

Therefore, the main focus of this chapter was to use our newly established cell labelling techniques to label CTLL2 cells and examine the potential and efficacy of labelling the cells with both ^{89}Zr-oxine and ^{89}Zr-DFO-NCS. Additionally, to validate the utility of our cell labelling methods as a PET method for tracking cells, we will label the same cell line in accordance with the Man *et al*.,[318] cell labelling method.

4.2 Methods and materials

I would like to acknowledge the contributions of Dr Stephen Paisey, my supervisor, who assisted me in the specific experiments described below. Because of a health and wellness problem arising from direct contact with rodents, as encouraged by the Occupational Health Department at Cardiff University, I was advised not to participate in direct animal handling. Consequently, Dr Paisey undertook all tasks entailing direct animal contact, including mouse injection and imaging procedures.

4.2.1 Radiolabelling of CTLL2 cells using the optimised parameters from EL4 cells and tracking the radiolabelled cells *in vivo* using PET/CT imaging in a mouse model.

CTLL2 cells were labelled using the three cell labelling methods. 1) The optimised ^{89}Zr-oxine method described in Chapter 3, 2) ^{89}Zr-DFO-NCS as described in chapter 3 and 3) the ^{89}Zr-oxine-kit formulation method as described by Man *et al.*,[318]. Following cell labelling, the viability, proliferation, and tracer retention abilities of the cells were assessed *in vitro* and using PET/CT imaging, labelled cells were tracked noninvasively after administration into wild-type C57BL/6 mice for *in vivo* assessment. *In vitro* and *in vivo* assessments of the cells were conducted for up to seven days following labelling.

4.2.1.1 Cell culture and mice

CTLL2 cells are clones of cytotoxic T cells derived from C57BL/6 mice. Cells were purchased from the ATCC (item code ATCC TIB-214). This cell line was cultured under specific conditions as per the ATCC guidelines.[314] CTLL2 cells were cultured in RPMI 1640 medium (4.5 g/L glucose), enriched with 2 mM L-glutamine, 1 mM sodium pyruvate, 100 IU penicillin, 100 µg/ml streptomycin, 10 % FCS, and 10 % T. stim with Concanavalin A (Scientific Laboratory Supplies, product code 354115). Cells were maintained in suspension and incubated in a 5 % CO_2 incubator at 37 °C within a humidified atmosphere. The culture medium for cells was refreshed two to three times a week. Subculturing of actively growing suspension cultures was performed before the cell density reaching 2×10^5 cells/ml to prevent rapid depletion of interleukin-2 (IL-2) and subsequent loss of cell viability. The cultures were inoculated at densities ranging from 1×10^4 to 2×10^4 viable cells/ml. For this process, T-75 flasks were utilized for subculturing these cells. This

approach ensured optimal growth conditions and maintained cell culture health. Cells were tested for mycoplasma contamination at regular intervals, typically every 4 weeks on actively growing cell lines and upon receipt of externally sourced cells and upon thawing of frozen cell lines, and no mycoplasma contamination was detected during this project.

Cells were counted, and viability was determined using automated cell counting. Two automated cell counters were used in this project. Within the primary tissue culture laboratory of the Immunity and Infection Department, cell counts were performed using the LUNA-FL™ Dual Fluorescence Cell Counter, which operates with either a 1:1 Trypan Blue solution or a 1:10 acridine orange/propidium iodide (AO/PI) Cell Viability Reagent, supplied by Logos Biosystems and Thermo Fisher Scientific. In the R & D preclinical laboratory a LUNA-II™ Automated cell Counter, which utilizes a 0.4% trypan blue stain was employed.

The thawing process began by rapidly warming the cryovial in a water bath. Once thawed, the cells were transferred to 10 ml of cell complete medium. After centrifugation at 350 g for 5 min, the supernatant was discarded, and the pellet was resuspended in RPMI 1640 medium (4.5 g/L glucose), enriched with 2 mM L-glutamine, 1 mM sodium pyruvate, 100 IU penicillin, 100 μg/ml streptomycin, 10 % FCS, and 10 % T. stim with Concanavalin A. This was then cultivated in a T 75 cell culture flask. For the freezing procedure, cells were transferred to 50 ml Falcon tubes, centrifuged at 350 g for 5 min, resuspended in 1 ml of freezing medium (FCS with 10 % DMSO), and placed in a cryovial. For effective cryopreservation and recovery, the vials were stored in a freezing container with isopropyl alcohol at -80 ºC overnight before long-term storage in liquid nitrogen.

Throughout our project, we used female C57BL/6 mice (aged 6 to 12 weeks) acquired from Charles River Laboratories in the UK as donor and recipient mice. All experimental

protocols and animal handling were performed in accordance with PPL, PIL, and UK Home Office guidelines.

4.2.1.2 Radiolabelling of cells

CTLL2 cells were radiolabelled with ^{89}Zr complexes using three methods 1) the ^{89}Zr-oxine method optimised on EL4 cells in chapter 3, 2) the ^{89}Zr-DFO-NCS methods described in chapter 3 and 3) the kit formulation of ^{89}Zr-oxine described by Man *et al.*,[318]. Detailed descriptions of the ^{89}Zr separation, purification, and synthesis of ^{89}Zr complexes are provided in Chapter 2. This section includes only the cell labelling procedures.

The following compositions were used to label CTLL2 cells with ^{89}Zr-oxine and ^{89}Zr-DFO-NCS. For methods 1) and 3) a total of 18 MBq of ^{89}Zr-oxine was added per 7.5×10^6 cells in 1.5 ml of complete medium (RPMI, 2mM L-glutamine, 1 mM sodium pyruvate, 100 IU penicillin, 100 μg/ml streptomycin, 10 % FCS, and 10 % T.stim with ConA) containing 0.75 mg oxine in 1.5 ml of suspensions. For method 2) A total of 18 MBq of ^{89}Zr-DFO-NCS was added per 7.5×10^6 cells in 1.5 ml of PBS (n = 3). Cells and radioactivity from all three methods, in 2 ml Eppendorf tubes, were placed in a thermoshaker for mixing at 300 rpm for 30 min at 37 °C. The cells were centrifuged immediately after the cell labelling reaction was completed for 5 min at RT and 350 g. The supernatants were discarded, and the labelled cells were washed three times with 1 ml of PBS to remove any unattached ^{89}Zr-oxine or ^{89}Zr-DFO-NCS. After each wash, the activity of cell pellets and supernatants was measured using a Capintec CRC-25R dose calibrator set to calibrator setting 465 to determine the cell labelling efficiency (CLE). CLE % was calculated by dividing the radioactivity in the pellet by the total radioactivity added. The cell count and viability were then calculated using a Luna II automated cell counter as described above.

4.2.1.3 *In vitro* monitoring of cells

After the cell labelling was accomplished, for each of the three labelling methods, triplicate samples containing 1.47×10^6 labelled CTLL2 cells were prepared. In parallel, triplicate samples of an equivalent number of unlabelled CTLL2 cells were also arranged. These samples were then introduced into flasks containing complete culture medium. Subsequently, the flasks were incubated at 37°C in a CO_2 incubator, where they were maintained for a seven-day period to facilitate *in vitro* analysis. The *in vitro* assessment focused on monitoring cell viability and proliferation, alongside the retention of the tracer by both labelled and unlabelled cells post-incubation. Tracer retention was quantified by measuring radioactivity in the cell supernatant and pellet using a Wallac Wizard 1470-20 gamma counter. These radioactivity measurements were taken, and the culture medium was refreshed on days 1, 4, and 7, following procedures detailed in section 4.2.1.1.

4.2.1.4 *In vivo* tracking of cells

In vivo tracking of a portion of the radiolabelled CTLL2 cells from section 4.2.1.2 was conducted using PET/CT imaging on wild-type, C57BL/6 female mice to determine whether the biodistribution of the labelled cells provided useful information and enabled an *in vivo* comparison of the three labelling products. The mice were intravenously injected with approximately 0.4 – 0.8 MBq of ^{89}Zr activity. The cell loading concentration of the injected ^{89}Zr-oxine labelled CTLL2 cells was 0.68 - 0.85 MBq/10^6 cells for ^{89}Zr-oxine (method 1), 0.53 – 0.59 MBq/10^6 cells for ^{89}Zr-DFO-NCS labelled CTLL2 cells (method 2) and 0.61 - 0.85 MBq/10^6 cells for the kit formulation of ^{89}Zr-oxine (method 3).

Mice were scanned 30 – 60 min after the labelled cells were administered using a Mediso PET/CT Imaging System (NanoScan122S PET/CT, Mediso, Hungary). To conduct PET/CT scanning, mice were anaesthetised, and anaesthesia was maintained using the scanner bed's nose cone (1 - 2 % isoflurane in oxygen gas, 1 – 2 l/min). At the same time, respiration was monitored using a pressure pad connected to differential pressure transducers to monitor low-range pressures. PET imaging of the whole body was performed on mice for 1 h, followed by a 3-min CT scan. The PET scan was acquired with the following PET settings: spatial resolution of 0.4 mm and energy lower/upper limits of 400/600 KeV. The CT scan was acquired at a tube voltage of 50 kVp, tube current of 1 mA, exposure time of 300 ms, and maximum projection count of 400. When reconstructed, the CT had a 0.25 mm resolution. The anaesthetised mice were then placed in a Capintec CRC-25 dose calibrator set to calibrator setting 465 to determine the total radioactivity of the whole body. The mice were scanned again at 20 h, 43 h, 67 h, 138 h, and 187 h after tracer administration.

4.2.1.5 Image processing and analysis

Using VivoQuant 4.0, patch 3 software, the acquired PET/CT images were processed and analysed. Three-dimensional regions of interest (ROIs) were drawn around the target organs: the lungs, liver, spleen, kidneys, and skeleton. ROI sum outputs were decay-corrected to the injection time to calculate the percentage of the injected dose (%IA) and the normalised percentage of the injected dose per organ (%IA/organ).

4.2.1.6 Statistical analysis

In this section, the data were analysed using GraphPad Prism software version 8.2.1. For comparisons between two groups, unpaired two-tailed t-tests were used, whereas one-way

ANOVAs with multiple comparisons were used for comparisons between more than two groups. The comparison was analysed using the statistical test indicated in the legend of each table and/or figure. Therefore, the results are presented as mean ± standard deviation (SD). P values < 0.05 were considered statistically significant, with * indicating that p values were ≤ 0.05, ** indicating that p values were ≤ 0.01, *** indicating that p values were ≤ 0.001, **** indicating that p values were ≤ 0.0001, while ns represents no significance for p values > 0.05.

4.3 Results

4.3.1 Radiolabelling of CTLL2 cells using the optimised parameters from EL4 cells and track the radiolabelled cells *in vivo* using PET/CT imaging in a mouse model.

4.3.1.1 Radiolabelling of cells

CTLL2 cells were radiolabelled with the ^{89}Zr-oxine complex using our developed method (method 1) and the method of Man *et al*. (method 3),[318] with a labelling efficiency of 23 – 27 % and radioactivity concentrations of 0.68 – 0.85 MBq/10^6 and 0.61 – 0.85 MBq/10^6 cells from a starting activity of 18 MBq for each method, respectively. In contrast, the labelling efficiency of CTLL2 cells using the ^{89}Zr-DFO-NCS complex obtained by our developed method (method 2) from a starting activity of 18 MBq was 20 %, resulting in a cell loading concentration of 0.53 – 0.59 MBq/10^6 cells. Cell viability was not significantly altered by the three cell labelling methods, with more than 4×10^6 cells labelled by each method.

4.3.1.2 *In vitro* monitoring of cells

4.3.1.2.1 ^{89}Zr-oxine labelled CTLL2 cells labelled by method 1

The ^{89}Zr-oxine labelling efficiency of CTLL2 cells was 23 – 27 % at 18 MBq with radiolabelled cell viability of 94.03 % ± 0.58 %. A radioactivity concentration of 0.68 – 0.85 MBq/10^6 cells was determined in ^{89}Zr-oxine labelled CTLL2 cells. The ^{89}Zr-oxine labelled CTLL2 cells were tested for viability and proliferative ability using an automated cell counter immediately following labelling and at 1, 4, and seven days after labelling. The cell viability values were 94.03 % ± 0.58 %, 95 % ± 0.53 %, 93.27 % ± 0.84 %, and 92.2 % ± 0.87 %, respectively, and the cell proliferation values were 1.77×10^6 ± 0.15, 3.78×10^6 ± 0.17, and 5.15×10^6 ± 0.45, respectively. During days 1, 4, and 7 post labelling, 27.03 % ± 1.57 %, 42.97 % ± 1.27 %, and 52.10 % ± 0.76 %, respectively, of the radiolabelled activity were released from the ^{89}Zr-oxine labelled CTLL2 cells, Figure 4-7, Table 4-6, and Table 4-7.

^{89}Zr-labelled and unlabelled cells were compared for viability and proliferation using the unpaired t-test with Welch's correction test. Individual variances were calculated for each comparison (Brown-Forsythe and Welch ANOVA tests). No statistically significant difference was observed between cells labelled with ^{89}Zr and those that were not labelled in terms of viability and proliferation ability ($p > 0.05$). In Table 4-1, Figure 4-1, and Figure 4-2, the *in vitro* viability and proliferation of ^{89}Zr- labelled and unlabelled CTLL2 cells are compared statistically at 0, 1, 4, and 7 days following the cell labelling procedure.

Result	Time	Unpaired t with Welch's correction test	Mean difference	Significant?	Summary	P Value
Cell Viability (%)	0 h	Unlabelled vs ^{89}Zr-oxine	1.43	No	ns	0.07
	1 d	Unlabelled vs ^{89}Zr-oxine	0.07	No	ns	0.91
	4 d	Unlabelled vs ^{89}Zr-oxine	0.93	No	ns	0.25
	7 d	Unlabelled vs ^{89}Zr-oxine	1.57	No	ns	0.07
Cell proliferation ($\times 10^6$)	0 h	Unlabelled vs ^{89}Zr-oxine	0.00	No	ns	0.65
	1 d	Unlabelled vs ^{89}Zr-oxine	0.12	No	ns	0.49
	4 d	Unlabelled vs ^{89}Zr-oxine	0.20	No	ns	0.32
	7 d	Unlabelled vs ^{89}Zr-oxine	-0.13	No	ns	0.68

Table 4-1: ***In vitro* cell viability and cell proliferation comparison results between the ^{89}Zr-oxine labelled and unlabelled CTLL2 cells at 0 h, day 1, day 4, and day 7 after cell labelling.** CTLL2 cells were labelled with 18 MBq of ^{89}Zr-oxine with a radioactivity concentration of 0.68 – 0.85 MBq/10^6 cells. Values are shown as mean ± SD, n = 3. No statistically significant difference was observed in viability and proliferation results between labelled and unlabelled cells. Significance was calculated using the unpaired t-test with Welch's correction test, with individual variances computed for each comparison (Brown-Forsythe and Welch ANOVA tests). p values < 0.05 were considered statistically significant. ns represents no significance for p values > 0.05.
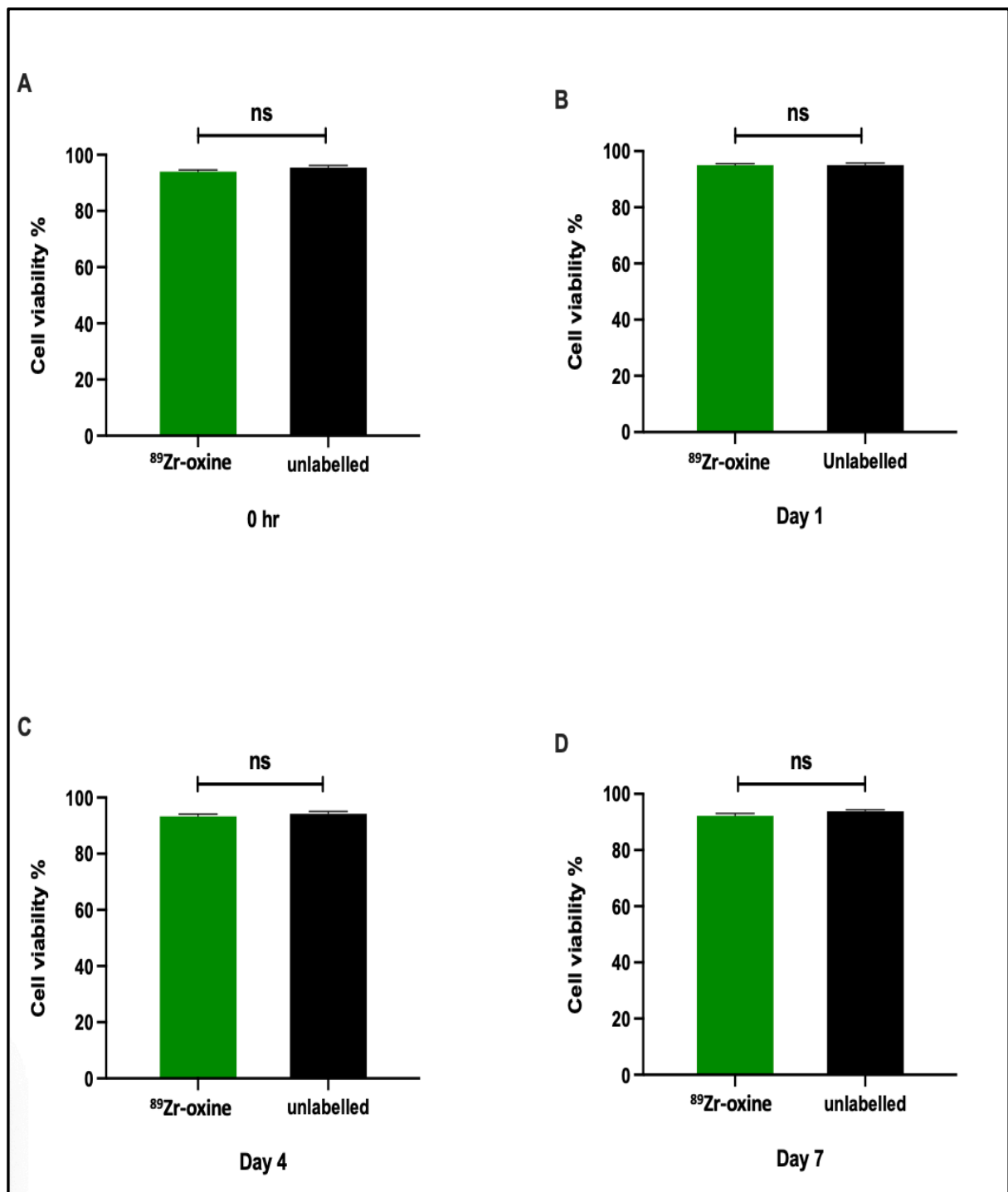
Figure 4-1: *In vitro* **cell viability results for** ^{89}**Zr-oxine labelled and unlabelled CTLL2 cells at 0 h, day 1, day 4, and day 7 after cell labelling.** CTLL2 cells were labelled with 18 MBq of ^{89}Zr-oxine with a radioactivity concentration of $0.68 – 0.85$ MBq/10^6 cells. All values are shown as mean $\pm$ SD, n = 3. A statistically significant difference in viability was not found between the labelled and unlabelled cells. Significance was calculated using the unpaired t-test with Welch's correction test, with individual variances computed for each comparison (Brown-Forsythe and Welch ANOVA tests). p values < 0.05 were considered statistically significant. ns represents no significance for p values > 0.05.

Figure 4-2: *In vitro* **proliferation results for unlabelled and** ⁸⁹**Zr-oxine labelled CTLL2 cells after 0 h, 1 d, 4 d, and 7 d following cell labelling.** CTLL2 cells were labelled with 18 MBq of ^{89}Zr-oxine to produce a radioactivity concentration of $0.68 - 0.85$ MBq/10^6 cells. Data are presented as mean $\pm$ SD, n = 3. Proliferation results between labelled and unlabelled cells did not differ statistically significantly. Each comparison was assessed through analysis of variance using the Brown– Forsythe and Welch ANOVA tests). p values < 0.05 were considered statistically significant. ns represents no significance for p values > 0.05.

4.3.1.2.2 ^{89}Zr-DFO-NCS labelled CTLL2 cells labelled by method 2

CTLL2 cells were labelled with 18 MBq of ^{89}Zr-DFO-NCS, and 95.4 % ± 0.26 % of those labelled cells survived with a radioactivity concentration of 0.53 – 0.59 MBq/10^6 cells. The viability and proliferation of ^{89}Zr-DFO-NCS labelled CTLL2 cells were evaluated using an automated cell counter immediately, at 1, 4, and seven days following labelling. The results show that cell viability values were 95.4 % ± 0.26 %, 94.5 % ± 0.4 %, 94.5 % ± 0.26 %, and 93.3 % ± 0.4 %, respectively. Cell proliferation values were 1.47×10^6 ± 0.01, 1.81×10^6 ± 0.05, 3.09×10^6 ± 0.16, and 3.80×10^6 ± 0.21, in that order. A total of 11.4 % ± 1.25 %, 24.5 % ± 0.7 %, and 35.3 % ± 1.5 %, respectively, of the radiolabelled activity was released from CTLL2 cells labelled with ^{89}Zr-DFO-NCS on days 1, 4, and day 7 after labelling, Figure 4-7, Table 4-6, and Table 4-7.

The viability and proliferation of ^{89}Zr-labelled and unlabelled cells were compared using the unpaired t-test with Welch's correction test, with individual variances computed for each comparison (Brown-Forsythe and Welch ANOVA tests). Cell viability was not significantly different between ^{89}Zr-DFO-NCS labelled and unlabelled CTLL2 cells ($p > 0.05$). However, ^{89}Zr-DFO-NCS labelled cells demonstrated a time-dependent decrease in cell proliferation ability. The proliferation ability of cells after one day of labelling did not differ significantly from that of unlabelled cells ($p = 0.62$). Nevertheless, labelled CTLL2 cells demonstrated significantly lower cell proliferation abilities than unlabelled CTLL2 cells at days 4 ($p = 0.01$) and 7 ($p = 0.003$) following labelling. Table 4-2, Figure 4-3, and Figure 4-4 present statistical comparisons of the *in vitro* viability and proliferation of labelled and unlabelled CTLL2 cells.

Result	Time	Unpaired t with Welch's correction test	Mean difference	Significant?	Summary	P Value
Cell Viability (%)	0 h	Unlabelled vs ^{89}Zr-DFO-NCS	0.06	No	ns	0.9
	1 d	Unlabelled vs ^{89}Zr-DFO-NCS	0.53	No	ns	0.36
	4 d	Unlabelled vs ^{89}Zr-DFO-NCS	0.3	No	ns	0.61
	7 d	Unlabelled vs ^{89}Zr-DFO-NCS	0.46	No	ns	0.34
Cell proliferation ($\times 10^6$)	0 h	Unlabelled vs ^{89}Zr-DFO-NCS	0.00	No	ns	0.65
	1 d	Unlabelled vs ^{89}Zr-DFO-NCS	0.08	No	ns	0.62
	4 d	Unlabelled vs ^{89}Zr-DFO-NCS	0.89	Yes	*	0.01
	7 d	Unlabelled vs ^{89}Zr-DFO-NCS	1.23	Yes	**	0.003

Table 4-2: ***In vitro* cell viability and cell proliferation comparison results between the ^{89} Zr-DFO-NCS labelled and unlabelled CTLL2 cells at 0 h, day 1, day 4, and day 7 after cell labelling.** CTLL2 cells were labelled with 18 MBq of ^{89} Zr-DFO-NCS, and 95.4 % ± 0.26 % of the labelled cells survived with a radioactivity concentration of 0.53 – 0.59 MBq/10^6 cells. Values are shown as mean ± SD, n = 3. No statistically significant difference was observed in viability results, however there was a statistically significant difference in proliferation results between labelled and unlabelled cells. Significance was calculated using the unpaired t-test with Welch's correction test, with individual variances computed for each comparison (Brown-Forsythe and Welch ANOVA tests). P values < 0.05 were considered statistically significant, with * indicating that p values were ≤ 0.05 and ** indicating that p values were ≤ 0.01. ns represents no significance for p values > 0.05.
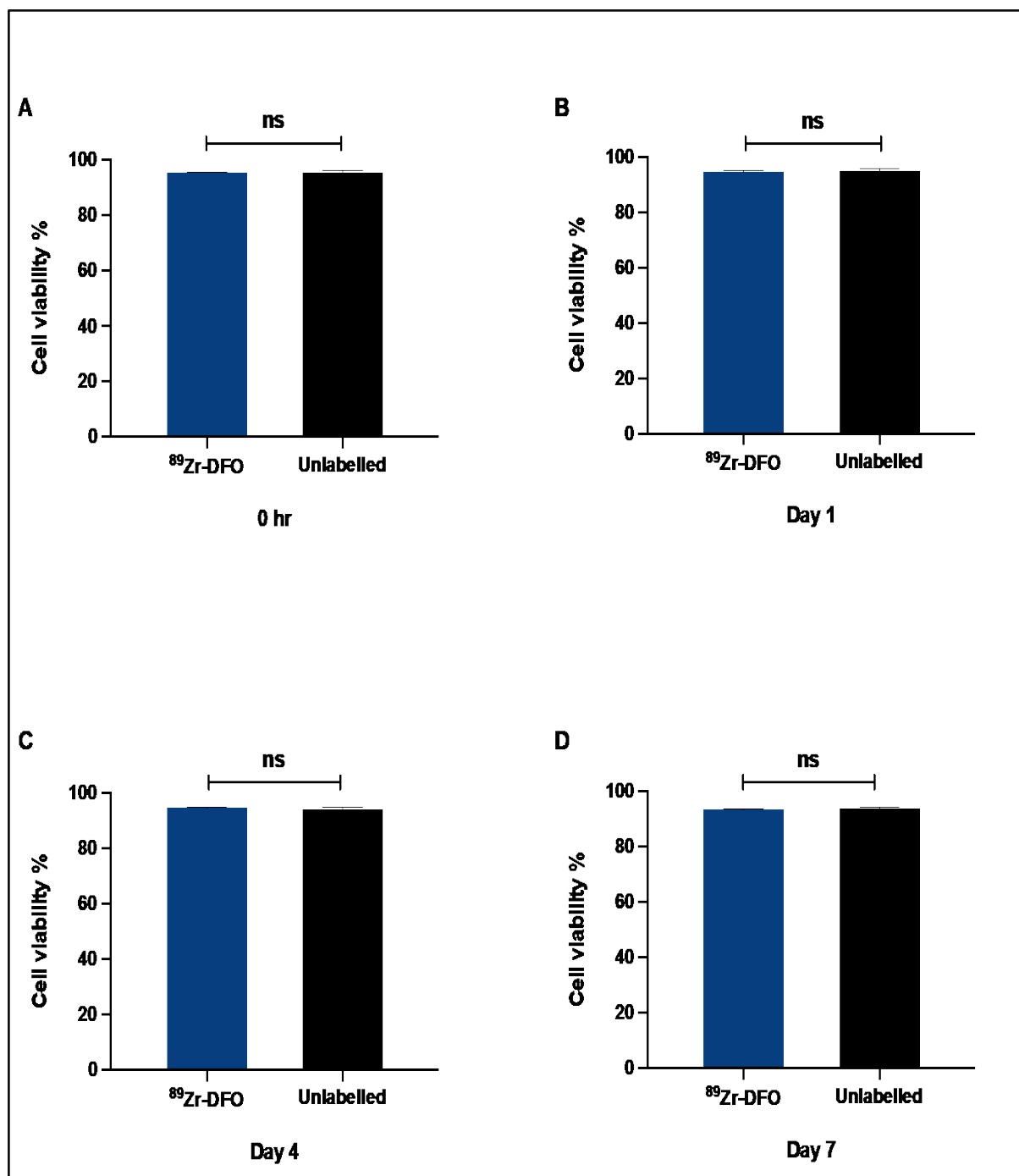
Figure 4-3: *In vitro* cell viability results for the ^{89}Zr-DFO-NCS labelled and unlabelled CTLL2 cells at 0 h, day 1, day 4, and day 7 post-cell labelling. CTLL2 cells were labelled with 18 MBq of ^{89}Zr-DFO-NCS, and 95.4 % ± 0.26 % of the labelled cells survived with a radioactivity concentration of 0.53 – 0.59 MBq/10^6 cells. All values are shown as mean ± SD, n = 3. A statistically significant difference in viability was not found between the labelled and unlabelled cells. Significance was calculated using the unpaired t-test with Welch's correction test. Individual variances were calculated for each comparison (Brown-Forsythe and Welch ANOVA tests). P values < 0.05 were considered statistically significant. ns represents no significance for p values > 0.05.

Figure 4-4: *In vitro* **cell count results for the** [89] **Zr-DFO-NCS labelled and unlabelled CTLL2 cells at 0 h, day 1, day 4, and day 7 post-cell labelling.** CTLL2 cells were labelled with 18 MBq of [89] Zr-DFO-NCS, and 95.4 % ± 0.26 % of the labelled cells survived with a radioactivity concentration of $0.53 - 0.59$ MBq/10^6 cells. All values are shown as mean ± SD, n = 3. A statistically significant difference in proliferation ability was found between the labelled and unlabelled cells. Significance was calculated using the unpaired t-test with Welch's correction test. Individual variances were calculated for each comparison (Brown-Forsythe and Welch ANOVA tests). P values < 0.05 were considered statistically significant, with * indicating that p values were ≤ 0.05 and ** indicating that p values were ≤ 0.01. ns represents no significance for p values > 0.05.

4.3.1.2.3 ^{89}Zr-oxine Kit labelled CTLL2 cells labelled by method 3

CTLL2 cells were labelled using 18 MBq of ^{89}Zr-oxine. The radioactivity concentration of the surviving cells, which accounted for 94.23 % ± 0.49 % of the labelled population, was found to be between 0.61 and 0.85 MBq/10^6 cells. The viability and proliferation of the labelled cells were then evaluated using an automated cell counter immediately after labelling and at 1, 4 and 7 days following the labelling process. The viability values for the labelled cells at each time point were 94.23 % ± 0.49 %, 94.27 % ± 0.15%, 93.80 % ± 1.25 %, and 94.13 % ± 0.90 %, respectively, while the proliferation values were $1.48{\times}10^6$ ± 0.01, $1.70{\times}10^6$ ± 0.17, $3.79{\times}10^6$ ± 0.14, and $4.66{\times}10^6$ ± 0.47. The total activity released from the labelled CTLL2 cells on days 1, 4, and 7 after labelling was 27.37 % ± 0.90 %, 43.33 % ± 1.53 %, and 51.63 % ± 1.19 %, respectively, Figure 4-7, Table 4-6, and Table 4-7.

To compare the viability and proliferation of labelled and unlabelled cells, an unpaired t-test with Welch's correction was performed. Brown– Forsythe and Welch ANOVA tests were performed to calculate individual variances for each comparison. The results showed no statistically significant differences in viability and proliferation between the labelled and unlabelled cells ($p > 0.05$). In Table 4-3, Figure 4-5, and Figure 4-6, the *in vitro* viability and proliferation of ^{89}Zr- labelled CTLL2 cells were compared at different time points following the labelling procedure.

Result	Time	Unpaired t with Welch's correction test	Mean difference	Significant?	Summary	P Value
Cell Viability (%)	**0 h**	Unlabelled vs ^{89}Zr-oxine-Kit	1.23	No	ns	0.09
	1 d	Unlabelled vs ^{89}Zr-oxine-Kit	0.80	No	ns	0.20
	4 d	Unlabelled vs ^{89}Zr-oxine-Kit	0.40	No	ns	0.67
	7 d	Unlabelled vs ^{89}Zr-oxine-Kit	-0.37	No	ns	0.59
Cell proliferation (×10^6)	**0 h**	Unlabelled vs ^{89}Zr-oxine-Kit	0.00	No	ns	0.82
	1 d	Unlabelled vs ^{89}Zr-oxine-Kit	-0.19	No	ns	0.32
	4 d	Unlabelled vs ^{89}Zr-oxine-Kit	-0.19	No	ns	0.33
	7 d	Unlabelled vs ^{89}Zr-oxine-Kit	-0.36	No	ns	0.33

Table 4-3: Results of a comparison between the *in vitro* viability and proliferation of CTLL2 cells labelled with ^{89}Zr-oxine-Kit and those that were not. The labelled cells were created using 18 MBq of ^{89}Zr-oxine and had a radioactivity concentration of $0.61 - 0.85$ MBq/10^6 cells. The results are shown as mean ± standard deviation, with n = 3 for each comparison. The viability and proliferation of the labelled and unlabelled cells did not differ statistically significantly. ANOVA tests were used to calculate significance using the unpaired t-test with Welch's correction and individual variances for each comparison (Brown-Forsythe and Welch ANOVA tests). Statistical significance was defined as p values < 0.05. For p values > 0.05, ns indicates no significance.
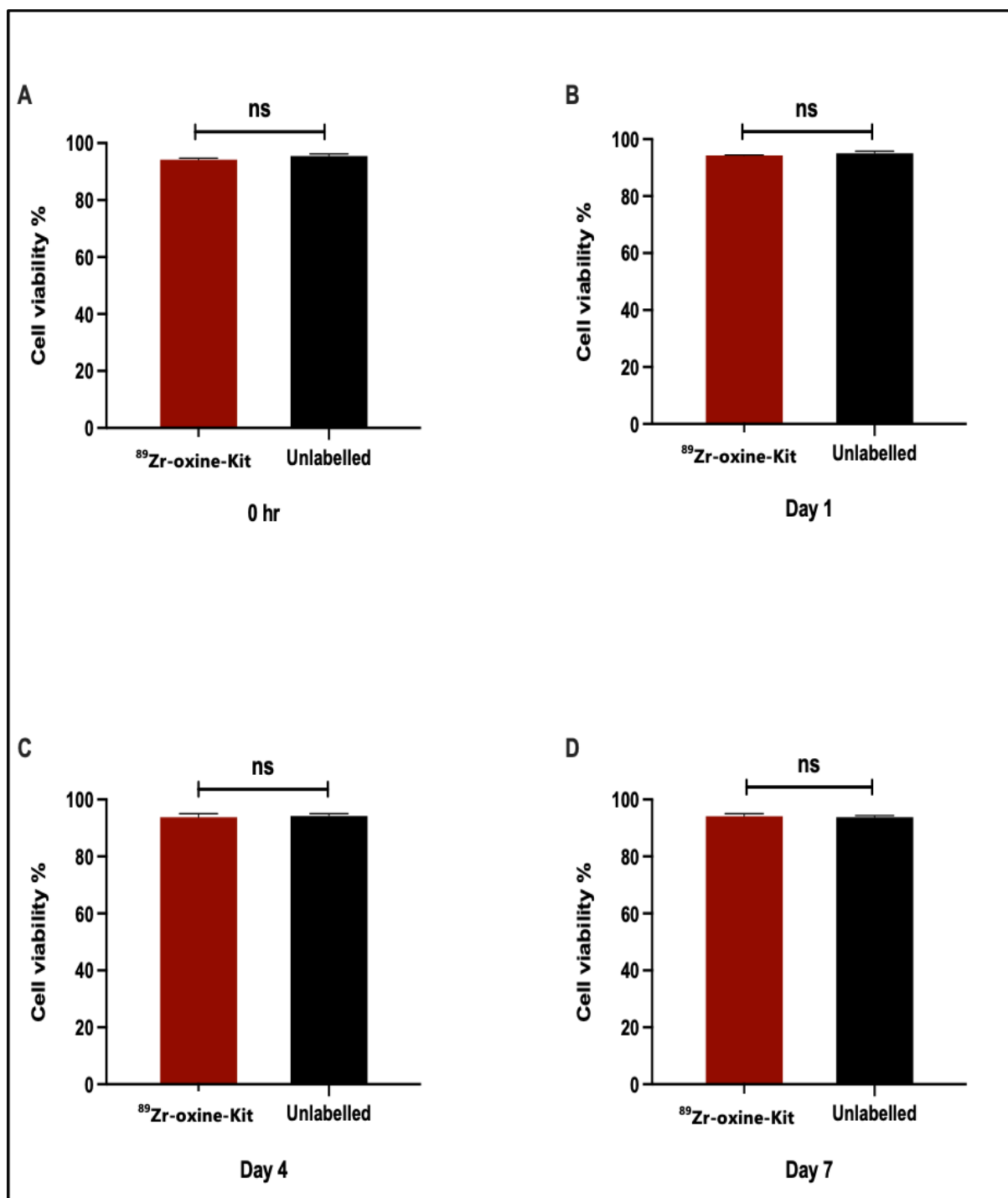
Figure 4-5: *In vitro* **cell viability results for** ⁸⁹**Zr-oxine labelled and unlabelled CTLL2 cells at 0 h, day 1, day 4, and day 7 after cell labelling.** The cells were radiolabelled using 18 MBq of ^{89}Zr-oxine and had a radioactivity concentration of $0.61 – 0.85$ MBq/10^6 cells. The results are shown as mean $\pm$ standard deviation, with n = 3 for each comparison. The viability and proliferation of the labelled and unlabelled cells did not differ statistically significantly. ANOVA tests were used to calculate significance using the unpaired t-test with Welch's correction and individual variances for each comparison (Brown-Forsythe and Welch ANOVA tests). Statistical significance was defined as p values < 0.05. For p values > 0.05, ns indicates no significance.
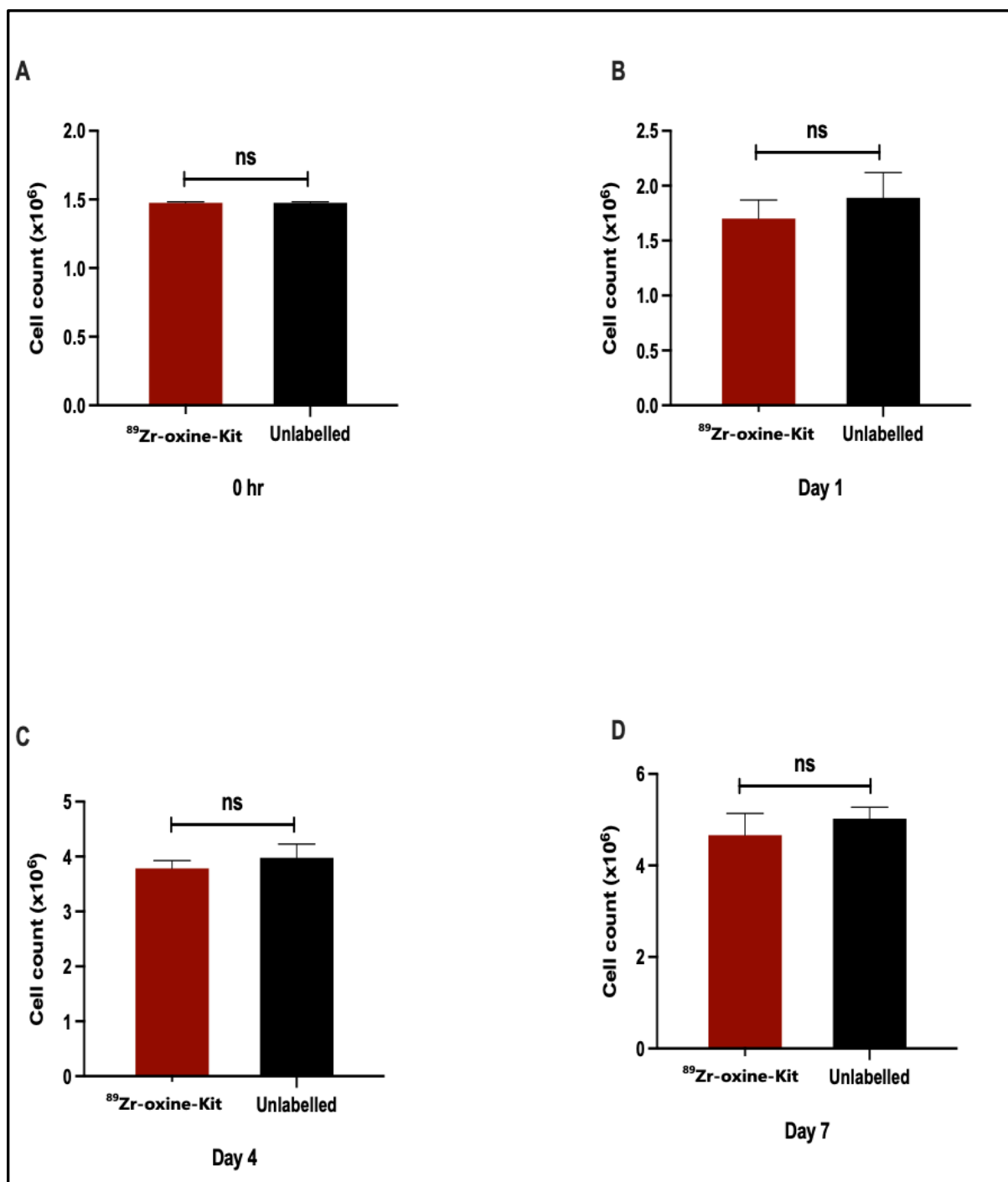
Figure 4-6: Results of *in vitro* cell count for CTLL2 cells labelled with ⁸⁹Zr-oxine and unlabelled cells at various time points after labelling. The labelled cells were prepared using 18 MBq of ^{89}Zr-oxine and had a radioactivity concentration of $0.61 - 0.85$ MBq/10^6 cells. The data, displayed as mean ± standard deviation, were derived from three replicates per comparison and analysed using Brown–Forsythe and Welch ANOVA tests. There were no statistically significant differences in viability or proliferation between labelled and unlabelled cells. Statistical significance was determined to be present at p values less than 0.05, whereas p values greater than 0.05 are denoted as "ns" to indicate a lack of significance.

Time	Sample	Cell viability (%)			
		UNLABELLED CTLL2 Cells (%)	LABELLED CTLL2 Cells		
			^{89}Zr-oxine-CTLL2 (%)	^{89}Zr-DFO-NCS-CTLL2 (%)	^{89}Zr-oxine KIT-CTLL2 (%)
0 d	1	96.1	93.8	95.3	93.9
	2	94.6	94.7	95.2	94
	3	95.7	93.6	95.7	94.8
1 d	1	94.3	94.8	94.6	94.4
	2	95.1	95.6	94.1	94.1
	3	95.8	94.6	94.9	94.3
4 d	1	94.3	93.8	94.7	92.8
	2	93.3	92.3	94.6	95.2
	3	95	93.7	94.2	93.4
7 d	1	93.2	91.8	92.9	95
	2	93.7	93.2	93.3	93.2
	3	94.4	91.6	93.7	94.2

Table 4-4: **Summary of the *in vitro* cell viability results obtained from the radiolabelling of CTLL2 cells** using our developed methods of ^{89}Zr-oxine and ^{89}Zr-DFO-NCS, as well as the cell labelling method developed by Man *et al*.,[318] for labelling cells with ^{89}Zr-oxine. The cells were labelled using 18 MBq of ^{89}Zr, and data were collected from three replicates per comparison. Labelled and unlabelled CTLL2 cells were tracked *in vitro* at 0 hr, day 1, day 4, and day 7 post cell labelling.

Time	Sample	Cell Proliferation			
		UNLABELLED CTLL2 Cells ($\times 10^6$)	LABELLED CTLL2 Cells		
			^{89}Zr-oxine-CTLL2 ($\times 10^6$)	^{89}Zr-DFO-NCS-CTLL2 ($\times 10^6$)	^{89}Zr-oxine Kit-CTLL2 ($\times 10^6$)
1 d	1	1.63	1.6	1.87	1.53
	2	1.97	1.8	1.8	1.87
	3	2.07	1.9	1.77	1.7
4 d	1	3.97	3.93	3.27	3.9
	2	3.73	3.8	2.97	3.83
	3	4.23	3.6	3.03	3.63
7 d	1	5.27	5.1	3.63	5.03
	2	5.03	4.73	4.03	4.83
	3	4.77	5.63	3.73	4.13

Table 4-5: **Summary of *in vitro* cell proliferation results for unlabelled and labelled CTLL2 cells** using the methods developed by us for ^{89}Zr-oxine and ^{89}Zr-DFO-NCS, as well as the method developed by Man *et al*.,[318] for labelling cells with ^{89}Zr-oxine. Data were collected from three replicates per comparison after labelling the cells with 18 MBq of ^{89}Zr. Cells were tracked *in vitro* at 0 h, day 1, day 4, and day 7 after cell labelling.

Time	Sample	EFFLUX% of ^{89}Zr activity in labelled cells		
		^{89}Zr-oxine-CTLL2 cells (%)	^{89}Zr-DFO-NCS-CTLL2 cells (%)	^{89}Zr-oxine Kit-CTLL2 cells (%)
1 d	1	25.8	11.3	27.3
	2	26.5	10.2	28.3
	3	28.8	12.7	26.5
4 d	1	41.6	25	45
	2	44.1	23.7	42
	3	43.2	24.8	43
7 d	1	51.3	37	53
	2	52.2	35	50.9
	3	52.8	34	51

Table 4-6: **Summary of efflux % of ^{89}Zr activity from the labelled CTLL2 cells** using the methods developed by us for ^{89}Zr-oxine and ^{89}Zr-DFO-NCS, as well as the method developed by Man *et al*.,[318] for labelling cells with ^{89}Zr-oxine. Data were collected from three replicates per comparison after labelling the cells with 18 MBq of ^{89}Zr. The data are presented as the total efflux percentage off ^{89}Zr activity calculated at days 1, 4, and 7 post cell labelling for each cell labelling method.

Time	Brown– Forsythe and Welch ANOVA tests of EFFLUX percentage of activity from labelled cells	Mean efflux difference (%)	Significant?	Summary	P Value
1 d	^{89}Zr-oxine vs ^{89}Zr-DFO-NCS	15.63	Yes	***	< 0.001
	^{89}Zr-oxine vs ^{89}Zr-oxine-Kit	-0.33	No	ns	0.77
	^{89}Zr-DFO-NCS vs ^{89}Zr-oxine-Kit	-15.97	Yes	***	< 0.001
4 d	^{89}Zr-oxine vs ^{89}Zr-DFO-NCS	18.47	Yes	***	< 0.001
	^{89}Zr-oxine vs ^{89}Zr-oxine-Kit	-0.37	No	ns	0.77
	^{89}Zr-DFO-NCS vs ^{89}Zr-oxine-Kit	-18.83	Yes	***	< 0.001
7 d	^{89}Zr-oxine vs ^{89}Zr-DFO-NCS	16.77	Yes	***	< 0.001
	^{89}Zr-oxine vs ^{89}Zr-oxine-Kit	0.47	No	ns	0.60
	^{89}Zr-DFO-NCS vs ^{89}Zr-oxine-Kit	-16.30	Yes	***	< 0.001

Table 4-7: **Summary of the statistical comparison results of the efflux % of ^{89}Zr activity from the labelled CTLL2 cells** using the methods developed by us for ^{89}Zr-oxine and ^{89}Zr-DFO-NCS, as well as the method developed by Man *et al*.,[318] for labelling cells with ^{89}Zr-oxine. Data were collected from three replicates per comparison after labelling the cells with 18 MBq of ^{89}Zr. Significance was calculated using the unpaired t-test with Welch's correction test. Individual variances were calculated for each comparison (Brown-Forsythe and Welch ANOVA tests). P values < 0.05 were considered statistically significant, with *** indicating that p values were ≤ 0.001, and ns represents no significance for p values > 0.05.
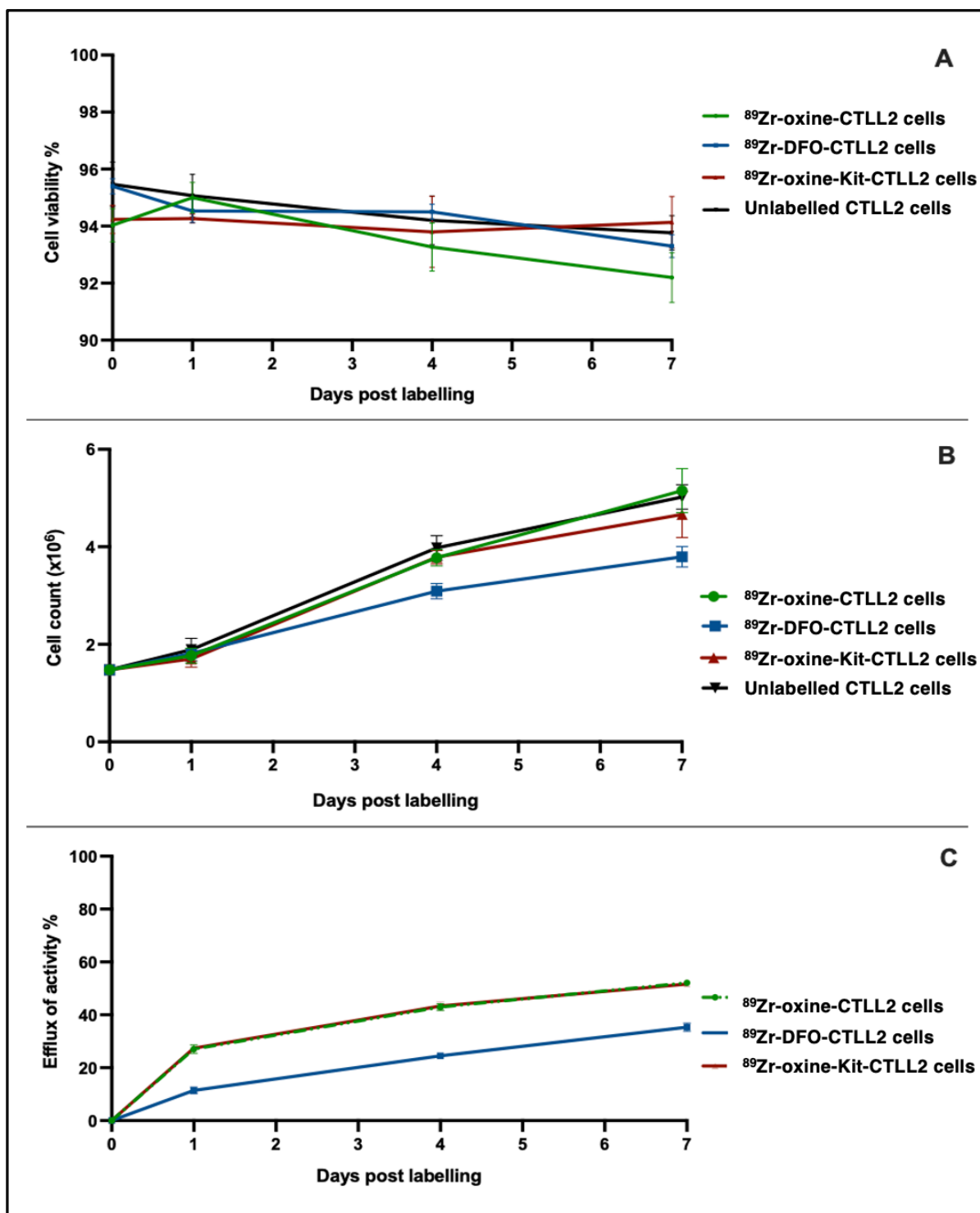
Figure 4-7: Plots comparing cell behaviour after radiolabelling via 3 methods. Results for *in vitro* monitoring of unlabelled and labelled CTLL2 cells using the methods developed by us for ^{89}Zr-oxine and ^{89}Zr-DFO-NCS, as well as the method developed by Man *et al.,*[318] for labelling cells with ^{89}Zr-oxine. Data were collected after labelling the cells with 18 MBq of ^{89}Zr. The results of cell viability **(A)**, cell count **(B)**, and efflux of activity from cells **(C)** were plotted vs time at the following intervals post cell labelling: 0 hr, day 1, day 4, and day 7 post cell labelling. The displayed data are mean ± SD, (n = 3).

4.3.1.3 *In vivo* tracking of the cells

4.3.1.3.1 ^{89}Zr-oxine labelled CTLL2 cells

A series of PET/CT imaging was performed after injecting CTLL2 cells labelled with ^{89}Zr-oxine into mice (n = 3) intravenously to allow for non-invasive longitudinal *in vivo* tracking of the injected cells. Primarily, ^{89}Zr activity was detected in the lungs, liver, skeleton, and kidneys. At 30 min post-activity administration, most of the activity was accumulated in the lungs (%IA: 46.5 % ± 2.34 %), with a minor accumulation of activity seen in the liver (%IA :7.5 % ± 2.33 %) and skeleton (%IA: 5.6 % ± 4.39 %). After 20 h, lung activity (%IA: 25.3 % ± 1.3 %) migrated and accumulated primarily in the liver (%IA: 24.2 % ± 1.9 %), followed by the skeleton (%IA: 10.8 % ± 2.2 %), with minor accumulations in the spleen (%IA: 3.1 % ± 2.1 %) and kidneys (%IA: 1.1 % ± 2.0 %). In these organs, activity remained until the end of the scanning process.

Figure 4-8 and Figure 4-11 display PET/CT imaging and uptake percentage of ^{89}Zr-oxine labelled CTLL2 cells, respectively, in a mouse model, acquired at 0.55 h, 20 h, 43 h, 67 h, 138 h, and 187 h following tracer injection (n = 3). Quantitative data extracted from PET scans of mice injected with CTLL2 cells labelled with ^{89}Zr-DFO-NCS-CTLL2 cells at 0 h, 20 h, 43 h, 67 h, 138 h, and 187 h after injection are presented in Table 4-8.
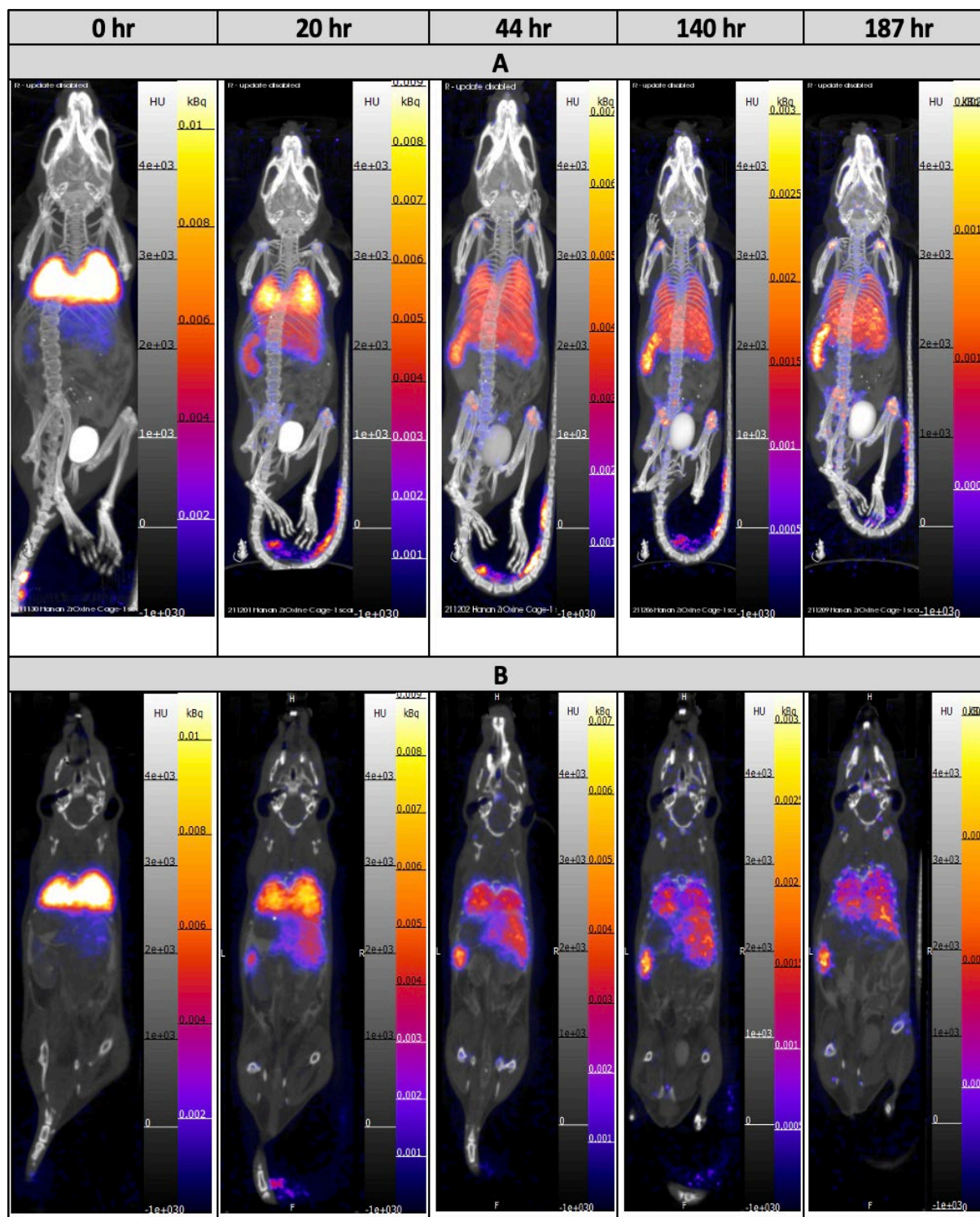
Figure 4-8: PET/CT imaging of ⁸⁹Zr-oxine labelled CTLL2 cells in a mouse model. CTLL2 cells were labelled using our developed ⁸⁹Zr-oxine cell labelling method. **(A)** Serial whole-body MIP representations of PET/CT images and **(B)** PET/CT coronal slice images for a C57BL/6 mouse injected with ⁸⁹Zr-oxine labelled CTLL2 cells via intravenous tail injection. PET/CT scans were acquired at 0.5 h, 20 h, 43 h, 67 h, 138 h, and 187 h post-tracer administration (n = 3). PET images are displayed as KBq and the maximum intensity setting chosen to best highlight tissues of interest in scan 2 was decay corrected backward/forward for other scans in the series based upon the half-life of ⁸⁹Zr.

4.3.1.3.2 ^{89}Zr-DFO-NCS labelled CTLL2 cells

The *in vivo* biodistribution of intravenously injected CTLL2 cells labelled with ^{89}Zr-DFO-NCS in mice (n = 4) was examined using PET/CT imaging at 0.5 h, 20 h, 43 h, 67 h, 138 h, and 187 h. It was found that ^{89}Zr activity was primarily present in the lungs, liver, skeleton, spleen, and kidney. Also, of note in the images of the mouse presented in Figure 4-9 is the two bright spots of focal activity one in the lungs and one in the liver. These bright spots were not observed in the other 3 mice injected with this batch of cells but are similar to those observed for the ^{89}Zr-DFO-NCS labelled mixed lymphocytes imaged in chapter 3. This unwanted effect has not been observed in ^{89}Zr-oxine labelled cells. Approximately 30 min after the activity administration, most of the activity accumulated in the lungs (%IA: 69.4 % ± 5.3 %), with only a minor amount in the skeleton (%IA: 3.7 % ± 1.2 %) and liver (%IA: 2.9 % ± 1.0 %). There was a significant decrease in lung activity (%IA: 17.2 % ± 2.3 %) after 20 h, associated with a significant increase in liver activity (%IA: 34.5 % ± 0.9 %), followed by skeletal activity (%IA: 6.3 % ± 0.9 %) and minor accumulations in the spleen (%IA: 4.7 % ± 0.7 %) and kidneys (%IA: 3.5 % ± 0.4 %).

Figure 4-9 displays PET/CT imaging and uptake % ^{89}Zr-DFO-NCS labelled CTLL2 cells, respectively, in a mouse model, acquired at 0 h, 20 h, 43 h, 67 h, 138 h, and 187 h following tracer injection (n = 4). Quantitative data extracted from PET scans of mice injected with CTLL2 cells labelled with ^{89}Zr-DFO-NCS-CTLL2 cells at 0 h, 20 h, 43 h, 67 h, 138 h, and 187 h after injection are presented in Table 4-8.
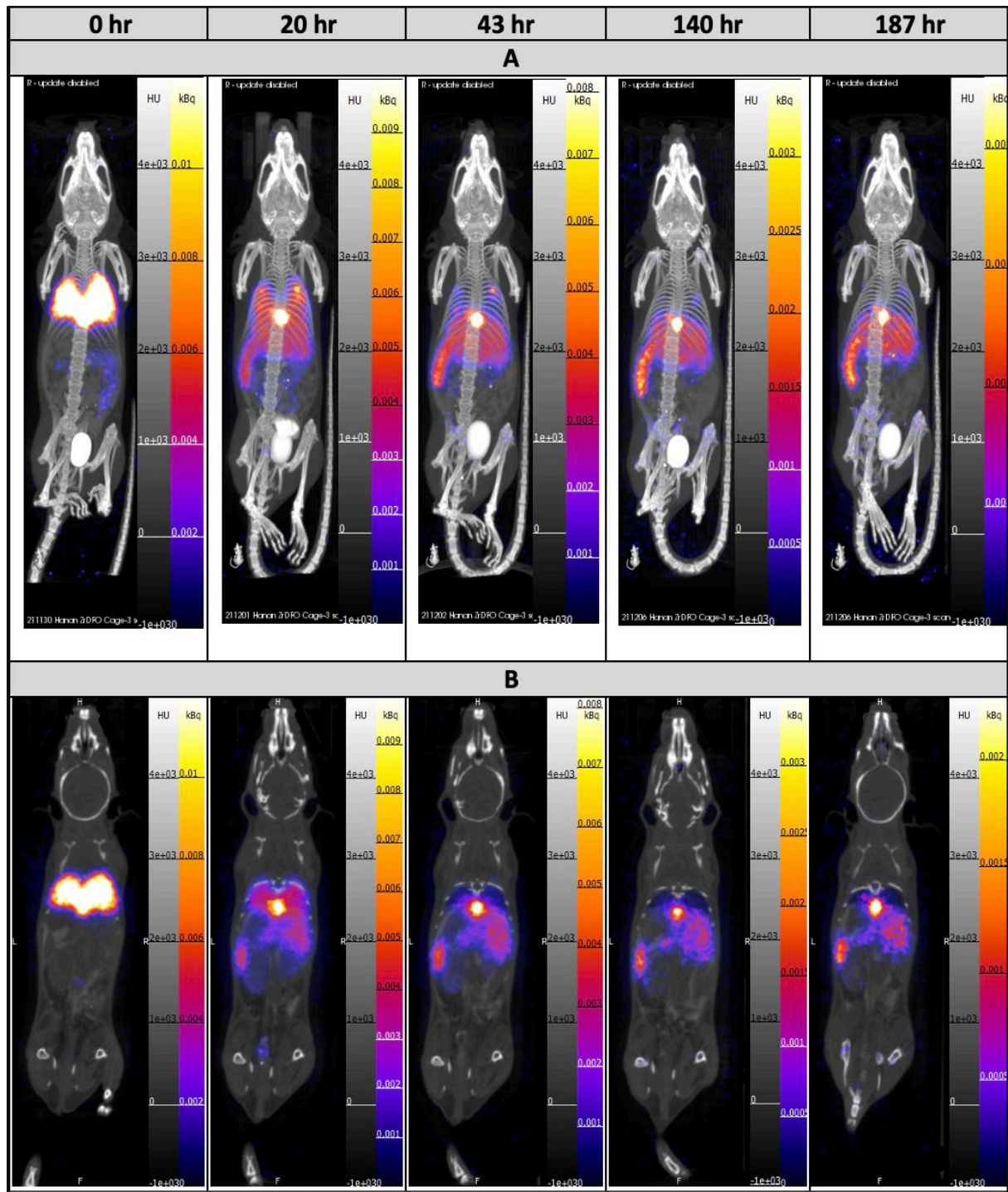
Figure 4-9: *In vivo* **tracking of** [89]**Zr-DFO-NCS labelled CTLL2 cells in a mouse model using PET/CT imaging.** In this study, our developed [89]Zr-DFO-NCS cell labelling method was employed to label CTLL2 cells. **(A)** MIP representation of a series of whole-body PET/CT images and **(B)** Coronal slice views of the same PET/CT images of a C57BL/6 mouse injected with the labelled cells via intravenous tail injection. PET/CT scans were acquired at 0.5 h, 20 h, 43 h, 67 h, 138 h, and 187 h following injection of the tracer (n = 4). PET images are displayed as KBq, and the maximum intensity setting chosen to best highlight tissues of interest in scan 2 was decay corrected backwards/forward for other scans in the series based upon the half-life of [89]Zr.

4.3.1.3.3 ^{89}Zr-oxine Kit labelled CTLL2 cells

CTLL2 cells labelled with the ^{89}Zr-oxine Kit were intravenously injected into mice (n = 2) and tracked *in vivo* using PET/CT imaging at 0.5 h, 20 h, 43 h, 67 h, 138 h, and 187 h post injection to assess their biodistribution. According to the results, ^{89}Zr activity was primarily observed in the lungs, liver, skeleton, spleen, and kidney. At the early time point of administration of the activity, approximately 30 min after administration, most of the activity was accumulated in the lungs (%IA: 42.4 % ± 0.4 %), liver (%IA: 14.2 % ± 5.2 %), kidneys (%IA: 5.1 % ± 0.1 %), and skeleton (%IA: 4.0 % ± 0.3 %). The following day, the activity remained in those organs, but the activity in the lungs (7.4 % ± 1.6 %) decreased, whereas the activity in the liver (%IA: 26.9 % ± 8.7 %), skeleton (%IA: 13.4 % ± 1.2 %), and spleen (%IA: 4.8 % ± 0.4 %) increased.

Figure 4-10 and Figure 4-11 display PET/CT imaging and uptake percentages of ^{89}Zr-oxine labelled CTLL2 cells, respectively, in a mouse model, acquired at 0.5 h, 20 h, 43 h, 67 h, 138 h, and 187 h following tracer injection (n = 2). Quantitative data extracted from PET scans of mice injected with CTLL2 cells labelled with the ^{89}Zr-oxine-Kit at 0.5 h, 20 h, 43 h, 67 h, 138 h, and 187 h after injection are presented in Table 4-8.
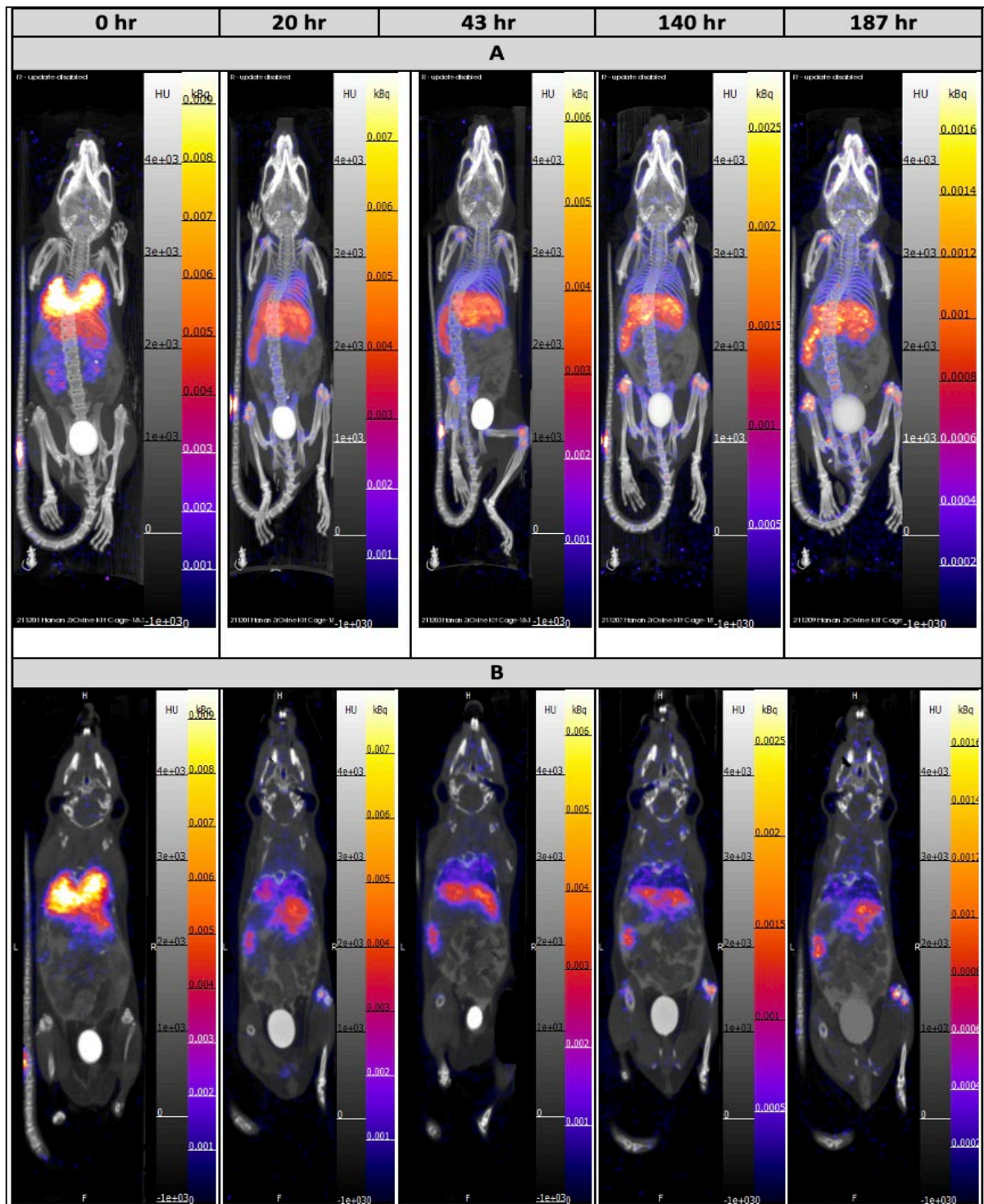
Figure 4-10: **PET/CT imaging of ⁸⁹Zr-oxine labelled CTLL2 cells in a mouse model.** CTLL2 cells were radiolabelled using the method developed by Man *et al*.,[318] for radiolabelling cells with [89]Zr-oxine. **(A)** MIP views of a series of whole-body PET/CT images and **(B)** Coronal slice PET/CT images of a C57BL/6 mouse injected with labelled cells. PET/CT scans were acquired at 0.5 h, 20 h, 43 h, 67 h, 138 h, and 187 h following injection of the tracer (n = 2). PET images are displayed as KBq and the maximum intensity setting chosen to best highlight tissues of interest in scan 2 was decay corrected backwards/forward for other scans in the series based upon the half-life of [89]Zr.

Radiolabelled cells	Organs	Scan 1 (1 hour)		Scan 2 (20 hour)		Scan 3 (43 hour)		Scan 4 (67 hour)		Scan 5 (138 hour)		Scan 6 (187 hour)	
		%IA	± SD	%IA	± SD	%IA	± SD	%IA	± SD	%IA	± SD	%IA	± SD
^{89}Zr-oxine-CTLL2 cells (A)	Bone	5.56	4.39	10.82	2.22	13.28	6.48	15.27	3.34	17.85	0.04	18.28	0.18
	Lungs	46.49	2.34	25.32	1.34	13.08	2.84	10.66	0.32	8.34	0.08	9.02	0.36
	Liver	7.49	2.23	24.22	1.98	29.66	3.16	30.70	2.11	29.36	0.40	29.59	0.21
	Spleen	0.24	2.69	3.05	2.10	4.56	2.68	4.88	1.83	5.28	0.11	5.51	0.49
	Kidneys	0.73	2.66	1.13	2.01	1.38	2.91	1.20	1.40	1.14	0.43	1.12	0.44
^{89}Zr-DFO-NCS-CTLL2 cells (B)	Bone	3.67	1.17	6.27	0.95	9.27	0.98	10.61	0.49	12.01	0.60	12.57	0.37
	Lungs	69.41	5.33	17.22	2.27	4.58	0.29	4.14	1.72	2.60	0.97	2.49	0.88
	Liver	2.96	1.03	34.45	0.93	43.67	3.18	42.05	2.22	42.48	1.47	43.80	3.07
	Spleen	0.04	0.03	4.65	0.72	6.88	1.40	7.39	1.47	7.54	0.80	7.84	1.30
	Kidneys	0.21	0.08	3.47	0.43	3.63	0.46	3.24	0.44	2.81	0.57	2.51	0.37

Radiolabelled cells	Organs	Scan 1 (1 hour)		Scan 2 (20 hour)		Scan 3 (43 hour)		Scan 4 (67 hour)		Scan 5 (138 hour)		Scan 6 (187 hour)	
		%IA	± SD	%IA	± SD	%IA	± SD	%IA	± SD	%IA	± SD	%IA	± SD
^{89}Zr-oxine KIT-CTLL2 cells (C)	Bone	4.04	0.32	13.37	1.21	15.54	0.56	17.18	1.21	17.72	1.65	19.83	0.55
	Lungs	42.43	0.41	7.36	1.64	5.61	0.53	4.10	0.95	3.22	0.05	2.70	0.54
	Liver	14.17	5.21	26.95	8.77	33.14	1.16	34.33	2.44	31.43	0.89	30.12	0.72
	Spleen	1.11	0.27	4.85	0.36	4.47	0.31	4.93	0.14	5.23	0.35	4.67	0.74
	Kidneys	5.13	0.14	1.59	0.27	1.46	0.53	1.50	0.03	1.38	0.09	1.59	0.16

Table 4-8: Summary of the quantitative analysis results (%IA) for labelled CTLL2 cells in target organs of C57BL/6 mice after PET/CT imaging. CTLL2 cells were labelled using the cell labelling methods developed by us for **(A)** ^{89}Zr-oxine, (n = 3), **(B)** ^{89}Zr-DFO-NCS, (n = 4), and **(C)** the method developed by Man *et al.,*[318] for labelled cells with ^{89}Zr-oxine, (n = 2). PET/CT scans were acquired at 0.5 h, 20 h, 43 h, 67 h, 138 h, and 187 h following injection of the tracer. The displayed data are mean ± SD.

Time	Šídák's multiple comparisons test for (%IA) SKELETON	Mean difference (%)	Below threshold?	Summary	Individual P Value
0 d (0.5 hr)	^{89}Zr-oxine vs ^{89}Zr-DFO-NCS	1.89	No	ns	0.69
	^{89}Zr-oxine vs ^{89}Zr-oxine Kit	1.53	No	ns	0.98
	^{89}Zr-DFO-NCS vs ^{89}Zr-oxine Kit	-0.37	No	ns	> 0.99
1 d	^{89}Zr-oxine vs ^{89}Zr-DFO-NCS	4.55	Yes	***	< 0.001
	^{89}Zr-oxine vs ^{89}Zr-oxine Kit	-2.55	No	ns	0.49
	^{89}Zr-DFO-NCS vs ^{89}Zr-oxine Kit	-7.10	Yes	***	< 0.001
4 d	^{89}Zr-oxine vs ^{89}Zr-DFO-NCS	4.01	Yes	**	0.00
	^{89}Zr-oxine vs ^{89}Zr-oxine Kit	-2.27	No	ns	0.69
	DFO vs ^{89}Zr-oxine Kit	-6.27	Yes	***	< 0.001
5 d	^{89}Zr-oxine vs ^{89}Zr-DFO-NCS	4.66	Yes	***	< 0.001
	^{89}Zr-oxine vs ^{89}Zr-oxine Kit	-1.91	No	ns	0.89
	^{89}Zr-DFO-NCS vs ^{89}Zr-oxine Kit	-6.57	Yes	***	< 0.001
6 d	^{89}Zr-oxine vs ^{89}Zr-DFO-NCS	5.84	Yes	***	< 0.001
	^{89}Zr-oxine vs ^{89}Zr-oxine Kit	0.14	No	ns	> 0.99
	^{89}Zr-DFO-NCS vs ^{89}Zr-oxine Kit	-5.71	Yes	***	< 0.001
7 d	^{89}Zr-oxine vs ^{89}Zr-DFO-NCS	5.71	Yes	***	< 0.001
	^{89}Zr-oxine vs ^{89}Zr-oxine Kit	-1.54	No	ns	0.98
	^{89}Zr-DFO-NCS vs ^{89}Zr-oxine Kit	-7.26	Yes	***	< 0.001

Table 4-9: **Comparisons of the percentage of injected dose (%IA) observed in the skeletons of C57BL/6 mice** (n = 9), Mice received labelled CTLL2 cells and were imaged by PET/CT. In this study, CTLL2 cells were labelled using the methods developed by us for ^{89}Zr-oxine, (n = 3), ^{89}Zr-DFO-NCS, (n = 4), and the method developed by Man *et al.,*[318] for labelling cells with ^{89}Zr-oxine, (n = 2). The significance of the results was determined using one-way ANOVA and Sidak's multiple comparison tests. P values < 0.05 were considered statistically significant, with *** showing that p values were ≤ 0.001, and ns showing no significance for p values > 0.05.

Time	Šídák's multiple comparisons test for (%IA/g) SKELETON	Mean Difference (%)	Below threshold?	Summary	Individual P Value
0 d (0.5 hr)	^{89}Zr-oxine vs ^{89}Zr-DFO-NCS	4.17	No	ns	0.21
	^{89}Zr-oxine vs ^{89}Zr-oxine Kit	4.85	No	ns	0.22
	^{89}Zr-DFO-NCS vs ^{89}Zr-oxine Kit	0.68	No	ns	0.85
1 d	^{89}Zr-oxine vs ^{89}Zr-DFO-NCS	11.93	Yes	***	< 0.001
	^{89}Zr-oxine vs ^{89}Zr-oxine Kit	-2.88	No	ns	0.46
	^{89}Zr-DFO-NCS vs ^{89}Zr-oxine Kit	-14.81	Yes	***	< 0.001
4 d	^{89}Zr-oxine vs ^{89}Zr-DFO-NCS	9.76	Yes	**	0.005
	^{89}Zr-oxine vs ^{89}Zr-oxine Kit	-3.27	No	ns	0.41
	^{89}Zr-DFO-NCS vs ^{89}Zr-oxine Kit	-13.03	Yes	**	0.001
5 d	^{89}Zr-oxine vs ^{89}Zr-DFO-NCS	10.41	Yes	**	0.003
	^{89}Zr-oxine vs ^{89}Zr-oxine Kit	0.26	No	ns	0.95
	^{89}Zr-DFO-NCS vs ^{89}Zr-oxine Kit	-10.15	Yes	**	0.009
6 d	^{89}Zr-oxine vs ^{89}Zr-DFO-NCS	15.36	Yes	***	< 0.001
	^{89}Zr-oxine vs ^{89}Zr-oxine Kit	3.04	No	ns	0.44
	^{89}Zr-DFO-NCS vs ^{89}Zr-oxine Kit	-12.32	Yes	**	0.002
7 d	^{89}Zr-oxine vs ^{89}Zr-DFO-NCS	13.64	Yes	***	< 0.001
	^{89}Zr-oxine vs ^{89}Zr-oxine Kit	-2.05	No	ns	0.6
	^{89}Zr-DFO-NCS vs ^{89}Zr-oxine Kit	-15.69	Yes	***	< 0.001

Table 4-10: Statistical comparison for the percentage of injected dose normalised with weight of organ (%IA/g) observed in the skeletons of C57BL/6 mice. Mice (n = 9) were injected with labelled CTLL2 cells and imaged with PET/CT images. The CTLL2 cells were labelled using the methods developed by us for ^{89}Zr-oxine, (n = 3), ^{89}Zr-DFO-NCS, (n = 4), and the method developed by Man *et al.,*[318] for labelling cells with ^{89}Zr-oxine, (n = 2). Significance was calculated using ordinary one-way ANOVA for multiple comparisons and uncorrected Fisher's LSD tests. P values < 0.05 were considered statistically significant, with ** indicating that p values were ≤ 0.01, *** indicating that p values were ≤ 0.001, and ns represents no significance for p values > 0.05.

Time	Šídák's multiple comparisons test for (%IA) LIVER	Mean Difference (%)	Below threshold?	Summary	Adjusted P Value
0 d (0.5 hr)	^{89}Zr-oxine vs ^{89}Zr-DFO-NCS	4.53	No	ns	0.41
	^{89}Zr-oxine vs ^{89}Zr-oxine Kit	-6.68	No	ns	0.14
	^{89}Zr-DFO-NCS vs ^{89}Zr-oxine Kit	-11.21	Yes	***	< 0.001
1 d	^{89}Zr-oxine vs ^{89}Zr-DFO-NCS	-10.22	Yes	***	< 0.001
	^{89}Zr-oxine vs ^{89}Zr-oxine Kit	-2.73	No	ns	> 0.99
	^{89}Zr-DFO-NCS vs ^{89}Zr-oxine Kit	7.50	Yes	*	0.04
4 d	^{89}Zr-oxine vs ^{89}Zr-DFO-NCS	-14.01	Yes	***	< 0.001
	^{89}Zr-oxine vs ^{89}Zr-oxine Kit	-3.48	No	ns	0.95
	^{89}Zr-DFO-NCS vs ^{89}Zr-oxine Kit	10.53	Yes	***	< 0.001
5 d	^{89}Zr-oxine vs ^{89}Zr-DFO-NCS	-11.36	Yes	***	< 0.001
	^{89}Zr-oxine vs ^{89}Zr-oxine Kit	-3.64	No	ns	0.93
	^{89}Zr-DFO-NCS vs ^{89}Zr-oxine Kit	7.72	Yes	*	0.03
6 d	^{89}Zr-oxine vs ^{89}Zr-DFO-NCS	-13.12	Yes	***	< 0.001
	^{89}Zr-oxine vs ^{89}Zr-oxine Kit	-2.06	No	ns	> 0.99
	^{89}Zr-DFO-NCS vs ^{89}Zr-oxine Kit	11.06	Yes	***	< 0.001
7 d	^{89}Zr-oxine vs ^{89}Zr-DFO-NCS	-14.21	Yes	***	<0.001
	^{89}Zr-oxine vs ^{89}Zr-oxine Kit	-0.53	No	ns	> 0.99
	^{89}Zr-DFO-NCS vs ^{89}Zr-oxine Kit	13.68	Yes	***	< 0.001

Table 4-11: **Comparison of the percentage of injected dose (%IA) observed in the livers of C57BL/6 mice.** Mice (n = 9) were injected with labelled CTLL2 cells, and imaged with PET/CT. CTLL2 cells were labelled using the methods developed by us for ^{89}Zr-oxine, (n = 3), ^{89}Zr-DFO-NCS, (n = 4), and the method developed by Man *et al.,*[318] for labelling cells with ^{89}Zr-oxine, (n = 2). For multiple comparisons, ordinary one-way ANOVA and Fisher's least significant difference (LSD) tests were used to calculate significance. P values < 0.05 were considered statistically significant, with * showing that p values were ≤ 0.05, ** showing that p values were ≤ 0.01, *** showing that p values were ≤ 0.001, and ns showing no significance for p values > 0.05.

Time	Šídák's multiple comparisons test for (%IA/g) LIVER	Mean Difference (%)	Below threshold?	Summary	Individual P Value
0 d (0.5 hr)	^{89}Zr-oxine vs ^{89}Zr-DFO-NCS	3.77	No	ns	0.42
	^{89}Zr-oxine vs ^{89}Zr-oxine Kit	-3.38	No	ns	0.54
	^{89}Zr-DFO-NCS vs ^{89}Zr-oxine Kit	-7.15	No	ns	0.18
1 d	^{89}Zr-oxine vs ^{89}Zr-DFO-NCS	-14.55	Yes	**	0.003
	^{89}Zr-oxine vs ^{89}Zr-oxine Kit	-3.69	No	ns	0.51
	^{89}Zr-DFO-NCS vs ^{89}Zr-oxine Kit	10.86	Yes	*	0.05
4 d	^{89}Zr-oxine vs ^{89}Zr-DFO-NCS	-22.17	Yes	***	< 0.001
	^{89}Zr-oxine vs ^{89}Zr-oxine Kit	1.23	No	ns	0.82
	^{89}Zr-DFO-NCS vs ^{89}Zr-oxine Kit	23.40	Yes	***	< 0.001
5 d	^{89}Zr-oxine vs ^{89}Zr-DFO-NCS	-21.37	Yes	***	< 0.001
	^{89}Zr-oxine vs ^{89}Zr-oxine Kit	-0.03	No	ns	> 0.99
	^{89}Zr-DFO-NCS vs ^{89}Zr-oxine Kit	21.34	Yes	***	< 0.001
6 d	^{89}Zr-oxine vs ^{89}Zr-DFO-NCS	-18.92	Yes	***	< 0.001
	^{89}Zr-oxine vs ^{89}Zr-oxine Kit	1.83	No	ns	0.74
	^{89}Zr-DFO-NCS vs ^{89}Zr-oxine Kit	20.75	Yes	***	< 0.001
7 d	^{89}Zr-oxine vs ^{89}Zr-DFO-NCS	-17.01	Yes	***	< 0.001
	^{89}Zr-oxine vs ^{89}Zr-oxine Kit	5.34	No	ns	0.34
	^{89}Zr-DFO-NCS vs ^{89}Zr-oxine Kit	22.35	Yes	***	< 0.001

Table 4-12: Comparison of the percentage of injected dose normalised by the weight of organ (%IA/g) observed in the livers of C57BL/6 mice. Mice (n = 9) were injected with labelled CTLL2 cells and imaged with PET/CT. CTLL2 cells were labelled using the methods developed by us for ^{89}Zr-oxine, (n = 3), ^{89}Zr-DFO-NCS, (n = 4), and the ^{89}Zr-oxine-Kit, (n = 2) Man *et al.,*[318] for labelling cells. For multiple comparisons, ordinary one-way ANOVA and Fisher's least significant difference (LSD) tests were used to calculate significance. P values < 0.05 were considered statistically significant, with * for p values ≤ 0.05, ** for p values ≤ 0.01, *** for p values ≤ 0.001, and ns showing no significance for p values > 0.05.

Time	Šídák's multiple comparisons test for (%IA) SPLEEN	Mean Difference (%)	Below threshold?	Summary	Adjusted P Value
0 d (0.5 hr)	[89]Zr-oxine vs [89]Zr-DFO-NCS	0.19	No	ns	> 0.99
	[89]Zr-oxine vs [89]Zr-oxine Kit	-0.87	No	ns	> 0.99
	[89]Zr-DFO-NCS vs [89]Zr-oxine Kit	-1.07	No	ns	0.92
1 d	[89]Zr-oxine vs [89]Zr-DFO-NCS	-1.60	No	ns	0.20
	[89]Zr-oxine vs [89]Zr-oxine Kit	-1.80	No	ns	0.27
	[89]Zr-DFO-NCS vs [89]Zr-oxine Kit	-0.20	No	ns	> 0.99
4 d	[89]Zr-oxine vs [89]Zr-DFO-NCS	-2.32	Yes	**	0.01
	[89]Zr-oxine vs [89]Zr-oxine Kit	0.09	No	ns	> 0.99
	[89]Zr-DFO-NCS vs [89]Zr-oxine Kit	2.41	Yes	*	0.02
5 d	[89]Zr-oxine vs [89]Zr-DFO-NCS	-2.52	Yes	**	0.00
	[89]Zr-oxine vs [89]Zr-oxine Kit	-0.05	No	ns	> 0.99
	[89]Zr-DFO-NCS vs [89]Zr-oxine Kit	2.47	Yes	*	0.02
6 d	[89]Zr-oxine vs [89]Zr-DFO-NCS	-2.26	Yes	*	0.01
	[89]Zr-oxine vs [89]Zr-oxine Kit	0.05	No	ns	> 0.99
	[89]Zr-DFO-NCS vs [89]Zr-oxine Kit	2.31	Yes	*	0.03
7 d	[89]Zr-oxine vs [89]Zr-DFO-NCS	-2.33	Yes	**	0.01
	[89]Zr-oxine vs [89]Zr-oxine Kit	0.84	No	ns	> 0.99
	[89]Zr-DFO-NCS vs [89]Zr-oxine Kit	3.17	Yes	***	< 0.001

Table 4-13: Statistical analysis of the percentage of injected dose (%IA/g) observed in the spleens of C57BL/6 mice. Mice (n = 9) were injected with labelled CTLL2 cells and imaged with PET/CT. CTLL2 cells were labelled using the methods developed by us for [89]Zr-oxine, (n = 3), [89]Zr-DFO-NCS, (n = 4), and the method developed by Man *et al.,*[318] for labelling cells with [89]Zr-oxine, (n = 2). The significance of multiple comparisons was assessed using ordinary one-way ANOVAs and Fisher's least significant difference (LSD) tests. Statistics were considered significant at p values < 0.05, with * indicating that p values were ≤ 0.05, ** indicating that p values were ≤ 0.01, *** showing that p values were ≤ 0.001 and ns showing no significance for p values > 0.05.

Time	Šídák's multiple comparisons test for (%IA/g) SPLEEN	Mean difference (%)	Below threshold?	Summary	Individual P Value
0 d **(0.5 hr)**	[89]Zr-oxine vs [89]Zr-DFO-NCS	0.05	No	ns	0.89
	[89]Zr-oxine vs [89]Zr-oxine Kit	-0.03	No	ns	0.95
	[89]Zr-DFO-NCS vs [89]Zr-oxine Kit	-0.07	No	ns	0.85
1 d	[89]Zr-oxine vs [89]Zr-DFO-NCS	-0.44	No	ns	0.2
	[89]Zr-oxine vs [89]Zr-oxine Kit	-0.16	No	ns	0.7
	[89]Zr-DFO-NCS vs [89]Zr-oxine Kit	0.29	No	ns	0.47
4 d	[89]Zr-oxine vs [89]Zr-DFO-NCS	-0.62	No	ns	0.08
	[89]Zr-oxine vs [89]Zr-oxine Kit	0.15	No	ns	0.71
	[89]Zr-DFO-NCS vs [89]Zr-oxine Kit	0.77	No	ns	0.05
5 d	[89]Zr-oxine vs [89]Zr-DFO-NCS	-0.78	Yes	*	0.03
	[89]Zr-oxine vs [89]Zr-oxine Kit	0.09	No	ns	0.83
	[89]Zr-DFO-NCS vs [89]Zr-oxine Kit	0.86	Yes	*	0.03
6 d	[89]Zr-oxine vs [89]Zr-DFO-NCS	-0.73	Yes	*	0.04
	[89]Zr-oxine vs [89]Zr-oxine Kit	0.28	No	ns	0.5
	[89]Zr-DFO-NCS vs [89]Zr-oxine Kit	1.01	Yes	*	0.01
7 d	[89]Zr-oxine vs [89]Zr-DFO-NCS	-0.84	Yes	*	0.02
	[89]Zr-oxine vs [89]Zr-oxine Kit	0.40	No	ns	0.33
	[89]Zr-DFO-NCS vs [89]Zr-oxine Kit	1.24	Yes	**	0.003

Table 4-14: Statistical analysis of the percentage of injected dose normalised by organ weight (%IA/g) observed in the spleens of C57BL/6 mice. Mice (n = 9) were injected with labelled CTLL2 cells and imaged with PET/CT. CTLL2 cells were labelled using the methods developed by us for [89]Zr-oxine, (n = 3), [89]Zr-DFO-NCS, (n = 4), and the method developed by Man *et al.,*[318] for labelling cells with [89]Zr-oxine, (n = 2). The significance of multiple comparisons was assessed using ordinary one-way ANOVAs and Fisher's least significant difference (LSD) tests. Statistics were considered significant at p values < 0.05, with * indicating that p values were ≤ 0.05, ** indicating that p values were ≤ 0.01, and ns showing no significance for p values > 0.05.
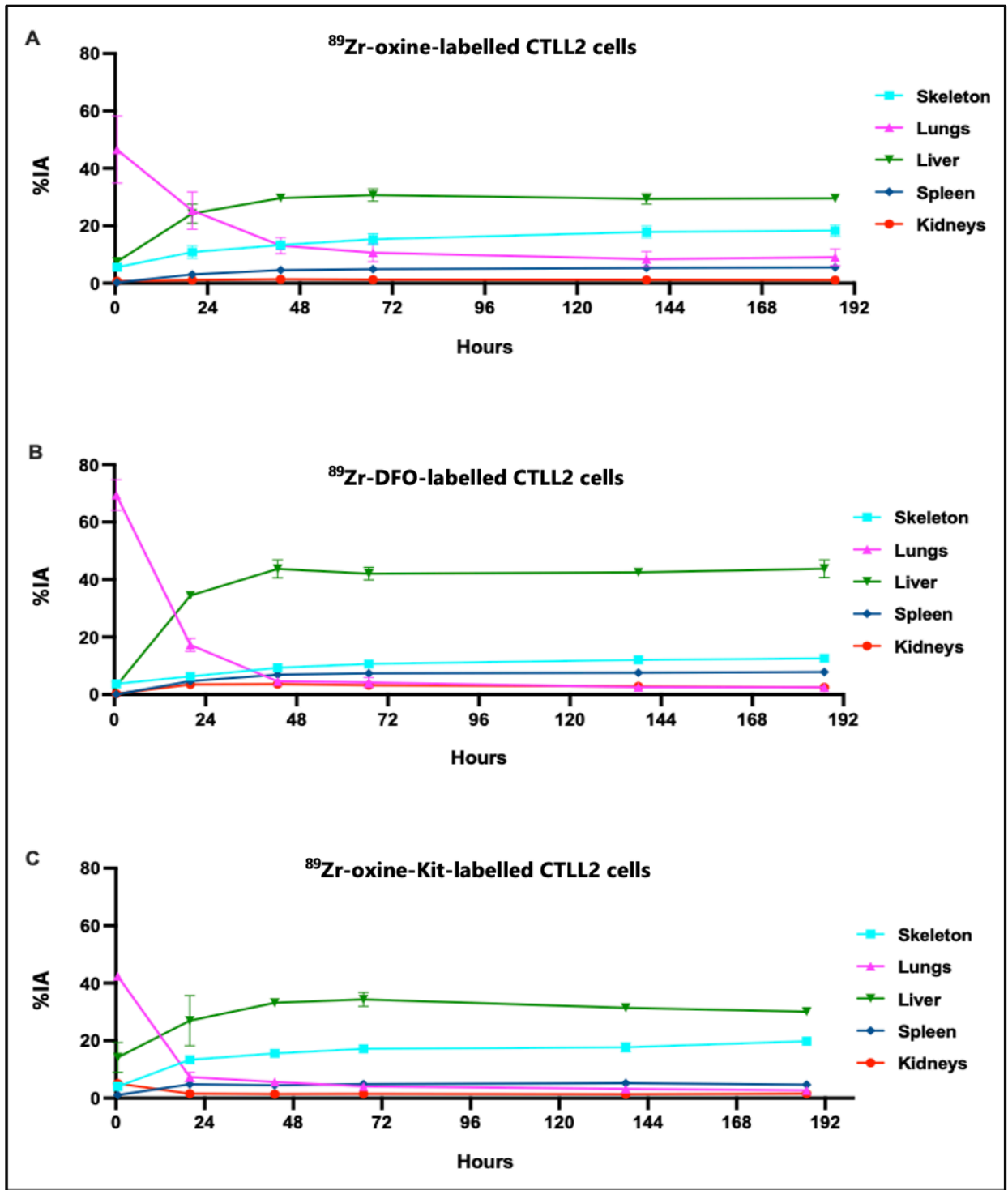
Figure 4-11: **Quantitative *in vivo* analysis of %IA in target organs from C57BL/6 mice post PET/CT with labelled CTLL2 cells.** Labelling was performed with our developed protocols for **(A)** [89]Zr-oxine (n = 3), **(B)** [89]Zr-DFO-NCS (n = 4), and (C) the method by Man *et al.,*[318] for [89]Zr-oxine labelled cells (n = 2). PET/CT imaging was conducted at 0.5 h, 20 h, 43 h, 67 h, 138 h, and 187 h after tracer injection. Data represent mean values ± SD.
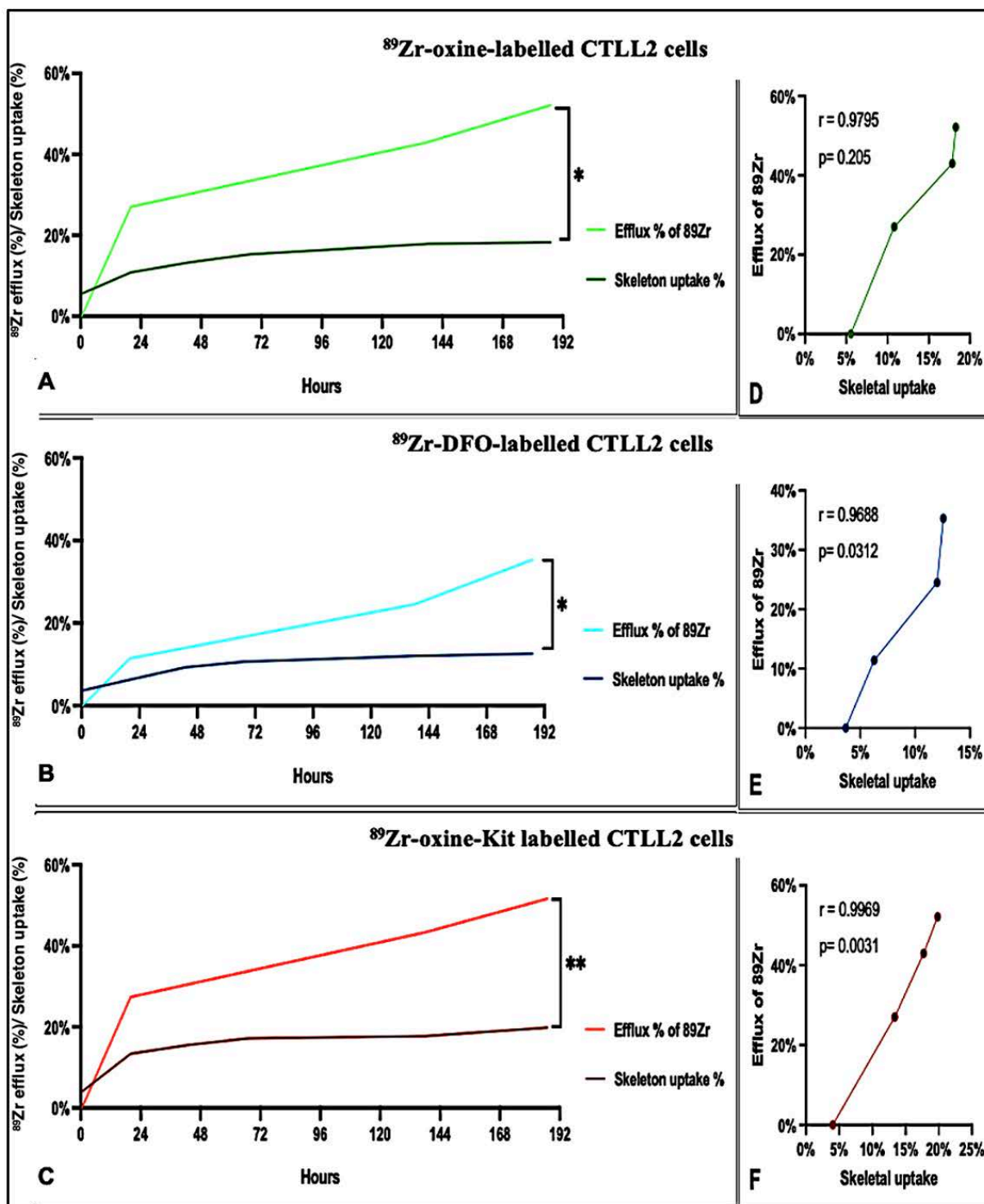
Figure 4-12: Relationship between ^{89}Zr efflux (*in vitro*) and skeletal uptake (*in vivo*) Results were obtained using the cell labelling methods developed by us ^{89}Zr-oxine **(A,D)**, ^{89}Zr-DFO-NCS **(B,E)**, and the method developed by Man *et al.,*[318] for ^{89}Zr-oxine labelling **(C,F)**. Correlations were determined using Pearson correlation coefficients (Pearson r). It was found that there exists a statistical correlation between 89Zr efflux and skeletal uptake percentage obtained from each method of labelling cells. Statistics were considered significant at p values < 0.05, with indicating that p values were ≤ 0.05, * indicating that p values were ≤ 0.01 and ** indicating that p values were ≤ 0.01.

4.4 Discussion

In chapter 3 several sets of optimisation experiments were conducted to develop radiolabelling methodologies for ^{89}Zr complexes in lymphocytes. In these experiments, several parameters were examined to optimise cell labelling methodologies and to minimise their effects on cell function. These parameters include the amount of initial ^{89}Zr activity, oxine concentration, labelling time and medium, and the speed at which cells and radioactivity are mixed. We collected the results from the optimisation experiments conducted on ELl4 cells to applied them to radiolabel our main cell line, CTLL2.

Thus, we used our developed ^{89}Zr-oxine and ^{89}Zr-DFO-NCS methodologies to label CTLL2 cells in parallel in this chapter. After labelling, the cells were monitored for seven days *in vitro* and *in vivo*. To assess the cellular retention of ^{89}Zr *in vitro* and its labelling effect, cellular functions such as viability and proliferation were analysed. For *in vivo* monitoring, the labelled cells were injected intravenously into wild-type syngeneic black mice (C57BL/6) so that they could be tracked in longitudinally without any invasive interventions. As a further evaluation of the efficacy of our developed cell labelling methods, CTLL2 cells were also labelled with ^{89}Zr-oxine complex prepared by the method published by Man *et al*.,[318] and referred to as the Kit method in this thesis.

In this chapter, the radiolabelling of CTLL2 cells with ^{89}Zr-oxine complexes revealed the following results: Cell labelling efficiencies of 27 % - 35 % were observed and radioactivity concentrations of 0.68 - 0.85 MBq/10^6 cells and 0.61 - 0.85 MBq/10^6 cells were achieved from starting activities of 18 MBq, for CTLL2 cells labelled with the ^{89}Zr-oxine complex using our developed method and the cell labelling method by Man *et al*.,[318] respectively. By comparison

a labelling efficiency of 20 % was achieved by labelling CTLL2 cells with the ^{89}Zr-DFO-NCS complex, also from a starting activity of 18 MBq, which resulted in a cell loading concentration of 0.53 – 0.59 MBq/10^6. With more than 4×10^6 cells being labelled by each labelling method, the viability of cells obtained by any of the three labelling methods was not significantly different from that of the cells obtained before labelling.

It has been reported in previous publications that ^{89}Zr-oxine and ^{89}Zr-DFO-NCS exhibit highly inconsistent cell labelling results, with CLE % varying between 13 % and 55 % [34],[35] for ^{89}Zr-oxine labelling reactions and 30 % to 72 % for ^{89}Zr-DFO-NCS labelling reactions [36],[37]. Gratifyingly the CLEs observed for our ^{89}Zr-oxine-labelling reactions in CTLL2 cells compare well to the equivalent CLEs reported in the literature for other cell lines [34],[35]. Conversely, the CLE we observed for the ^{89}Zr-DFO-NCS-labelling method was lower than that for our ^{89}Zr-oxine-labelling methods and other ^{89}Zr-DFO-NCS labelling methods reported in the literature.[36],[37] This may be because ^{89}Zr-DFO-NCS labelling is highly dependent on the abundance of free amines on the cell surface during labelling. In fact, this abundance may differ greatly between different cell types, which could affect the CLE of ^{89}Zr-DFO-NCS-CTLL2. Cell fragments can also affect the binding efficiency of ^{89}Zr-DFO-NCS-CTLL2 during cell labelling, resulting in a significant reduction in CLE. This can be attributed to the competition among amines that are exposed during labelling. However, the efficiency of cell labelling achieved using ^{89}Zr-DFO-NCS was sufficient to allow the planned *in vitro* and *in vivo* testing to be carried out.[38]

The *in vitro* monitoring of labelled CTLL2 cells obtained by the three labelling methods revealed the following results regarding the functions of the labelled cells. Regardless of which of the three cell labelling methods was used, the viability of labelled cells did not differ significantly from the

viability of unlabelled cells at any time after labelling. However, the proliferation results revealed that the proliferative abilities of the [89]Zr-DFO-NCS labelled CTLL2 cells were significantly impaired, unlike the [89]Zr-oxine labelled CTLL2 cells which could proliferate with similar proliferative abilities to unlabelled cells at any time after labelling. Interestingly the impairment of proliferation of the [89]Zr-DFO-NCS labelled CTLL2 cells was not immediate, with proliferative abilities remaining unchanged for the first 24 hours before statistically significant reductions were observed.

To cultivate and proliferate CTLL2 cells, cells were suspended in RPMI 1640 medium containing 2mM L-glutamine, 1 mM sodium pyruvate, 100 IU penicillin, 100 μg/ml streptomycin, 10 % FCS, and 10 % T.stim with Concanavalin A. ConA, is a lectin that binds to, and crosslinks glycosylated molecules on T cell surfaces, promoting cell proliferation.[346] Based on the fact that [89]Zr-DFO-NCS-CTLL2 binds to exposed amines on the cell membrane surface, it may be that DFO modifies the TCR or any molecules to which Concanavalin A binds. This could explain the reduced proliferation observed in CTLL2 cells labelled with [89]Zr-DFO-NCS after 24 h of labelling.

To allow long-term imaging of labelled cells, the cells must retain their activity for a long time. Keeping a sufficient count rate during scanning is critical when considering serial long-term PET imaging after dose administration, particularly during very delayed PET scans. To determine whether the cells retained [89]Zr activity after labelling for 7 days, we monitored them *in vitro*. Table 4-4 and Table 4-5 show a summary of the viability and proliferation of the labelled cells that have been monitored *in vitro*. A noteworthy observation from *the in vitro* efflux results was that [89]Zr-DFO-NCS labelled CTLL2 cells retained significantly more tracer than [89]Zr-oxine labelled CTLL2 cells using either the developed [89]Zr-oxine method or the [89]Zr-oxine-Kit method. [89]Zr-DFO-NCS-

CTLL2 cells retained 70 % of the tracer for up to 7 days after labelling, with no difference in viability between labelled and unlabelled cells. This improved cell retention is in line with literature examples and can be explained by the long-term stability of the covalent bonds between the [89]Zr-DFO-NCS complex and the cells. Although we observed significant efflux of the tracer from the [89]Zr-oxine labelled CTLL2 cells, our results indicated that 50 % of the tracer remained associated with the cells for seven days after labelling. CTLL2 cells labelled with [89]Zr-oxine had the same viability as unlabelled cells at any time after labelling. There was no statistically significant difference in the amount of [89]Zr activity released by CTLL2 cells labelled with the [89]Zr-oxine complex between our method and the Kit formulation method.

Bansal conducted a study where human immune cells were labelled with [89]Zr-DFO-NCS and found that radioactivity concentrations up to 0.5 MBq/10^6 did not adversely affect cell viability, and the labelled cells retained the radioactivity for seven days post-labelling.[36]

According to Man *et al*.,[319] [89]Zr-oxine retention varies with cell type. In this study, approximately 50 % of the [89]Zr incorporated in labelled cells was released during incubation for one week. [89]Zr-oxine has been studied by Charoenphun et *al.,*[34] and Sato *et al.,*[328] for its chemotoxicity and significant efflux from cells following labelling, two problems commonly encountered with oxine-based labelling. In their study, Charoenphun *et al*.,[34] observed a decrease in the viability of [89]Zr-oxine labelled 5 T33 myeloma cells from 93.3 % to 76.3 % ± 3.2 % in the first 24 h, as well as a significant efflux of 28.9 % of radioactivity 24 h following labelling. The same findings were observed by Sato *et al*.,[328] with [89]Zr-oxine labelled human and rhesus macaque natural killer cells. As a result of the radiolabelling of cells, they observed a wide range of viability levels from 60 % to 100 % within the first 24 h, which decreased after 6 days to 20 %

to 30 %. In addition, these viable ^{89}Zr-oxine labelled cells emitted significant amounts of radioactivity following culture. In the first 24 h, approximately 20 % – 25 % of the radioactivity was released from labelled cells, and after one week, 70 % – 80 % was excreted from the cells. Further previous studies on ^{111}In-oxine have demonstrated a cellular efflux of 70 % – 75 % within three to four days.[35],[351]

Our ^{89}Zr-DFO-NCS labelled CTLL2 cell method holds great promise and is comparable to that reported in the literature regarding cell viability and ^{89}Zr efflux results. Moreover, the developed ^{89}Zr-DFO-NCS labelled CTLL2 cell method demonstrated superior results for the retention of labelled activity compared with the developed ^{89}Zr-oxine labelled CTLL2 cell method. However, these benefits need to be weighed carefully against the observed reductions in proliferation. Meanwhile, despite our ^{89}Zr-oxine labelled CTLL2 exhibiting higher rates of ^{89}Zr efflux than our ^{89}Zr-DFO-NCS labelled cells the retention levels were comparable to those mentioned above in the literature and a substantial improvement over efflux rates observed for ^{111}In labelled cells [35],[351]. Most importantly, unlike the abovementioned results reported by Charoenphun *et al.,*[34] and Sato *et al.,*[328], our ^{89}Zr-oxine labelled CTLL2 cells demonstrated no significant change in cell viability between labelled and unlabelled cells up to 7 days after labelling.

The general biodistribution pattern of labelled CTLL2 cells by any of the three labelling methodologies can be summarised as follows: at early imaging times, the lungs accumulated most activity, with a minor accumulation of activity seen in the liver and kidneys. The high lung activity in the delayed imaging of 24 h shifted primarily to the liver, skeleton, spleen, and kidneys, where it remained for the remainder of the 7-day imaging period. Detailed quantitative results of PET

scans of mice following intravenous administration of CTLL2 cells at 0.5 h, 20 h, 43 h, 67 h, 138 h, and 187 h are presented in Table 4-8.

The key quantitative highlights of the PET scan results obtained for the wild-type mice injected intravenously with the labelled CTLL2 cells using the three different methods are as follows: Mice injected with [89]Zr-oxine labelled CTLL2 cells obtained by both [89]Zr-oxine methods did not demonstrate significant differences in the (%IA) and (%IA/g) values for the livers, spleens, and skeletons. The (%IA) and (%IA/g) values for the livers, spleens, and skeletons of mice injected with [89]Zr-oxine labelled CTLL2 cells, on the other hand, differed significantly from the (%IA) and (%IA/g) values for the liver, spleen, and skeletons of mice treated with [89]Zr-DFO-NCS labelled CTLL2 cells. Furthermore, on all PET scans except those taken 0.5 h after injection, mice injected with [89]Zr-DFO-NCS-CTLL2 cells had significantly more activity accumulating in their livers and spleens than mice injected with [89]Zr-oxine-CTLL2 cells. The high uptake of the livers and spleens observed in the mice injected with [89]Zr-DFO-NCS labelled CTLL2 cells was associated with significantly lower skeletal uptake compared with those treated with [89]Zr-oxine-CTLL2 cells, Table 4-9 to Table 4-14.

A closer look at the *in vitro* efflux data revealed that, except for 1 h after labelling, [89]Zr-DFO-NCS labelled CTLL2 cells showed significantly lower efflux of activity than their [89]Zr-oxine labelled counterparts at all time points. At the same time, no statistical difference in [89]Zr effluxes from [89]Zr-oxine labelled CTLL2 cells was observed using any of the [89]Zr-oxine methods. In the *in vivo* course of the experiment, free [89]Zr released by CTLL2 cells will likely be localised in the skeleton following rapid spread throughout the entire body during PET scanning.[349] As a result, mice injected with [89]Zr-DFO-NCS labelled CTLL2 cells demonstrated significantly less bone uptake

than mice injected with ^{89}Zr-oxine labelled CTLL2 cells. The relationship between ^{89}Zr efflux (*in vitro*) and skeletal uptake (*in vivo*) based on the cell labelling method is illustrated in Figure 4-12.

Considering the ability of cells to retain ^{89}Zr or not, the distribution of labelled CTLL2 cells in this study can be interpreted as follows: The majority of radioactivity was found in the lungs of all mice within an hour of being injected with labelled CTLL2 cells. After 24 hours of delayed imaging, radioactivity was redistributed from the lungs into the liver and spleen in mice injected with ^{89}Zr-DFO-NCS labelled CTLL2 cells, whereas radioactivity was rapidly redistributed to the liver and bone in mice injected with ^{89}Zr-oxine labelled CTLL2 cells. These findings are in line with the following publications regarding the *in vivo* biodistribution of ^{89}Zr-oxine and ^{89}Zr-DFO-NCS labelled cells. In his study, Charoenphun reported that ^{89}Zr-oxine labelled myeloma cells were injected intravenously and found in the lungs 30 min after the tracer was administered. However, within 24 h, the cells migrated to the liver and spleen, where they remained up to 7 days after administration.[34] In a study published by Sato, ^{89}Zr-oxine labelled dendritic cells were observed to have a similar distribution.[310] By comparing the *in vivo* tracking of CTLL2 cells labelled with ^{89}Zr-DFO-NCS using our developed method, a similar distribution was observed to that reported in a study on the distribution of CAR T cells labelled with ^{89}Zr-DFO-NCS.[37]

Our observation of the labelling method dictating the biodistribution is also in accordance with the recent study by Ida Friberger *et al.,*; which compared the *in vivo* biodistribution of cells labelled with ^{89}Zr-oxine or ^{89}Zr-DFO-NCS using PET. In this study, human decidual stromal cells (hDSCs) and rat macrophages (rMacs) were radiolabelled with ^{89}Zr-oxine and ^{89}Zr-DFO-NCS. Although interestingly our results reveal an opposite trend to that observed by Friberger *et al,.* Alongside the previously discussed reduced bone uptake for the ^{89}Zr-DFO-NCS labelled CTLL2 cells, from 20

h onwards we also observed a lower lung uptake and higher liver from our ^{89}Zr-DFO-NCS labelled CTLL2 cells compared to our ^{89}Zr-oxine labelled CTLL2 cells. An additional noteworthy observation from our studies was the focal hotspots of activity observed in the liver and lungs of one of the mice injected with ^{89}Zr-DFO-NCS labelled CTLL2 cells. This effect was only observed for one of the 4 mice injected with this batch of labelled cells, however it is similar to the effects seen in chapter 3 with the ^{89}Zr-DFO-NCS labelled lymphocytes. These focal hotspots which were not observed for any of the ^{89}Zr-oxine labelled cells are a considerable drawback of the ^{89}Zr-DFO-NCS labelling methodology and if observed in other radiolabelled cell lines would preclude its use in any studies wishing to image metastatic disease.

The *in vitro* and *in vivo* monitoring of radiolabelled cells revealed that both ^{89}Zr-oxine and ^{89}Zr-DFO-NCS facilitated successful labelling and *in vivo* monitoring of cell biodistribution. However, ^{89}Zr-oxine exhibited more favourable characteristics in terms of *in vitro* viability, proliferative ability of labelled cells and *in vivo* biodistribution than ^{89}Zr-DFO-NCS. Based on the *in vivo* biodistribution results, cells labelled with ^{89}Zr-oxine had better biodistribution profiles, showing lower uptake in the liver and spleen and did not cause any focal hotspots in any of the images. Accordingly, it appears that despite the higher rate of efflux and corresponding higher levels of bone uptake, ^{89}Zr-oxine may be more suitable for CTLL2 cell labelling and *in vivo* monitoring because it offers minimal impact on cell proliferation and viability.[39]

These findings demonstrated that our *in vitro* results for the labelled CTLL2 cells were consistent with the *in vivo* biodistribution of the labelled CTLL2 cells. As a further means of verifying these results, which unfortunately could not be achieved in this project due to the instrument being unavailable in our R&D laboratory, mice's target organ tissue can be dissected, examined, and

compared based on the number of cells trapped in these organs using a flow cytometer. Accordingly, to overcome this project limitation, considering tissue histology with a flow cytometer for future work would be of substantial value. This is because it would shed more light on previously murky findings such as liver, spleen, and bone uptake in all mice.

4.5 Conclusion

Cell labelling and tracking have become increasingly important in preclinical and clinical settings, particularly for monitoring and evaluating cellular therapies. Thus, it is important to understand the behaviour of cells and their movement within the body after their administration. This will facilitate the use of cell therapies in clinical practise.

Advancements in the development of direct cell labelling methodologies, especially with ^{89}Zr-oxine and ^{89}Zr-DFO-NCS chelators, have marked a significant stride in medical imaging and cellular therapy. The novel kit formulation for ^{89}Zr-oxinate preparation for PET imaging introduced by Man *et al.,* represents a breakthrough, streamlining the radiolabelling process to just 5 min. This innovation addresses the limitations of previous ^{89}Zr-oxine preparation methods in clinical applications and delivers better yields while ensuring safety for operators with minimal radiation exposure.[318]

Recent research by Friberger *et al.,* takes this research to a whole new level by extensively examining both ^{89}Zr-oxine and ^{89}Zr-DFO-NCS labelled cells. As a result of this study, we can understand the distinctive distribution patterns of these radiotracers and their dependence on cell type on biodistribution. Notably, cells labelled with ^{89}Zr-oxine showed immediate lung

uptake and later migration to the liver, which differed from the prolonged lung retention observed with [89]Zr-DFO-NCS labelled cells. Such findings are critical for understanding how the choice of radiotracer can influence the behaviour and distribution of labelled cells *in vivo*.[39] These impacts cell-based therapy design and optimisation.

In our research, we provided a detailed *in vitro* and *in vivo* comparison of [89]Zr-oxine and [89]Zr-DFO-NCS for CTLL2 cell labelling. Our radiolabelling findings demonstrate a labelling efficiency of 27 % and 35 % for [89]Zr-oxine and 20 % for [89]Zr-DFO-NCS, with notable maintenance of cell viability post labelling. These results not only align closely with the pioneering work of Man *et al.,*[318] but also present some interesting deviations from other studies in the literature. For example, the labelling efficiencies for [89]Zr-oxine in other research varied between 13 % and 55 % [34],[35] and between 30 % and 72 % [36],[37] for [89]Zr-DFO-NCS. We attribute these variations to differences in cell surface characteristics and labelling conditions. This underlines the critical role of cell type and methodology in radiolabelling effectiveness. In addition, our research provides insight into the *in vivo* distribution of labelled CTLL2 cells. The pattern was consistent across the three labelling methods examined in this study, with a predominant accumulation in the lungs followed by redistribution to the liver, spleen, and skeleton. However, the degree of uptake in these organs varied considerably.

It has been demonstrated in our research the correlation between *in vitro* and *in vivo* results. Furthermore, our study's differential biodistribution patterns have significant implications for radiolabelling research, showing further work is required to ascertain which tracers most closely reflect the true distribution of the native unlabelled cells. Additionally, the finding has

potential for researchers developing targeted therapies opening up the possibility of using the labelling agents as directing agents. For example, the higher liver uptake observed in ^{89}Zr-DFO-NCS labelled cells suggests their potential for assisting liver-targeted therapies, which are beneficial for conditions such as hepatic tumours or liver fibrosis. Conversely, the prolonged lung retention of ^{89}Zr-oxine labelled cells indicates their suitability for lung-specific treatments, which are essential for diseases such as pulmonary fibrosis or lung cancer. Furthermore, these distinct biodistribution patterns have broader implications for diseases affecting multiple organ systems, such as metastatic cancers. Utilizing a combination of cells labelled with both radiotracers could facilitate multi-organ targeting, potentially enhancing the efficacy of combination therapies. With regard to regenerative medicine, such as repairing heart tissue after myocardial infarction or promoting pancreatic cell regeneration in diabetes, the targeted delivery of therapeutic cells, guided by our understanding of biodistribution patterns, could significantly improve therapeutic outcomes.

As with any scientific project, our research has limitations. One primary limitation was our inability to dissect and examine target organ tissue in mice using flow cytometry. This limitation restricts a more detailed analysis of organ-specific cell uptake, which is crucial for a comprehensive understanding of biodistribution patterns. Future work should focus on incorporating advanced analytical techniques to provide a more detailed assessment of cell localisation after injection. One key weakness of direct cell labelling is that the there is no guarantee that the observed imaging signal is coming from healthy cells, or even that the radioactivity is still cell associated. Therefore, future work should focus upon developing ways to prove the imaging signals are still associated with viable cells particularly at later time points. Strategies could include *ex vivo* analysis of organ lysates to confirm the presence

of live cells, the use of biological blocking agents to modify *in vivo* cellular biodistributions, this could be particularly powerful if cellular distributions and hence radioactivity distributions could be modified *in vivo* several days after the injection of the radiolabelled cells. In addition, exploring other cell types and labelling methodologies is another crucial area of future research, particularly if the alternative cell lines are expected to have markedly different biodistributions. This approach would provide further evidence both in terms of the validity of the assumption that the cells maintain their viability *in vivo* and in terms of the wider applicability of the radiolabelling technologies. Given the variability in cell surface properties and the differential response to radiotracers across cell types, a one-size-fits-all approach may not be viable. Investigating a broader range of cells and conditions can help refine labelling techniques, making them more versatile and applicable to various cell-based therapies.

In conclusion, our study revealed promising insights into the use of ^{89}Zr-oxine and ^{89}Zr-DFO-NCS in direct cell labelling for PET imaging within cell-based therapies. By overcoming identified obstacles, we intend to boost cell labelling approaches for wider medical applications. Our direct cell labelling methodologies can be further refined by applying and exploring them for different types of cells and diseases, making them more versatile and useful for various cell-based therapies. Therefore, this work represents a significant step forward in the field of targeted therapy, and we are excited about the possibilities it may present for improving patient outcomes.

5 Chapter 5: Conclusion

5.1 Summary

Cell tracking and labelling have become rapidly growing areas of interest in clinical practice, particularly in the context of monitoring and evaluating immune cells and cell-based therapies. In order to effectively implement these therapies and bring them into clinical practice, it is essential to have a comprehensive understanding of how cells behave and distribute within the body post-administration. There have been numerous studies published on the use of ^{89}Zr-oxine and ^{89}Zr-DFO-NCS for cell labelling. However, there has yet to be a direct comparison made between these two methods to determine which is more suitable for long-term *in vivo* cell tracking, with the exception of a study published in 2023 by Ida Friberger *et al*.,[39] Therefore, the thesis aimed to optimise radiolabelling of T cells with zirconium-89 complexes, specifically ^{89}Zr-oxine and ^{89}Zr-DFO-NCS and compared these methods in a head-to-head cell labelling study for *in vivo* tracking via PET/CT imaging in a mouse model. In particular, the thesis addressed the following objectives. Chapter 2 presented initial attempts at labelling lymphocytes with ^{89}Zr-oxine and ^{89}Zr-DFO-NCS complexes and tracking the labelled cells *in vivo* via PET/CT imaging in a mouse model. Chapter 3 focused on the development of *in vitro* labelling methods for ^{89}Zr-oxine and EL4 cells, with the goal of facilitating *in vivo* PET imaging. Finally, the primary focus of chapter 4 was the use of recently developed cell labelling techniques to label CTLL2 cells and to evaluate the potential and effectiveness of labelling these cells with ^{89}Zr-oxine and ^{89}Zr-DFO-NCS. Additionally, to validate the utility of our cell labelling methods as a PET method for tracking cells, we also labelled the same cell line using the published cell labelling method by Man *et al*.,[318].

In chapter 2, it was evident that the process of labelling lymphocytes with ^{89}Zr-oxine and ^{89}Zr-DFO-NCS complexes and tracking the labelled cells *in vivo* via PET/CT imaging in a mouse model proved to be technically challenging. The mixed results revealed a number of individual processes that needed to work seamlessly in order to produce useful results. The constant failure of experiments due to varying reasons and the variability in cell isolation and labelling results made the process frustrating. To address this, more work was needed to understand the causes of this variability. The plan was to break down the processes into individual stages and assess in more detail which factors affected each individual stage of the process to ensure repeatability at each stage before any further *in vivo* imaging experiments were attempted. To achieve this, the team decided to optimise procedures on cell lines rather than donor cells, to reduce the number of animals used and to enable greater access to cells for multiple repeats of several labelling conditions to be run simultaneously. Once confidence in labelling repeatability was gained, the team could return to working with the desired donor cell population. Another issue was that the quality of the imaging results was entirely dependent on a successful tail vein injection, which required more work to hone this skill. Despite these challenges, there was still encouragement that when all the different stages of the experiments worked together, this cell labelling method could be a powerful tool in understanding the processes governing cell homing *in vivo*. One particularly interesting finding from these existing results was the unusual focal hotspots of radioactivity produced by the ^{89}Zr-DFO-NCS labelled cells with high viability after a successful tail vein injection. This unexpected distribution strongly suggested some sort of physical trapping mechanism within the tissues and organs of the mice. It was important to confirm these findings with repeat experiments and also to confirm with successful imaging of ^{89}Zr-oxine labelled cells that the hotspots were not due to this mixed cell population which had not been successfully imaged in a ^{89}Zr-oxine labelled form yet. However, if it was confirmed that the distribution pattern of the cells was

adversely affected by the choice of labelling method, this was a very significant finding that should be published.

In chapter 3, experiments were conducted to optimise the labelling of EL4 cells with ^{89}Zr-oxine. Conclusions were reached that variations in oxine concentration, caused by variations in extraction efficiency, were the main factor affecting cell viability during labelling, rather than the initial amount of ^{89}Zr-oxine activity or labelling duration. It was found that a concentration of oxine in the cell suspension of ≤1 mg/2 ml resulted in high cell viability. Additionally, it was determined that using a complete cell culture medium instead of PBS buffer and mixing cells at 300 rpm at 37 °C for 30 minutes or incubating in a CO_2 incubator at 37 °C for 30 minutes improved cell survival during labelling. The lack of a sterile environment in the lab also significantly decreased cell viability. Following the application of the optimised parameters, successful cell labelling results were obtained in terms of activity remaining in the reaction tube, labelling efficiency, cell viability, and cell yield. The method was then adapted for use with the main cell line to evaluate its efficiency.

Chapter 4 aimed to utilise the recently developed cell labelling techniques to label CTLL2 cells and evaluate the potential and efficiency of labelling the cells with ^{89}Zr-oxine and ^{89}Zr-DFO-NCS. Additionally, to validate the applicability of our cell labelling methods as a PET method for tracking cells, the same cell line was also labelled using the published cell labelling method by Man *et al*.,[318] Throughout the chapter, it was demonstrated that both ^{89}Zr-oxine and ^{89}Zr-DFO-NCS were effective at labelling the cells in terms of cell viability. Nevertheless, ^{89}Zr-DFO-NCS showed significantly higher long-term stability and retention in comparison to ^{89}Zr-oxine, whereas ^{89}Zr-oxine displayed higher labelling efficiency and the resultant ^{89}Zr-oxine labelled cells displayed a higher proliferative ability than ^{89}Zr-DFO-NCS labelled cells. Furthermore, labelling the CTLL2 cells with the method reported by Man *et al.,*[318] revealed

that this method and our developed ^{89}Zr-oxine method were both successful at labelling these cells. The results of the *in vitro* study on labelled CTLL2 cells were found to be consistent with the *in vivo* biodistribution of these cells as determined through the use of three distinct labelling methodologies. These findings indicate that the labelling methods used were successful in accurately tracking the movement and distribution of the labelled cells in mice using PET/CT imaging.

5.2 limitations and future work

In this work, we have examined the potential of the developed labelling methodologies of ^{89}Zr-oxine and ^{89}Zr-DFO-NCS as PET tracers for prolonged tracking of radiolabelled cells *in vivo* using CTLL2 cells. However, further verification of the consistency between the *in vitro* results of labelled CTLL2 cells and their *in vivo* biodistribution would be beneficial. Unfortunately, this was not feasible due to limitations in the equipment available in our research and development laboratory. One potential solution to this limitation is to use tissue histology with a flow cytometer for future work. This would provide more insights into previously unclear findings such as liver, spleen, and bone uptake in all mice.

References

[1]   S. I. Grivennikov, F. R. Greten, and M. Karin, 'Immunity, inflammation, and cancer. Cell. 2010;140(6):883–899.', *Cell*, vol. 140, no. 6, pp. 883–899, 2010.

[2]   S. A. Hoption Cann, J. P. van Netten, and C. van Netten, 'Dr William Coley and tumour regression: a place in history or in the future.', *Postgrad. Med. J.*, vol. 79, no. 938, pp. 672–680, Dec. 2003.

[3]   E. F. McCarthy, 'The toxins of William B. Coley and the treatment of bone and soft-tissue sarcomas.', *Iowa Orthop. J.*, vol. 26, pp. 154–158, 2006.

[4]   H. C. NAUTS, W. E. SWIFT, and B. L. COLEY, 'The treatment of malignant tumors by bacterial toxins as developed by the late William B. Coley, M.D., reviewed in the light of modern research.', *Cancer Res.*, vol. 6, pp. 205–216, Apr. 1946.

[5]   P. Dobosz and T. Dzieciątkowski, 'The Intriguing History of Cancer Immunotherapy', *Front. Immunol.*, vol. 10, no. December, 2019.

[6]   J. B. Murphy and J. J. Morton, 'The Lymphocyte as a Factor in Natural and Induced Resistance to Transplanted Cancer.', *Proc. Natl. Acad. Sci. U. S. A.*, vol. 1, no. 7, pp. 435–437, Jul. 1915.

[7]   G. P. Dunn, A. T. Bruce, H. Ikeda, L. J. Old, and R. D. Schreiber, 'Cancer immunoediting: from immunosurveillance to tumor escape.', *Nat. Immunol.*, vol. 3, no. 11, pp. 991–998, Nov. 2002.

[8]   O. Stutman, 'Chemical carcinogenesis in nude mice: comparison between nude mice

from homozygous matings and heterozygous matings and effect of age and carcinogen dose.', *J. Natl. Cancer Inst.*, vol. 62, no. 2, pp. 353–358, Feb. 1979.

[9]   O. Stutman, 'Delayed tumour appearance and absence of regression in nude mice infected with murine sarcoma virus.', *Nature*, vol. 253, no. 5487, pp. 142–144, Jan. 1975.

[10]   A. M. Abel, C. Yang, M. S. Thakar, and S. Malarkannan, 'Natural Killer Cells: Development, Maturation, and Clinical Utilization.', *Front. Immunol.*, vol. 9, p. 1869, 2018.

[11]   H. F. Pross and M. Jondal, 'Cytotoxic lymphocytes from normal donors. A functional marker of human non-T lymphocytes.', *Clin. Exp. Immunol.*, vol. 21, no. 2, pp. 226–235, Aug. 1975.

[12]   W. K. Decker *et al.*, 'Cancer Immunotherapy: Historical Perspective of a Clinical Revolution and Emerging Preclinical Animal Models.', *Front. Immunol.*, vol. 8, p. 829, 2017.

[13]   V. Shankaran *et al.*, "IFNγ and lymphocytes prevent primary tumour development and shape tumour immunogenicity," *Nature*, vol. 410, no. 6832, pp. 1107–1111, Apr. 2001, doi: 10.1038/35074122.

[14]   F. M. Burnet, 'The concept of immunological surveillance.', *Prog. Exp. Tumor Res.*, vol. 13, pp. 1–27, 1970.

[15]   S. J. Oiseth and M. S. Aziz, 'Cancer immunotherapy: a brief review of the history, possibilities, and challenges ahead', *J. Cancer Metastasis Treat.*, vol. 3, pp. 250–261,

2017.

[16] G. P. Dunn, L. J. Old, and R. D. Schreiber, 'The three Es of cancer immunoediting', *Annu. Rev. Immunol.*, vol. 22, no. 4, pp. 329–360, 2004.

[17] R. D. Schreiber, L. J. Old, and M. J. Smyth, 'Cancer immunoediting: integrating immunity's roles in cancer suppression and promotion.', *Science*, vol. 331, no. 6024, pp. 1565–1570, Mar. 2011.

[18] S. K. Kim and S. W. Cho, 'The Evasion Mechanisms of Cancer Immunity and Drug Intervention in the Tumor Microenvironment.', *Front. Pharmacol.*, vol. 13, p. 868695, 2022.

[19] A. D. Waldman, J. M. Fritz, and M. J. Lenardo, 'A guide to cancer immunotherapy: from T cell basic science to clinical practice', *Nat. Rev. Immunol.*, vol. 20, no. 11, pp. 651–668, 2020.

[20] D. S. Chen and I. Mellman, 'Oncology meets immunology: The cancer-immunity cycle', *Immunity*, vol. 39, no. 1, pp. 1–10, 2013.

[21] F. Galli, M. Varani, C. Lauri, G. G. Silveri, L. Onofrio, and A. Signore, 'Immune cell labelling and tracking: implications for adoptive cell transfer therapies', *EJNMMI Radiopharm. Chem.*, vol. 6, no. 1, p. 7, Feb. 2021.

[22] X. Zhang, L. Zhu, H. Zhang, S. Chen, and Y. Xiao, 'CAR-T Cell Therapy in Hematological Malignancies: Current Opportunities and Challenges.', *Front. Immunol.*, vol. 13, p. 927153, 2022.

[23]   R. Poojary, A. F. Song, B. S. Song, C. S. Song, L. Wang, and J. Song, 'Investigating chimeric antigen receptor T cell therapy and the potential for cancer immunotherapy (Review).', *Mol. Clin. Oncol.*, vol. 19, no. 6, p. 95, Dec. 2023.

[24]   M. C. Hanna, 'Advances in immunotherapy for Cancer Treatment', *Virol. Immunol. J.*, vol. 3, no. 3, pp. 1–8, 2019.

[25]   B. B. Kasten *et al.*, 'Positron emission tomography imaging with (89)Zr- labelled anti-CD8 cys-diabody reveals CD8(+) cell infiltration during oncolytic virus therapy in a glioma murine model.', *Sci. Rep.*, vol. 11, no. 1, p. 15384, Jul. 2021.

[26]   W. Wei, D. Jiang, E. B. Ehlerding, Q. Luo, and W. Cai, 'Noninvasive PET Imaging of T cells.', *Trends in cancer*, vol. 4, no. 5, pp. 359–373, May 2018.

[27]   K.-H. Jung, J. H. Lee, M. Kim, Y. S. Cho, and K.-H. Lee, '(89)Zr Immuno-PET Imaging of Tumor PD-1 Reveals That PMA Upregulates Lymphoma PD-1 through NFκB and JNK Signaling.', *Mol. Imaging*, vol. 2022, p. 5916692, 2022.

[28]   S. C. Srivastava and L. R. Chervu, 'Radionuclide- labelled red blood cells: current status and future prospects.', *Semin. Nucl. Med.*, vol. 14, no. 2, pp. 68–82, Apr. 1984.

[29]   P. J. Gawne, F. Man, P. J. Blower, and R. T. M. De Rosales, 'Direct Cell Radiolabeling for *in vivo* Cell Tracking with PET and SPECT Imaging', *Chem. Rev.*, vol. 122, no. 11, pp. 10266–10318, 2022.

[30]   Z.-Y. Chen *et al.*, 'Advance of molecular imaging technology and targeted imaging agent in imaging and therapy.', *Biomed Res. Int.*, vol. 2014, p. 819324, 2014.

[31] Ł. Kiraga *et al.*, 'Nuclear imaging for immune cell tracking *in vivo* – Comparison of various cell labeling methods and their application', *Coord. Chem. Rev.*, vol. 445, p. 214008, 2021.

[32] C. E. McCarthy, J. M. White, N. T. Viola, and H. M. Gibson, '*In vivo* Imaging Technologies to Monitor the Immune System', *Front. Immunol.*, vol. 11, Jun. 2020.

[33] A. Rahmim and H. Zaidi, 'PET versus SPECT: strengths, limitations and challenges', *Nucl. Med. Commun.*, vol. 29, no. 3, 2008.

[34] P. Charoenphun *et al.*, '[(89)Zr]oxinate4 for long-term *in vivo* cell tracking by positron emission tomography.', *Eur. J. Nucl. Med. Mol. Imaging*, vol. 42, no. 2, pp. 278–287, Feb. 2015.

[35] K. O. Asiedu, S. Koyasu, L. P. Szajek, P. L. Choyke, and N. Sato, 'Bone marrow cell trafficking analyzed by 89Zr-oxine positron emission tomography in a murine transplantation model', *Clin. Cancer Res.*, vol. 23, no. 11, pp. 2759–2768, Jun. 2017.

[36] A. Bansal *et al.*, 'Novel [89]Zr cell labeling approach for PET-based cell trafficking studies', *EJNMMI Res.*, vol. 5, no. 1, pp. 1–11, 2015.

[37] S. H. Lee *et al.*, 'Feasibility of real-time *in vivo* 89Zr-DFO- labelled CAR T-cell trafficking using PET imaging', *PLoS One*, vol. 15, no. 1, p. e0223814, Jan. 2020.

[38] I. Friberger *et al.*, 'Optimisation of the Synthesis and Cell Labelling Conditions for [89Zr]Zr-oxine and [89Zr]Zr-DFO-NCS: a Direct *In vitro* Comparison in Cell Types with Distinct Therapeutic Applications', *Mol. Imaging Biol.*, vol. 23, no. 6, pp. 952–962, 2021.

[39] I. Friberger *et al.*, 'Comparative *in vivo* biodistribution of cells labelled with [89Zr]Zr-(oxinate)4 or [89Zr]Zr-DFO-NCS using PET', *EJNMMI Res.*, vol. 13, no. 1, p. 73, 2023.

[40] N. C. Smith, M. L. Rise, and S. L. Christian, 'A Comparison of the Innate and Adaptive Immune Systems in Cartilaginous Fish, Ray-Finned Fish, and Lobe-Finned Fish', *Front. Immunol.*, vol. 10, Oct. 2019.

[41] E. Corsini and M. Iulini, 'Immune system', P. B. T.-E. of T. (Fourth E. Wexler, Ed. Oxford: Academic Press, 2024, pp. 471–495.

[42] B. A. Beutler, 'TLRs and innate immunity.', *Blood*, vol. 113, no. 7, pp. 1399–1407, Feb. 2009.

[43] O. Takeuchi and S. Akira, 'Pattern recognition receptors and inflammation.', *Cell*, vol. 140, no. 6, pp. 805–820, Mar. 2010.

[44] Y. Kumagai and S. Akira, 'Identification and functions of pattern-recognition receptors.', *J. Allergy Clin. Immunol.*, vol. 125, no. 5, pp. 985–992, May 2010.

[45] P. J. Delves and I. M. Roitt, 'The Immune System', *N. Engl. J. Med.*, vol. 343, no. 1, pp. 37–49, Jul. 2000.

[46] A. N. Al-Shura, '7 - Lymphocytes', A. N. B. T.-A. H. in I. C. C. M. Al-Shura, Ed. Academic Press, 2020, pp. 41–46.

[47] A. N. Al-Shura, 'Function of The Spleen Zang From The Chinese Medicine Perspectives Of Ascending Qi and Controlling Blood', *Adv. Hematol. Integr. Cardiovasc. Chinese Med.*, vol. 3, no. 2020, pp. 41–46, 2020.

[48] E. Corsini and M. B. T.-R. M. in B. S. Iulini, 'Immune system', Elsevier, 2023.

[49] B. Alberts, 'The Adaptive Immune System'. 2002.

[50] N. P. Restifo, M. J. Smyth, and A. Snyder, 'Acquired resistance to immunotherapy and future challenges.', *Nat. Rev. Cancer*, vol. 16, no. 2, pp. 121–126, Feb. 2016.

[51] D. S. Chen and I. Mellman, 'Elements of cancer immunity and the cancer-immune set point.', *Nature*, vol. 541, no. 7637, pp. 321–330, Jan. 2017.

[52] L. M. Lechermann, D. Lau, B. Attili, L. Aloj, and F. A. Gallagher, '*In vivo* cell tracking using pet: Opportunities and challenges for clinical translation in oncology', *Cancers (Basel).*, vol. 13, no. 16, pp. 1–19, 2021.

[53] B. M. Helfer *et al.*, 'Options for imaging cellular therapeutics *in vivo*: a multi-stakeholder perspective', *Cytotherapy*, vol. 23, no. 9, pp. 757–773, Sep. 2021.

[54] H. W. Lee, P. Gangadaran, S. Kalimuthu, and B. C. Ahn, 'Advances in Molecular Imaging Strategies for *in vivo* Tracking of Immune Cells', *Biomed Res. Int.*, vol. 2016, no. Dc, 2016.

[55] M. H. Kim, Y. J. Lee, and J. H. Kang, 'Stem Cell Monitoring with a Direct or Indirect Labeling Method', *Nucl. Med. Mol. Imaging (2010).*, vol. 50, no. 4, pp. 275–283, 2016.

[56] L. Lauwerys, E. Smits, T. Van den Wyngaert, and F. Elvas, 'Radionuclide Imaging of Cytotoxic Immune Cell Responses to Anti-Cancer Immunotherapy', *Biomedicines*, vol. 10, no. 5, pp. 1–23, 2022.

[57] A. Aicher *et al.*, 'Assessment of the Tissue Distribution of Transplanted Human Endothelial Progenitor Cells by Radioactive Labeling', *Circulation*, 2003.

[58] I. M. Barbash *et al.*, 'Systemic Delivery of Bone Marrow–Derived Mesenchymal Stem Cells to the Infarcted Myocardium', *Circulation*, 2003.

[59] H. Hong, Y. Yang, Y. Zhang, and W. Cai, 'Non-Invasive Cell Tracking in Cancer and Cancer Therapy', *Curr. Top. Med. Chem.*, 2010.

[60] F. Shao, Y. Long, H. Ji, D. Jiang, P. Lei, and X. Lan, 'Radionuclide-based molecular imaging allows CAR-T cellular visualization and therapeutic monitoring.', *Theranostics*, vol. 11, no. 14, pp. 6800–6817, 2021.

[61] A. Khatri, Y. Husaini, and P. J. Russell, 'Murine CTLL-2 cells respond to mIL12: prospects for developing an alternative bioassay for measurement of murine cytokines IL12 and IL18.', *J. Immunol. Methods*, vol. 326, no. 1–2, pp. 41–53, Sep. 2007.

[62] C. Love and C. J. Palestro, 'Radionuclide Imaging of Infection', *J. Nucl. Med. Technol.*, vol. 32, no. 2, pp. 47 LP – 57, Jun. 2004.

[63] J. T. Emslie, K. Zarnegar, M. E. Siegel, and R. W. Beart, 'Technetium-99m- labelled red blood cell scans in the investigation of gastrointestinal bleeding', *Dis. Colon Rectum*, vol. 39, no. 7, pp. 750–754, 1996.

[64] G. G. Winzelberg, K. A. McKusick, H. W. Strauss, A. C. Waltman, and A. J. Greenfield, 'Evaluation of gastrointestinal bleeding by red blood cells labelled *in vivo* with technetium-99m.', *J. Nucl. Med.*, vol. 20, no. 10, pp. 1080–1086, Oct. 1979.

[65] C. M. Griessinger *et al.*, '*In vivo* tracking of Th1 cells by PET reveals quantitative and temporal distribution and specific homing in lymphatic tissue.', *J. Nucl. Med.*, vol. 55, no. 2, pp. 301–307, Feb. 2014.

[66] K. Kumar, 'Radio labelled Compounds for Diagnosis and Treatment of Cancer.', *Molecules (Basel, Switzerland)*, vol. 26, no. 20. Switzerland, Oct-2021.

[67] W. Dai *et al.*, 'Radiolabeling of Nanomaterials: Advantages and Challenges.', *Front. Toxicol.*, vol. 3, p. 753316, 2021.

[68] T. Yeh, W. Zhang, S. T. Ildstad, and C. Ho, 'Intracellular Labeling of T-cells With Superparamagnetic Contrast Agents', *Magn. Reson. Med.*, 1993.

[69] T.-H. Chung *et al.*, 'Iron Oxide Nanoparticle-Induced Epidermal Growth Factor Receptor Expression in Human Stem Cells for Tumor Therapy', *ACS Nano*, 2011.

[70] J. J. Lukawska *et al.*, 'Real-time differential tracking of human neutrophil and eosinophil migration *in vivo*', *J. Allergy Clin. Immunol.*, vol. 133, no. 1, pp. 233–240, 2014.

[71] M. R. Puncher and P. J. Blower, 'Autoradiography and density gradient separation of technetium-99m-exametazime (HMPAO) labelled leucocytes reveals selectivity for eosinophils.', *Eur. J. Nucl. Med.*, vol. 21, no. 11, pp. 1175–1182, Nov. 1994.

[72] E. Sharif-Paghaleh *et al.*, '*In vivo* SPECT reporter gene imaging of regulatory T cells.', *PLoS One*, vol. 6, no. 10, p. e25857, 2011.

[73] R. Tavaré *et al.*, 'Monitoring of *in vivo* function of superparamagnetic iron oxide labelled murine dendritic cells during anti-tumour vaccination.', *PLoS One*, vol. 6, no.

5, p. e19662, 2011.

[74] S. Edmonds *et al.*, 'Exploiting the Metal-Chelating Properties of the Drug Cargo for *In vivo* Positron Emission Tomography Imaging of Liposomal Nanomedicines.', *ACS Nano*, vol. 10, no. 11, pp. 10294–10307, Nov. 2016.

[75] Y. Noh, Y. T. Lim, and B. H. Chung, 'Noninvasive imaging of dendritic cell migration into lymph nodes using near-infrared fluorescent semiconductor nanocrystals', *FASEB J.*, vol. 22, no. 11, pp. 3908–3918, 2008.

[76] F. Galli *et al.*, '*In vivo* imaging of natural killer cell trafficking in tumors', *J. Nucl. Med.*, vol. 56, no. 10, pp. 1575–1580, 2015.

[77] N. P. van der Meulen, K. Strobel, and T. V. M. Lima, 'New Radionuclides and Technological Advances in SPECT and PET Scanners', *Cancers (Basel).*, vol. 13, no. 24, p. 6183, Dec. 2021.

[78] J. M. Leech *et al.*, 'Whole-body imaging of adoptively transferred T cells using magnetic resonance imaging, single photon emission computed tomography and positron emission tomography techniques, with a focus on regulatory T cells.', *Clin. Exp. Immunol.*, vol. 172, no. 2, pp. 169–177, May 2013.

[79] S. Iwano *et al.*, 'Single-Cell Bioluminescence Imaging of Deep Tissue in Freely Moving Animals', *Science (80-.).*, 2018.

[80] J. Nakayama *et al.*, 'High Sensitivity *in vivo* Imaging of Cancer Metastasis Using a Near-Infrared Luciferin Analogue seMpai', *Int. J. Mol. Sci.*, 2020.

[81]   M. A. Pysz, S. S. Gambhir, and J. K. Willmann, 'Molecular Imaging: Current Status and Emerging Strategies', *Clin. Radiol.*, 2010.

[82]   A. Hellebust and R. Richards-Kortum, 'Advances in Molecular Imaging: Targeted Optical Contrast Agents for Cancer Diagnostics', *Nanomedicine*, 2012.

[83]   Y. Liu, G. Yu, M. Tian, and H. Zhang, 'Optical Probes and the Applications in Multimodality Imaging', *Contrast Media Mol. Imaging*, 2011.

[84]   K. W. Kang, 'Preliminary Pre-Clinical Results and Overview on PET/MRI/Fluorescent Molecular Imaging', *Open Nucl. Med. J.*, 2010.

[85]   J. E. Lemaster, F. Chen, T. Kim, A. Hariri, and J. V Jokerst, 'Development of a Trimodal Contrast Agent for Acoustic and Magnetic Particle Imaging of Stem Cells', *Acs Appl. Nano Mater.*, 2018.

[86]   F. Chen and J. V Jokerst, 'Stem Cell Tracking With Nanoparticle-Based Ultrasound Contrast Agents', 2020.

[87]   G. J. Czarnota *et al.*, 'Ultrasound Imaging of Apoptosis: High-Resolution Non-Invasive Monitoring of Programmed Cell Death *in vitro*, in Situ and *in vivo*', *Br. J. Cancer*, 1999.

[88]   N. Çiledağ, K. Arda, B. K. Arıbaş, E. Aktaş, and S. K. Köse, 'The Utility of Ultrasound Elastography and MicroPure Imaging in the Differentiation of Benign and Malignant Thyroid Nodules', *Am. J. Roentgenol.*, 2012.

[89]   G. J. Czarnota *et al.*, 'Ultrasound Biomicroscopy of Cancer Therapy Effects: Correlation Between Light and Electron Microscopy, and a New Non-Invasive Ultrasound Imaging

Method for Detecting Apoptosis', *Microsc. Microanal.*, 2000.

[90] J. Belfield and C. Findlay-Line, 'Testicular Germ Cell Tumours—The Role of Conventional Ultrasound', *Cancers (Basel).*, 2022.

[91] E. Vazquez-Sequeiros and M. J. Wiersema, 'The Role of Endoscopic Ultrasonography in Diagnosis Staging, and Management of Pancreatic Disease States', *Curr. Gastroenterol. Rep.*, 2000.

[92] C. X. Deng, X. Hong, and J. P. Stegemann, 'Ultrasound Imaging Techniques for Spatiotemporal Characterization of Composition, Microstructure, and Mechanical Properties in Tissue Engineering', *Tissue Eng. Part B Rev.*, 2016.

[93] C. Sciallero and A. Trucco, 'Concentration Estimation of Ultrasound Targeted Microbubbles for Improving Cancer Detection: A Preliminary *in vivo* Study', 2015.

[94] N. Bhat, 'A Review on Analysis of Speckle Reduction in Ultra Sound Images', *Int. J. Res. Appl. Sci. Eng. Technol.*, 2018.

[95] F. Chen *et al.*, 'Exosome-Like Silica Nanoparticles: A Novel Ultrasound Contrast Agent for Stem Cell Imaging', *Nanoscale*, 2017.

[96] P. Dierks and M. C. Berman, 'Renal Cell Carcinoma', *J. Diagnostic Med. Sonogr.*, 1987.

[97] J. Sun, G. Teng, S. Ju, Z. Ma, X. Mai, and M. Ma, 'MR Tracking of Magnetically labelled Mesenchymal Stem Cells in Rat Kidneys With Acute Renal Failure', *Cell Transplant.*, 2008.

[98] V. Hoerr *et al.*, 'Bacteria Tracking by *in vivo*magnetic Resonance Imaging', *BMC Biol.*, 2013.

[99] H. E. Daldrup-Link *et al.*, '*In vivo* tracking of genetically engineered, anti-HER2/neu directed natural killer cells to HER2/neu positive mammary tumors with magnetic resonance imaging.', *Eur. Radiol.*, vol. 15, no. 1, pp. 4–13, Jan. 2005.

[100] S. A. Anderson *et al.*, 'Magnetic resonance imaging of labelled T-cells in a mouse model of multiple sclerosis', *Ann. Neurol.*, vol. 55, no. 5, p. 654—659, May 2004.

[101] D. Baumjohann, A. Hess, L. Budinsky, K. Brune, G. Schuler, and M. B. Lutz, '*In vivo* magnetic resonance imaging of dendritic cell migration into the draining lymph nodes of mice.', *Eur. J. Immunol.*, vol. 36, no. 9, pp. 2544–2555, Sep. 2006.

[102] C. M. Long, H. W. M. van Laarhoven, J. W. M. Bulte, and H. I. Levitsky, 'Magnetovaccination as a novel method to assess and quantify dendritic cell tumor antigen capture and delivery to lymph nodes.', *Cancer Res.*, vol. 69, no. 7, pp. 3180–3187, Apr. 2009.

[103] S. R. Alam *et al.*, 'Ultrasmall superparamagnetic particles of iron oxide in patients with acute myocardial infarction: early clinical experience.', *Circ. Cardiovasc. Imaging*, vol. 5, no. 5, pp. 559–565, Sep. 2012.

[104] J. L. Gaglia *et al.*, 'Noninvasive imaging of pancreatic islet inflammation in type 1A diabetes patients.', *J. Clin. Invest.*, vol. 121, no. 1, pp. 442–445, Jan. 2011.

[105] M. G. Harisinghani *et al.*, 'Noninvasive detection of clinically occult lymph-node metastases in prostate cancer.', *N. Engl. J. Med.*, vol. 348, no. 25, pp. 2491–2499, Jun.

2003.

[106] T. T. Sibov *et al.*, 'Umbilical cord mesenchymal stem cells labelled with multimodal iron oxide nanoparticles with fluorescent and magnetic properties: application for *in vivo* cell tracking.', *Int. J. Nanomedicine*, vol. 9, pp. 337–350, 2014.

[107] H. Markides, O. Kehoe, R. H. Morris, and A. J. El Haj, 'Whole body tracking of superparamagnetic iron oxide nanoparticle-labelled cells--a rheumatoid arthritis mouse model.', *Stem Cell Res. Ther.*, vol. 4, no. 5, p. 126, Oct. 2013.

[108] M. Srinivas, M. S. Turner, J. M. Janjic, P. A. Morel, D. H. Laidlaw, and E. T. Ahrens, '*In vivo* cytometry of antigen-specific t cells using 19F MRI.', *Magn. Reson. Med.*, vol. 62, no. 3, pp. 747–753, Sep. 2009.

[109] Z. Liu and Z. Li, 'Molecular Imaging in Tracking Tumor-Specific Cytotoxic T Lymphocytes (CTLs)', *Theranostics*, vol. 4, no. 10, pp. 990–1001, 2014.

[110] 'Advancing Nuclear Medicine Through Innovation', Sep. 2007.

[111] J. L. Prekeges, 'Nuclear Medicine and PET/CT Technology and Techniques', *J. Nucl. Med. Technol.*, 2012.

[112] P. J. Ell, 'Nuclear medicine.', *Postgrad. Med. J.*, vol. 68, no. 796, pp. 82–105, Feb. 1992.

[113] B. Palumbo *et al.*, 'SPECT and PET Serve as Molecular Imaging Techniques and *in vivo* Biomarkers for Brain Metastases', *Int. J. Mol. Sci.*, 2014.

[114] S. A. R. Naqvi, '99mTc- labelled Antibiotics for Infection Diagnosis: Mechanism,

Action, and Progress', *Chem. Biol. Drug Des.*, 2021.

[115] S. Tiepolt *et al.*, 'Current Radiotracers to Image Neurodegenerative Diseases', *Ejnmmi Radiopharm. Chem.*, 2019.

[116] S. J. Ryder, A. Love, E. L. Duncan, and D. A. Pattison, 'PET Detectives: Molecular Imaging for Phaeochromocytomas and Paragangliomas in the Genomics Era', *Clin. Endocrinol. (Oxf).*, 2020.

[117] Y. Güzel, İ. Kaplan, F. Kepenek, N. Söğütçü, and H. Kömek, 'Perirenal Infiltration of Signet Ring Cell Colon Carcinoma Shown by 68Ga-Fapi PET/CT', *Clin. Nucl. Med.*, 2022.

[118] G. Treglia, V. Rufini, M. Salvatori, A. Giordano, and L. Giovanella, 'PET Imaging in Recurrent Medullary Thyroid Carcinoma', *Int. J. Mol. Imaging*, 2012.

[119] O. Schillaci, A. Spanu, B. Palumbo, and R. Danieli, 'SPECT/CT in Neuroendocrine Tumours', *Clin. Transl. Imaging*, 2014.

[120] P. R. Bhatt *et al.*, 'Parathyroid Imaging With Simultaneous Acquisition of 99mTc-Sestamibi and 123I: The Relative Merits of Pinhole Collimation and SPECT/CT', *J. Nucl. Med. Technol.*, 2015.

[121] J. G. McAfee and M. L. Thakur, 'Survey of radioactive agents for *in vitro* labeling of phagocytic leukocytes. I. Soluble agents.', *J. Nucl. Med.*, vol. 17, no. 6, pp. 480–487, Jun. 1976.

[122] P. Zanzonico *et al.*, '[131I]FIAU labeling of genetically transduced, tumor-reactive

lymphocytes: cell-level dosimetry and dose-dependent toxicity.', *Eur. J. Nucl. Med. Mol. Imaging*, vol. 33, no. 9, pp. 988–997, Sep. 2006.

[123] G. M. Currie, P. A. Towers, and J. M. Wheat, 'A role for subtraction scintigraphy in the evaluation of lower gastrointestinal bleeding in the athlete.', *Sports Med.*, vol. 37, no. 10, pp. 923–928, 2007.

[124] H. Q. Dam *et al.*, 'The SNMMI Procedure Standard/EANM Practice Guideline for Gastrointestinal Bleeding Scintigraphy 2.0', *J. Nucl. Med. Technol.*, vol. 42, no. 4, pp. 308–317, 2014.

[125] L. M. Lechermann *et al.*, 'Detection limit of 89Zr- labelled T cells for cellular tracking: an *in vitro* imaging approach using clinical PET/CT and PET/MRI', *EJNMMI Res.*, vol. 10, no. 1, 2020.

[126] B. F. Hutton, 'The origins of SPECT and SPECT/CT.', *Eur. J. Nucl. Med. Mol. Imaging*, vol. 41 Suppl 1, pp. S3-16, May 2014.

[127] R. J. Jaszczak, 'The early years of single photon emission computed tomography ({SPECT}): an anthology of selected reminiscences', *Phys. Med. Biol.*, vol. 51, no. 13, pp. R99--R115, Jun. 2006.

[128] B. Bybel, R. C. Brunken, F. P. DiFilippo, D. R. Neumann, G. Wu, and M. D. Cerqueira, 'SPECT/CT Imaging: Clinical Utility of an Emerging Technology', *RadioGraphics*, vol. 28, no. 4, pp. 1097–1113, 2008.

[129] C. S. Cutler, H. M. Hennkens, N. Sisay, S. Huclier-Markai, and S. S. Jurisson, 'Radiometals for combined imaging and therapy', *Chem. Rev.*, vol. 113, no. 2, pp. 858–

883, 2013.

[130] F. Caobelli *et al.*, 'Simultaneous dual-isotope solid-state detector SPECT for improved tracking of white blood cells in suspected endocarditis', *Eur. Heart J.*, vol. 38, no. 6, pp. 436–443, Feb. 2017.

[131] 'CARL DAVID ANDERSON.Biographical Memoirs'. Jun-1998.

[132] S. Basu, T. C. Kwee, S. Surti, E. A. Akin, D. Yoo, and A. Alavi, 'Fundamentals of PET and PET/CT imaging', *Ann. N. Y. Acad. Sci.*, vol. 1228, no. 1, pp. 1–18, Jun. 2011.

[133] W. H. Sweet, 'The use of nuclear disintegration in diagnosis and treatment of brain tumors', *N. Engl. J. Med.*, vol. 245, no. 23, pp. 875–878, Dec. 1951.

[134] R. Nutt, 'The history of positron emission tomography', *Mol. Imaging Biol.*, vol. 4, no. 1, pp. 11–26, 2002.

[135] D. W. Townsend, 'Combined positron emission tomography-computed tomography: the historical perspective.', *Semin. Ultrasound. CT. MR*, vol. 29, no. 4, pp. 232–235, Aug. 2008.

[136] D. W. Townsend, J. P. J. Carney, J. T. Yap, and N. C. Hall, 'PET/CT today and tomorrow.', *J. Nucl. Med.*, vol. 45 Suppl 1, pp. 4S-14S, Jan. 2004.

[137] S. R. Cherry, T. Jones, J. S. Karp, J. Qi, W. W. Moses, and R. D. Badawi, 'Total-Body PET: Maximizing Sensitivity to Create New Opportunities for Clinical Research and Patient Care.', *J. Nucl. Med.*, vol. 59, no. 1, pp. 3–12, Jan. 2018.

[138] G. Crișan, N. S. Moldovean-Cioroianu, D.-G. Timaru, G. Andrieș, C. Căinap, and V. Chiș, 'Radiopharmaceuticals for PET and SPECT Imaging: A Literature Review over the Last Decade', *International Journal of Molecular Sciences*, vol. 23, no. 9. 2022.

[139] 'Molecular Imaging and Its Biological Applications', *Eur. J. Nucl. Med. Mol. Imaging*, vol. 31, no. 11, p. 1544, 2004.

[140] M. Partridge, A. Spinelli, W. Ryder, and C. Hindorf, 'The effect of β+ energy on performance of a small animal PET camera', *Nucl. Instruments Methods Phys. Res. Sect. A Accel. Spectrometers, Detect. Assoc. Equip.*, vol. 568, no. 2, pp. 933–936, 2006.

[141] G. A. M. S. van Dongen *et al.*, 'The Role of (89)Zr-Immuno-PET in Navigating and Derisking the Development of Biopharmaceuticals.', *J. Nucl. Med.*, vol. 62, no. 4, pp. 438–445, Apr. 2021.

[142] I. Verel, G. W. M. Visser, and G. A. van Dongen, 'The Promise of Immuno-PET in Radioimmunotherapy', *J. Nucl. Med.*, vol. 46, no. 1 suppl, pp. 164S LP-171S, Jan. 2005.

[143] A. A. M. Van der Veldt, E. F. Smit, and A. A. Lammertsma, 'Positron emission tomography as a method for measuring drug delivery to tumors *in vivo*: The example of [11C]docetaxel', *Front. Oncol.*, vol. 3 AUG, no. August, pp. 1–7, 2013.

[144] C. Johnson *et al.*, 'Evaluation of 3D reconstruction algorithms for a small animal PET camera', 1997.

[145] J. Qi, R. M. Leahy, S. R. Cherry, A. Chatziioannou, and T. H. Farquhar, 'High-resolution 3D Bayesian image reconstruction using the microPET small-animal scanner.', *Phys. Med. Biol.*, vol. 43, no. 4, pp. 1001–1013, Apr. 1998.

[146] C. Kuntner and D. Stout, 'Quantitative preclinical PET imaging: Opportunities and challenges', *Front. Phys.*, vol. 2, no. February, pp. 1–12, 2014.

[147] T. Jones and D. Townsend, 'History and future technical innovation in positron emission tomography', *J. Med. Imaging*, vol. 4, no. 1, p. 011013, 2017.

[148] A. Kiani, A. Esquevin, N. Lepareur, P. Bourguet, F. Le Jeune, and J. Gauvrit, 'Main applications of hybrid {PETMRI} contrast agents: a review', *Contrast Media Mol. Imaging*, vol. 11, no. 2, pp. 92–98, Dec. 2015.

[149] R. Hicks, E. Lau, and D. Binns, 'Hybrid imaging is the future of molecular imaging', *Biomed. Imaging Interv. J.*, vol. 3, no. 3, 2007.

[150] B. J. Pichler, M. S. Judenhofer, and C. Pfannenberg, 'Multimodal imaging approaches: PET/CT and PET/MRI.', *Handb. Exp. Pharmacol.*, no. 185 Pt 1, pp. 109–132, 2008.

[151] H. Hricak *et al.*, 'Global Trends in Hybrid Imaging', *Radiology*, vol. 257, no. 2, pp. 498–506, 2010.

[152] R. Seifert *et al.*, 'Clinical Use of PET/MR in Oncology: An Update.', *Semin. Nucl. Med.*, vol. 52, no. 3, pp. 356–364, May 2022.

[153] R. Weissleder and M. J. Pittet, 'Imaging in the era of molecular oncology.', *Nature*, vol. 452, no. 7187, pp. 580–589, Apr. 2008.

[154] E. A. Osborn and F. A. Jaffer, 'Advances in molecular imaging of atherosclerotic vascular disease.', *Curr. Opin. Cardiol.*, vol. 23, no. 6, pp. 620–628, Nov. 2008.

[155] M. L. James and S. S. Gambhir, 'A molecular imaging primer: Modalities, imaging agents, and applications', *Physiol. Rev.*, vol. 92, no. 2, pp. 897–965, 2012.

[156] S. Rizzo, F. Petrella, L. S. Politi, and P. Wang, 'Molecular Imaging of Stems Cells}: *In vivo* Tracking and Clinical Translation', *Stem Cells Int.*, vol. 2017, pp. 1–2, 2017.

[157] Y. Ouyang, T. J. Kim, and G. Pratx, 'Evaluation of a BGO-Based PET System for Single-Cell Tracking Performance by Simulation and Phantom Studies.', *Mol. Imaging*, vol. 15, 2016.

[158] B. Palumbo *et al.*, 'SPECT and PET serve as molecular imaging techniques and *in vivo* biomarkers for brain metastases', *International Journal of Molecular Sciences*, vol. 15, no. 6. pp. 9878–9893, 2014.

[159] M. Rodriguez-Porcel, '*In vivo* imaging and monitoring of transplanted stem cells: clinical applications.', *Curr. Cardiol. Rep.*, vol. 12, no. 1, pp. 51–58, Jan. 2010.

[160] S. T. Langford, C. S. Wiggins, R. Santos, M. Hauser, J. M. Becker, and A. E. Ruggles, 'Three-dimensional spatiotemporal tracking of fluorine-18 radio labelled yeast cells via positron emission particle tracking.', *PLoS One*, vol. 12, no. 7, p. e0180503, 2017.

[161] L. C. Wu *et al.*, 'A Review of Magnetic Particle Imaging and Perspectives on Neuroimaging.', *AJNR. Am. J. Neuroradiol.*, vol. 40, no. 2, pp. 206–212, Feb. 2019.

[162] Y. Xing, J. Zhao, P. S. Conti, and K. Chen, 'Radio labelled nanoparticles for multimodality tumor imaging.', *Theranostics*, vol. 4, no. 3, pp. 290–306, 2014.

[163] E. B. Olasz, L. Lang, J. Seidel, M. V Green, W. C. Eckelman, and S. I. Katz, 'Fluorine-

18 labelled mouse bone marrow-derived dendritic cells can be detected in vivo by high resolution projection imaging.', *J. Immunol. Methods*, vol. 260, no. 1–2, pp. 137–148, Feb. 2002.

[164] I. J. M. De Vries *et al.*, 'Effective migration of antigen-pulsed dendritic cells to lymph nodes in melanoma patients is determined by their maturation state.', *Cancer Res.*, vol. 63, no. 1, pp. 12–17, Jan. 2003.

[165] H. W. Lee *et al.*, 'Tracking of dendritic cell migration into lymph nodes using molecular imaging with sodium iodide symporter and enhanced firefly luciferase genes.', *Sci. Rep.*, vol. 5, p. 9865, May 2015.

[166] H. S. Kim *et al.*, '*In vivo* Tracking of Dendritic Cell using MRI Reporter Gene, Ferritin.', *PLoS One*, vol. 10, no. 5, p. e0125291, 2015.

[167] S. Kang *et al.*, 'Combined Fluorescence and Magnetic Resonance Imaging of Primary Macrophage Migration to Sites of Acute Inflammation Using Near-Infrared Fluorescent Magnetic Nanoparticles.', *Mol. imaging Biol.*, vol. 17, no. 5, pp. 643–651, Oct. 2015.

[168] H. E. Daldrup-Link *et al.*, 'MRI of tumor-associated macrophages with clinically applicable iron oxide nanoparticles.', *Clin. cancer Res. an Off. J. Am. Assoc. Cancer Res.*, vol. 17, no. 17, pp. 5695–5704, Sep. 2011.

[169] A. Gramoun *et al.*, 'Monitoring the effects of dexamethasone treatment by MRI using *in vivo* iron oxide nanoparticle- labelled macrophages.', *Arthritis Res. Ther.*, vol. 16, no. 3, p. R131, Jun. 2014.

[170] H. W. Lee *et al.*, 'Dual reporter gene imaging for tracking macrophage migration using

the human sodium iodide symporter and an enhanced firefly luciferase in a murine inflammation model.', *Mol. imaging Biol.*, vol. 15, no. 6, pp. 703–712, Dec. 2013.

[171] J. H. Seo *et al.*, 'Trafficking macrophage migration using reporter gene imaging with human sodium iodide symporter in animal models of inflammation.', *J. Nucl. Med.*, vol. 51, no. 10, pp. 1637–1643, Oct. 2010.

[172] A. Blykers *et al.*, 'PET Imaging of Macrophage Mannose Receptor-Expressing Macrophages in Tumor Stroma Using 18F-Radio labelled Camelid Single-Domain Antibody Fragments.', *J. Nucl. Med.*, vol. 56, no. 8, pp. 1265–1271, Aug. 2015.

[173] M. Srinivas, P. A. Morel, L. A. Ernst, D. H. Laidlaw, and E. T. Ahrens, 'Fluorine-19 MRI for visualization and quantification of cell migration in a diabetes model.', *Magn. Reson. Med.*, vol. 58, no. 4, pp. 725–734, Oct. 2007.

[174] H. Kim *et al.*, 'Engineering human tumor-specific cytotoxic T cells to function in a hypoxic environment.', *Mol. Ther.*, vol. 16, no. 3, pp. 599–606, Mar. 2008.

[175] C. J. Shu *et al.*, 'Quantitative PET reporter gene imaging of CD8+ T cells specific for a melanoma-expressed self-antigen.', *Int. Immunol.*, vol. 21, no. 2, pp. 155–165, Feb. 2009.

[176] D. L. J. Thorek, P. Y. Tsao, V. Arora, L. Zhou, R. A. Eisenberg, and A. Tsourkas, '*In vivo*, multimodal imaging of B cell distribution and response to antibody immunotherapy in mice.', *PLoS One*, vol. 5, no. 5, p. e10655, May 2010.

[177] M. Walther *et al.*, 'Implementation of89Zr production and *in vivo* imaging of B-cells in mice with89Zr- labelled anti-B-cell antibodies by small animal PET/CT', *Appl. Radiat.*

Isot., vol. 69, no. 6, pp. 852–857, 2011.*Isot. Incl. data, Instrum. methods use Agric. Ind. Med.*, vol. 69, no. 6, pp. 852–857, Jun. 2011.

[178] S. Tavri *et al.*, 'Optical imaging of cellular immunotherapy against prostate cancer.', *Mol. Imaging*, vol. 8, no. 1, pp. 15–26, 2009.

[179] R. J. Melder, A. L. Brownell, T. M. Shoup, G. L. Brownell, and R. K. Jain, 'Imaging of activated natural killer cells in mice by positron emission tomography: preferential uptake in tumors.', *Cancer Res.*, vol. 53, no. 24, pp. 5867–5871, Dec. 1993.

[180] L. Zamai *et al.*, 'NK cells and cancer.', *J. Immunol.*, vol. 178, no. 7, pp. 4011–4016, Apr. 2007.

[181] N. C. Gupta, D. J. Esterbrooks, D. E. Hilleman, and S. M. Mohiuddin, 'Comparison of adenosine and exercise thallium-201 single-photon emission computed tomography SPECT myocardial perfusion imaging', *J. Am. Coll. Cardiol.*, vol. 19, no. 2, pp. 248–257, 1992.

[182] I. MATSUNARI *et al.*, 'Attenuation-corrected rest thallium-201/stress technetium 99m sestamibi myocardial {SPECT} in normals*', *J. Nucl. Cardiol.*, vol. 5, no. 1, pp. 48–55, 1998.

[183] M. J. Manyak *et al.*, 'Immunoscintigraphy with indium-111-capromab pendetide: evaluation before definitive therapy in patients with prostate cancer', *Urology*, vol. 54, no. 6, pp. 1058–1063, 1999.

[184] R. ter Heine *et al.*, 'Bench to bedside development of GMP grade Rhenium-188-HEDP, a radiopharmaceutical for targeted treatment of painful bone metastases', *Int. J. Pharm.*,

vol. 465, no. 1–2, pp. 317–324, 2014.

[185] A. Gholamrezanezhad *et al.*, 'Cytotoxicity of 111In-oxine on mesenchymal stem cells: a time-dependent adverse effect', *Nucl. Med. Commun.*, vol. 30, no. 3, pp. 210–216, 2009.

[186] B. Nowak *et al.*, 'Indium-111 oxine labelling affects the cellular integrity of haematopoietic progenitor cells.', *Eur. J. Nucl. Med. Mol. Imaging*, vol. 34, no. 5, pp. 715–721, May 2007.

[187] E. P. Balaban, T. R. Simon, and E. P. Frenkel, 'Toxicity of indium-111 on the radio labelled lymphocyte.', *J. Nucl. Med.*, vol. 28, no. 2, pp. 229–233, Feb. 1987.

[188] D. Blocklet *et al.*, '111In-oxine and 99mTc-HMPAO labelling of antigen-loaded dendritic cells: *in vivo* imaging and influence on motility and actin content.', *Eur. J. Nucl. Med. Mol. Imaging*, vol. 30, no. 3, pp. 440–447, Mar. 2003.

[189] A. Gholamrezanezhad *et al.*, '*In vivo* tracking of 111In-oxine labelled mesenchymal stem cells following infusion in patients with advanced cirrhosis.', *Nucl. Med. Biol.*, vol. 38, no. 7, pp. 961–967, Oct. 2011.

[190] P. H. Rosado-de-Castro *et al.*, 'Biodistribution of bone marrow mononuclear cells after intra-arterial or intravenous transplantation in subacute stroke patients.', *Regen. Med.*, vol. 8, no. 2, pp. 145–155, Mar. 2013.

[191] I. Ak, M. P. Stokkel, and E. K. Pauwels, 'Positron emission tomography with 2-[18F]fluoro-2-deoxy-D-glucose in oncology. Part II. The clinical value in detecting and staging primary tumours.', *J. Cancer Res. Clin. Oncol.*, vol. 126, no. 10, pp. 560–574,

Oct. 2000.

[192] J. H. F. Rudd *et al.*, 'Imaging atherosclerotic plaque inflammation with [18F]-fluorodeoxyglucose positron emission tomography.', *Circulation*, vol. 105, no. 23, pp. 2708–2711, Jun. 2002.

[193] S. Osman and H. J. Danpure, 'The use of 2-[18F]fluoro-2-deoxy-D-glucose as a potential *in vitro* agent for labelling human granulocytes for clinical studies by positron emission tomography.', *Int. J. Radiat. Appl. instrumentation. Part B, Nucl. Med. Biol.*, vol. 19, no. 2, pp. 183–190, Feb. 1992.

[194] L. A. Forstrom, B. P. Mullan, J. C. Hung, V. J. Lowe, and L. M. Thorson, '18F-FDG labelling of human leukocytes.', *Nucl. Med. Commun.*, vol. 21, no. 7, pp. 691–694, Jul. 2000.

[195] J. N. Rini *et al.*, 'PET with FDG- labelled leukocytes versus scintigraphy with 111In-oxine- labelled leukocytes for detection of infection.', *Radiology*, vol. 238, no. 3, pp. 978–987, Mar. 2006.

[196] N. Dumarey *et al.*, 'Imaging infection with 18F-FDG- labelled leukocyte PET/CT: initial experience in 21 patients.', *J. Nucl. Med.*, vol. 47, no. 4, pp. 625–632, Apr. 2006.

[197] K. K. Bhargava, R. K. Gupta, K. J. Nichols, and C. J. Palestro, '*In vitro* human leukocyte labeling with 64Cu: an intraindividual comparison with 111In-oxine and 18F-FDG', *Nucl. Med. Biol.*, vol. 36, no. 5, pp. 545–549, 2009.

[198] H. M. Prince *et al.*, '*In vivo* tracking of dendritic cells in patients with multiple myeloma.', *J. Immunother.*, vol. 31, no. 2, pp. 166–179, 2008.

[199] M. Hofmann *et al.*, 'Monitoring of bone marrow cell homing into the infarcted human myocardium.', *Circulation*, vol. 111, no. 17, pp. 2198–2202, May 2005.

[200] C. Botti *et al.*, 'Comparison of three different methods for radiolabelling human activated T lymphocytes.', *Eur. J. Nucl. Med.*, vol. 24, no. 5, pp. 497–504, May 1997.

[201] B. Doyle *et al.*, 'Dynamic tracking during intracoronary injection of 18F-FDG- labelled progenitor cell therapy for acute myocardial infarction.', *J. Nucl. Med.*, vol. 48, no. 10, pp. 1708–1714, Oct. 2007.

[202] K. Stojanov, E. F. J. de Vries, D. Hoekstra, A. van Waarde, R. A. J. O. Dierckx, and I. S. Zuhorn, '[18F]FDG labeling of neural stem cells for *in vivo* cell tracking with positron emission tomography: inhibition of tracer release by phloretin.', *Mol. Imaging*, vol. 11, no. 1, pp. 1–12, Feb. 2012.

[203] C. Fersing, A. Bouhlel, C. Cantelli, P. Garrigue, V. Lisowski, and B. Guillet, 'A Comprehensive Review of Non-Covalent Radiofluorination Approaches Using Aluminum [(18)F]fluoride: Will [(18)F]AlF Replace (68)Ga for Metal Chelate Labeling?', *Molecules*, vol. 24, no. 16, Aug. 2019.

[204] J. E. Blower *et al.*, 'The Radiopharmaceutical Chemistry of the Radionuclides of Gallium and Indium BT - Radiopharmaceutical Chemistry', J. S. Lewis, A. D. Windhorst, and B. M. Zeglis, Eds. Cham: Springer International Publishing, 2019, pp. 255–271.

[205] M. D. Bartholomä, A. S. Louie, J. F. Valliant, and J. Zubieta, 'Technetium and Gallium Derived Radiopharmaceuticals: Comparing and Contrasting the Chemistry of Two

Important Radiometals for the Molecular Imaging Era', *Chem. Rev.*, vol. 110, no. 5, pp. 2903–2920, May 2010.

[206] M. D. Bartholomä, 'Recent developments in the design of bifunctional chelators for metal-based radiopharmaceuticals used in Positron Emission Tomography', *Inorganica Chim. Acta*, vol. 389, pp. 36–51, 2012.

[207] S. R. Banerjee and M. G. Pomper, 'Clinical applications of Gallium-68', *Appl. Radiat. Isot.*, vol. 76, pp. 2–13, 2013.

[208] M. Fani, J. P. André, and H. R. Maecke, '68Ga-PET: a powerful generator-based alternative to cyclotron-based PET radiopharmaceuticals.', *Contrast Media Mol. Imaging*, vol. 3, no. 2, pp. 67–77, 2008.

[209] M. Brandt, J. Cardinale, M. L. Aulsebrook, G. Gasser, and T. L. Mindt, 'An Overview of PET Radiochemistry, Part 2: Radiometals.', *J. Nucl. Med.*, vol. 59, no. 10, pp. 1500–1506, Oct. 2018.

[210] M. J. Welch, M. L. Thakur, R. E. Coleman, M. Patel, B. A. Siegel, and M. Ter-Pogossian, 'Gallium-68 labelled red cells and platelets: new agents for positron tomography.', *J. Nucl. Med.*, vol. 18, no. 6, pp. 558–562, Jun. 1977.

[211] D. A. Goodwin *et al.*, 'Viability and biodistribution of 68Ga MPO-labelled human platelets.', *Nucl. Med. Commun.*, vol. 14, no. 11, pp. 1023–1029, Nov. 1993.

[212] Y. Yano *et al.*, 'Gallium-68 lipophilic complexes for labeling platelets.', *J. Nucl. Med.*, vol. 26, no. 12, pp. 1429–1437, Dec. 1985.

[213] C. J. Anderson, T. S. Pajeau, W. B. Edwards, E. L. Sherman, B. E. Rogers, and M. J. Welch, '*In vitro* and *in vivo* evaluation of copper-64-octreotide conjugates.', *J. Nucl. Med.*, vol. 36, no. 12, pp. 2315–2325, Dec. 1995.

[214] N. Adonai *et al.*, 'Ex vivo cell labeling with 64Cu-pyruvaldehyde-bis(N4-methylthiosemicarbazone) for imaging cell trafficking in mice with positron-emission tomography.', *Proc. Natl. Acad. Sci. U. S. A.*, vol. 99, no. 5, pp. 3030–3035, Mar. 2002.

[215] J. Huang, C. C. I. Lee, J. L. Sutcliffe, S. R. Cherry, and A. F. Tarantal, 'Radiolabeling rhesus monkey CD34+ hematopoietic and mesenchymal stem cells with 64Cu-pyruvaldehyde-bis(N4-methylthiosemicarbazone) for microPET imaging.', *Mol. Imaging*, vol. 7, no. 1, pp. 1–11, 2008.

[216] J.-J. Park *et al.*, 'Comparison of cell-labeling methods with [124]I-FIAU and ^{64}Cu-PTSM for cell tracking using chronic myelogenous leukemia cells expressing HSV1-tk and firefly luciferase.', *Cancer Biother. Radiopharm.*, vol. 27, no. 10, pp. 719–728, Dec. 2012.

[217] Z.-B. Li, K. Chen, Z. Wu, H. Wang, G. Niu, and X. Chen, '64Cu- labelled PEGylated polyethylenimine for cell trafficking and tumor imaging.', *Mol. imaging Biol.*, vol. 11, no. 6, pp. 415–423, 2009.

[218] P. J. Blower, J. S. Lewis, and J. Zweit, 'Copper radionuclides and radiopharmaceuticals in nuclear medicine.', *Nucl. Med. Biol.*, vol. 23, no. 8, pp. 957–980, Nov. 1996.

[219] Y. Zhou *et al.*, '(64)Cu-based Radiopharmaceuticals in Molecular Imaging.', *Technol. Cancer Res. Treat.*, vol. 18, p. 1533033819830758, Jan. 2019.

[220] E. A. Pérès *et al.*, '(64)Cu-ATSM/(64)Cu-Cl(2) and their relationship to hypoxia in glioblastoma: a preclinical study.', *EJNMMI Res.*, vol. 9, no. 1, p. 114, Dec. 2019.

[221] B. M. Cork JM, LeBlanc JM, Martin DW, Nester WH, 'Nuclear levels associated with zirconium 95 and niobium 95.', *Phys Rev.*, vol. 90, no. 4, pp. 579–581, 1953.

[222] J. J. MEALEY, '[Turn-over of carrier-free zirconium-89 in man].', *Nature*, vol. 179, no. 4561, pp. 673–674, Mar. 1957.

[223] B. N. McKnight and N. T. Viola-Villegas, '89Zr-ImmunoPET companion diagnostics and their impact in clinical drug development.', *J. Labelled Comp. Radiopharm.*, vol. 61, no. 9, pp. 727–738, Jul. 2018.

[224] Y. Kurebayashi, P. L. Choyke, and N. Sato, 'Imaging of cell-based therapy using89 zr-oxine ex vivo cell labeling for positron emission tomography', *Nanotheranostics*, vol. 5, no. 1, pp. 27–35, 2021.

[225] P. J. Gawne *et al.*, 'PET Imaging of Liposomal Glucocorticoids using (89)Zr-oxine: Theranostic Applications in Inflammatory Arthritis.', *Theranostics*, vol. 10, no. 9, pp. 3867–3879, 2020.

[226] N. Li, Z. Yu, T. T. Pham, P. J. Blower, and R. Yan, 'A generic (89)Zr labeling method to quantify the *in vivo* pharmacokinetics of liposomal nanoparticles with positron emission tomography.', *Int. J. Nanomedicine*, vol. 12, pp. 3281–3294, 2017.

[227] I. Verel, G. W. M. Visser, R. Boellaard, M. Stigter-van Walsum, G. B. Snow, and G. A. M. S. van Dongen, '89Zr immuno-PET: comprehensive procedures for the production of 89Zr- labelled monoclonal antibodies.', *J. Nucl. Med.*, vol. 44, no. 8, pp. 1271–1281,

Aug. 2003.

[228] G. W. Severin, J. W. Engle, T. E. Barnhart, and R. J. Nickles, '89Zr radiochemistry for positron emission tomography.', *Med. Chem.*, vol. 7, no. 5, pp. 389–394, Sep. 2011.

[229] Y. W. S. Jauw *et al.*, '(89)Zr-Immuno-PET: Toward a Noninvasive Clinical Tool to Measure Target Engagement of Therapeutic Antibodies *In vivo*.', *J. Nucl. Med.*, vol. 60, no. 12, pp. 1825–1832, Dec. 2019.

[230] G. Fischer, U. Seibold, R. Schirrmacher, B. Wängler, and C. Wängler, '(89)Zr, a radiometal nuclide with high potential for molecular imaging with PET: chemistry, applications and remaining challenges.', *Molecules*, vol. 18, no. 6, pp. 6469–6490, Jun. 2013.

[231] M. T. La, V. H. Tran, and H.-K. Kim, 'Progress of Coordination and Utilization of Zirconium-89 for Positron Emission Tomography (PET) Studies', *Nucl. Med. Mol. Imaging (2010).*, vol. 53, no. 2, pp. 115–124, 2019.

[232] M. Conti and L. Eriksson, 'Physics of pure and non-pure positron emitters for PET: a review and a discussion.', *EJNMMI Phys.*, vol. 3, no. 1, p. 8, Dec. 2016.

[233] S. M. Qaim, 'The Present and Future of Medical Radionuclide Production', *Radiochim. Acta*, 2012.

[234] P. Martini *et al.*, 'In-House Cyclotron Production of High-Purity Tc-99m and Tc-99m Radiopharmaceuticals', *Appl. Radiat. Isot.*, 2018.

[235] A. Boschi, P. Martini, V. Costa, A. Pagnoni, and L. Uccelli, 'Interdisciplinary Tasks in

the Cyclotron Production of Radiometals for Medical Applications. The Case of 47Sc as Example', *Molecules*, 2019.

[236] J. Link, K. A. Krohn, and M. J. O'Hara, 'A Simple Thick Target for Production of 89Zr Using an 11 MeV Cyclotron', *Appl. Radiat. Isot.*, 2017.

[237] A. Fesas, M. R. Pourkhessalian, and A. Vrachimis, 'Single Center Experience on the Production of Fluorine-18 Radiopharmaceuticals Using a 7.5 MeV Cyclotron: Capabilities and Challenges', *Sn Appl. Sci.*, 2020.

[238] G. B. Saha, N. T. Porile, and L. Yaffe, '(P,Xn) and (P,Pxn) Reactions of yttrium-89 with 5-85-mev protons', *Phys. Rev.*, vol. 144, no. 3, pp. 962–971, Apr. 1966.

[239] M. Sadeghi, T. Kakavand, and M. Taghilo, 'Targetry of Y2O3 on a copper substrate for the non-carrier-added 89Zr production via 89Y(p,n)89Zr reaction', *Kerntechnik*, vol. 75, no. 5, pp. 298–302, Sep. 2010.

[240] Y. Zhang, H. Hong, and W. Cai, 'PET tracers based on Zirconium-89.', *Curr. Radiopharm.*, vol. 4, no. 2, pp. 131–139, Apr. 2011.

[241] D. Degering, S. Unterricker, and W. Stolz, 'Excitation function of the89Y/d,2n/89Zr reaction', *J. Radioanal. Nucl. Chem. Lett.*, vol. 127, no. 1, pp. 7–11, 1988.

[242] *Cyclotron Produced Radionuclides: Physical Characteristics and Production Methods*, no. 468. Vienna: INTERNATIONAL ATOMIC ENERGY AGENCY, 2009.

[243] J. M. Link *et al.*, ' 89Zr for antibody labeling and positron emission tomography', *J. Label. Compd. Radiopharm.*, vol. 23, no. 10–1, pp. 1297–1298, 1986.

[244] W. E. Meijs *et al.*, 'Production of highly pure no-carrier added 89Zr for the labelling of antibodies with a positron emitter', *Appl. Radiat. Isot.*, vol. 45, no. 12, pp. 1143–1147, 1994.

[245] P. P. Kumbhar and C. D. Lokhande, 'Electrodeposition of yttrium from a nonaqueous bath', *Met. Finish.*, vol. 93, no. 4, pp. 28–31, 1995.

[246] A. M. Dabkowski, S. J. Paisey, E. Spezi, J. Chester, and C. Marshall, 'Optimization of zirconium-89 production in IBA Cyclone 18/9 cyclotron with COSTIS solid target system', *AIP Conf. Proc.*, vol. 1845, no. 1, p. 20005, 2017.

[247] A. Infantino *et al.*, 'Prediction of (89)Zr production using the Monte Carlo code FLUKA.', *Appl. Radiat. Isot. Incl. data, Instrum. methods use Agric. Ind. Med.*, vol. 69, no. 8, pp. 1134–1137, Aug. 2011.

[248] A. L. Wooten, G. D. Schweitzer, L. A. Lawrence, E. Madrid, and S. E. Lapi, 'An automated system for production of 89Zr', *AIP Conf. Proc.*, vol. 1509, no. 1, pp. 201–205, 2012.

[249] F. Wang *et al.*, 'Production of the next-generation positron nuclide zirconium-89 ((89) Zr) guided by Monte Carlo simulation and its good quality for antibody labeling.', *J. Labelled Comp. Radiopharm.*, vol. 64, no. 1, pp. 47–56, Jan. 2021.

[250] M. Sadeghi, M. Enferadi, and M. Bakhtiari, 'Accelerator production of the positron emitter zirconium-89', *Ann. Nucl. Energy*, vol. 41, pp. 97–103, 2012.

[251] M. K. Pandey, A. Bansal, H. P. Engelbrecht, J. F. Byrne, A. B. Packard, and T. R. DeGrado, 'Improved production and processing of ^{89}Zr using a solution target.', *Nucl.*

Med. Biol., vol. 43, no. 1, pp. 97–100, Jan. 2016.

[252] T. R. DeGrado, M. K. Pandey, and J. Byrne, 'Solution target for cyclotron production of radiometals'. Mar-2022.

[253] M. A. Synowiecki, L. R. Perk, and J. F. W. Nijsen, 'Production of novel diagnostic radionuclides in small medical cyclotrons.', *EJNMMI Radiopharm. Chem.*, vol. 3, no. 1, p. 3, 2018.

[254] J. Rousseau *et al.*, 'Synthesis and evaluation of bifunctional tetrahydroxamate chelators for labeling antibodies with (89)Zr for imaging with positron emission tomography.', *Bioorg. Med. Chem. Lett.*, vol. 28, no. 5, pp. 899–905, Mar. 2018.

[255] F. Guérard, Y. Lee, R. Tripier, L. P. Szajek, J. R. Deschamps, and M. W. Brechbiel, 'Investigation of Zr(IV) and 89Zr(IV) complexation with Hydroxamates: progress toward designing a better chelator than desferrioxamine B for immuno-PET imaging', vol. 1002–1004. Jan-2013.

[256] D. N. Pandya *et al.*, 'Zirconium tetraazamacrocycle complexes display extraordinary stability and provide a new strategy for zirconium-89-based radiopharmaceutical development.', *Chem. Sci.*, vol. 8, no. 3, pp. 2309–2314, Mar. 2017.

[257] J. P. Holland, Y. Sheh, and J. S. Lewis, 'Standardized methods for the production of high specific-activity zirconium-89', *Nucl. Med. Biol.*, vol. 36, no. 7, pp. 729–739, 2009.

[258] Y. Tang *et al.*, 'A simple and convenient method for production of (89)Zr with high purity.', *Appl. Radiat. Isot. Incl. data, Instrum. methods use Agric. Ind. Med.*, vol. 118, pp. 326–330, Dec. 2016.

[259] O. T. Dejesus and R. J. Nickles, 'Production and purification of 89Zr, a potential PET antibody label', *Int. J. Radiat. Appl. instrumentation. Part A. Appl. Radiat. Isot.*, vol. 41, no. 8, pp. 789–790, 1990.

[260] M. Seif, H. Einsele, and J. Löffler, 'CAR T Cells Beyond Cancer: Hope for Immunomodulatory Therapy of Infectious Diseases.', *Front. Immunol.*, vol. 10, p. 2711, 2019.

[261] J. Siikanen, T. A. Tran, T. G. Olsson, S.-E. Strand, and A. Sandell, 'A solid target system with remote handling of irradiated targets for PET cyclotrons.', *Appl. Radiat. Isot. Incl. data, Instrum. methods use Agric. Ind. Med.*, vol. 94, pp. 294–301, Dec. 2014.

[262] S. L. Queern *et al.*, 'Production of Zr-89 using sputtered yttrium coin targets (89)Zr using sputtered yttrium coin targets.', *Nucl. Med. Biol.*, vol. 50, pp. 11–16, Jul. 2017.

[263] M. K. Pandey, H. P. Engelbrecht, J. P. Byrne, A. B. Packard, and T. R. DeGrado, 'Production of 89Zr via the 89Y(p,n)89Zr reaction in aqueous solution: effect of solution composition on in-target chemistry.', *Nucl. Med. Biol.*, vol. 41, no. 4, pp. 309–316, Apr. 2014.

[264] A. Kasbollah, P. Eu, S. Cowell, and P. Deb, 'Review on production of 89Zr in a medical cyclotron for PET radiopharmaceuticals.', *J. Nucl. Med. Technol.*, vol. 41, no. 1, pp. 35–41, Mar. 2013.

[265] L. E. McInnes, S. E. Rudd, and P. S. Donnelly, 'Copper, gallium and zirconium positron emission tomography imaging agents: The importance of metal ion speciation', *Coord. Chem. Rev.*, vol. 352, pp. 499–516, 2017.

[266] G. A. Van Dongen *et al.*, '89Zr-immuno-PET for imaging of long circulating drugs and disease targets: why, how and when to be applied?', *Q. J. Nucl. Med. Mol. imaging Off. Publ. Ital. Assoc. Nucl. Med. [and] Int. Assoc. Radiopharmacol. (IAR),[and] Sect. Soc. of...*, vol. 59, no. 1, pp. 18–38, Mar. 2015.

[267] J. P. Holland, Y. Sheh, and J. S. Lewis, 'Standardized methods for the production of high specific-activity zirconium-89.', *Nucl. Med. Biol.*, vol. 36, no. 7, pp. 729–739, Oct. 2009.

[268] N. Bhatt, D. Pandya, and T. Wadas, 'Recent advantages in zirconium-89 chelator development', *Molecules*, vol. 23, no. 3, p. 638, Mar. 2018.

[269] A. G. Kazakov, R. A. Aliev, V. S. Ostapenko, A. B. Priselkova, and S. N. Kalmykov, 'Separation of 89Zr from irradiated yttrium targets by extraction chromatography', *J. Radioanal. Nucl. Chem.*, vol. 317, no. 1, pp. 605–611, 2018.

[270] O. F. Ikotun and S. E. Lapi, 'The rise of metal radionuclides in medical imaging: copper-64, zirconium-89 and yttrium-86', *Future Med. Chem.*, vol. 3, no. 5, pp. 599–621, 2011.

[271] J. Zweit, S. Downey, and H. L. Sharma, 'Production of no-carrier-added zirconium-89 for positron emission tomography', *Int. J. Radiat. Appl. instrumentation. Part A. Appl. Radiat. Isot.*, vol. 42, no. 2, pp. 199–201, 1991.

[272] B. Dutta, M. Maiti, and S. Lahiri, 'Production of 88,89Zr by proton induced activation of natY and separation by SLX and LLX', *J. Radioanal. Nucl. Chem.*, vol. 281, no. 3, pp. 663–667, 2009.

[273] W. E. Meijs, J. D. Herscheid, H. J. Haisma, and H. M. Pinedo, 'Evaluation of desferal

as a bifunctional chelating agent for labeling antibodies with Zr-89.', *Int. J. Radiat. Appl. instrumentation. Part A, Appl. Radiat. Isot.*, vol. 43, no. 12, pp. 1443–1447, Dec. 1992.

[274] A. Kasbollah, P. Eu, S. Cowell, and P. Deb, 'Review on Production of 89Zr in a Medical Cyclotron for PET Radiopharmaceuticals', *J. Nucl. Med. Technol.*, vol. 41, no. 1, pp. 35–41, 2013.

[275] E. Tugce Sarcan, M. Silindir-Gunay, A. Yekta Ozer, and N. Hartman, '89Zr as a promising radionuclide and it's applications for effective cancer imaging', *J. Radioanal. Nucl. Chem.*, vol. 330, no. 1, pp. 15–28, 2021.

[276] S. A. Kandil, B. Scholten, Z. A. Saleh, A. M. Youssef, S. M. Qaim, and H. H. Coenen, 'A comparative study on the separation of radiozirconium via ion-exchange and solvent extraction techniques, with particular reference to the production of 88Zr and 89Zr in proton induced reactions on yttrium', *J. Radioanal. Nucl. Chem.*, vol. 274, no. 1, pp. 45–52, 2007.

[277] V. I. Fadeeva, T. I. Tikhomirova, I. B. Yuferova, and G. V Kudryavtsev, 'Preparation, properties and analytical application of silica with chemically grafted hydroxamic acid groups', *Anal. Chim. Acta*, vol. 219, pp. 201–212, 1989.

[278] S. A. Graves *et al.*, 'Evaluation of a chloride-based (89)Zr isolation strategy using a tributyl phosphate (TBP)-functionalized extraction resin.', *Nucl. Med. Biol.*, vol. 64–65, pp. 1–7, 2018.

[279] A. Singhal, L. M. Toth, J. S. Lin, and K. Affholter, 'Zirconium(IV) Tetramer/Octamer Hydrolysis Equilibrium in Aqueous Hydrochloric Acid Solution', *J. Am. Chem. Soc.*,

vol. 118, no. 46, pp. 11529–11534, Jan. 1996.

[280] R. Borjas Nevarez, S. M. Balasekaran, E. Kim, P. Weck, and F. Poineau, 'Zirconium tetrachloride revisited.', *Acta Crystallogr. Sect. C, Struct. Chem.*, vol. 74, no. Pt 3, pp. 307–311, Mar. 2018.

[281] J. R. de Laeter *et al.*, 'Atomic weights of the elements. Review 2000 (IUPAC Technical Report)', vol. 75, no. 6, pp. 683–800, 2003.

[282] T. W. Price, J. Greenman, and G. J. Stasiuk, 'Current advances in ligand design for inorganic positron emission tomography tracers 68Ga, 64Cu, 89Zr and 44Sc', *Dalt. Trans.*, vol. 45, no. 40, pp. 15702–15724, 2016.

[283] M. K. Moi, C. F. Meares, M. J. McCall, W. C. Cole, and S. J. DeNardo, 'Copper chelates as probes of biological systems: Stable copper complexes with a macrocyclic bifunctional chelating agent', *Anal. Biochem.*, vol. 148, no. 1, pp. 249–253, 1985.

[284] T. SASAKI, T. KOBAYASHI, I. TAKAGI, and H. MORIYAMA, 'Hydrolysis Constant and Coordination Geometry of Zirconium(IV)', *J. Nucl. Sci. Technol.*, vol. 45, no. 8, pp. 735–739, Aug. 2008.

[285] 'Multi-Agency Radiological Laboratory Analytical Protocols Manual (NUREG-1576, Initial Report)'. .

[286] L. R. Perk *et al.*, '(89)Zr as a PET surrogate radioisotope for scouting biodistribution of the therapeutic radiometals (90)Y and (177)Lu in tumor-bearing nude mice after coupling to the internalizing antibody cetuximab.', *J. Nucl. Med.*, vol. 46, no. 11, pp. 1898–1906, Nov. 2005.

[287] M. Patra *et al.*, 'An octadentate bifunctional chelating agent for the development of stable zirconium-89 based molecular imaging probes', *Chem. Commun.*, vol. 50, no. 78, pp. 11523–11525, 2014.

[288] D. Parker, K. Pulukkody, F. C. Smith, A. Batsanov, and J. A. K. Howard, "Structures of the yttrium complexes of 1,4,7,10-tetraazacyclododecane-N,N′,N″,N‴-tetraacetic acid (H4dota) and N,N″-bis(benzylcarbamoylmethyl)diethylenetriamine-N,N′,N″-triacetic acid and the solution structure of a zirconium complex of H4dota," J. Chem. Soc., Dalton Trans., no. 5, pp. 689–693, 1994, doi: 10.1039/dt9940000689.

[289] A. B. Ilyukhin, R. L. Davidovich, I. N. Samsonova, and L. V. Teplukhina, "Eightfold-coordinated diethylenetriaminepentaacetates: Crystal structures of K[M(Dtpa)] ·3H2O (M = Zr or Hf) and NH4[Sn(Dtpa)] · H2O," Crystallography Reports, vol. 45, no. 1, pp. 39–43, Jan. 2000, doi: 10.1134/1.171134.

[290] A. I. Pozhidaev, T. N. Polynova, M. A. Porai-Koshits, and V. G. Dudakov, 'Crystal structure of disodium magnesium ethylenediaminetetraacetate tetrahydrate', *J. Struct. Chem.*, vol. 15, no. 1, pp. 149–150, 1974.

[291] E. Boros, B. V Marquez, O. F. Ikotun, S. E. Lapi, and C. L. Ferreira, 'Coordination chemistry and ligand design in development of metal based radiopharmaceuticals', *Ligand Des. Med. Inorg. Chem.*, pp. 47–79, May 2014.

[292] M. A. Deri, B. M. Zeglis, L. C. Francesconi, and J. S. Lewis, 'PET imaging with 89Zr: From radiochemistry to the clinic', *Nucl. Med. Biol.*, vol. 40, no. 1, pp. 3–14, 2013.

[293] J. P. Holland, V. Divilov, N. H. Bander, P. M. Smith-Jones, S. M. Larson, and J. S.

Lewis, '89Zr-DFO-J591 for immunoPET of prostate- specific membrane antigen expression *in vivo*', *J. Nucl. Med.*, vol. 51, no. 8, pp. 1293–1300, Jul. 2010.

[294] A. J. Chang, R. Desilva, S. Jain, K. Lears, B. Rogers, and S. Lapi, '89Zr-Radio labelled Trastuzumab Imaging in Orthotopic and Metastatic Breast Tumors.', *Pharmaceuticals (Basel).*, vol. 5, no. 1, pp. 79–93, Jan. 2012.

[295] J. S. Khurana, *Bone {Pathology}*. Springer Science & Business Media, 2009.

[296] G. A. Ulaner, D. M. Hyman, S. K. Lyashchenko, J. S. Lewis, and J. A. Carrasquillo, '89Zr-Trastuzumab PET/CT for detection of human epidermal growth factor receptor 2- positive metastases in patients with human epidermal growth factor receptor 2-negative primary breast cancer', *Clin. Nucl. Med.*, vol. 42, no. 12, pp. 912–917, 2017.

[297] Y. W. S. Jauw *et al.*, 'Immuno-positron emission tomography with zirconium-89-labelled monoclonal antibodies in oncology: What can we learn from initial clinical trials?', *Front. Pharmacol.*, vol. 7, no. MAY, pp. 1–15, 2016.

[298] J. N. Tinianow *et al.*, 'Site-specifically 89Zr-labelled monoclonal antibodies for immunoPET', *Nucl. Med. Biol.*, vol. 37, no. 3, pp. 289–297, 2010.

[299] S. Liu, 'Bifunctional coupling agents for radiolabeling of biomolecules and target-specific delivery of metallic radionuclides', *Adv. Drug Deliv. Rev.*, vol. 60, no. 12, pp. 1347–1370, 2008.

[300] L. R. Perk *et al.*, 'P-Isothiocyanatobenzyl-desferriozamine: a new bifunctional chelate for facile radiolabelling of monoclonal antibodies with zirconium-89 for immuno-PET imaging', *Eur. J. Nucl. Med. Mol. Imaging*, vol. 37, no. 2, pp. 250–259, Sep. 2009.

[301] M. J. W. D. Vosjan *et al.*, 'Conjugation and radiolabeling of monoclonal antibodies with zirconium-89 for PET imaging using the bifunctional chelate p-isothiocyanatobenzyl-desferrioxamine', *Nat. Protoc.*, vol. 5, no. 4, pp. 739–743, 2010.

[302] S. Heskamp, R. Raavé, O. Boerman, M. Rijpkema, V. Goncalves, and F. Denat, '89Zr-Immuno-Positron Emission Tomography in Oncology: State-of-the-Art 89Zr Radiochemistry', *Bioconjug. Chem.*, vol. 28, no. 9, pp. 2211–2223, Sep. 2017.

[303] J. P. Holland, 'Predicting the Thermodynamic Stability of Zirconium Radiotracers.', *Inorg. Chem.*, vol. 59, no. 3, pp. 2070–2082, Feb. 2020.

[304] R. T. Dhawan and A. M. Peters, 'Withdrawal of indium-111: implications for white-cell imaging. The nuclear medicine community must act.', *Nuclear medicine communications*, vol. 35, no. 8. England, pp. 789–791, Aug-2014.

[305] V. Oliveri and G. Vecchio, '8-Hydroxyquinolines in medicinal chemistry: A structural perspective', *Eur. J. Med. Chem.*, vol. 120, pp. 252–274, 2016.

[306] S. Prachayasittikul, V., Prachayasittikul, V., Prachayasittikul, S., & Ruchirawat, '8-Hydroxyquinolines: a review of their metal chelating properties and medicinal applications', *Drug Des. Devel. Ther.*, p. 1157, 2013.

[307] B. L. ELLIS and H. L. SHARMA, 'Co, Fe and Ga chelates for cell labelling: A potential use in PET imaging?', *Nucl. Med. Commun.*, vol. 20, no. 11, 1999.

[308] T. J. Ferris, P. Charoenphun, L. K. Meszaros, G. E. D. D. Mullen, P. J. Blower, and M. J. Went, 'Synthesis and characterisation of zirconium complexes for cell tracking with Zr-89 by positron emission tomography', *Dalt. Trans.*, vol. 43, no. 39, pp. 14851–14857,

2014.

[309] L. Southcott and C. Orvig, 'Inorganic radiopharmaceutical chemistry of oxine', *Dalt. Trans.*, vol. 50, no. 45, pp. 16451–16458, 2021.

[310] N. Sato, H. Wu, K. O. Asiedu, L. P. Szajek, G. L. Griffiths, and P. L. Choyke, '(89)Zr-Oxine Complex PET Cell Imaging in Monitoring Cell-based Therapies.', *Radiology*, vol. 275, no. 2, pp. 490–500, May 2015.

[311] K. O. Asiedu, S. Koyasu, L. P. Szajek, P. L. Choyke, and N. Sato, 'Bone marrow cell trafficking analyzed by 89Zr-oxine positron emission tomography in a murine transplantation model', *Clin. Cancer Res.*, vol. 23, no. 11, pp. 2759–2768, Jun. 2017.

[312] A. M. Dabkowski, S. J. Paisey, M. Talboys, and C. Marshall, 'Optimization of cyclotron production for radiometal of Zirconium 89', *Acta Phys. Pol. A*, vol. 127, pp. 1479–1482, 2015.

[313] 'EL4 - TIB-39 | ATCC'. [Online]. Available: https://www.atcc.org/products/tib-39. [Accessed: 19-Jan-2024].

[314] 'CTLL-2 - TIB-214 | ATCC'. [Online]. Available: https://www.atcc.org/products/tib-214. [Accessed: 04-Jan-2024].

[315] 'Using a Hemocytometer for Cell Counting | Protocol'. [Online]. Available: https://www.stemcell.com/how-to-count-cells-with-a-hemocytometer.html#materials. [Accessed: 18-Oct-2023].

[316] N. S. Sta Maria *et al.*, 'Spatio-temporal biodistribution of 89Zr-oxine labelled huLym-

1-A-BB3z-CAR T-cells by PET imaging in a preclinical tumor model', *Sci. Rep.*, vol. 11, no. 1, pp. 1–13, 2021.

[317] A. Bansal, S. Sharma, B. Klasen, F. Rösch, and M. K. Pandey, 'Evaluation of different 89Zr- labelled synthons for direct labeling and tracking of white blood cells and stem cells in healthy athymic mice', *Sci. Rep.*, vol. 12, no. 1, p. 15646, Sep. 2022.

[318] F. Man, A. A. Khan, A. Carrascal-Miniño, P. J. Blower, and R. T.M. de Rosales, 'A kit formulation for the preparation of [89Zr]Zr(oxinate)4 for PET cell tracking: White blood cell labelling and comparison with [111In]In(oxinate)3', *Nucl. Med. Biol.*, vol. 90–91, pp. 31–40, 2020.

[319] F. Man *et al.*, '*In vivo* PET Tracking of 89 Zr- labelled Vγ9Vδ2 T Cells to Mouse Xenograft Breast Tumors Activated with Liposomal Alendronate', *Mol. Ther.*, vol. 27, no. 1, pp. 219–229, 2019.

[320] S. Wang *et al.*, 'Biodistribution of 89Zr-Oxine- labelled Human Bone Marrow-Derived Mesenchymal Stem Cells by Micro-Pet/Computed Tomography Imaging in Sprague–Dawley Rats', *Nucl. Med. Commun.*, 2022.

[321] L. Weston, A. Geczy, and C. Farrell, 'A convenient and reliable IL-2 bioassay using frozen CTLL-2 to improve the detection of helper T lymphocyte precursors.', *Immunol. Cell Biol.*, vol. 76, no. 2, pp. 190–192, Apr. 1998.

[322] M. Kahts et al., "89Zr-leukocyte labelling for cell trafficking: in vitro and preclinical investigations," EJNMMI Radiopharmacy and Chemistry, vol. 8, no. 1, Nov. 2023, doi: 10.1186/s41181-023-00223-1.

[323] P. S. Patrick *et al.*, 'Lung delivery of MSCs expressing anti-cancer protein TRAIL visualised with 89Zr-oxine PET-CT', *Stem Cell Res. Ther.*, vol. 11, no. 1, p. 256, 2020.

[324] K. O. Asiedu, M. Ferdousi, P. T. Ton, S. S. Adler, P. L. Choyke, and N. Sato, 'Bone marrow cell homing to sites of acute tibial fracture: 89 Zr-oxine cell labeling with positron emission tomographic imaging in a mouse model', *EJNMMI Res.*, vol. 8, 2018.

[325] M. R. Weist *et al.*, 'PET of adoptively transferred chimeric antigen receptor T Cells with 89Zr-Oxine', *J. Nucl. Med.*, vol. 59, no. 10, pp. 1531–1537, 2018.

[326] P. Leland, D. Kumar, S. Nimaggada, S. R. Bauer, R. K. Puri, and B. Joshi, 'Characterization of Chimeric Antigen Receptor Modified T Cells Expressing scFv-IL-13Rα2 After Radiolabeling With 89Zirconium Oxine for PET Imaging', 2023.

[327] J. Jacob *et al.*, 'Radiolabelling of Polyclonally Expanded Human Regulatory T Cells (Treg) With 89Zr-Oxine for Medium-Term *in vivo* Cell Tracking', *Molecules*, 2023.

[328] N. Sato *et al.*, '*In vivo* Tracking of Adoptively Transferred Natural Killer Cells in Rhesus Macaques Using 89Zirconium-Oxine Cell Labeling and PET Imaging', *Clin. Cancer Res.*, vol. 26, no. 11, pp. 2573–2581, 2020.

[329] J. Perrin *et al.*, 'Cell Tracking in Cancer Immunotherapy', *Front. Med.*, vol. 7, no. February, pp. 1–16, 2020.

[330] N. Shalaby, V. P. Dubois, and J. Ronald, 'Molecular imaging of cellular immunotherapies in experimental and therapeutic settings', *Cancer Immunol. Immunother.*, vol. 71, no. 6, pp. 1281–1294, 2022.

[331] F. Man *et al.*, '*In vivo* PET Tracking of 89Zr- labelled Vγ9Vδ2 T Cells to Mouse Xenograft Breast Tumors Activated With Liposomal Alendronate', *Mol. Ther.*, 2019.

[332] P. S. Patrick *et al.*, 89Zr-Oxine Labelling and PET Imaging Shows Lung Delivery of a Cell/Gene Cancer Therapy', 2019.

[333] D. S. Abou, T. Ku, and P. M. Smith-Jones, '*In vivo* biodistribution and accumulation of 89Zr in mice', *Nucl. Med. Biol.*, vol. 38, no. 5, pp. 675–681, 2011.

[334] P. S. Patrick *et al.*, 'Lung delivery of MSCs expressing anti-cancer protein TRAIL visualised with (89)Zr-oxine PET-CT.', *Stem Cell Res. Ther.*, vol. 11, no. 1, p. 256, Jun. 2020.

[335] M. S. De Feo, M. Pontico, V. Frantellizzi, F. Corica, F. De Cristofaro, and G. De Vincentis, "89Zr-PET imaging in humans: a systematic review," Clinical and Translational Imaging, vol. 10, no. 1, pp. 23–36, Sep. 2021, doi: 10.1007/s40336-021-00462-9.

[336] P. Laverman *et al.*, 'Immuno-PET and Immuno-SPECT of Rheumatoid Arthritis with Radio labelled Anti–Fibroblast Activation Protein Antibody Correlates with Severity of Arthritis', *J. Nucl. Med.*, vol. 56, no. 5, pp. 778 LP – 783, May 2015.

[337] D. S. Abou, T. W. Ku, and P. Smith-Jones, '*In vivo* Biodistribution and Accumulation of 89Zr in Mice', *Nucl. Med. Biol.*, 2011.

[338] C. Bailly *et al.*, 'What Is the Best Radionuclide for Immuno-Pet of Multiple Myeloma? A Comparison Study Between 89Zr- And 64Cu- labelled Anti-Cd138 in a Preclinical Syngeneic Model', *Int. J. Mol. Sci.*, 2019.

[339] H. Damerow *et al.*, 'Toward Optimized 89Zr-Immuno-PET: Side-by-Side Comparison of [89Zr]Zr-DFO-,[89Zr]Zr-3,4,3-(LI-1,2-HOPO)- and [89Zr]Zr-DFO*-Cetuximab for Tumor Imaging: Which Chelator Is the Most Suitable?', *Pharmaceutics*, vol. 14, no. 10, p. 2114, Oct. 2022.

[340] M. Chomet *et al.*, 'Head-to-Head Comparison of DFO* and DFO Chelators: Selection of the Best Candidate for Clinical 89Zr-Immuno-Pet', *Eur. J. Nucl. Med. Mol. Imaging*, 2020.

[341] J. J. Bartnicka, F. Al-Salemee, G. Firth, and P. J. Blower, 'L-Cysteine-mediated modulation of copper trafficking in prostate cancer cells: An: *In vitro* and *in vivo* investigation with 64Cu and 64Cu-PET', *Metallomics*, vol. 12, no. 10, pp. 1508–1520, 2020.

[342] L. Zhang, S. Bhatnagar, E. Deschenes, and G. M. Thurber, 'Mechanistic and quantitative insight into cell surface targeted molecular imaging agent design', *Sci. Rep.*, vol. 6, no. 1, p. 25424, 2016.

[343] F. Man, P. J. Gawne, and R. T.M. de Rosales, 'Nuclear imaging of liposomal drug delivery systems: A critical review of radiolabelling methods and applications in nanomedicine', *Adv. Drug Deliv. Rev.*, vol. 143, pp. 134–160, 2019.

[344] J. Davidson-Moncada *et al.*, 'A Novel Method to Study the *in vivo* Trafficking and Homing of Adoptively Transferred NK Cells in Rhesus Macaques and Humans', *Blood*, vol. 124, no. 21, p. 659, Dec. 2014.

[345] J. P. Holland, V. Divilov, N. H. Bander, P. M. Smith-Jones, S. M. Larson, and J. S.

Lewis, '89 Zr-DFO-J591 for immunoPET of prostate-specific membrane antigen expression *in vivo*', *J. Nucl. Med.*, vol. 51, no. 8, pp. 1293–1300, 2010.

[346] R. Palacios, "Concanavalin A triggers T lymphocytes by directly interacting with their receptors for activation.," *The Journal of Immunology*, vol. 128, no. 1, pp. 337–342, Jan. 1982, doi: 10.4049/jimmunol.128.1.337.

[347] D. S. Abou, T. Ku, and P. M. Smith-Jones, '*In vivo* biodistribution and accumulation of 89Zr in mice', *Nucl. Med. Biol.*, vol. 38, no. 5, pp. 675–681, Jul. 2011.

[348] M. L. Thakur, R. E. Coleman, C. G. Mayhall, and M. J. J. Welch, 'Preparation and evaluation of 111In- labelled leukocytes as an abscess imaging agent in dogs.', *Radiology*, vol. 119, no. 3, p. 731, Jun. 1976.

[349] D. J. Vugts *et al.*, 'Comparison of the octadentate bifunctional chelator DFO*-pPhe-NCS and the clinically used hexadentate bifunctional chelator DFO-pPhe-NCS for 89Zr-immuno-PET', *Eur. J. Nucl. Med. Mol. Imaging*, vol. 44, no. 2, pp. 286–295, 2017.

[350] R. J. M. Berge, A. T. Natarajan, E. A, and T. A. Schellekens, 'PHYSICS AND RADIATION Labeling with Indium-i 11 has Detrimental Effects on Human Lymphocytes : ConciseCommunication', vol. 24, no. 7, pp. 615–620, 1983.

[351] J. Kuyama *et al.*, 'Indium-111 labelled lymphocytes: Isotope distribution and cell division', *Eur. J. Nucl. Med.*, vol. 24, no. 5, pp. 488–496, May 1997.

[352] J. R. Giles, A.-M. Globig, S. M. Kaech, and E. J. Wherry, 'CD8+ T cells in the cancer-immunity cycle', *Immunity*, vol. 56, no. 10, pp. 2231–2253, 2023.

[353] S.-W. Lee, G.-W. Lee, H.-O. Kim, and J.-H. Cho, 'Shaping Heterogeneity of Naive CD8(+) T Cell Pools.', *Immune Netw.*, vol. 23, no. 1, p. e2, Feb. 2023.

[354] W. E. Biddison, G. M. Shearer, and T. W. Chang, 'Regulation of influenza virus-specific cytotoxic T cell responses by monoclonal antibody to a human T cell differentiation antigen.', *J. Immunol.*, vol. 127, no. 6, pp. 2236–2240, Dec. 1981.

[355] A. R. Townsend and J. J. Skehel, 'Influenza A specific cytotoxic T-cell clones that do not recognize viral glycoproteins.', *Nature*, vol. 300, no. 5893, pp. 655–657, Dec. 1982.

[356] F. A. Ennis, W. J. Martin, and M. W. Verbonitz, 'Hemagglutinin-specific cytotoxic T-cell response during influenza infection.', *J. Exp. Med.*, vol. 146, no. 3, pp. 893–898, Sep. 1977.

[357] J. W. Yewdell, J. R. Bennink, G. L. Smith, and B. Moss, 'Influenza A virus nucleoprotein is a major target antigen for cross-reactive anti-influenza A virus cytotoxic T lymphocytes.', *Proc. Natl. Acad. Sci. U. S. A.*, vol. 82, no. 6, pp. 1785–1789, Mar. 1985.

[358] A. R. Townsend, F. M. Gotch, and J. Davey, 'Cytotoxic T cells recognize fragments of the influenza nucleoprotein.', *Cell*, vol. 42, no. 2, pp. 457–467, Sep. 1985.

[359] M. D. Martin and V. P. Badovinac, 'Defining Memory CD8 T Cell.', *Front. Immunol.*, vol. 9, p. 2692, 2018.

[360] H. Choi, Y. Kim, and Y. W. Jung, 'The Function of Memory CD8+ T Cells in Immunotherapy for Human Diseases.', *Immune Netw.*, vol. 23, no. 1, p. e10, Feb. 2023.

[361] E. J. Wherry and R. Ahmed, 'Memory CD8 T-cell differentiation during viral infection.', *J. Virol.*, vol. 78, no. 11, pp. 5535–5545, Jun. 2004.

[362] N. Zhang and M. J. Bevan, 'CD8(+) T cells: foot soldiers of the immune system.', *Immunity*, vol. 35, no. 2, pp. 161–168, Aug. 2011.

[363] E. J. Wherry, 'T cell exhaustion.', *Nat. Immunol.*, vol. 12, no. 6, pp. 492–499, Jun. 2011.

[364] M. Ando, M. Ito, T. Srirat, T. Kondo, and A. Yoshimura, 'Memory T cell, exhaustion, and tumor immunity.', *Immunol. Med.*, vol. 43, no. 1, pp. 1–9, Mar. 2020.

[365] L. M. McLane, M. S. Abdel-Hakeem, and E. J. Wherry, 'CD8 T Cell Exhaustion During Chronic Viral Infection and Cancer.', *Annu. Rev. Immunol.*, vol. 37, pp. 457–495, Apr. 2019.

[366] K. Perica, J. C. Varela, M. Oelke, and J. Schneck, 'Adoptive T cell immunotherapy for cancer.', *Rambam Maimonides Med. J.*, vol. 6, no. 1, p. e0004, Jan. 2015.

[367] M. St Paul and P. S. Ohashi, 'The Roles of CD8(+) T Cell Subsets in Antitumor Immunity.', *Trends Cell Biol.*, vol. 30, no. 9, pp. 695–704, Sep. 2020.

[368] H. Aghajanian, J. G. Rurik, and J. A. Epstein, 'CAR-based therapies: opportunities for immuno-medicine beyond cancer.', *Nat. Metab.*, vol. 4, no. 2, pp. 163–169, Feb. 2022.